CLAY COLLOID MOBILIZATION IN AN IRON OXIDE–COATED SAND

by

Joseph N. Ryan

B.S.C.E. Princeton University 1983
M.S.C.E. Massachusetts Institute of Technology 1988

Submitted to the
Department of Civil and Environmental Engineering
in partial fulfillment of the requirements for the degree of

Doctor of Philosophy

Massachusetts Institute of Technology

July 1992

Author _____
Joseph N. Ryan
Civil and Environmental Engineering Department

Certified by _____
Professor Philip M. Gschwend
Thesis Supervisor

Accepted by _____
Professor Eduardo A. Kausel
Chair, Departmental Committee on Graduate Studies

CLAY COLLOID MOBILIZATION IN AN IRON OXIDE–COATED SAND

by
Joseph N. Ryan

Submitted to the Department of Civil and Environmental Engineering
on 14 July 1992 in partial fulfillment of the requirements of the Degree of
Doctor of Philosophy in Environmental Engineering

ABSTRACT

The goal of these studies was to develop an understanding of the geochemical mechanisms responsible for the mobilization of clay colloids in an iron oxide–coated sediment. Starting with the hypothesis that the infiltration of anoxic, organic matter–rich groundwater caused the dissolution of the Fe(III) oxides and the release of clay colloids in the New Jersey Coastal Plain Cohansey Sand formation, two major efforts to elucidate the source of clay colloids were made.

The first effort involved examining distributions of minerals and elements in soil and sediment samples taken from the Cohansey Sand formation. In this investigation, we showed that the clay and Fe(III) oxides that coated the quartz grains were diagenetic alterations of the original sediment and that the clay–sized fraction and Fe(III) oxide contents in the anoxic sediments below the swamp were lower than those in the oxic sediments. The influx of organic matter–rich water from the swamp dissolved the Fe(III) oxide coatings and released kaolinite. To determine the abundance of the secondary Fe(III) oxides in the New Jersey Coastal Plain sands, we devised a new selective extraction method that targeted the dissolution of Fe(III) oxides in soils and sediments using a mixed chelate Ti(III) complex as the reductant. The Ti(III) method was more selective than the widely–used dithionite method.

The second effort involved a laboratory study of the effect of changing the *p*H, ionic strength, reductant concentration, and surfactant concentration of the flushing solution on the rate of clay release from the sediment. We showed that the electrostatic energy between approaching surfaces exerted the primary control over clay release. The electrostatic energy were made more repulsive and clay release was accelerated by the reductive dissolution of Fe(III) oxides. Surface potentials of the clay colloids were estimated from their surface potentials with an empirical relationship between the zeta potentials and calculated surface potentials of two simple oxides.

As a prelude to these experiments, we tested the appropriateness of two models of colloid detachment kinetics: (1) the energy barrier model, in which the release rate is controlled be the size of the potential energy barrier and (2) an equilibrium model, in which the release rate is controlled by both thermodynamic and hydrodynamic conditions. Experiments in which the ionic strength and the flow rate of the flushing solution were varied showed that the equilibrium model better described the colloid detachment kinetics. Nevertheless, the detachment energies could only be qualitatively related to the trends in the colloid release rates.

Thesis Supervisor: Dr. Philip M. Gschwend

Title: Associate Professor of Civil and Environmental Engineering

ACKNOWLEDGMENTS

Only one name appears on the cover of this thesis, but many people generously contributed in many ways. On these pages, I hope to properly acknowledge their contributions.

I am most grateful to Phil Gschwend, my thesis advisor, for his intellectual energy and guidance and for his fairness and directness. I also thank Harry Hemond and François Morel, members of my thesis committee, for their insights and many helpful reviews.

The financial support of the U.S. Department of Energy's Subsurface Science Program and Dr. Frank Wobber is gratefully acknowledged. The research was supported under contracts DE–FG02–86ER60413 and DE–FG02–89ER60846.

This thesis also benefited from discussions with Prof. Dieke Postma of the Technical University of Denmark (who also provided a very thorough review of Chapter 2), Prof. Keith Stolzenbach of Cal Tech, Dr. Bob Hudson of UC Santa Barbara, Dr. Lynn Roberts of MIT, Prof. Dave Dzombak of Carnegie–Mellon University, Prof. Janet Hering of UCLA, and Dr. Niels Ryde of Clarkson University.

I am indebted to Pat Johnsson and Julia Barringer of the U.S. Geological Survey, West Trenton, NJ, for access to and tours of the sampling site and many helpful discussions, and to Mr. Christian Bethmann, Lebanon State Forest, NJ, for access to the sampling site.

Many people contributed by providing access to equipment, instruments, and instructions on their use, including Harry Hemond (drilling rig), Shiela Frankel (various electonics and optics), and Henry Spliethoff (ICP–AES) of Parsons Lab, Mike Frongillo (environmental SEM) and Joe Adario (XRD) of the MIT Center for Materials Science and Engineering, Steve Rudolph of the MIT Civil Engineering Department (SEM/EDX), Prof. Raymond Siever of the Harvard Earth and Planetary Sciences Department (petrologic microscope), and Larry Poppe of the US Geological Survey (XRD).

Two colleagues in my research group, with whom I often shared lunch and much more, deserve special recognition. John MacFarlane made many important contributions to this work, spanning the range from lab and field assistance to preparation of graphics to golfing advice. deb backhus, even after she went to Minnesota, supported my efforts with discussions, much encouragement, St. Joseph Day cards (March 19), and delivery of the critical thesis–finishing wax at the end. Unfornately, now, "lunch over", but I'm sure we'll share more burritos with each other in the future.

Other members of the Gschwend research group helped with good questions and comments. Many of my fellow students aided me in the lab and field, including Mike Ernst (drilling and electronics) and Jonathan Clapp (drilling). Many others contributed indirectly – by making me laugh, be being good friends. Thanks also to all those who competed as Hydros over the years, especially the team captains and to those who organized events and parties at the lab.

My family has filled my life with love and support throughout these sometimes arduous years at MIT. I especially thank my mother and father, Evelyn and Joe Sr., for instilling in me the value of learning, and my grandfather, Edward C. Smith, for teaching me to do things the right way. I save the final thanks for my wife Martha, who has always understood the demands on my time, has always been interested in my work and achievements, and has loved me in more sweet, supportive ways than I ever could have imagined.

TABLE OF CONTENTS

(continued)

FIGURES

TABLES

Chapter One

INTRODUCTION

I entered upon the small enterprise of "learning" twelve or thirteen hundred miles of the great Mississippi River with the easy confidence of my time of life. If I had really known what I was about to require of my faculties, I should not have had the courage to begin. I supposed that all a pilot had to do was to keep his boat in the river, and I did not consider that that could be much of a trick, since it was so wide.

— Mark Twain, *Life on the Mississippi* (1874).

MOTIVATION

Concern over the genesis of colloids in groundwater has recently escalated as investigators have observed colloid–facilitated transport of radionuclides, metals, and hydrophobic organic compounds through aquifers (Buddemeier and Hunt, 1988, McCarthy and Zachara, 1989; Penrose *et al.*, 1990; Magaritz *et al.*, 1990) and laboratory soil columns (Enfield and Bengtsson, 1988; Torok *et al.*, 1990; Dunnivant *et al.*, 1992, Puls and Powell, 1992). In some cases, the colloidal matter itself is hazardous; for example, viruses and bacteria (Wood and Ehrlich, 1978; Keswick and Gerba, 1980; Keswick *et al.*, 1982; Harvey *et al.*, 1989) and asbestos (Hayward, 1984; Gronow, 1987) are mobile in groundwater. Colloidal material has also been implicated in the movement of precious metals and radionuclides to and away from ore bodies (Horzempa and Helz, 1979; Giblin *et al.*, 1981; Short *et al.*, 1988; Turner–Peterson, 1985; Benedetti and Boulègue, 1991) and in mineral weathering and precipitation (Fritz and Mohr, 1984; Williams and Crerar, 1985).

The distribution and texture of clays may be diagenetically altered by "mechanical" infiltration in sediments (Walker *et al.*, 1978; Owens *et al.*, 1983; Molenaar, 1986; Passaretti and Eslinger, 1987; Matlack *et al.*, 1989; Moraes and De Ros, 1990) and illuviation in soils (Folks and Riecken, 1956; Dijkerman *et al.*, 1967; Bond, 1986). The mobilization and entrapment of colloids in pore throats has led to reductions in formation permeability that hamper enhanced oil recovery efforts (Muecke, 1978; Morris and Shepperd, 1982; Gruesbeck and Collins, 1982; Khilar and Fogler, 1983; Lin, 1985), artificial recharge (Goss *et al.*, 1973; Nightingale and Bianchi, 1977; Brown and Silvey, 1977), water withdrawal from coastal aquifers (Goldenberg *et al.*, 1983; 1984; Goldenberg, 1985), and soil infiltration (Frenkel *et al.*, 1978; Suarez *et al.*, 1984).

Colloid–associated transport of metals and organic compounds depends on

(1) the abundance and nature of colloids present, (2) the association of the low–solubility species with colloids, and (3) the mobility of colloids in aquifers. Sorption of metals and organic compounds to colloidal material is relatively well understood (Sposito, 1984; Karickhoff, 1984). Due to interest in the factors that control wastewater filtration, the transport of colloids through porous media has been modeled accurately in the absence of repulsive forces between colloids and immobile grains (Yao *et al.*, 1971; Rajagopalan and Tien, 1976;); however, when repulsive forces exist, the extent of colloid deposition has been vastly underpredicted (O'Melia, 1990). Knowledge of the nature and abundance of colloids in groundwater, and thus the potential impact of colloid–facilitated transport of contaminants, is still largely scattered and anecdotal. Unfortunately, most of the studies in which colloid–facilitated transport of contaminants has been observed do not address the nature and source of the colloids.

Colloids in groundwater may be operationally defined as inorganic particles and organic macromolecules that remain suspended at groundwater flow rates. Inorganic colloids are generated by precipitation of supersaturated mineral phases and by mobilization of aquifer materials. Precipitated colloidal phases of radionuclides have been observed in laboratory experiments (Giblin *et al.*, 1981; Ho and Miller, 1986). Precipitated hydrous ferric oxide (Langmuir, 1969; Postma and Brockenhuus–Schack, 1987) and ferrous phosphate (Gschwend and Reynolds, 1987) colloids have been observed in groundwater. Mobilization of colloid–sized aquifer materials has been attributed to erosion of secondary minerals in fractures (Buddemeier and Hunt, 1988; Degueldre *et al.*, 1989), mobilization of existing colloids by changes in ionic strength and *p*H (Khilar and Fogler, 1984; Cerda, 1987), and dissolution of cementing minerals (Harris *et al.*, 1987; Ryan and Gschwend, 1990; Gschwend *et al.*, 1990; Ronen *et al.*, 1992). Colloidal organic matter in groundwater includes mainly humic substances, tannins, lignins, and other large

organic molecules generated by the decomposition of organic detritus (Thurman, 1986). Organic colloids may be mobilized by changes in *p*H or ionic strength (McCarthy *et al.*, 1992).

The goal of this study was to examine the geochemical conditions that produced widely varying concentrations of suspended clay particles in groundwater from an iron oxide–coated sand aquifer on the New Jersey Coastal Plain, the Cohansey Sand (Ryan, 1988; Ryan and Gschwend, 1990). The groundwater was collected from two wells located only 60 meters apart, one screened 8 m below the peat layer of a swamp and the other screened 10 m below highly permeable soils in the nearby uplands. The groundwater below the swamp contained ≤ 30 μM dissolved oxygen and about 60 mg L^{-1} colloids, mainly kaolinite fragments. Colloids were essentially absent from the oxic groundwater below the upland terrain. We hypothesized that clay colloids were mobilized by the dissolution of Fe(III) oxide coatings on the quartz grains in the anoxic zone of the aquifer. In contrast, the Fe(III) oxide coatings that persisted in the oxic zones of the aquifer acted as a cementing phase that promoted attachment of the kaolinite colloids to the quartz grains.

Iron oxide–coated sands are common constituents of not only Atlantic Coastal Plain sediments, but potentially of any oxic sediment containing unstable ferrous iron–bearing primary minerals. Some idea of the ubiquity of such sediments can be gleaned from the widespread location of "red beds," sediments colored red by ferric oxides, mainly hematite. Red bed formation has been described in surficial or near–surface sediments currently exposed to arid, tropical, and temperate climates throughout the world (Van Houten, 1973; Pye, 1983).

IRON DIAGENESIS AND CLAY MOBILIZATION

The first major approach to testing the hypothesis that clay transport was controlled by the presence of Fe(III) oxide coatings involved the collection of soil and sediment cores near the groundwater wells to examine distributions of minerals and elements and grain–scale mineral associations (Ryan and Gschwend, 1992; Chapter 2). The cores were subdivided in layers based on color and texture and examined with x–ray diffraction, scanning electron microscopy, energy–dispersive x–ray spectroscopy, thin–section microscopy, physical separations, and chemical extractions of phases.

We anticipated that clay colloid concentration in the pore water would be inversely related to the clay content of the soil and sediment; therefore, variations in the abundance of the clay–sized fraction and surface Fe in the oxidized and reduced soil and sediment layers were examined. We also wanted to determine the role of Fe diagenesis in clay transport, so we investigated the appearance and composition of the Fe–bearing primary minerals and secondary Fe(III) oxides.

The investigation of the sediment cores had potential ramifications for contaminant transport as well as for diagenetic alteration of sediments. Using the organic matter–rich water infiltrating from the swamp as an analog for anoxic leachate from landfills, we intended to show that colloids could be mobilized from iron oxide–coated sands. Furthermore, we wanted to explore commonly–accepted diagenetic interpretations of clay transport in sediments. Generally, clay transport in sediments has been linked exclusively to the vertical infiltration of clay through the unsaturated zone in arid climates (Walker *et al.*, 1978; Matlack *et al.*, 1989; Moraes and De Ros, 1990).

DETACHMENT RATES AND DLVO ENERGY

Experiments testing the effect of changing ionic strength on the rate of clay release from the iron oxide–coated sands revealed that a decrease in the ionic strength accelerated the clay release rate (Chapter 4). When we compared the rate of clay release to DLVO (Derjaguin–Landau–Verwey–Overbeek) detachment energies that represented the generally accepted model of colloid detachment kinetics (Dahneke, 1975; Ruckenstein and Prieve, 1976), a negative correlation was observed. This led us to formulate a new model of colloid detachment kinetics based on the DLVO energy difference between the attached and detached colloids and their rate of diffusion across a hydrodynamic boundary layer (Chapter 3). The new model, dubbed the equilibrium model, produced detachment energies that were positively correlated with the increase in clay release rates with the decrease in ionic strength.

Solution ionic strength, *p*H, electrolyte composition, and other physical–chemical factors that affect colloid and grain surface properties have been related to the kinetics of diffusion–driven colloid release using DLVO interaction potentials as Arrhenius activation energies (Dahneke, 1975; Ruckenstein and Prieve, 1976). According to this "energy barrier" model, a potential energy barrier limits the rate of diffusional transport of colloids from the grain surface to the bulk fluid. Kallay *et al.* (1987) summarized the results of a series of colloid detachment experiments in which a qualitative agreement between the rate of colloid release and the DLVO energy barrier inhibiting detachment was observed (Kolakowski and Matijević, 1979; Kuo and Matijević, 1979; 1980; Kallay and Matijević, 1981; Thompson *et al.*, 1984; Kallay *et al.*, 1986).

The relationship that we observed between the clay release rates and DLVO detachment energy implied that (1) the transport of colloids over the energy barrier

was relatively rapid and (2) the transport of colloids through the diffusion boundary layer to the bulk fluid was the rate–determining step for laminar flow through porous media. To test this "equilibrium" model, we compared the dependence of colloid release rates measured in the model systems summarized in Kallay *et al.* (1987) to the size of the energy barrier and to the equilibrium energy difference. In calculating the DLVO energy for the model systems, we replaced zeta potentials measured in the studies summarized by Kallay *et al.* (1987) with surface potentials estimated with a surface complexation/double layer (SCDL) model to assess the usefulness of zeta potentials.

We were particularly interested in experiments in which the flushing solution ionic strength was varied at constant *p*H. According to our model calculations, a decrease in release rate with increasing ionic strength would suggest that the equilibrium energy difference controlled detachment, while an increase in release rate with increasing ionic strength would suggest that the energy barrier controlled detachment. In most of experiments summarized by Kallay *et al.* (1987) and in field and laboratory observations (Nightingale and Bianchi, 1977; Khilar and Fogler, 1984; McDowell–Boyer, 1992), release rates decrease when ionic strength is increased; however, Kallay *et al.* (1986) observed an increase in release rate when ionic strength was increased in a system of hematite colloids and glass (amorphous SiO_2) grains. To resolve this contradictory evidence, we measured colloid detachment kinetics in a hematite colloid–quartz grain system. We also varied the flow rate in our hematite–quartz system to test the hypothesis that transport of the detached colloids through the diffusion boundary layer was the rate–determining step in colloid release.

SOLUTION CHEMISTRY AND CLAY RELEASE

The second major approach to testing the hypothesis that the infiltration of organic matter–rich water dissolved Fe(III) oxides and released the clay colloids involved laboratory column experiments on clay release from samples of the iron oxide–coated sand (Chapter 4). We wanted to determine whether the mobilization of the clay colloids would require the breaking of strong chemical bonds between the Fe(III) oxide cement and the kaolinite colloids, or the breaking of the weak, electrostatic bonds between colloid surfaces. To test this, we subjected a sample of the oxic sediment to changes in ionic strength, *p*H, and reductant and surfactant concentrations and measured the rates of clay and Fe release. The release rates were compared to Fe(III) oxide dissolution rates and detachment energies to evaluate the relative importance of chemical *vs.* physical binding of colloids.

The detachment energies were chosen to represent two models of colloid detachment kinetics. In the first model, the energy barrier model, the rate–limiting step is the diffusion of colloids over the potential energy barrier near the surface (Dahneke, 1975; Ruckenstein and Prieve, 1976). In the second model, the equilibrium model, colloids are rapidly re–distributed between the primary and secondary minima in potential energy preceding the rate–limiting transport through a diffusion boundary layer separating the grain surface from the bulk fluid (discussed in detail in Chapter 3). Because zeta potential is insensitive to surface potential at high ionic strength and surface charge (Hunter, 1981), we replaced zeta potentials with surface potentials estimated by an empirical relationship between zeta potentials, ionic strength, and surface potentials determined by surface complexation/double layer (SCDL) models for two model oxides (Appendix 2).

SELECTIVE EXTRACTION OF IRON(III) OXIDES

During the examination of the Pine Barrens sediment cores, we tried to selectively extract the surface, or "free," secondary Fe(III) oxide phases to determine the abundance of the Fe(III) oxide cement binding clay colloids (Ryan and Gschwend, 1990; Appendix 1). Initially, we found that hydroxylamine–acetic acid (Chester and Hughes, 1967) and hydroxylamine–citrate (Robbins *et al.*, 1984) were not capable of dissolving the crystalline Fe(III) oxide, goethite, present in the sediments. We turned to the widely–used dithionite-citrate-bicarbonate treatment (Mehra and Jackson, 1960). This combination of reductant, ligand, and buffer, augmented by heating to 80° C, is capable of dissolving crystalline Fe(III) oxides (hematite, goethite). However, the strong reducing capability comes at the expense of diminished selectivity, particularly when sediments contain Fe^{3+}–bearing smectite clays (Rozenson and Heller–Kallai, 1976; Heath and Dymond, 1977; Stucki *et al.*, 1984; Ericsson *et al.*, 1984). Frequently, multiple extractions are necessary to completely remove crystalline Fe oxides from some sediments (Mendelovici *et al.*, 1979), so unintended removal of structural elements may be increased.

In preliminary tests on our samples, multiple dithionite extractions were required to completely remove the free Fe oxides. In some cases, the same amount of Fe was dissolved in each successive extraction, suggesting that Fe from layer silicates and heavy minerals was being dissolved. We suspected that 80° C heating and the high citrate concentration (0.27 M) contributed to non–selective, ligand–promoted dissolution. These concerns led us to develop a new treatment for the extraction of Fe oxides from a technique used to distinguish between extra– and intracellular Fe in marine phytoplankton (Hudson and Morel, 1989). The new treatment uses the ternary complex of titanium(III)-citrate-ethylenediaminetetraacetic acid (in a molar ratio of 1:1:1) reported by Fujiwara *et*

al. (1964) as a reducing agent and HCO_3^- as a *p*H buffer. In the new technique, the free ligand concentration ligand content was lowered and the heating step was eliminated. The two treatments were tested on synthetic Fe(III) oxides, standard clay minerals, and natural sediments from the Pine Barrens.

REFERENCES

Benedetti M. and Boulègue J. (1991) Mechanism of gold transfer and deposition in a supergene environment. *Geochim. Cosmochim. Acta* **55**, 1539–1547.

Bond W.J. (1986) Illuvial band formation in a laboratory column of sand. *Soil Sci. Soc. Amer. J.* **50**, 265–267.

Brown D.L. and Silvey W.D. (1977) Artificial recharge to a freshwater–sensitive brackish–water sand aquifer, Norfolk, Virginia. U.S. Geol. Survey Prof. Paper 939, 53 pp.

Buddemeier R.W. and Hunt J.R. (1988) Transport of colloidal contaminants in groundwater: radionuclide migration at the Nevada Test Site. *Appl. Geochem.* **3**, 535–548.

Cerda C.M. (1987) Mobilization of kaolinite fines in porous media. *Colloids Surfaces* 27, 219–241.

Chester R. and Hughes M.J. (1967) A chemical technique for the separation of ferro–manganese minerals, carbonate minerals and adsorbed trace elements from pelagic sediments. *Chem. Geol.* **2**, 249–262.

Dahneke B. (1975) Kinetic theory of the escape of colloids from surfaces. *J. Colloid Interface Sci.* **50**, 89–107.

Degueldre C., Baeyens B., Goerlich W., Riga J., Verbist J., and Stadelmann P. (1989) Colloids in water from a subsurface fracture in granitic rock, Grimsel Test Site, Switzerland. *Geochim. Cosmochim. Acta* **53**, 603–610.

Dijkerman J.C., Cline M.G., and Olson G.W. (1967) Properties and genesis of textural subsoil lamellae. *Soil Sci.* **104**, 7–16.

Dunnivant F.M., Jardine P.M., Taylor D.L., and McCarthy J.F. (1992) Cotransport of cadmium and hexachorobiphenyl by dissolved organic carbon through columns containing aquifer material. *Environ. Sci. Technol.* **26**, 360–368.

Enfield C.G. and Bengtsson G. (1988) Macromolecular transport of hydrophobic contaminants in aqueous environments. *Ground Water* **26**, 71–79.

Ericsson T., Linares J., and Lotse E. (1984) A Mössbauer study of the effect of dithionite–citrate–bicarbonate treatment on a vermiculite, a smectite, and a soil. *Clay Min.* **19**, 85–91.

Folks H.C. and Riecken F.F. (1956) Physical and chemical properties of some Iowa soil profiles with clay–iron bands. *Soil Sci. Soc. Amer. Proc.* **21**, 575–580.

Frenkel H., Goertzen J.O., and Rhoades J.D. (1978) Effect of clay type and content, exchangeable sodium percentage, and electrolyte concentration on clay dispersion and hydraulic conductivity. *Soil Sci. Soc. Amer. J.* **42**, 32–39.

Fritz S.J. and Mohr D.W. (1984) Chemical alteration in the micro weathering environment within a spheroidally–weathered anorthosite boulder. *Geochim. Cosmochim. Acta* **48**, 2527–2535.

Fujiwara S., Nagashima K., and Codell M. (1964) Mixed chelate compounds of titanium(III) as studied by electron paramagnetic resonance and spectroscopy. *Bull. Chem. Soc. Japan* **37**, 773–779.

Giblin A.M., Batts B.D., and Swaine D.J. (1981) Laboratory simulation of uranium mobility in natural waters. *Geochim. Cosmochim. Acta* **45**, 699–709.

Goldenberg L.C. (1985) Decrease of hydraulic conductivity in sand at the interface between seawater and dilute clay suspensions. *J. Hydrol.* **78**, 183–199.

Goldenberg L.C., Magaritz M., and Mandel S. (1983) Experimental investigation on irreversible changes of hydraulic conductivity on the seawater–freshwater interface in coastal aquifers. *Water Resour. Res.* **19**, 77–85.

Goldenberg L.C., Magaritz M., Amiel A.J., and Mandel S. (1984) Changes in hydraulic conductivity of laboratory sand–clay mixtures caused by a seawater–freshwater interface. *J. Hydrol.* **70**, 329–336.

Goss D.W., Smith S.J., Stewart B.A., and Jones O.R. (1973) Fate of suspended sediment during basin recharge. *Water Resour. Res.* 9, 668–675.

Gronow J.R. (1987) The dissolution of asbestos fibres in water. *Clay Min.* **22**, 21–35.

Gruesbeck C. and Collins R.E. (1982) Entrainment and deposition of fine particles in porous media. *Soc. Petrol. Eng. J.* **22**, 847–856.

Gschwend P.M. and Reynolds M.D. (1987) Monodisperse ferrous phosphate colloids in an anoxic groundwater plume. *J. Contam. Hydrol.* **1**, 307–320.

Gschwend P.M., Backhus D.A., MacFarlane J.K., and Page A.L. (1990) Mobilization of colloids in groundwater due to infiltration of water at a coal ash disposal site. *J. Contam. Hydrol.* **6**, 307–320.

Hayward S.B. (1984) Field monitoring of chrysotile asbestos in California waters. *J. Amer. Water Works Assoc.* **76**, 66–73.

Harris W.G., Carlisle V.W., and Chesser S.L. (1987) Clay mineralogy as related to morphology of Florida soils with sandy epipedons. *Soil Sci. Soc. Amer. J.* **51**, 1673–1677.

Harvey R.W., George L.H., Smith R.L., and LeBlanc D.R. (1989) Transport of microspheres and indigenous bacteria through a sandy aquifer: Results of natural– and forced–gradient tracer experiments. *Environ. Sci. Technol.* **23**, 51–56.

Heath G.R. and Dymond J. (1977) Genesis and transformation of metalliferous sediments from the East Pacific Rise, Bauer Deep and central region northwest Nazca plate. *Geol. Soc. Amer. Bull.* **88**, 723–733.

Ho C.H. and Miller N.H. (1986) Formation of uranium oxide sols in bicarbonate solutions. *J. Colloid Interface Sci.* **113**, 232–240.

Horzempa L.M. and Helz G.R. (1979) Controls on the stability of sulfide sols: colloidal covellite as an example. *Geochim. Cosmochim. Acta* **43**, 1645–1650.

Hudson R.J.M. and Morel F.M.M. (1989) Distinguishing between extra– and intracellular Fe in marine phytoplankton. *Limnol. Oceanogr.* **34**, 1113–1120.

Hunter R.J. (1981) *Zeta Potential in Colloid Science.* Academic Press, p. 209.

Kallay N., Barouch E., and Matijević E. (1987) Diffusional detachment of colloidal particles from solid/solution interfaces. *Adv. Colloid Interface Sci.* **27**, 1–42.

Kallay N., Biškup B., Tomić M., and Matijević E. (1986) Particle adhesion and removal in model systems X. The effect of electrolytes on colloid detachment. *J. Colloid Interface Sci.* 114, 357–362.

Kallay N. and Matijević E. (1981) Particle adhesion and removal in model systems Part 2.– Monodispersed ferric oxide on steel. *J. Colloid Interface Sci.* **83**, 289–300.

Karickhoff S.W. (1984) Organic pollutant sorption in aquatic systems. *J. Hydraul. Eng.* **110**, 707–735.

Keswick B.H. and Gerba C.P. (1980) Viruses in groundwater. *Environ. Sci. Technol.* **14**, 1290–1297.

Keswick B.H., Wang D.–S., and Gerba C.P. (1982) The use of microorganisms as ground–water tracers: A review. *Ground Water* **20**, 142–149.

Khilar K.C. and Fogler H.S. (1983) Water sensitivity of sandstones. *Soc. Petrol. Eng. J.* **23**, 55–64.

Khilar K.C. and Fogler H.S. (1984) The existence of a critical salt concentration for particle release. *J. Colloid Interface Sci.* **101**, 214–224.

Kolakowski J.E. and Matijević E. (1979) Particle adhesion and removal in model systems Part 1.–Monodispersed chromium hydroxide on glass. *J. Chem. Soc. Faraday Trans. I* **75**, 65–78.

Kuo R.J. and Matijević E. (1979) Particle adhesion and removal in model systems Part 2.–Monodispersed chromium hydroxide on steel. *J. Chem. Soc. Faraday Trans. I* **75**, 2014–2026.

Kuo R.J. and Matijević E. (1980) Particle adhesion and removal in model systems Part 3.–Monodispersed ferric oxide on steel. *J. Colloid Interface Sci.* **78**, 407–421.

Langmuir D. (1969) Geochemistry of iron in a coastal–plain groundwater of the Camden, New Jersey area. U.S. Geological Survey Prof. Paper 650–C, C224–C235.

Lin F.–C. (1985) Clay–coating reduction of permeability during oil–sand testing. *Clays Clay Min.* **33**, 76–78.

Magaritz M., Amiel A.J., Ronen D., and Wells M.C. (1990) Distribution of metals in a polluted aquifer: A comparison of aquifer suspended material to fine sediments of the adjacent environment. *J. Contam. Hydrol.* **5**, 333–347.

Matlack K.S., Houseknecht D.W., and Applin K.R. (1989) Emplacement of clay into sand by infiltration. *J. Sediment. Petrol.* **59**, 77–87.

McCarthy J.F., Liang L., Jardine P.M., and Williams T.M. (1992) Mobility of natural organic matter injected into a sandy aquifer. In *Concepts in Manipulation of Groundwater Colloids for Environmental Restoration* (eds. J.F. McCarthy and F.J. Wobber), Lewis Publishers.

McCarthy J.F. and Zachara J.M. (1989) Subsurface transport of contaminants. *Environ. Sci. Technol.* **23**, 496–503.

McDowell–Boyer L.M. (1992) Chemical mobilization of micron–sized colloids in saturated porous media under steady flow conditions. *Environ. Sci. Technol.* **26**, 586–593.

McDowell–Boyer L.M., Hunt J.R., and Sitar N. (1986) Particle transport through porous media. *Water Resour. Res.* 22, 1901–1921.

Mehra O.P. and Jackson M.L. (1960) Fe oxide removal from soils and clays by a dithionite–citrate system buffered with sodium bicarbonate. In *Proceedings of Seventh National Conference on Clays and Clay Minerals* (ed. A. Swineford). Pergamon Press, Washington, DC, 317–327.

Mendelovici E., Yariv Sh., and Villalba R. (1979) Fe–bearing kaolinite in Venezuelan laterites: I. Infrared spectroscopy and chemical dissolution evidence. *Clay Min.* **14**, 323–331.

Molenaar N. (1986) The interrelation between clay infiltration, quartz cementation, and compaction in Lower Givetian terrestrial sandstones, northern Ardennes, Belgium. *J. Sediment. Petrol.* **56**, 359–369.

Moraes M.A.S. and De Ros L.F. (1990) Infiltrated clays in fluvial Jurassic sandstones of Reconcavo Basin, northeastern Brazil. *J. Sediment. Petrol.* **60**, 809–819.

Morris K.A. and Shepperd C.M. (1982) The role of clay minerals in influencing porosity and permeability characteristics in the Bridport Sands of Wytch Farm, Dorset. *Clay Min.* **17**, 41–54.

Muecke T.W. (1979) Formation fines and factors controlling their movement in porous media. *J. Petrol. Technol.* **31**, 144–150

Nightingale H.I. and Bianchi W.C. (1977) Ground–water turbidity resulting from artificial recharge. *Ground Water* **15**, 146–152.

O'Melia C.R. (1990) Kinetics of colloid chemical processes in aquatic systems. In *Aquatic Chemical Kinetics* (ed. W. Stumm), Wiley & Sons, 447–474.

Owens J.P., Hess M.M., Denny C.S., and Dwornik E.J. (1983) Postdepositional alteration of surface and near–surface minerals in selected Coastal Plain formations of the middle Atlantic states. U.S. Geol. Survey Prof. Paper 1067–F, F1–F45.

Passaretti M.L. and Eslinger E.V. (1987) Dissolution and relic textures in framework grains of Holocene sediments from the Brazos River and Gulf Coast of Texas. *J. Sediment. Petrol.* **57**, 94–97.

Penrose W.R., Polzer W.L., Essington E.H., Nelson D.M., and Orlandini K.A. (1990) Mobility of plutonium and americium through a shallow aquifer in a semiarid region. *Environ. Sci. Technol.* **24**, 228–234.

Postma D. and Brockenhuus–Schack B.S. (1987) Diagenesis of iron in proglacial sand deposits of late– and post–Weichselian age. *J. Sediment. Petrol.* **57**, 1040–1053.

Puls R.W. and Powell R.M. (1992) Transport of inorganic colloids through natural aquifer material: implications for contaminant transport. *Environ. Sci. Technol.* **26**, 614–621.

Pye K. (1983) Red beds. In *Chemical Sediments and Geomorphology* (eds. A.S. Goudie and K. Pye), Academic Press, 227–263.

Rajagopalan R. and Tien C. (1976) Trajectory analysis of deep–bed filtration with the sphere–in–cell porous media model. *AIChE J.* **22**, 523–533.

Robbins J.M., Lyle M., and Heath G.R. (1984) A sequential extraction procedure for partitioning elements among co–existing phases in marine sediments. Reference 84–3, College of Oceanography, Oregon State University, Corvallis, OR, 64 pp.

Ronen D., Magaritz M., Weber U., Amiel A., and Klein E. (1992) Characterization of suspended colloids collected in groundwater under natural groundwater flow conditions. *Water Resour. Res.* **28**, 1279–1291.

Rozenson I. and Heller–Kallai L. (1976) Reduction and oxidation of Fe^{3+} in dioctahedral smectites–1: Reduction with hydrazine and dithionite. *Clays Clay Min.* **24**, 271–282.

Ruckenstein E. and Prieve D.C. (1976) Adsorption and desorption of particles and their chromatographic separation. *AIChE J.* **22**, 276–283.

Ryan J.N. (1988) Colloid mobilization in two Atlantic Coastal Plain aquifers: Colloid formation and stability. M.S. thesis, Dept. of Civil Eng., Massachusetts Institute of Technology, 250 pp.

Ryan J.N. and Gschwend P.M. (1990) Colloid mobilization in two Atlantic Coastal Plain aquifers: field studies. *Water Resour. Res.* **26**, 307–322.

Ryan J.N. and Gschwend P.M. (1991) Extraction of iron oxides from soils and sediments using reductive dissolution by titanium(III). *Clays Clay Min.* **39**, 509–518.

Ryan J.N. and Gschwend P.M. (1992) Effect of iron diagenesis on the transport of colloidal clay in an unconfined sand aquifer. *Geochim. Cosmochim. Acta* **56**, 1507–1521.

Short S.A., Lowson R.T., and Ellis J. (1988) $^{234}U/^{238}U$ and $^{230}Th/^{234}U$ activity ratios in the colloidal phases of aquifers in lateritic weathered zones. *Geochim. Cosmochim. Acta* **52**, 2555–2563.

Sposito G. (1984) *The Surface Chemistry of Soils.* Oxford University Press.

Stucki J.W., Golden D.C., and Roth C.B. (1984) Effects of reduction and reoxidation of structural iron on the surface charge and dissolution of dioctahedral smectites. *Clays Clay Min.* **32**, 350–356.

Suarez D.L., Rhoades J.D., Lavado R., and Grieve C.M. (1984) Effect of *p*H on saturated hydraulic conductivity and soil dispersion. *Soil. Sci. Soc. Amer. J.* **48**, 50–55.

Thompson G., Kallay N., and Matijević E. (1984) Particle adhesion and removal in model systems–IX Detachment of rod–like β–FeOOH colloids from steel. *Chem. Eng. Sci.* **39**, 1271–1276.

Thurman E.M. (1986) *Organic Geochemistry of Natural Waters.* Martinus Nijhoff/Dr W. Junk, p. 70.

Torok J., Buckley L.P., and Woods B.L. (1990) The separation of radionuclide migration by solution and particle transport in soil. *J. Contam. Hydrol.* **6**, 185–203.

Turner–Peterson C.E. (1985) Lacustrine–humate model for primary uranium ore deposits, Grants Uranium Region, New Mexico. *Bull. Amer. Assoc. Petrol. Geol.* **69**, 1999–2020.

Van Houten F.B. (1973) Origin of red beds; a review – 1961–1972. *Ann. Rev. Earth Planet. Sci.* **1**, 39–61.

Walker T.R., Waugh B., and Crone A.J. (1978) Diagenesis in first–cycle desert alluvium of Cenozoic age, southwestern United States and northwestern Mexico. *Geol. Soc. Amer. Bull.* **89**, 19–32.

Williams L.A. and Crerar D.A. (1985) Silica diagenesis, II. General mechanisms. *J. Sediment. Petrol.* **55**, 312–321.

Wood W.W. and Ehrlich G.G. (1978) Use of baker's yeast to trace microbial movement in ground water. *Ground Water* **16**, 398–403.

Yao K.–M., Habibian M.T., and O'Melia C.R. (1971) Water and wastewater filtration: concepts and applications. *Environ. Sci. Technol.* **11**, 1105–1112.

Chapter Two

EFFECT OF IRON DIAGENESIS ON THE TRANSPORT OF COLLOIDAL CLAY IN AN UNCONFINED SAND AQUIFER

J.N. Ryan and P.M. Gschwend (1992)
Geochimica et Cosmochimica Acta **56**, 1507–1521

"Could I have some water?" I said to Fred.

"Hell, yes," he said. "That isn't my water. That's God's water. That's God's water. That right, Bill?"

"I *guess* so," said Bill, without looking up. "It's good water, I can tell you that."

— John McPhee, *The Pine Barrens* (1967).

ABSTRACT

The role of Fe diagenesis in the transport of clay colloids was investigated in the Cohansey Sand, an Fe(III) oxide–coated quartz arenite that covers most of the New Jersey Coastal Plain. Based on our past work, we hypothesized that clay had been transported into the sediments, that the clay distribution was controlled by attachment to surface Fe(III) oxides, and that anoxic water infiltrating from a swamp had dissolved Fe(III) oxides and released clay colloids into flowing groundwater.

Sediment cores were collected from upland and swamp terrains and the composition and distribution of the clay–sized and heavy mineral fractions were examined by x–ray diffraction, optical and electron microscopy, separations, and elemental analyses. Throughout the Upland core and below 6.1 m in the Swamp core, oxidized soil and sediment layers contained goethite and > 15 μmol g^{-1} surface Fe (extractable by Ti(III) reduction), but the Swamp reduced soils and sediments lacked goethite and contained < 5 μmol g^{-1} surface Fe. The clay–sized content of the oxidized sediments was roughly double that of the reduced sediments. Electron microscopy revealed that coatings on the quartz grains had the appearance of infiltrated clay particles.

The relationship between clay and surface Fe content indicated that the onset of reducing conditions below the swamp remobilized clay colloids by dissolving Fe(III) oxide cement. Surface Fe(III) oxides were derived from weathering of ilmenite and pseudorutile, Fe–Ti oxides found in the heavy mineral fraction. In the oxidized sediments, Fe was transported from the Fe–Ti oxide grains to quartz surfaces, where it was deposited as surface Fe(III) oxides mixed with kaolinite. Thus, weathering of Fe–bearing minerals and the formation and dissolution of secondary Fe(III) oxides influenced the mobility of clay in the Cohansey Sand.

INTRODUCTION

The transport of radionuclides, metals, and hydrophobic organic compounds through aquifers and laboratory soil columns is enhanced by sorption to mobile colloidal phases (Giblin *et al.*, 1981; Brownawell and Farrington, 1986; Short *et al.*, 1988; Buddemeier and Hunt, 1988; Enfield and Bengtsson, 1988; Penrose *et al.*, 1990; Magaritz *et al.*, 1990). Colloidal material may also be implicated in the mobilization of ore metals (Horzempa and Helz, 1979; Turner–Peterson, 1985). The degree of enhancement or mobilization depends on the abundance and nature of colloids present, the extent of association with colloids, and the transport of colloids through the porous medium. While the sorption of low–solubility species to colloidal phases and the transport of colloids through porous media have been investigated and even quantitatively modeled with some success, only a few researchers have studied the factors that influence the abundance and nature of colloids in groundwater (*e.g.*, Langmuir, 1969; Khilar and Fogler, 1984; Degueldre *et al.*, 1989). With this in mind, we undertook a study of the geochemical conditions that produced widely varying concentrations of suspended clay particles in a sandy surficial aquifer located on the Atlantic Coastal Plain.

Unconfined sandy aquifers composed primarily of Fe(III) oxide–coated quartz are common on the Atlantic Coastal Plain. In past work, we investigated groundwater from a surficial aquifer on the New Jersey Coastal Plain, the Cohansey Sand (Ryan and Gschwend, 1990). The groundwater was collected from two wells located only 60 meters apart, one screened 8 m below the peat layer of a swamp ("Swamp") and the other screened 10 m below highly permeable soils in the nearby uplands ("Upland"). The groundwater below the swamp contained $\leq$ 30 μM dissolved oxygen and 60 mg L^{-1} colloids, mainly kaolinite fragments, but colloids were absent from the oxic groundwater below the upland terrain. We hypothesized

that clay colloids were removed from suspension by Fe(III) oxide coatings on the the quartz grains in the oxic zone of the aquifer. In contrast, clay transport was facilitated below the swamp because Fe(III) oxide coatings were absent in the anoxic zone.

To test the hypothesis that clay transport was controlled by the presence of Fe(III) oxide coatings, we collected soil and sediment cores near the groundwater wells to examine distributions of minerals and elements and grain–scale mineral associations. We assumed that clay abundance in the pore water would be inversely related to the clay content of the soil and sediment; therefore, variations in the abundance of the clay–sized fraction and surface Fe in the oxidized and reduced soil and sediment layers were examined. We also wanted to determine the role of Fe diagenesis in clay transport, so we investigated the appearance and composition of the Fe–bearing primary minerals and secondary Fe(III) oxides.

METHODS AND MATERIALS

Site Description

Two core samples were collected near the head of the McDonalds Branch watershed in Lebanon State Forest, southern New Jersey in August, 1989 (Fig. 2.1). The site is located in a low–relief, pine–dominated region of the New Jersey Coastal Plain known as the Pine Barrens. The cores were taken from two locations (Upland and Swamp) about 50 meters down–gradient from groundwater wells sampled in the previous study (Ryan and Gschwend, 1990) to prevent contamination of the wells.

The surficial aquifer underlying of most of the Pine Barrens is the Late Miocene Cohansey Sand, a poorly–sorted quartz arenite wedge, 0 to 61 m thick, composed of marine sheet sands intercalated with distributary, swamp, and marsh deposits (Carter, 1978). Laminated clays deposited in tidal channels and marshes are usually thin (< 1 m) but laterally extensive, spanning distances of the hundreds of meters (Rhodehamel, 1979a). Overall, however, clay is a minor constituent of the Cohansey (generally less than 5 to 10 percent). Moderate wave energy separated the sediment load by size and density, leaving sand layers relatively clay–free (Carter, 1978). The sand fraction in the Cohansey is made up almost entirely of quartz, usually coated by goethite, $\leq$ 3% heavy mineral grains (85% ilmenite and its weathering products; Markewitz, 1969), and trace amounts of feldspar and muscovite. The clay and silt fractions are dominated by kaolinite, with trace amounts of muscovite, illite, and quartz (Rhodehamel, 1979a).

Deposition of the Cohansey Sand began about 20 million years ago and ended about 5 million years ago when the sea completed its final regression from the New Jersey Coastal Plain (Rhodehamel, 1979a). During the Pleistocene, glaciers lowered sea levels more than 100 meters below the present level, resulting in vigorous and continuous fluvial and aeolian erosion and redeposition of Cohansey sediments.

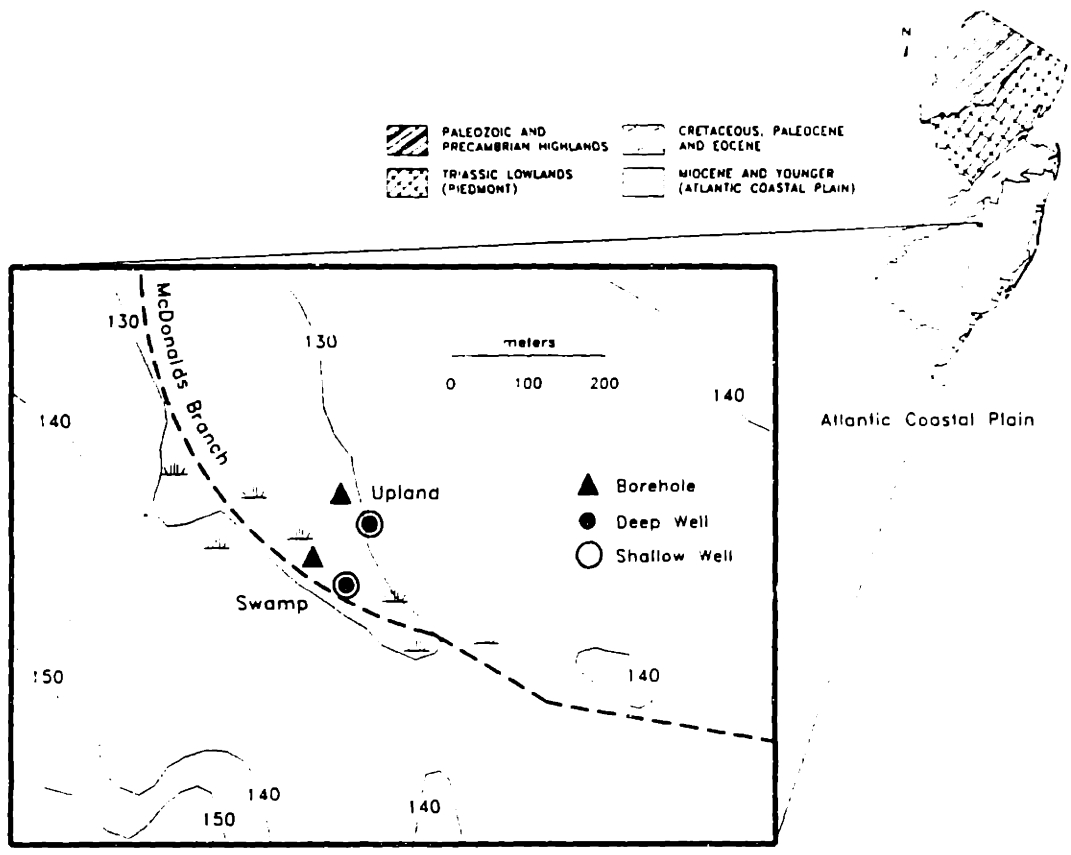

Fig. 2.1. Sampling site showing location of sampling site in relation to the geological provinces of New Jersey (after Olsson, 1963), topography (contours in feet), intermittent stream (McDonalds Branch), boreholes, and wells sampled previously (Ryan and Gschwend, 1990).

During the most recent glaciation (Wisconsin, 100,000 to 10,000 years ago), the Pine Barrens may have resembled present–day northern Greenland, with strong winds blowing off ice sheets over a sandy surface devoid of vegetation (Minard, 1966). Following the Wisconsin, the topography and flora of the region took on its present form. Ecologically, the Pine Barrens can be divided into two distinct systems: (1) uplands, characterized by pine–oak vegetation and well–drained soils; and (2) lowlands, distinguished by cedar and hardwood swamps, *Sphagnum*, and soils made up of muck and peat (Little, 1979).

The groundwater hydrology of the site may be influenced by the strike and dip of a thick (< 1 m), impermeable clay–silt layer below the permeable sands of the unconfined aquifer (Lord *et al.*, 1990). Local groundwater flow directions and gradients were estimated from hydraulic head measurements in the four groundwater wells (Fig. 2.1). Downward hydraulic gradients appear to exist between the shallow and deep Swamp wells (0.17 $m \cdot m^{-1}$) and between the shallow Swamp and deep Upland wells (0.02 $m \cdot m^{-1}$), but not between the shallow and deep Upland wells. The hydraulic head data suggest that the swampy area around McDonalds Branch is a recharge zone despite its location in a topographic depression (if the groundwater sampled by these wells is hydraulically connected).

Field Procedures

The boreholes were drilled without fluids using hollow–stem augers at locations geographically similar to the location of the groundwater wells upstream (Fig. 2.1). The core samples were collected using a 61 cm steel split–tube sampler lined with 3.8 cm inside–diameter clear cellulose acetate butyrate (CAB) tubes. Plastic basket retainers were used to hold the unconsolidated samples in the sampler during withdrawal. The split–tube sampler was driven into the sediment with a 63.5 kg hammer and the CAB tube with the sediments was removed, capped, and

stored upright in a cooler. The sampler was washed and rinsed with distilled water between samples.

The sampler was driven into the undisturbed sediment below the auger. Two samples were taken for every 1.5 m section of auger added to the drill string until we reached wet, unconsolidated sand that entered the auger flight and inhibited sampling of undisturbed sediment. At these points, we measured the distance that running sands penetrated the auger to determine how much of each sample was collected outside the auger. The split–tube sampler retrieved undisturbed samples representing about 71% of the Upland soil and sediment above 5.8 m and about 53% of the Swamp soil and sediment. Below 5.8 m in the Upland core, running sands became so fluid that samples could not be taken below the auger because the auger was filled to heights greater than the length of the split–tube sampler. Consequently, samples from below 5.8 m were retrieved from the auger flights and placed in plastic zipper–lock bags. We stopped drilling when we reached the thick clay–silt layer at depths of about 10 meters below the uplands and 8 meters below the swamp.

Laboratory Procedures

The cores were split and subsampled (based on changes in sediment color and texture) for chemical analyses and preparation of oriented thin sections. Subsamples were collected from core centers to avoid edge smearing and contamination.

Total Fe, Al, and Ti for the sediments were determined by $HF/HCl/HNO_3$ digestion of 0.1 g portions of the samples in teflon–lined bombs at 110° C for 1 h (Lim and Jackson, 1982) and inductively–coupled plasma/atomic emission spectroscopy (ICP/AES). Calibration curves were prepared with blanks and standards made up with the digestion solution. Method precision for triplicate

analyses of two samples was [Fe] ± 8%, [Ti] ± 5%, and [Al] ± 14%.

"Surface" Fe and Al were determined by selective dissolution of the Fe(III) oxide fraction using the Ti(III)–citrate–ethylenediaminetetraacetate (EDTA) ternary complex as the reductant (Ryan and Gschwend, 1991; Appendix 1). The reducing solution was combined with sample portions (0.3 g), sonicated for 5 min, shaken for 10 min, and centrifuged at 26,900 g (maximum) for 1 h. The supernatant was analyzed for Fe and Al by ICP/AES. The extractions were repeated until the amount of Fe removed in the last extraction was < 5% of the cumulative removed. In almost all of the samples, Fe was > 95% removed in the first extraction; however, in three of the samples from the Swamp reduced sediments, more than two extractions were required. The method precision for quintuplicate analyses of three samples was [Fe] ± 3% and [Al] ± 6%. Fe and Al removed by this method are presumed to include organically–bound elements and amorphous and crystalline oxides. Fe and Al left behind are referred to as "structural" Fe and Al and are presumed to reside in aluminosilicates and Fe(II)–bearing oxides.

Organic matter content was determined gravimetrically by loss on ignition. Sample portions (5 to 10 g) were dried at 105° C for 6 h and combusted at 450° C for 6 h and desiccated prior to weighing. Method precision for duplicate analyses of six samples was ± 12%.

Clay–sized (< 2 μm) content was determined by sonication and sedimentation of suspensions of 0.5 g sample portions in 30 mL distilled water. The suspension was sonicated for 10 min in an 80 W sonicating bath and added to a cylinder containing 1 L distilled water. Sonication appeared to adequately dislodge clay– and silt–sized minerals from the sand–sized grains. The turbidity of the < 2 μm suspensions were compared to a turbidity calibration curve made using dilutions of a 500 mg L^{-1} < 2 μm "colloidal kaolin powder" (EM Science, Cherry Hill, NJ) stock solution separated by the same method. Method precision for six

duplicate samples was ± 12%.

Heavy mineral content was determined by suspending 5 to 10 g portions of selected samples in 100 mL of bromoform ($CHBr_3$, specific gravity 2.89) in a separatory funnel. The suspensions were shaken and allowed to settle for 5 min two times, then the heavy minerals were trapped on filter paper. The entire procedure was repeated for the heavy minerals trapped in the first separation. Method precision for four duplicate samples was ± 8%.

Minerals of whole sediments, clay–sized fractions, and heavy mineral fractions were identified by powder X–ray diffraction (XRD) using a Diano XRD–5 diffractometer with Ni–filtered Cu Kα radiation (35 kV, 15 mA, 3° divergence slit, 1° scatter slit, and 0.2 mm receiving slit, 2° 2θ min^{-1} scan rate). Randomly oriented mounts of whole sediment samples were prepared by drying in a desiccator, grinding by mortar and pestle to pass through a 400 mesh (< 37 μm) sieve, and packing into aluminum sample holders. Oriented samples of the < 2 μm clay suspensions were prepared by vacuum–filtering the suspensions through Nuclepore 0.45 μm Ag membrane filters (Poppe and Hathaway, 1979). Identification of clay mineral peaks was aided by glycolation and heating. The heavy minerals were ground to pass through a 400 mesh sieve, suspended in distilled water, and vacuum–filtered onto Ag membrane filters. The raw diffraction patterns were digitized and the 2θ angles were calibrated to the sharp Ag peak at d = 2.044 Å.

Thin sections of oriented samples were prepared by Mineral Optics, Inc. (Wilder, VT) by vacuum–impregnating with epoxy and diamond–polishing selected subsamples. Modal abundances of grain types and pore fillings were determined by 400–point counts per sample. Quartz grain sizes were also determined for 100 grains in each sample. The thin sections were also examined by environmental scanning electron microscopy (ESEM; ElectroScan Inc., Wilmington, MA) at 20 to 30 kV accelerating voltage. Uncoated thin sections were attached to stubs with

carbon tape and placed in a sample chamber under a water vapor atmosphere of 2 to 10 Torr.

Selected whole sediment, thin section, and heavy mineral samples were examined by scanning electron microscopy (SEM) and energy–dispersive X–ray (EDX) spectroscopy with a Cambridge Stereoscan 240 SEM and Link EDX. The heavy mineral samples were suspended in distilled water and sonicated for 10 min to remove particles obscuring surface features. Samples were air–dried, Au–coated, and analyzed in back–scatter and secondary electron mode at an accelerating voltages of 20 and 30 kV. Element profiles across quartz grain coatings were acquired in some samples by series of spot EDX analyses made at intervals in a path across the coating perpendicular to the quartz surfaces. Spot surface and wide–area interior EDX analyses were made in Fe–Ti oxide grains. EDX spectra were acquired at rates of 1,000 to 3,000 counts s^{-1} in 100 s scans and were converted to molar concentrations of Fe, Al, Si, Ti, K, Cl (epoxy), and Au (coating) using built–in x–ray absorption, fluorescence, and atomic number corrections.

RESULTS

Soil and Sediment Description

The Upland and Swamp cores both exhibited well–developed soil zones containing organic detritus, thick sandy layers, and thin ($\leq$ 3 cm), dark, fine–grained layers from the surface to depths of 2.3 m. The sandy layers of the Upland soils appeared light gray to very pale brown (dry sediments, 10YR7/1 to 10YR7/3, Munsell Soil Color Chart). The Swamp soils appeared gray to light brownish gray (10YR6/1 to 10YR6/2). The water table approximately coincided with the bottom of the soil zone in the Upland core and was at the surface in the Swamp. Below the soil zone (> 2.3 m depth), Upland sediments consisted of unconsolidated very pale brown to yellow (10YR7/3 to 10YR7/8) sands. The Swamp sediments also consisted mainly of unconsolidated sands. Swamp sediment color changed distinctly at 6.1 m from white to light gray (5YR8/1 to 5YR7/1) above to yellow to reddish yellow (10YR8/6 to 7.5YR6/6) below. The color boundary did not coincide with any abrupt change in sediment grain size.

Thin section point counting showed that the sediments consisted mainly of subrounded quartz grains (Table 2.1). Other grains identified in minor and trace quantities included opaque and transparent heavy minerals (identified as zircon and augite), feldspar, and mica. The fine–grained matrix fillings and coatings were evenly dispersed throughout the sediments and showed no preferred orientation. They often extended into and blocked the smaller pore spaces between grains. Sediments from the Upland core and those from below 6.1 m in the Swamp core contained slightly more matrix and coating than the Swamp sediments and soils above 6.1 m (13.8±3.8 % *vs.* 9.0±5.2 %). More than 90% of the quartz grains were between 0.25 and 1.0 mm in diameter. The quartz grain size distributions of the samples were quite similar; thus, we interpreted changes in clay and surface Fe

Table 2.1. Results of thin section point counting for selected samples. Headings include quartz (qtz), feldspar and mica (fsp + mica), heavy minerals (hvy min), matrix and coatings (matx + coat) and void space (void).

sample	depth (m)	qtz (%)	fsp+ mica (%)	hvy min (%)	matx+ coat (%)	void (%)
Upland						
U.2.2	0.8–1.5	56.5	0.5	2.2	14.0	26.8
U.3.2	1.7–2.0	57.5	0.8	1.5	16.2	24.0
U.4.3	2.4–2.8	53.5	0.5	1.0	17.0	28.0
U.6.1	3.7–4.1	59.2	0.5	0.5	6.0	33.8
U.8.1*	4.9–5.3	52.8	0.5	0.8	13.0	33.0
Swamp						
S.1.3	0.6–0.9	65.5	0.8	1.5	5.2	27.2
S.3.3	1.6–1.8	57.0	0.8	1.2	19.2	21.8
S.4.1	2.3–2.4	60.2	0.5	0.8	10.5	28.0
S.5.1	2.7–3.3	59.2	0.2	1.2	9.8	29.5
S.7.1	4.3–4.6	52.5	0.5	1.2	6.2	39.5
S.8.1	5.8–6.1	61.5	0.2	2.2	3.2	32.8
S.8.2	6.1–6.3	61.0	0.0	0.2	16.8	22.0

*Sample U.8.1 is not an oriented sample.

content as the result of post–depositional processes.

The white to light gray color of the Swamp soil and sediments above 6.1 m suggested an apparent lack of Fe(III) oxides, so we assumed that water infiltrating through the peat layer below the swamp was organic matter–rich, anoxic, and acidic like the Swamp groundwater sampled 50 m upstream (Ryan and Gschwend, 1990). The pale brown to yellow color of the Upland soil and sediment and the Swamp sediment below 6.1 m suggested that this groundwater was oxic and that Fe(III) oxide formation was promoted. We divided the Upland core into a soil zone above the fine–grained layer (< 2.3 m) and a sediment zone below (> 2.3 m). The Swamp core was divided into soil and sediment zones at 2.3 m and into reduced and

oxidized sediments at the color change at 6.1 m (Fig. 2.2). The oxidized surface layer of organic detritus is not included in the Swamp soil zone. Results are presented as values for the designated zones of the cores as mean values and sample standard deviations (Table 2.2) and for individual layers in depth profiles (Fig. 2.2; Table 2.3). The means and standard deviations are weighted by the thickness of the layer over which each value was obtained (thicknesses given in Table 2.3).

Table 2.2. Mean values and sample standard deviations (weighted by layer thicknesses) of clay, organic matter and total and surface elements in the Upland and Swamp cores.

	Upland		Swamp		
	oxidized soil	oxidized sediment	reduced soil	reduced sediment	oxidized sediment
depth range (m)	0–2.3	2.3–10.4	0–2.3	2.3–6.1	6.1–7.8
clay–sized (wt%)	0.8±0.6	2.6±1.1	2.3±3.2	1.2±0.3	2.6±0.5
goethite/kaol	0.04±0.03	0.06±0.02	0	0	0.10±0.01
surf Fe (μmol g^{-1})	23±14	34±8.3	1.5±1.6	3.0±2.5	42±3.5
surf Al (μmol g^{-1})	5.7±2.7	6.4±1.4	5.6±6.5	3.8±1.0	4.4±0.4
surf Al/Al+Fe	0.21±0.04	0.16±0.02	0.72±0.16	0.61±0.12	0.10±0.00
org matter (wt%)	1.4±2.2	0.2±0.1	5.0±7.2	0.4±0.1	0.2±0.1
total Fe (μmol g^{-1})	70±13	75±12	55±12	47±21	67±5.5
total Ti (μmol g^{-1})	100±23	79±14	120±28	96±43	39±7.8
total Al (μmol g^{-1})	820±210	830±170	690±180	700±49	580±100
struc Fe (μmol g^{-1})	47±12	41±7.4	53±12	44±19	25±6.2
struc Fe/Ti	0.47±0.05	0.52±0.05	0.44±0.02	0.47±0.04	0.66±0.11

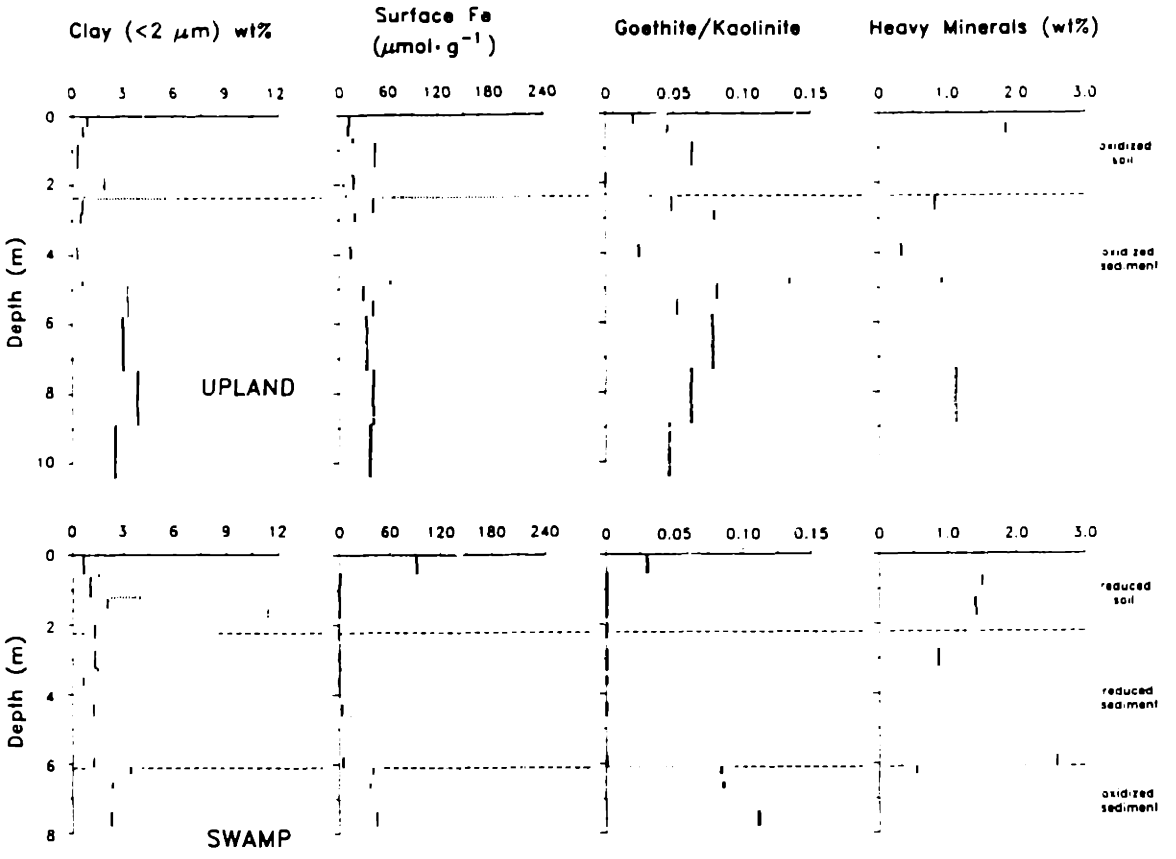

Fig. 2.2. Vertical profiles of element and mineral concentrations in Upland (above) and Swamp (below) cores: clay–sized (< 2 μm) fraction; surface Fe; ratio of goethite d_{110} peak area/kaolinite d_{001} peak area from XRD; and heavy mineral fraction. Layer thicknesses are shown by solid vertical bars for samples taken by split–tube sampler and by open bars for samples taken from auger flights. Horizontal dashed lines show grouping of layers into soil and sediment zones for mean element and mineral contents presented in Table 2.2.

Table 2.3. Element and mineral distributions and derived quantities for individual sample layers.

sample	depth (m)	org matter (wt%)	surf Al	tot Fe	tot Ti	tot Al	struc Fe	struc Fe/Ti	surf Al/(Al+Fe)
			——— μmol g^{-1} ———						
Upland									
U.1.1	0.00–0.30	3.7	3.6	81	150	1100	70	0.48	0.24
U.1.2	0.30–0.61	0.32	2.3	69	110	980	59	0.55	0.18
U.2.1	0.65–0.80	7.3	6.1	61	89	720	46	0.51	0.28
U.2.2	0.80–1.52	0.21	8.9	81	96	590	39	0.41	0.18
U.3.1	1.70–1.73	5.9	5.1	67	100	680	53	0.51	0.27
U.3.2	1.73–1.98	0.14	4.8	53	75	900	37	0.49	0.23
U.3.3	1.98–2.03	0.70	2.2	36	58	1100	32	0.55	0.33
U.3.2	2.03–2.13	0.14	4.8	53	75	900	37	0.49	0.23
U.4.1	2.29–2.34	0.31	1.9	44	80	650	37	0.46	0.21
U.4.2	2.34–2.39	1.3	35	340	78	1100	120	1.54	0.14
U.4.3	2.39–2.79	0.30	9.3	99	120	1200	60	0.49	0.19
U.5.1	2.79–3.05	0.03	3.2	52	71	1000	34	0.49	0.16
U.6.1	3.73–4.11	0.12	2.5	49	67	1000	37	0.55	0.17
U.7.1	4.72–4.88	0.19	8.8	88	41	790	28	0.69	0.13
U.8.1	4.88–5.33	0.22	6.5	67	74	750	40	0.54	0.19
U.9.1	5.33–5.8	0.13	6.1	77	88	870	38	0.43	0.13
U.10.1	5.8–7.3	0.12	6.3	66	74	900	35	0.48	0.17
U.11.1	7.3–8.8	0.45	7.2	77	72	860	48	0.52	0.15
U.12.1	8.8–10.4	0.17	6.1	85	86	590	49	0.58	0.15
Swamp									
S.1.1	0.00–0.53	17	30	150	110	560	57	0.53	0.24
S.1.2	0.53–0.61	1.8	3.6	52	120	480	49	0.40	0.56
S.1.3	0.61–0.91	0.68	1.4	46	98	620	44	0.45	0.47
S.2.1	0.91–1.19	0.18	3.8	50	110	670	49	0.44	0.85
S.2.2	1.19–1.24	0.50	3.8	52	120	730	51	0.41	0.74
S.2.3	1.24–1.52	0.67	3.8	59	150	660	58	0.39	0.72
S.3.2	1.55–1.57	5.3	8.9	71	130	620	57	0.43	0.38
S.3.3	1.57–1.78	1.2	21	81	180	1200	80	0.45	0.94
S.4.1	1.98–2.24	0.46	2.6	44	96	740	43	0.45	0.76
S.4.2	2.24–2.26	2.0	16	55	100	1200	51	0.49	0.81
S.4.1	2.26–2.39	0.46	2.6	44	96	740	43	0.45	0.76
S.5.1	2.74–3.25	0.38	3.4	33	68	670	32	0.47	0.72
S.5.2	3.25–3.33	0.47	3.8	41	78	860	39	0.50	0.66
S.6.1	3.51–3.73	0.16	2.4	28	49	690	27	0.55	0.70
S.7.1	4.27–4.62	0.38	4.4	45	96	670	41	0.43	0.51
S.7.2	4.62–4.65	0.57	8.3	86	150	870	72	0.48	0.37
S.8.1	5.79–6.10	0.29	4.7	86	180	710	80	0.45	0.45
S.8.2	6.10–6.30	0.38	4.0	59	26	750	20	0.79	0.09
S.9.1	6.55–6.71	0.14	4.1	75	48	560	37	0.78	0.10
S.10.1	7.37–7.80	0.13	4.8	68	41	500	23	0.56	0.10

Clay–Sized and Heavy Mineral Fractions Distribution and Composition

The clay–sized fractions contained mainly kaolinite, minor amounts of goethite and quartz, and trace amounts of muscovite. Ferrihydrite ($5Fe_2O_3 \cdot 9H_2O$), gibbsite ($Al(OH)_3$), and other Fe and Al oxide phases were not detected. Goethite (relative abundance represented by peak area ratio of goethite d_{110}/kaolinite d_{001}) was present in most layers of the Upland core, but absent from most layers of the Swamp core above 6.1 m. Only the major goethite peak (d_{110} = 4.18 Å) was detectable in the clay–sized fraction. The d_{110} peak was broad and shifted to slightly smaller *d*–spacings (as low as 4.16 Å) in some samples, most noticeably in the Upland soils and sediments.

The deeper Upland sediments and Swamp oxidized sediments contained about two to three times as much clay–sized material as the Swamp reduced sediments. Clay–sized materials were about three times more abundant in the deeper Upland sediments than in the Upland soils, but Swamp soils contained about twice as much clay–sized material as Swamp reduced sediments.

Organic matter was much more abundant in the Swamp core, especially in the soil zone. The organic matter content of both cores generally decreased with depth. Organic matter and clay contents were high in the thin layers separating the soil and sediment zones, suggesting that these constituents were eluviated from the soil by infiltrating water and deposited in these layers.

The heavy mineral suite separated from five Upland and six Swamp layers consisted mainly of 50 to 200 μm subangular to rounded grains. Heavy mineral contents measured in these samples varied considerably with depth in both cores. Bromoform separations gave heavy mineral contents in the same range as those determined by point counting for different samples. XRD indicated that the heavy minerals are mainly pseudorutile, with minor amounts of ilmenite, rutile, zircon, and quartz, and trace amounts of augite. The presence of quartz was an artifact

related to incomplete separation.

Soil and Sediment Elemental Composition

Surface Fe was much more abundant in the oxidized soils and sediments than in the reduced soils and sediments with the exception of the surface layer in the swamp, which contained the highest surface Fe content (Fig. 2.2). We suspect that Fe^{2+} diffusing up from the reduced soils was oxidized because dissolved O_2 is present. Fe^{2+} oxidation may have been accelerated by microbial action, as in the case of bog iron formation (Crerar *et al.*, 1979). Soils and sediments with high surface Fe were colored shades of yellow (corresponding to oxidized zones), while those with low surface Fe ($\leq$ 5 μmol g^{-1}) were generally white to light gray (corresponding to reduced zones). Surface Fe and goethite abundance are correlated in both cores (R^2 = 0.70, n = 17, Upland; R^2 = 0.64, n = 20, Swamp). Other less crystalline Fe(III) oxides in the sediments, such as ferrihydrite, may also constitute a portion of the surface Fe.

The amount of surface Fe may have been overestimated by extraction of Fe from the Fe–Ti oxides in the heavy mineral fractions, particularly in the Swamp soils and reduced sediments where goethite was not detected by XRD. Generally, for samples with high surface Fe content and goethite abundance, Fe removed from the heavy minerals probably constituted < 2% of surface Fe, but for samples with low surface Fe and high heavy mineral contents (especially the reduced sediments in the Swamp core), the heavy mineral contribution to surface Fe may be as much as 60% of the surface Fe measured (Ryan and Gschwend, 1991). Fe(III) in pseudorutile may be particularly susceptible to dissolution by the reducing solution.

Surface Al was > 95% removed in the first extraction of all of the Upland and Swamp samples containing goethite. For samples that did not contain goethite, the amount of Al extracted did not significantly decrease with succeeding

extractions, suggesting that Al was dissolved mainly from aluminosilicate minerals. High surface Al and Fe contents coincided with high organic matter in some thin soil layers in which goethite was not detected. In these cases, Al and Fe may have been associated with organic matter and removed by the selective extractions.

Total Fe was divided into two fractions, surface Fe and structural Fe, where structural Fe is the difference between total and surface Fe. The structural Fe estimates were used to represent the amount of Fe in the Fe–Ti oxides of the heavy mineral fraction because structural Fe correlated far better with the heavy mineral content ($R^2 = 0.53$, $n = 11$) than with other possible sources of Fe–bearing primary minerals (clay– and silt–sized fractions). We assumed that total Ti represented the amount of Ti in the Fe–Ti oxides because total Ti also correlated with heavy mineral content ($R^2 = 0.63$, $n = 11$). Thus, the ratio of structural Fe/total Ti (struc Fe/Ti) was considered to be a gauge of the overall composition of the ilmenite–pseudorutile–rutile suite that dominated the heavy mineral fraction. Corrections for the overestimation of surface Fe by dissolution of Fe–Ti oxides did not significantly change the structural Fe/Ti ratios in the samples for which heavy mineral content was measured. Subtle differences in structural Fe/Ti may be discerned between the oxidized and reduced sediments and between the soils and sediments in both cores, but the magnitude of the differences is similar to that of the uncertainties in the ratios.

Total Al was roughly 50 to 200 times as abundant as surface Al and was not correlated with surface Al, clay–sized, or heavy mineral content. Total Al concentrations matched the expected contributions of Al from feldspar, mica, kaolinite, and the heavy mineral fraction if we assumed that the portion of the coating and matrix volume determined by point counting in excess of the estimated volume of the clay–sized fraction (Table 2.1) was composed of aluminosilicates (kaolinite or muscovite).

Scanning Electron Microscopy and Energy–Dispersive X–Ray Spectroscopy

SEM examination of disoriented sediments showed that the quartz grain surfaces in the Upland soil and sediments and the Swamp oxidized sediments were extensively covered by clay plates in the < 5 μm size range. Occasionally, bridges between grains were preserved despite the disoriented nature of the samples (Fig. 2.3a). In the Swamp soil and reduced sediments, grain surfaces were relatively free of coatings (Fig. 2.3b).

ESEM analysis of the uncoated thin sections revealed details regarding the nature of the coatings on quartz grain surfaces. We concentrated on the Swamp sediments at the redox boundary at 6.1 meters depth. In the Swamp oxidized sediment (S.8.2), pore spaces between quartz grains were commonly filled with fine–grained, densely–packed material. In addition to matrix buildup in constricted pore spaces, grains were coated on surfaces exposed to open pore spaces (Fig. 2.4a). The coatings and matrix fillings did not show any preferential arrangement. The thickness of the coatings in the open pores varied from zero to 10 μm thick, and in the constricted pores, the matrix fillings spanned thicknesses up to 100 μm. The grain coatings adjacent to the large pore spaces appeared to be composed of clay plates in the ≤ 1 μm size range (Fig. 2.4b). In contrast, the Swamp reduced sediment (S.8.1) showed accumulation of clay in some restricted pore spaces (Fig. 2.4c), but open pores were predominantly free of coatings. The fine–grained material collected in the restricted pore spaces consisted mainly of elongated, fibrous minerals loosely jumbled on the quartz surface (Fig. 2.4d).

Element profiles across quartz grain coatings acquired by EDX (Fig. 2.5) revealed that coatings in the oxidized sediments (U.8.1 and S.8.2) contained far more Fe than those in the reduced sediment (S.8.1). Fe/Si ratios vary widely in the coatings, but the minimum Fe/Si in the oxidized sediments was still about four times greater than the maximum Fe/Si detected in the reduced sediment. If the

2 to 50 mole% Fe (where Fe concentration is reported as molar percentage of Fe relative to the total content of Fe, Al, Si, Ti, K, and Cl, but not O) was present entirely as goethite and Al and Si are present as kaolinite, then goethite may constitute 1.4 to 58 wt% of the coatings. The ratio of Al/Si ranged from 0.1 to 0.9 in the coatings, gradually reaching a plateau at approximately 0.8 at distances of 2 to 3 μm from the quartz grain surface. Low Al/Si ratios recorded at the quartz–coating interface probably reflect the averaging of Al and Si contents of quartz and kaolinite in the volume penetrated by the electron beam.

SEM/EDX analysis of the heavy minerals revealed primarily Fe– and Ti–rich mineral grains tentatively identified as pseudorutile, ilmenite, and rutile (based on Fe/Ti_{edx}), as well as trace amounts of grains that contained Mg, Al, Si, and Ca. The trace minerals may have included augite and sphene ($CaTiSiO_5$). Fe–Ti oxide grains with Fe/Ti_{edx} ratios closest to the ideal ratio of pseudorutile, Fe/Ti = 0.67, were most abundant in the samples. Rutile grains ($Fe/Ti_{edx} \leq 0.1$) were larger and more rounded than the pseudorutile grains. The surfaces of pseudorutile grains in each of the soil and sediment samples showed signs of advanced weathering in the form of etch pits, cracks, and generally degraded surfaces. EDX profiles across Fe–Ti oxide grains showed that surfaces were depleted in Fe relative to Ti compared to interiors (surface Fe/Ti_{edx} = 0.33 to 0.49; interior Fe/Ti_{edx} = 0.47 to 0.76). The difference between surface and interior Fe/Ti_{edx} was greater in the oxidized sediments (S.8.2, U.8.1). The structural Fe/Ti ratios estimated for these samples fell between the surface and interior Fe/Ti_{edx} ratios, indicating that the structural Fe/Ti ratio determined by chemical means provided an accurate overall Fe/Ti ratio reflecting mainly structural Fe and Ti in the Fe–Ti oxides in the heavy mineral fraction.

Figure 2.3 is shown on the following page.

Fig. 2.3. SEM photographs of quartz grain surfaces in Swamp oxidized sediment (sample S.8.2) and Swamp reduced sediment (sample S.8.1). Scale bars show dimension.
(a) sample S.8.2: kaolinite particles completely coating quartz surfaces and bridging distance between grains (left); kaolinite packed into the bridge in a manner characteristic of colloidally transported clay (right; 8× zoom of bright region at left).
(b) sample S.8.1: quartz surface relatively free of kaolinite particles; the few kaolinite particles attached are located in protected cracks and corners of the angular quartz grains. Numbers refer to EDX spectra not shown.

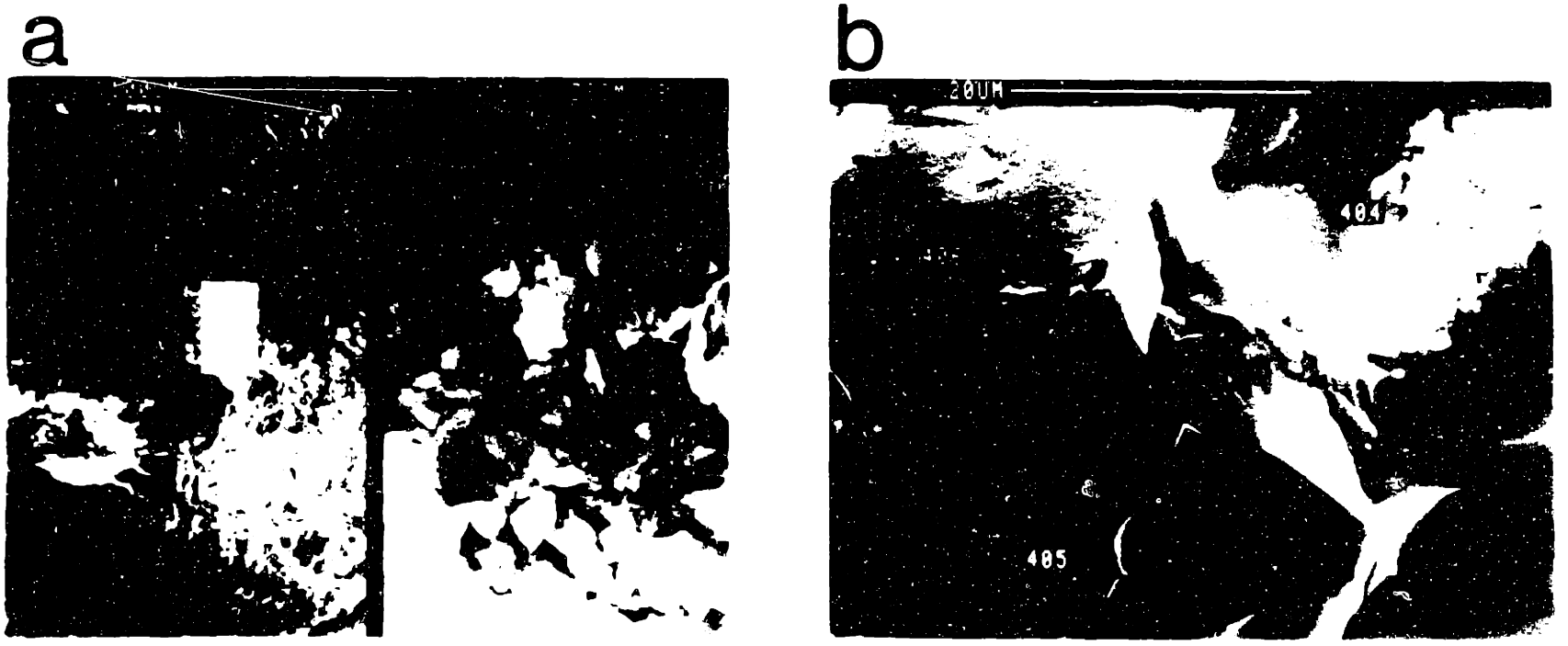
a
b
20UM
404
405

Figure 2.4 is shown on the following page.

Fig. 2.4. Environmental SEM photographs of polished, oriented thin sections of oxidized sediment (sample S.8.2) and reduced sediment (sample S.8.1) from the Swamp core. Photographs arranged properly with respect to the orientation of the sediments in the cores. Scale bars show dimension.
Sample S.8.2:
(a) coatings in open pores and matrix fillings between quartz grains.
(b) coating composed of particles resembling clay plates in enlargement of enclosed area in (a).
Sample S.8.1:
(c) retention of clay particles in restricted pore space between quartz grains. Open pore surfaces, more exposed to groundwater flow, are uncoated.
(d) coatings contain loosely packed, larger, elongated clay particles in enlargement of of enclosed area in (c).

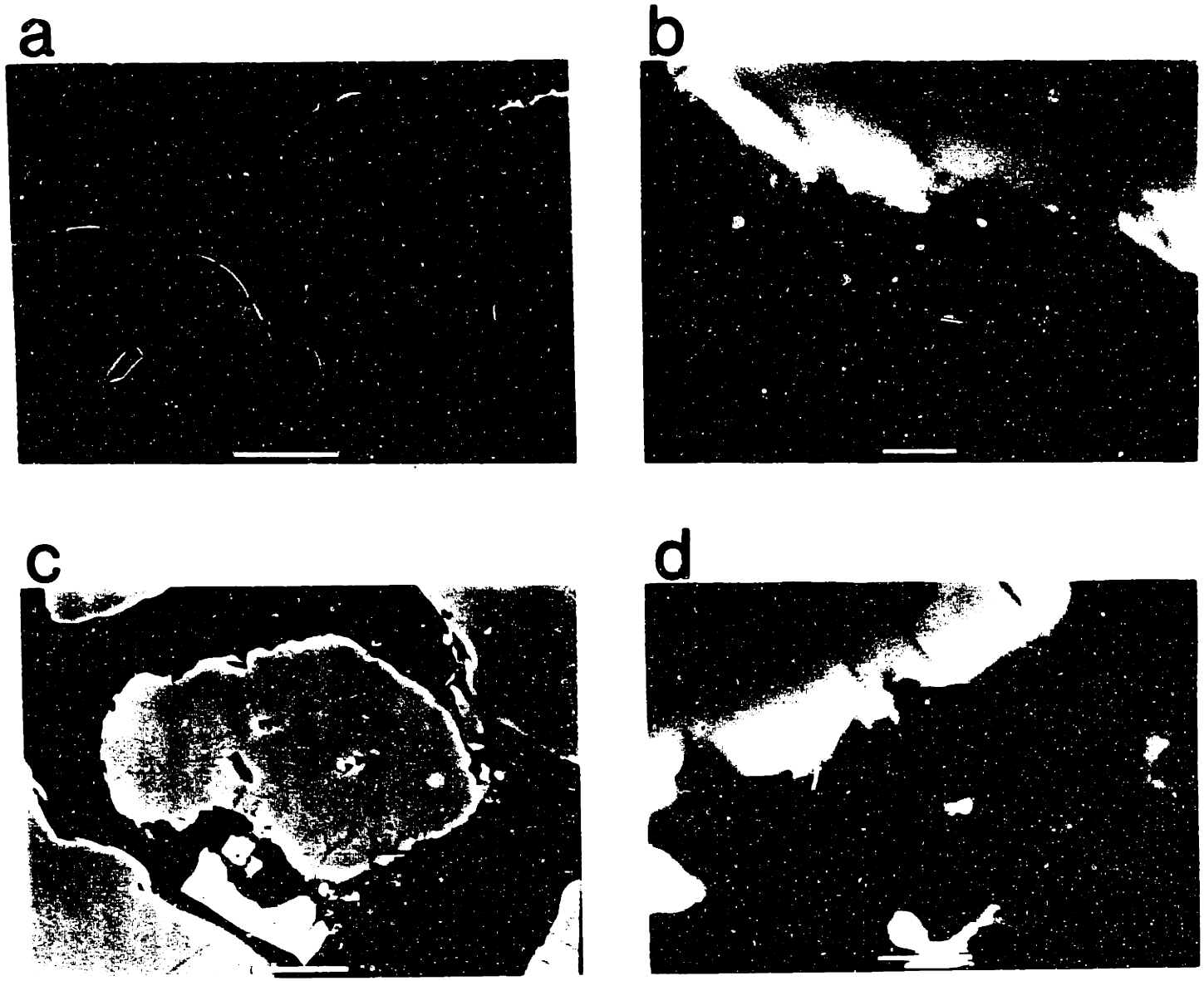
a
b
c
d

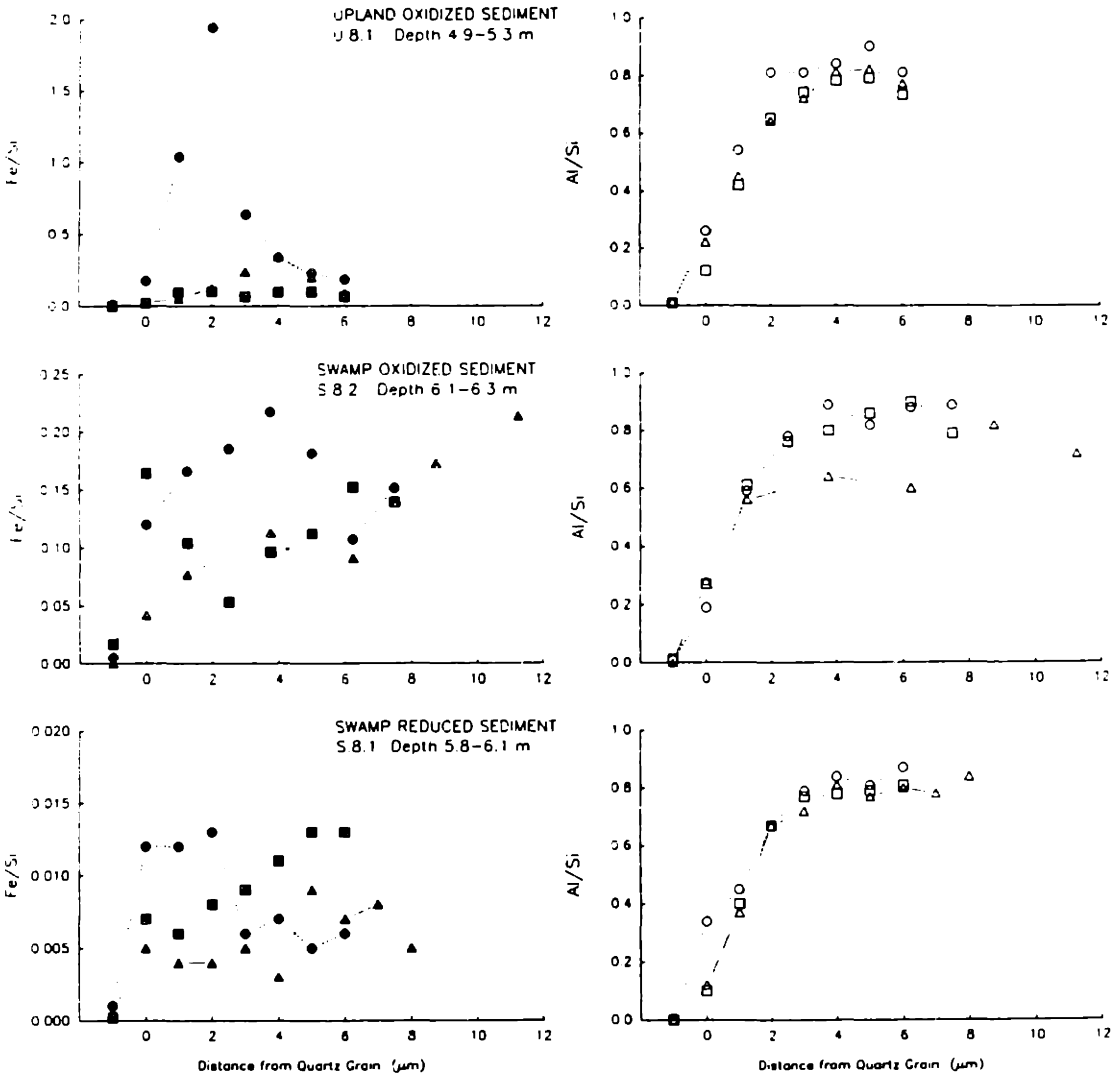

Fig. 2.5. Element profiles across kaolinite–Fe(III) oxide coatings on quartz grains in Upland oxidized sediment (U.8.1), Swamp oxidized sediment (S.8.2), and Swamp reduced sediment (S.8.1) obtained by spot EDX analyses in Au–coated thin sections. Note that the Fe/Si axis for the Swamp reduced sediment covers a much smaller range. Connected data points represent profiles across three different grain coatings in each sample. Note that the Fe/Si axis for the Swamp reduced sediment covers a much smaller range.

DISCUSSION

Evidence of Colloidal Clay Transport

Two lines of evidence support our contention that clay colloids have been and, under some conditions, still are transported by groundwater flow in the Cohansey Sand. First, clay appears to have been delivered into the sand layers of the Cohansey after deposition. Second, suspended clay can currently be found in zones of anoxic groundwater (Ryan and Gschwend, 1990).

The anisopachous, mineralogically heterogeneous coatings of randomly–oriented kaolinite and Fe(III) oxides particles appear to have been formed by accumulation of kaolinite particles from flowing groundwater, based on criteria applied by Matlack *et al.* (1989) and Moraes and De Ros (1990). Interbedded clay–silt laminations, from which infiltrating water may have eluviated kaolinite particles into underlying sand layers, are likely sources of clay. The overlying source of clay for these sediments may have been removed by erosion. Detrital or authigenic origins of kaolinite particles in the Cohansey Sands are unlikely. The wave– and wind–winnowed sand sheets of the Cohansey Sand were deposited relatively free of detrital clay–sized particles (Carter, 1978). Sources of authigenic clay, primarily feldspars, are scarce in the Cohansey because very little feldspar was deposited in the Cohansey Sand (Rhodehamel, 1979a). Furthermore, kaolinite coatings are evenly distributed throughout the sediments and not concentrated near aluminosilicate parent grains.

Clay observed in the Cohansey Sand has been attributed to vertical transport in the unsaturated zone ("illuviation" or "mechanical infiltration"). Owens *et al.* (1983) found halloysite in upper layers of the Cohansey only in locations where it was overlain by the Late Miocene Bridgeton Formation, in which halloysite is common. Infiltrated clay has also been observed in halos that mark the former

menisci of perched water above small, impermeable clay lenses (W.L. Newell, U.S.G.S., Reston, VA, personal communication, 1991). In contrast, the mobilization of kaolinite colloids in the anoxic groundwater below the swamp suggests that kaolinite is being transported in the saturated zone as well as in the unsaturated zone.

In the saturated zone, colloids are operationally defined as particles that remain suspended and are mobile at groundwater flow rates. The mobility of colloids is controlled by the frequency of colloid collisions with grains and the probability of attachment to grain surfaces following collisions. Collision frequency depends on particle size and flow velocity. At typical groundwater velocities, collisions of particles < 0.1 μm are mainly caused by Brownian diffusion; for particles > 1 μm, collisions are caused primarily by sedimentation (Yao *et al.*, 1971). Particles in the 0.1 to 1 μm size range experience the fewest collisions. Kaolinite colloids observed in the Swamp groundwater (Ryan and Gschwend, 1990) and kaolinite particles attached to quartz grains are generally in the < 2 μm size range, so the expected collision frequency of these particles is relatively low. We estimate that a particle of 0.5 μm diameter experiences only one collision for every five grains passed, using a groundwater velocity of 10^{-4} cm s^{-1}, temperature of 15° C, average grain diameter of 250 μm, and particle thickness of 50 nm in the analytical equations developed by Yao *et al.* (1971).

The probability of an attachment of a colloid to a grain following a collision is controlled by attractive and repulsive forces acting between the colloid and grain surfaces. We estimated the total potential energy of interaction between colloid and grain as the sum of Born repulsion, van der Waals attraction, and electrostatic repulsion between spherical colloid and grain as a function of distance. Born repulsion was calculated using the expression derived by Ruckenstein and Prieve (1976) with a collision diameter $\sigma = 8$ Å, colloid radius of 0.4 μm, and grain radius

of 250 μm. The van der Waals energy was calculated using the expression derived by Verwey and Overbeek (1948) with the Hamaker constant $A = 1.7 \cdot 10^{-20}$ J (Hough and White, 1980) and kaolinite plate thickness of 50 nm. Electrostatic repulsion was calculated using the expression derived by Hogg *et al.* (1966) with ionic strength of 260 μM, kaolinite surface potential of –0.11 V determined by electrophoretic mobility (Ryan and Gschwend, 1990), and quartz surface potential estimated at –0.20 V from electrophoretic mobility data of Kia *et al.* (1987) at *p*H 4.6. With these assumptions and parameter values, we estimated that an energy barrier of 55 **k**T (where **k** is the Boltzmann constant and T is absolute temperature) inhibits the attachment of kaolinite colloids to quartz grains in the Swamp groundwater. The magnitude of this energy barrier corresponds to very low attachment probability. With low collision frequency and low attachment probability, the observed mobility of kaolinite colloids in the Swamp groundwater (*p*H = 4.5) seems likely.

Role of Fe(III) Oxides in Clay Transport

The energy barrier inhibiting attachment of kaolinite to quartz is estimated to be larger (78 **k**T) in the oxic Upland groundwater (*p*H = 4.8) because surface potentials are higher, but colloids are essentially absent in the water (Ryan and Gschwend, 1990). We hypothesized that the barrier to attachment had been removed by the accumulation of Fe(III) oxides on the quartz surfaces because (1) Fe(III) oxides are positively charged at the groundwater *p*H ($pH_{zpc} \cong 7.0$ to 8.5; Parks, 1967) and (2) silica surface charge can be reversed from negative to positive by adsorption of metal ions (James and Healy, 1972). We expected that correlations between clay and surface Fe contents would illustrate the role of Fe(III) oxides in the attachment of kaolinite colloids.

The relationship between the surface Fe and clay content of the sediment layers highlights three groups of sediments (Fig. 2.6): (1) high surface Fe and clay in the deeper oxidized sediments in both cores, (2) low surface Fe and clay in the reduced sediments, and (3) high surface Fe and low clay in the oxidized sediments just below the soil zone in the Upland core. If the four Upland sediment layers of the third group are dismissed on the basis that soil zone processes diminished the supply of clay to these layers, surface Fe and clay content are correlated ($R^2 = 0.74$, $n = 15$). However, clay content remained substantial even when surface Fe content was very low. The residual clay content (about 1.0 wt%) may represent kaolinite released by Fe(III) oxide dissolution and trapped in restricted pore spaces (Fig. 2.5). Alternatively, small amounts of Fe(III) oxides may remain in the restricted pores cementing the residual kaolinite particles.

The removal of suspended kaolinite by goethite coatings must require a continuous supply of Fe to maintain the positive surface charge of the framework grains. Without constant Fe supply, the attachment of a kaolinite layer would result in a return to repulsive interactions between colloid and grain surfaces as colloids encountered a colloid–coated grain (42 kT energy barrier at *p*H 4.8). EDX analyses showed that Fe is distributed throughout the coatings (Fig. 2.5), suggesting that Fe has been continually supplied to grain surfaces. The source of the Fe is the slow, ongoing dissolution of the Fe–Ti oxides, ilmenite and pseudorutile.

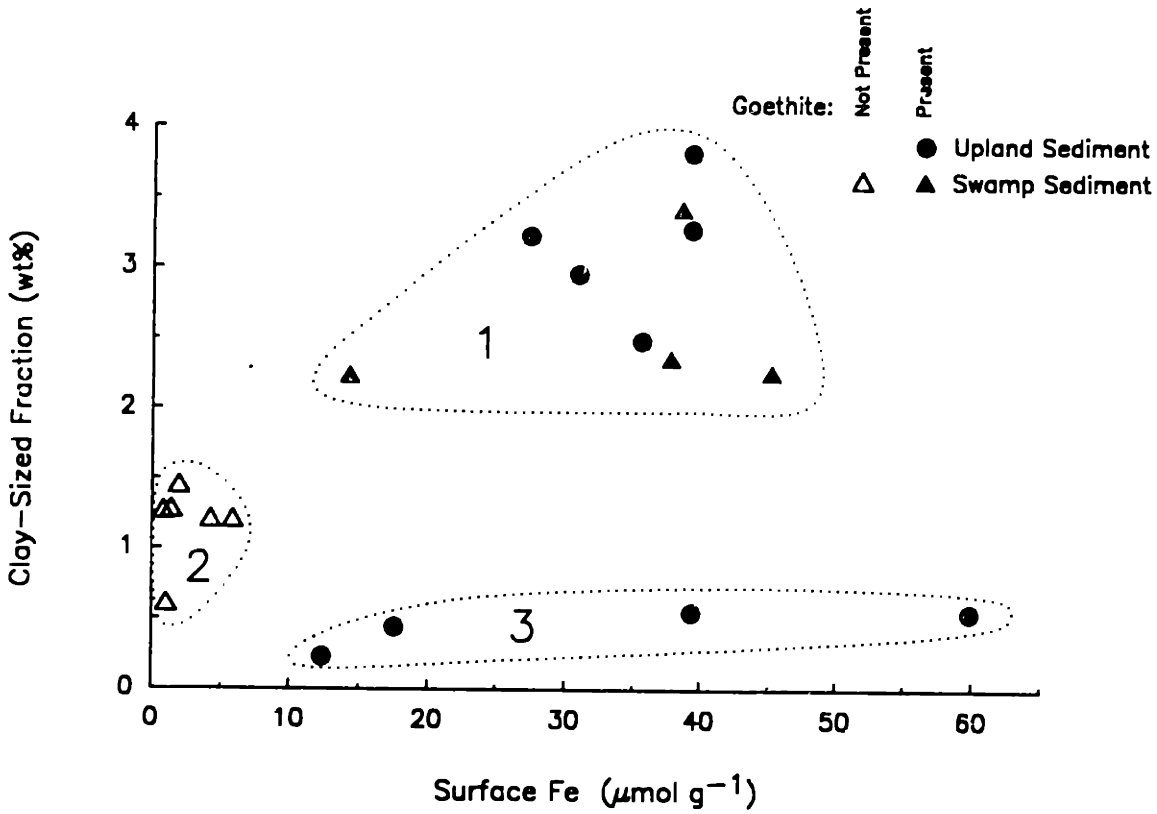

Fig. 2.6. Relationship of clay–sized content to surface Fe content for Upland and Swamp sediments. Sediment layers containing goethite marked by filled symbols. Enclosed areas represent (1) high surface Fe/high clay layers from oxidized sediments in both cores, (2) low surface Fe/low clay layers from reduced sediments in Swamp core, and (3) high surface Fe/low clay layers from oxidized sediments just below soil zone in Upland core.

Release of Iron from Fe–Ti Oxides

The major Fe–bearing primary minerals in the Cohansey sediments are pseudorutile ($Fe_2O_3 \cdot 3TiO_2$) and ilmenite ($FeO \cdot TiO_2$). The XRD results, structural Fe/Ti, and Fe/Ti_{edx} indicate that most of the ilmenite has been converted to pseudorutile, releasing Fe^{3+} to solution. Pseudorutile is formed only as an intermediate weathering product of ilmenite under oxidizing conditions (Teufer and Temple, 1966). Ilmenite alteration to pseudorutile is slow (Temple, 1966) because it involves the solid–state oxidation of Fe(II) in ilmenite and diffusion of one–third of the resulting Fe(III) out of the structure to maintain charge balance:

$$3\ FeO \cdot TiO_2 \longrightarrow Fe_2O_3 \cdot 3TiO_2 + Fe^{3+} + 3e^-.$$

The Cohansey sediments were probably oxidized following subaerial exposure about 5 million years ago (Rhodehamel, 1979a). It is unlikely that much Fe was released from ilmenite prior to the onset of oxidizing conditions in the sediments. Ilmenite is congruently dissolved under acidic, reducing conditions, producing Fe^{2+} and authigenic TiO_2 (Temple, 1966; Grey and Reid, 1975), but we did not find any authigenic TiO_2 in these sediments. The pore waters of the Cohansey sediments were probably reducing and alkaline during the 15 million years that the sediments were submerged. Thus, most of the Fe released in the Cohansey sediments has come from the alteration of ilmenite to pseudorutile over the past 5 million years. Minor amounts of Fe may also have been derived from the complete dissolution of Fe–bearing silicates (amphiboles, pyroxenes) and aluminosilicates (augite) that are no longer present in the sediments, but these minerals were apparently never present in significant amounts in the initial deposits (Markewitz, 1969; Rhodehamel, 1979a)

The structural Fe/Ti and Fe/Ti_{edx} in the soils and reduced sediment are slightly lower than those in the oxidized sediments, suggesting that acidic, reducing conditions that developed in the soils and below the swamp perhaps as recently as

10,000 years ago probably promoted the removal of Fe(III) from pseudorutile surfaces following adsorption of reduced species and protons. Signs of more advanced weathering in the reduced sediments and soils were not evident in SEM examination of the pseudorutile grain surfaces.

Iron Mobility in the Sediments

The fate of Fe released by the weathering of Fe–Ti oxides in the Cohansey Sand depends on the redox potential, *p*H, and complexing ligand concentration of the pore water. To determine whether Fe released from Fe–bearing primary minerals was deposited as secondary Fe(III) oxides in the same layer or transported away from the layer as dissolved Fe, we estimated the amounts of Fe deposited and released in each layer. Fe deposited was estimated using the surface Fe measurements. Fe released was estimated by assuming that (1) Fe originates entirely from the weathering of Fe–Ti oxides, (2) the Fe–Ti oxides were originally deposited as ilmenite, and (3) Ti is conserved in the parent grains during weathering of Fe–Ti oxides. Thus, the amount of Fe released by weathering is the difference between total Ti and structural Fe.

These calculations suggest that Fe released from the Fe–Ti oxides in the Swamp soil and reduced sediments was removed by groundwater flow (Fig. 2.7). Fe released in acidic, reduced sediments is most likely present as soluble Fe^{2+} species, resulting in loss of Fe from the soil or sediment (Anand and Gilkes, 1984; Morad and Aldahan, 1986). Fe in excess of intrastratal supply may have been deposited in the oxidized layers below 6.1 m by infiltrating water. Fe deposited in the surface soil layer of the Swamp core may be delivered by diffusion of dissolved Fe from the reduced soil layers below.

In the Upland core, Fe is removed from the soil zone and deposited in the thin layer at 2.3 m depth. In the upper sediments, Fe may have also been

redistributed downward between the 2.3 and 4.9 m. Below 4.9 m, Fe release and deposition are nearly balanced. However, even in the oxidized sediment layers in which Fe released and Fe deposited were roughly balanced, Fe^{3+} released by Fe–Ti oxide weathering was transported over at least pore–scale distances. Quartz grains were ubiquitously coated by kaolinite–Fe(III) oxide mixtures without regard to proximity to Fe–Ti oxides grains. The pore–scale transport of Fe in oxidized sediments implies that Fe^{3+} temporarily formed soluble complexes or colloidal Fe(III) oxides stabilized by organic coatings. Organic acid components of the dissolved organic matter (present at 4 mM C; Ryan and Gschwend, 1990) may have been the most important complexing ligands for complexing Fe^{3+}. Crerar *et al.* (1981) determined that most of the dissolved Fe in Pine Barrens groundwater was associated with dissolved organic matter. Colloidal Fe(III) oxides have also been observed in Pine Barrens groundwater (Langmuir, 1969).

Formation of Surface Fe(III) Oxides

Weathered ilmenite in oxidized sediments is frequently replaced by hematite and rutile (Grey and Reid, 1975), suggesting that rapid hydrolysis of Fe and Ti led to epitactic precipitation of Fe and Ti oxides. Instead of epitactic precipitation of hematite in oxidized sediments, we observed that Fe was transported away from the Fe–Ti oxides and spread uniformly throughout the sediments. The transport of Fe^{3+} away from the parent Fe–Ti oxides implies that Fe^{3+} activity was not sufficiently high to precipitate Fe(III) oxides on the parent Fe–Ti oxides. Because Fe(III) oxides were not precipitated even at the source of Fe, it is unlikely that pore waters would be supersaturated with respect to Fe(III) oxides near the surfaces of quartz grains distant from the source. MINEQL (Westall *et al.*, 1976) calculations using groundwater chemistry data (Ryan and Gschwend, 1990; Lord *et al.*, 1991)

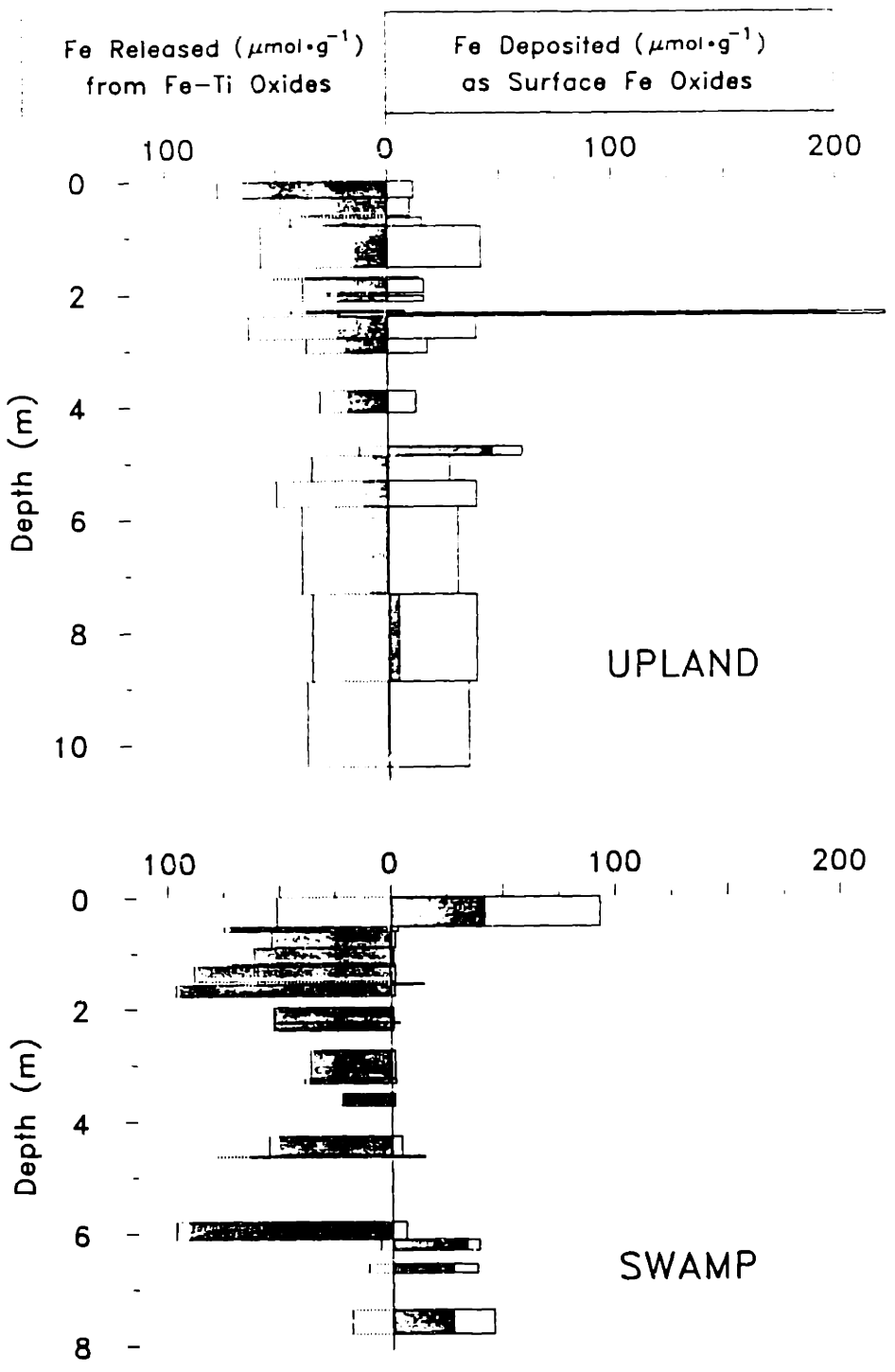

Fig. 2.7. Balance between Fe released by weathering of Fe–Ti oxides and deposition of secondary Fe(III) oxides in individual layers. Open bars with dotted horizontal lines on negative x axis show Fe released from ilmenite and pseudorutile; open bars with solid horizontal lines on positive x axis show surface Fe measured. Filled bars show difference between Fe weathered and Fe deposited as surface Fe. Net Fe export from a layer is shown as a negative difference; net Fe import to a layer is shown as a positive difference.

confirmed that the Upland groundwater is undersaturated with respect to Fe(III) oxides (without including the effect of organic acid ligands, which would increase dissolved [Fe^{3+}]).

We suspect that Fe(III) oxides on quartz grains originated as adsorbed surface complexes. Silanol groups on quartz and amorphous silica surfaces strongly adsorb hydrolyzed Fe^{3+} species (Dugger *et al.*, 1964; Schindler *et al.*, 1976). Continued adsorption of successive layers of Fe^{3+} leads to formation of Fe oxyhydroxide surface deposits (Anderson *et al.*, 1984; Taylor *et al.*, 1990). Given the extensive coverage of quartz surfaces by kaolinite–goethite coatings, it is apparent that Fe^{3+} adsorption has not been limited to patches or surface imperfections on the quartz surface; instead, Fe^{3+} is present in significant quantities over a high percentage of quartz surfaces. The distribution of Fe throughout the coatings indicates that additional Fe^{3+} was adsorbed by the kaolinite particles following their attachment to previously accumulated Fe(III) oxides. Positively–charged surfaces favorable for the continued removal of kaolinite from suspension could have been maintained in this way.

Following the accumulation of Fe^{3+} on the quartz and kaolinite surfaces, goethite formation is favored over the formation of ferrihydrite or lepidocrocite (γ–FeOOH) in the Cohansey Sand because Fe(III) oxide nucleation is probably slow. Nucleation may be slowed by (1) slow release of Fe^{3+} (Graham *et al.*, 1989) from the Fe–Ti oxides, (2) complexation of Fe^{3+} by organic acids (Kämpf and Schwertmann, 1982), and (3) slow oxidation of Fe^{2+} at low *p*H (Schwertmann, 1988). Despite slow nucleation, goethite crystal size appeared to be limited to $\ll 1$ μm in most quartz coatings, possibly by the continuous attachment of kaolinite. Larger, discrete Fe(III) oxide crystals with the lath–like appearance of goethite formed only in locations where Fe concentration exceeded 10 mole%, or about 13 wt% FeOOH (if all Fe was present as goethite).

Goethite in the Cohansey Sand appeared to be considerably substituted by Al, as indicated by correlation of surface Fe and Al contents of sediment layers containing goethite ($R^2 = 0.65$, $n = 18$), shifts in the goethite d_{110} peaks to slightly smaller d–spacings in some samples (Schulze, 1984), and the lack of any Al oxyhydroxide phase in the sediments. The extent of Al substitution in goethite was estimated by the ratio of surface Al/(surface Fe + surface Al) in each layer (weighted mean values in Table 2.2). Goethite in the unsaturated Upland soil had the highest proportion of AlOOH (20 mole%), perhaps due to lower H_2O activity (Tardy and Nahon, 1985). In the saturated sediments, goethite is less substituted by Al (Upland sediment, 16 mole% AlOOH; Swamp oxidized sediment, 9.6 mole% AlOOH). The difference between Al substitution of sediment goethites may be caused by transport of excess Fe into the Swamp oxidized sediments from the overlying reduced sediments, resulting in higher ratios of dissolved Fe/Al. Thermodynamic stability calculations indicate that Al substitution increases goethite stability relative to hematite (Tardy and Nahon, 1985).

Kinetics of Fe(III) Oxide Dissolution and Clay Mobilization

If kaolinite is cemented to quartz surfaces by Fe(III) oxides, the kinetics of kaolinite release must be linked to the kinetics of Fe(III) oxide dissolution. Because Fe is distributed throughout the kaolinite coatings, kaolinite remobilization should commence at the onset of Fe(III) oxide dissolution and continue until Fe(III) oxide is completely dissolved given suitably dispersive conditions of *p*H and ionic strength. Harris *et al.* (1987) envisioned a similar decementation process leading to vertical redistribution of clays in Fe(III) oxide–cemented soils in Florida. In the anoxic groundwater below the swamp, the goethite cementing phase is probably dissolved by reduction using organic carbon (represented by CH_2O) as an electron source:

$$FeOOH + \frac{1}{4} CH_2O + 2\,H^+ \longrightarrow Fe^{2+} + \frac{1}{4} CO_2 + \frac{7}{4} H_2O$$

A minimum of 12.5 pore volumes of infiltrating water are necessary to dissolve the goethite within a volume of sediment if we assume that (1) the sediments underlying the swamp originally contained 35 μmol g^{-1} surface Fe as goethite, (2) the sediment bulk density is 1.8 g cm^{-3} and porosity is 0.3, (3) the total organic carbon concentration in the water was 4 mM C, and (4) the reaction proceeds to completion in each pore volume. In (4) it is assumed that goethite dissolution is fast relative to the flushing of a pore volume. However, goethite dissolution may be slowed by low surface area (blocking of active sites by attached kaolinite) and reductants that are not extensively adsorbed or that do not transfer their electrons efficiently. With the hydraulic gradient measured between the Swamp shallow and deep wells (0.17 $m \cdot m^{-1}$) and a representative range of hydraulic conductivities (10^{-2} to 10^{-4} cm s^{-1}; Rhodehamel, 1979b), a minimum of 50 to 5,000 years is required to dissolve goethite in the 6 meters of reduced sediment below the swamp. This estimate assumes that our rudimentary knowledge of local groundwater flow adequately describes the actual flow, both now and in the past. Nevertheless, it appears reasonable that a reduced zone of 6 m depth may have formed in the 10,000 years following glacial retreat.

The kinetics of Fe(III) oxide dissolution and clay release may be important in considering the environmental importance of decementation. The swampy terrain around McDonalds Branch could be considered a natural analog of a waste site that generates reducing leachates capable of dissolving Fe and Mn oxides. Plumes of reducing leachate have been reported to alter sediment color from yellow and brown to white and grey over periods of tens of years in sediments similar to the Cohansey Sand (Kimmel and Braids, 1980; Nicholson *et al.*, 1983). In addition to the potential for clay colloid mobilization, trace metals (Baedecker and Back, 1979) and colloidal organic matter (e.g., humic substances) adsorbed to oxide phases would be released following oxide dissolution. The potential mobilization of trace

metals, organic matter, and clay particles in reducing plumes produces two deleterious effects: (1) the concentration of suspended colloids increases, enhancing the potential for colloid–facilitated transport of contaminants, and (2) the adsorptive capacity of the sediment decreases, diminishing the retardation of contaminants. Colloid mobilization by reducing plumes may be a wide–spread problem because sandy, Fe(III) oxide–coated sediments are common along the entire Atlantic Coastal Plain. Colloidal phases can also be mobilized by changes in groundwater chemistry in sediments cemented by other secondary mineral phases (carbonates, silica, evaporites). Gschwend *et al.* (1990) reported that silicate colloids were mobilized in a carbonate–cemented aquifer where they suspected that an increase in P_{CO_2} had dissolved calcite cement.

Implications for Clay and Iron Diagenesis

Clay infiltration is considered an unsaturated zone process (Walker, 1976; Passaretti and Eslinger, 1987); thus, the occurrence of infiltrated clay in sediments is cited as evidence for arid climates, deep water tables, and vertical redistribution of clay minerals early in the diagenetic sequence (Walker *et al.*, 1978; Owens *et al.*, 1983; Molenaar, 1986; Matlack *et al.*, 1989; Moreas and De Ros, 1990). Much of the clay in the Cohansey Sand was probably emplaced by unsaturated zone infiltration during times of low sea level and deep water tables. However, our observations of the Cohansey Sand demonstrate that clays may be redistributed in saturated sediments as well. Horizontal redistribution of colloids is often important in the saturated zone as colloids follow the direction of groundwater advection. For example, Short *et al.* (1988), Buddemeier and Hunt (1988), and Penrose *et al.* (1990) each reported lateral transport of colloid–associated radionuclides away from their sources. Clay mobilization in saturated sediments has also been caused by reductions in ionic strength at sea water–fresh water interfaces (Goldenberg *et al.*,

1983) resulting in horizontal movement of colloids in response to changes in sea level. Thus, evidence of colloidal clay morphologies and textures in sediments is not a certain indicator of unsaturated zone infiltration.

The development of red beds by intrastratal dissolution of unstable Fe–bearing primary minerals and subsequent precipitation of hematite is often considered to be an indicator of arid and tropical environments (Walker, 1967; 1974). In this research, we have observed another example of intrastratal weathering of Fe–bearing primary minerals leading to the formation of secondary Fe(III) oxides in temperate climates. Goethite, the stable Fe(III) oxide in low–temperature, saturated surface sediments (Tardy and Nahon, 1985) is transformed to hematite through dehydration initiated by a decrease in H_2O activity following sediment uplift or an increase in temperature following sediment burial (Berner, 1969; Langmuir, 1971). Sediments containing Fe(III) oxide–coated skeletal grains have also been observed in other temperate climates (Schluger and Roberson, 1975; Postma and Brockenhuus–Schack, 1987).

CONCLUSIONS

Based on our observations and those of others who have investigated this Atlantic Coastal Plain deposit, we surmise that the diagenesis of Fe and clay in the Cohansey Sand followed this sequence of events. As initially deposited about 20 million years ago, the Cohansey Sand contained predominantly quartz and ilmenite grains in sheets of sand intercalated by clay– and silt–rich laminations. The marine sediments were presumably reducing and slightly alkaline, thus ilmenite remained relatively unweathered. Oxidizing and acidic conditions developed in the sediments upon emergence from the sea about 5 million years ago. Ilmenite weathered to pseudorutile under oxidizing conditions and slowly released Fe to the sediments. Fe^{3+} released by Fe–Ti oxide weathering spread over pore–scale distances throughout the sediment. The quartz surfaces adsorbed Fe^{3+}, which accumulated on the surfaces primarily as microcrystalline, Al–substituted (9.6 to 20 mole% AlOOH) goethite. The accumulation of Fe(III) oxides eventually reversed the surface charge of the grains from negative to positive. As sea level declined, the water table deepened. Infiltrating water passed through clay–bearing layers and carried kaolinite particles downward into the sediments. The kaolinite was removed from suspension by attachment to the Fe(III) oxides on quartz surfaces through electrostatic attraction. Coatings on quartz grains of up to 10 μm thickness accumulated. The coatings consist of goethite, and perhaps other less crystalline ferric oxides, intimately mixed with kaolinite. Conditions favorable for kaolinite attachment were maintained by the continued release of Fe from the Fe–Ti oxide weathering. The influx of organic matter–rich water from the swamp, beginning about 10,000 years ago, dissolved Fe(III) oxide coatings and released kaolinite particles, leading to the difference in clay content we observed between the Swamp reduced sediments and the oxidized sediments of the Upland and Swamp cores.

Acidic, reducing conditions accelerated the weathering of the Fe–Ti oxides in the soils and reduced sediments as revealed by surface and interior Fe/Ti ratios measured by EDX.

Given the widespread occurrence of Fe(III) oxide–coated sands, especially on the Atlantic Coastal Plain, the mobilization of kaolinite particles by dissolution of Fe(III) oxide cement may be a significant process affecting clay and Fe diagenesis and colloid–facilitated transport. The mobilization and lateral transport of clay in response to changes in pore water chemistry in saturated sediments suggests alternative interpretations of "illuviated" or "mechanically infiltrated" clay morphologies in sediments. The redistribution of Fe from sparsely distributed ilmenite and pseudorutile grains to secondary Fe(III) oxide coatings spread throughout the sediments further supports the contention that precursor red beds can be formed in temperate climates. Finally, changes or gradients in groundwater chemistry may incur decementation and clay mobilization, leading to colloid–facilitated transport of low–solubility species.

REFERENCES

Anand R.R. and Gilkes R.J. (1984) Weathering of ilmenite in a lateritic pallid zone. *Clays Clay Min.* **32**, 363–374.

Anderson M.A., Palm–Gennen M.H., Renard P.N., Defosse C., and Rouxhet P.G. (1984) Chemical and XPS study of the adsorption of iron (III) onto porous silica. *J. Colloid Interface Sci.* **102**, 328–336.

Baedecker M.J. and Back W. (1979) Modern marine sediments as a natural analog to the chemically stressed environment of a landfill. *J. Hydrol.* **43**, 393–414.

Berner R.A. (1969) Goethite stability and the origin of red beds. *Geochim. Cosmochim. Acta* **33**, 267–273.

Brownawell B.J. and Farrington J.W. (1986) Biogeochemistry of PCBs in interstitial waters of a coastal marine sediment. *Geochim. Cosmochim. Acta* **50**, 157–169.

Buddemeier R.W. and Hunt J.R. (1988) Transport of colloidal contaminants in groundwater: radionuclide migration at the Nevada Test Site. *Appl. Geochem.* **3**, 535–548.

Carter C.H. (1978) A regressive barrier and barrier–protected deposit: depositional environments and geographic setting of the Late Tertiary Cohansey Sand. *J. Sediment. Petrol.* **48**, 933–950.

Crerar D.A., Knox G.W., and Means J.L. (1979) Biogeochemistry of bog iron in the New Jersey Pine Barrens. *Chem. Geol.* **24**, 111–136.

Crerar D.A., Means J.L., Yuretich R.F., Borcsik M.P., Amster J.L., Hastings D.W., Knox G.W., Lyon K.E., and Quiett R.F. (1981) Hydrogeochemistry of the New Jersey Coastal Plain 2. Transport and deposition of iron, aluminum, dissolved organic matter, and selected trace elements in stream, ground–, and estuary water. *Chem. Geol.* **33**, 23–44.

Degueldre C., Baeyens B., Goerlich W., Riga J., Verbist J., and Stadelmann P. (1989) Colloids in water from a subsurface fracture in granitic rock, Grimsel Test Site, Switzerland. *Geochim. Cosmochim. Acta* **53**, 603–610.

Dugger D.L., Stanton J.H., Irby B.N., McConnell B.L., Cummings W.W., and Maatman R.W. (1964) The exchange of twenty metal ions with the weakly acidic silanol group of silica gel. *J. Phys. Chem.* **68**, 757–760.

Enfield C.G. and Bengtsson G. (1988) Macromolecular transport of hydrophobic contaminants in aqueous environments. *Ground Water* **26**, 71–79.

Giblin A.M., Batts B.D., and Swaine D.J. (1981) Laboratory simulation studies of uranium mobility in natural waters. *Geochim. Cosmochim. Acta* **45**, 699–709.

Goldenberg L.C., Magaritz M., and Mandel S. (1983) Experimental investigation on irreversible changes of hydraulic conductivity on the seawater–freshwater interface in coastal aquifers. *Water Resour. Res.* **19**, 77–85.

Graham R.C., Weed S.B., Bowen L.H., and Buol S.W. (1989) Weathering of iron–bearing minerals in soils and saprolite on the North Carolina Blue Ridge front: I. Sand–size primary minerals. *Clays Clay Min.* **37**, 19–28.

Grey I.E. and Reid A.F. (1975) The structure of pseudorutile and its role in the natural alteration of ilmenite. *Amer. Mineral.* **60**, 898–906.

Gschwend P.M., Backhus D.A., MacFarlane J.K., and Page A.L. (1990) Mobilization of colloids in groundwater due to infiltration of water at a coal ash disposal site. *J. Contam. Hydrol.* **6**, 307–320.

Harris W.G., Carlisle V.W., and Chesser S.L. (1987) Clay mineralogy as related to morphology of Florida soils with sandy epipedons. *Soil Sci. Soc. Amer. J.* **51**, 1673–1677.

Hogg R., Healy T.W., Fuerstenau D.W. (1966) Mutual coagulation of colloidal dispersions. *Trans. Faraday Soc.* **62**, 1638–1651.

Horzempa L.M. and Helz G.R. (1979) Controls on the stability of sulfide sols: colloidal covellite as an example. *Geochim. Cosmochim. Acta* **43**, 1645--1650.

Hough D.B. and White L.R. (1980) The calculation of Hamaker constants from Lifshitz theory with applications to wetting phenomena. *Adv. Colloid Interface Sci.* **14**, 3–41.

James R.O. and Healy T.W. (1972) Adsorption of hydrolyzable metal ions at the oxide–water interface II. Charge reversal of SiO_2 and TiO_2 colloids by adsorbed Co(II), La(III), and Th(IV) as model systems. *J. Colloid Interface Sci.* **40**, 53–64.

Kämpf N. and Schwertmann U. (1982) Goethite and hematite in a climosequence in southern Brazil and their application in classification of kaolinitic soils. *Geoderma* **29**, 27–39.

Khilar K.C. and Fogler H.S. (1984) The existence of a critical salt concentration for particle release. *J. Colloid Interface Sci.* **101**, 214–224.

Kia S.F., Fogler H.S., and Reed M.G. (1987) Effect of *p*H on colloidally induced fines migration. *J. Colloid Interface Sci.* **118**, 158–168.

Kimmel G.E. and Braids O.C. (1980) Leachate plumes in ground water from Babylon and Islip landfills, Long Island, New York. U.S. Geological Survey Prof. Paper 1085, 38 pp.

Langmuir D. (1969) Geochemistry of iron in a coastal–plain groundwater of the Camden, New Jersey area. U.S. Geological Survey Prof. Paper 650–C, C224–C235.

Langmuir D. (1971) Particle size effect on the reaction goethite = hematite + water. *Amer. J. Sci.* **271**, 147–156.

Lim C.H. and Jackson M.L. (1982) Dissolution for total analysis. In *Methods of Soil Analysis, Part 2* (ed. A.L. Page), Amer. Soc. Agron., Madison, WI, 5–7.

Little S. (1979) Fire and plant succession in the New Jersey Pine Barrens. In *Pine Barrens: Ecosystem and Landscape* (ed. R.T.T. Forman), Academic Press, San Diego, CA, 297–314.

Lord D.G., Barringer J.L., Johnsson P.A., Schuster P.F., Walker R.L., Fairchild J.E., Sroka B.N., and Jacobsen E. (1990) Hydrogeochemical data from an acidic deposition study at McDonalds Branch basin in the New Jersey Pinelands, 1983–1986. U.S. Geological Survey Open–File Report 88–500, 128 pp.

Magaritz M., Amiel A.J., Ronen D., and Wells M.C. (1990) Distribution of metals in a polluted aquifer: A comparison of aquifer suspended material to fine sediments of the adjacent environment. *J. Contam. Hydrol.* **5**, 333–347.

Markewitz F.J. (1969) Ilmenite deposits of the New Jersey Coastal Plain. In *Geology of Selected Areas in New Jersey and Eastern Pennsylvania and Guidebook of* Excursions (ed. S. Subitzky), Rutgers Univ. Press, New Brunswick, NJ, 363–382.

Matlack K.S., Houseknecht D.W., and Applin K.R. (1989) Emplacement of clay into sand by infiltration. *J. Sediment. Petrol.* **59**, 77–87.

Minard J.R. (1966) Sandblasted blocks on a hill the Coastal Plain of New Jersey. U.S. Geological Survey Prof. Paper 550–B, B87–B90.

Molenaar N. (1986) The interrelation between clay infiltration, quartz cementation, and compaction in Lower Givetian terrestrial sandstones, northern Ardennes, Belgium. *J. Sediment. Petrol.* **56**, 359–369.

Morad S. and Aldahan A.A. (1986) Alteration of detrital Fe–Ti oxides in sedimentary rocks. *Bull. Geol. Soc. Amer.* **97**, 567–578.

Moreas M.A.S. and De Ros L.F. (1990) Infiltrated clays in fluvial Jurassic sandstones of Reconcavo Basin, northeastern Brazil. *J. Sediment. Petrol.* **60**, 809–819.

Nicholson R.V., Cherry J.A., and Reardon E.J. (1983) Migration of contaminants in groundwater at a landfill: a case study. 6. Hydrogeochemistry. *J. Hydrol.* **63**, 131–176.

Olsson R.K. (1963) Latest Cretaceous and earliest Tertiary stratigraphy of New Jersey Coastal Plain. *Bull. Amer. Assoc. Petrol. Geol.* **47**, 643–665.

Owens J.P., Hess M.M., Denny C.S., and Dwornik E.J. (1983) Postdepositional alteration of surface and near–surface minerals in selected Coastal Plain formations of the Middle Atlantic states. U.S. Geological Survey Prof. Paper 1067–F, F1–F45.

Parks G.A. (1967) Aqueous surface chemistry of oxides and complex oxide minerals. In *Equilibrium Concepts in Natural Water Systems* (ed. W. Stumm), Advan. Chem. Ser. 67, Amer. Chem. Soc., Washington , DC, 121–160.

Passaretti M.L. and Eslinger E.V. (1987) Dissolution and relic textures in framework grains of Holocene sediments from the Brazos River and Gulf Coast of Texas. *J. Sediment. Petrol.* **57**, 94–97.

Penrose W.R., Polzer W.L., Essington E.H., Nelson D.M., and Orlandini K.A. (1990) Mobility of plutonium and americium through a shallow aquifer in a semiarid region. *Environ. Sci. Technol.* **24**, 228–234.

Poppe L.J. and Hathaway J.C. (1979) A metal–membrane mount for X–ray powder diffraction. *Clays Clay Min.* **27**, 152–153.

Postma D. and Brockenhuus–Schack B.S. (1987) Diagenesis of iron in proglacial sand deposits of late– and post–Weichselian age. *J. Sediment. Petrol.* **57**, 1040–1053.

Rhodehamel E.C. (1979a) Geology of the Pine Barrens of New Jersey. In *Pine Barrens: Ecosystem and Landscape* (ed. R.T.T. Forman), Academic Press, San Diego, CA, 39–60.

Rhodehamel E.C. (1979b) Hydrology of the New Jersey Pine Barrens. In *Pine Barrens: Ecosystem and Landscape* (ed. R.T.T. Forman), Academic Press, San Diego,.CA, 39–60.

Ruckenstein E. and Prieve D.C. (1976) Adsorption and desorption of particles and their chromatographic separation. *Amer. Inst. Chem. Eng. J.* **22**, 276–283.

Ryan J.N. and Gschwend P.M. (1990) Colloid mobilization in two Atlantic Coastal Plain aquifers: field studies. *Water Resour. Res.* **26**, 307–322.

Ryan J.N. and Gschwend P.M. (1991) Extraction of iron oxides from soils and sediments using reductive dissolution by titanium(III). *Clays Clay Min.* **39**, 509–518.

Schindler P.W., Fürst B., Dick R., and Wolf P.U. (1976) Ligand properties of surface silanol groups I. Surface complex formation with Fe^{3+}, Cu^{2+}, Cd^{2+}, and Pb^{2+}. *J. Colloid Interface Sci.* **55**, 469–475.

Schluger P.R. and Roberson H.E. (1975) Mineralogy and chemistry of the Patapsco Formation, Maryland, related to the groundwater geochemistry and flow system: a contribution to the origin of red beds. *Bull. Geol. Soc. Amer.* **86**, 153–158.

Schulze D.G. (1984) The influence of aluminum of iron oxides. VIII. Unit–cell dimensions of Al–substituted goethites and estimation of Al from them. *Clays Clay Min.* **32**, 36–44.

Schwertmann U. (1988) Occurrence and formation of iron oxides in various pedoenvironments. In *Iron in Soils and Clay Minerals* (eds. J.W. Stucki, B.A. Goodman, and U. Schwertmann), D. Reidel, Dordrecht, pp. 267–308.

Short S.A., Lowson R.T., and Ellis J. (1988) $^{234}U/^{238}U$ and $^{230}Th/^{234}U$ activity ratios in the colloidal phases of aquifers in lateritic weathered zones. *Geochim. Cosmochim. Acta* **52**, 2555–2563.

Tardy Y. and Nahon D. (1985) Geochemistry of laterites, stability of Al–goethite, Al–hematite, and Fe^{3+}–kaolinite in bauxites and ferricretes: an approach to the mechanism of concretion formation. *Amer. J. Sci.* **285**, 865–903.

Taylor R.M., Raupach M., and Chartres C.J. (1990) Simulation of soil reactions: Aluminum–iron (III) hydroxy species react with silica to give deposits on particle surfaces. *Clay Minerals* **25**, 375–389.

Temple A.K. (1966) Alteration of ilmenite. *Econ. Geol.* **61**, 695–714.

Teufer G. and Temple A.K. (1966) Pseudorutile – a new mineral intermediate between ilmenite and rutile in the N alteration of ilmenite. *Nature* **211**, 179–181.

Turner–Peterson C.E. (1985) Lacustrine–humate model for primary uranium ore deposits, Grants Uranium Region, New Mexico. *Bull. Amer. Assoc. Petrol. Geol.* **69**, 1999–2020.

Verwey E.J.W. and Overbeek J.Th.G. (1948) *Theory of the Stability of Lyophobic Colloids.* Elsevier Press, Amsterdam.

Walker T.R. (1967) Formation of red beds in modern and ancient deserts. *Bull. Geol. Soc. Amer.* **78**, 353–368.

Walker T.R. (1974) Formation of red beds in moist tropical climates: a hypothesis. *Bull. Geol. Soc. Amer.* **85**, 633–638.

Walker T.R. (1976) Diagenetic origin of continental red beds. In *The Continental Permian in Central, West and South Europe* (ed. H. Falke), D. Reidel, Dordrecht, 240–482.

Walker T.R., Waugh B., and Crone A.J. (1978) Diagenesis in first–cycle desert alluvium of Cenozoic age, southwestern United States and northwestern Mexico. *Bull. Geol. Soc. Amer.* **89**, 19–32.

Westall J.C., Zachary J.L., and Morel F.M.M. (1976) MINEQL: A computer program for the calculation of chemical equilibrium composition of aqueous systems. Tech. Note 18, R.M. Parsons Laboratory, Dept. Civil Eng., Mass. Inst. of Technol., Cambridge, MA.

Yao K.–M., Habibian M.T., and O'Melia C.R. (1971) Water and wastewater filtration: concepts and applications. *Environ. Sci. Technol.* **11**, 1105–1112.

Chapter Three

DEPENDENCE OF COLLOID DETACHMENT KINETICS ON INTERSURFACE POTENTIAL ENERGY

Frequently we experience the existence of adhesive forces between small particles.

— H.C. Hamaker (1937) *Physica* **4**, 1058.

ABSTRACT

The kinetics of colloid detachment from surfaces have been described by an "energy barrier" model, in which the rate–limiting step is colloid transport over an intersurface potential energy barrier composed of van der Waals, double layer, and Born potential energies. We propose an alternative "equilibrium" model, in which the detachment rate is controlled by both thermodynamic and hydrodynamic mechanisms. The thermodynamic mechanism depends on the energy difference between the primary and secondary minima in intersurface potential energy. The hydrodynamic mechanism depends on the length scale of diffusive colloid transport to the bulk fluid and to sites of lower potential energy associated with surface irregularities. In calculating the intersurface potential energy, we compared the use of zeta potentials with the use of surface potentials estimated with a surface complexation/double layer model.

To test these concepts, we examined colloid detachment data measured under varying solution conditions and, hence, different potential energy profiles, and varying hydrodynamic conditions. Increasing the ionic strength of the solutions flushing oxide colloids from grains resulted in slower detachment and fewer colloids ultimately released. Increasing the flow rate hastened detachment without affecting the number of colloids ultimately released. The relation between release rate constants and detachment energies indicated that the equilibrium model better described the detachment kinetics. The rate of colloid transport from the secondary minimum to the bulk fluid was related to the length scale of diffusion to the bulk fluid. The competing removal of colloids to irregular surface sites was related to the proximity of the secondary minimum to the surface.

INTRODUCTION

The detachment of colloids from surfaces is a concern in many fields, including wastewater filtration, subsurface transport of viruses and bacteria, and enhanced transport of colloid–associated contaminants in groundwater. Colloid–facilitated transport of low–solubility contaminants (*e.g.*, radionuclides, trace metals, and hydrophobic organic compounds) has been observed in aquifers (Buddemeier and Hunt, 1988; Short *et al.*, 1988; Penrose *et al.*, 1990; Magaritz *et al.*, 1990); however, the presence of colloids detected in these studies has not always been related to chemical and physical factors affecting their genesis. Some sources of colloids in groundwater include precipitation of supersaturated phases (Langmuir, 1969; Gschwend and Reynolds, 1987), erosion of secondary minerals from fractures (Degueldre *et al.*, 1989), mobilization by changes in ionic strength and *p*H (Nightingale and Bianchi, 1977; Khilar and Fogler, 1984), and release by dissolution of cementing minerals (Gschwend *et al.*, 1990; Ronen *et al.*, 1992).

Based on groundwater samples and sediment cores, we have hypothesized that clay colloids were mobilized from an iron oxide–coated sand aquifer by infiltration of organic matter–rich, anoxic groundwater that dissolved the Fe(III) oxide cement binding colloids to the framework grains (Ryan and Gschwend, 1990; 1992). More recently, we measured rates of clay release from columns containing the iron oxide–coated sand (Ryan and Gschwend, submitted; Chapter 4). The columns were subjected to solutions of varying ionic strength, *p*H, and reductant and surfactant concentrations. The results of these experiments suggested that the infiltrating organic matter mobilizes colloids most effectively as a dispersant and not as a reductant.

Solution ionic strength (I), *p*H, electrolyte composition, and other physical–chemical factors that affect colloid and grain surface properties have been

related to the kinetics of diffusion–driven colloid release by using the intersurface potential energy as an Arrhenius activation energy (Dahneke, 1975a; 1975b; Ruckenstein and Prieve, 1976). According to this "energy barrier" model, the potential energy barrier $\phi_{max}-\phi_{min1}$ limits the rate of diffusional transport of colloids from the grain surface to the bulk fluid (Fig. 3.1).

Rates of colloid coagulation and deposition predicted with potential energy barriers are orders of magnitude smaller than those measured in experiments (Hull and Kitchener, 1969; Bowen and Epstein, 1979; Gregory and Wishart, 1980). In contrast, Kallay *et al.* (1987) summarized the results of a series of colloid detachment experiments in which a qualitative agreement between the rate of colloid release and the potential energy barrier inhibiting detachment was observed.

When we related the rates of clay colloid release from the iron oxide–coated sand to detachment energies (Ryan and Gschwend, submitted; Chapter 4), we found that the energy barrier model did not adequately describe the trends in the release rates when ionic strength was varied. Instead, the rates were related to the difference between the primary and secondary minima of intersurface potential energy (Fig. 3.1). This implied that (1) the transport of colloids over the energy barrier was relatively rapid and (2) the transport of colloids through the diffusion boundary layer to the bulk fluid was the rate–determining step. To test this "equilibrium" model, we compared the dependence of colloid release rates measured in the model systems summarized in Kallay *et al.* (1987) to the size of the energy barrier and to the equilibrium energy difference. Because zeta potentials are insensitive to surface potentials at high surface charge and high I (Hunter, 1981), we used both zeta potentials measured in the studies summarized by Kallay *et al.* (1987) and surface potentials estimated with a surface complexation/double layer (SCDL) model in calculating the potential energy for the model systems.

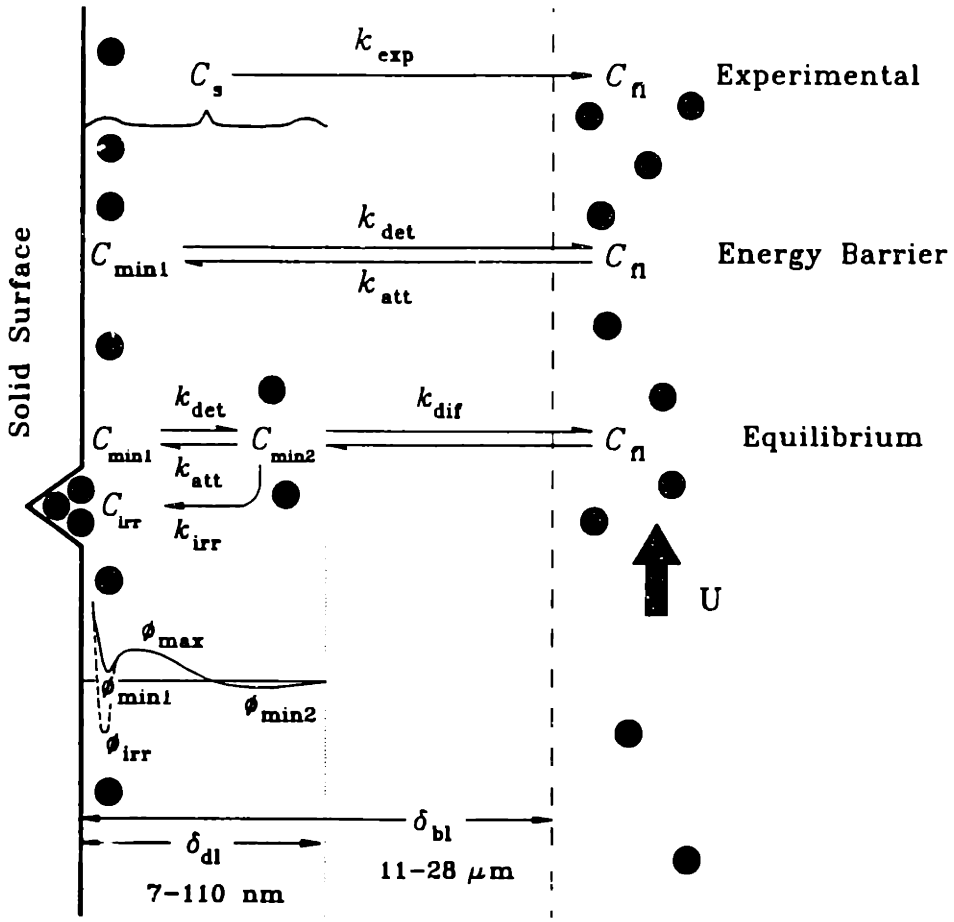

Fig. 3.1. A comparison of the energy barrier and equilibrium model of colloid detachment. The rate–limiting step in the energy barrier model is the diffusion–driven transport of colloids from the primary minimum (C_{min1}) over the potential energy barrier [$-(\phi_{max}-\phi_{min1})$]. In the equilibrium model, a rapid equilibration of colloids between C_{min1} and C_{min2} in the double layer region (δ_{dl}) precedes the rate–limiting step, diffusion of colloids from the secondary minimum (C_{min2}) through the diffusion boundary layer (δ_{bl}) to the bulk fluid (C_{fl}) moving at velocity U. Colloids may also be removed to surface sites of irregular geometry (C_{irr}) from C_{min2}. The equilibrium colloid distribution at the surface is controlled by the potential energy difference [$-(\phi_{min2}-\phi_{min1})$]. The experimentally–determined surface–bound colloids C_s and release rate constant k_{exp} may be related to the corresponding model parameters.

We were particularly interested in experiments in which the flushing solution I was varied at constant pH. Because the size of the energy barrier detachment energy decreases with increasing I, an increase in colloid release rate with increasing I would suggest that the energy barrier controlled detachment. On the other hand, the primary minimum becomes more stable with respect to the secondary minimum as I increases; thus, a decrease in release rate with increasing I would suggest that the equilibrium model better described colloid detachment. In most of experiments summarized by Kallay *et al.* (1987), release rates decreased when I was increased; however, Kallay *et al.* (1986) observed an increase in release rate when I was increased in a system of hematite colloids and glass (amorphous SiO_2) grains. To assess this contradictory evidence, we experimentally re–examined the kinetics of hematite colloid detachment from quartz grains. We also varied the flow rate in our hematite–quartz system to test the hypothesis that transport of the detached colloids through the diffusion boundary layer was the rate–determining step in colloid release.

MODELS OF COLLOID DETACHMENT

Kinetics of Colloid Detachment

Energy Barrier Model – In the diffusion boundary layer near the grain surface, where fluid motion is negligible relative to colloid diffusion, colloid attachment and detachment have been described as a first order exchange (Dahneke, 1975; Ruckenstein and Prieve, 1976) between colloids in the primary minimum (C_{min1}) and colloids in the bulk fluid (C_{fl}):

$$C_{min1} \underset{k_{att}}{\overset{k_{det}}{\rightleftharpoons}} C_{fl} \qquad [3.1]$$

where k_{det} and k_{att} (s^{-1}) are the detachment and attachment rate constants (Fig. 3.1). We assume that $[C_{min1}]$, the concentration of colloids in the primary minimum (g m^{-3}), is proportional to $[C_s]$, the experimentally–determined concentration of attached colloids (expressed as g m^{-3} where the volume (m^3) is defined as the product of the grain surface area (m^2) and the colloid diameter (m)). $[C_{fl}]$ is the concentration of colloids in the bulk fluid eluting from the column (g m^{-3}). In an analogy with Arrhenius kinetics, the rate constants have been exponentially related to the size of the activation energy barriers (Ruckenstein and Prieve, 1976):

$$k_{det} \approx D_c(x_{max}) \frac{(\gamma_{max}\gamma_{min1})^{0.5}}{2\pi kT} \exp\left[-\frac{\phi_{max}-\phi_{min1}}{kT}\right] \qquad [3.2a]$$

$$k_{att} \approx D_c(x_{max}) \frac{(\gamma_{max}\gamma_{min2})^{0.5}}{2\pi kT} \exp\left[-\frac{\phi_{max}-\phi_{min2}}{kT}\right] \qquad [3.2b]$$

where $D_c(x_{max})$ is the colloid diffusion coefficient (m^2 s^{-1}) at the separation distance x_{max} of the primary maximum in intersurface potential energy (ϕ_{max}), k is the Boltzmann constant (J K^{-1}), T is the absolute temperature (K), and

$$\gamma_i = -\,d^2\phi_i/dx^2\big|_{x_i} \qquad [3.3]$$

where ϕ_i is the potential energy at the primary minimum (min1), primary maximum (max), or secondary minimum (min2), and x_i is the separation distance of the primary minimum, the primary maximum, and the secondary minimum. When $[C_{fl}]$ is maintained at low concentrations by advection of colloid–free fluid, the attachment rate is negligible and the overall colloid release rate may be expressed as:

$$\begin{aligned} d[C_{fl}]/dt &= k_{exp}\,[C_s] \\ &= k_{det}\,[C_{min1}] \end{aligned} \qquad [3.4]$$

where k_{exp} is the experimental rate constant (s^{-1}). Because $[C_s]$ is taken as a measure of $[C_{min1}]$, k_{exp} can be equated with k_{det}. In terms of Arrhenius kinetics,

$$\log k_{exp} = -\frac{(\phi_{max}-\phi_{min1})}{2.303\mathbf{kT}} + \log\left[D_c\,\frac{(\gamma_{max}\gamma_{min1})^{0.5}}{2\pi\mathbf{k}T}\right] \qquad [3.5]$$

Equilibrium Model – Three steps are proposed to describe colloid release: (1) the rapid redistribution of colloids from the primary minimum (C_{min1}) to the secondary minimum (C_{min2}), (2) the rate–limiting transport of colloids from C_{min2} through the diffusion boundary layer to C_{fl}, and (3) transport of colloids from C_{min2} along the surface to more firmly bound sites at surface irregularities (C_{irr}):

$$C_{min1} \underset{k_{att}}{\overset{k_{det}}{\rightleftharpoons}} C_{min2} \xrightarrow{k_{dif}} C_{fl} \qquad [3.6]$$

$$C_{irr} \xleftarrow{k_{irr}} \text{(from } C_{min2}\text{)}$$

where k_{dif} and k_{irr} (s^{-1}) are the rate constants for transport to the bulk fluid and to the irregular surface sites, respectively.

Upon introduction of a flushing solution promoting more repulsive interactions between colloids and grains, a portion of colloids attached in C_{min1} will

be destabilized and rapidly redistributed to C_{min2}. The number of particles initially eligible for diffusion depends on the stability of C_{min1} relative to C_{min2}. The secondary minimum may be considered a temporary staging area for diffusion to C_{fl} and C_{irr} instead of an energy "well" where colloids reside because the energy well represented by ϕ_{min2} is very small compared to ϕ_{min1} under most conditions. Advection of the bulk fluid maintains $[C_{fl}]$ at low levels, so diffusion of colloids to the bulk fluid may be considered irreversible. Transport of colloids from C_{min2} to C_{irr} represents colloid diffusion and attachment to cracks, crevices, and kinks where the potential energy is lower than ϕ_{min1} owing to irregular geometry. If ϕ_{irr} is sufficiently deep relative to ϕ_{min1} under the conditions of a given experiment, colloid diffusion to C_{irr} may be considered irreversible. Colloid transport from C_{min1} to C_{irr} may be considered negligible because colloids in the primary minimum are tightly bound and virtually unable to diffuse laterally to lower energy sites.

The rate of colloid removal from the secondary minimum location may be expressed as

$$\frac{d[C_{min2}]}{dt} = k_{det}[C_{min1}] - k_{att}[C_{min2}] - k_{dif}[C_{min2}] - k_{irr}[C_{min2}] \qquad [3.7]$$

If the exchange of colloids between the primary and secondary minima is rapid relative to the diffusion of colloids from C_{min2}, the distribution of colloids between the primary and secondary minima can be described using an equilibrium constant:

$$K_s = \frac{k_{det}}{k_{att}} = \frac{[C_{min2}]}{[C_{min1}]} \qquad [3.8]$$

If $[C_{min1}]$ is replaced with $\frac{k_{att}}{k_{det}}[C_{min2}]$ in Eqn. 3.7 and the initial concentration of colloids in the secondary minimum, $[C_{min2}]_0$, is $K_s\,[C_{min1}]_0$, then the time–varying concentration of colloids in the secondary minimum is

$$[C_{min2}] = K_s\,[C_{min1}]_0 \exp\,[-\,(k_{dif} + k_{irr})\,t] \qquad [3.9]$$

The rate of colloid transport to the bulk fluid can be expressed as

$$\begin{aligned} d[C_{fl}]/dt &= k_{dif}\,[C_{min2}] \\ &= k_{dif}\,K_s\,[C_{min1}]_0 \exp\,[-\,(k_{dif} + k_{irr})\,t] \end{aligned} \qquad [3.10]$$

The initial colloid surface concentration $[C_s]_0$ is the sum of contributions from $[C_{min1}]_0$ and $[C_{irr}]_0$. $[C_{min1}]_0$ will be less than or equal to the experimentally–determined $[C_s]_0$.

We can relate k_{dif} to hydrodynamic parameters. If $[C_{fl}] \approx 0$, then the rate of diffusion of particles from the secondary minimum to the bulk fluid can be described by

$$\begin{aligned} d[C_{min2}]/dt &= -\,k_{dif}\,[C_{min2}] \\ &= -\,D_c \left.\frac{d^2[C]}{dx^2}\right|_{C_{min2}}^{C_{fl}} \\ &\approx \frac{D_c}{\delta_{bl}^2}\,[C_{min2}] \end{aligned} \qquad [3.11]$$

where δ_{bl} is the thickness of the diffusion boundary layer (m). Thus, the diffusion rate constant depends on hydrodynamic parameters:

$$k_{dif} = \frac{D_c}{\delta_{bl}^2} \qquad [3.12]$$

D_c is given by the Stokes–Einstein equation,

$$D_c = \mathbf{k}T/6\pi\mu_{fl}a_c \qquad [3.13]$$

where μ_{fl} is the viscosity of the fluid (kg m^{-1} s^{-1}) and a_c is the radius of the colloid (m). The average thickness of the boundary layer around a single spherical colloid in laminar flow may be estimated by (Batchelor, 1979)

$$\delta_{bl} = 2a_c \Big/ \left[1 + 0.625\left[\frac{\mu_{fl}}{\rho_{fl}D_p}\right]^{1/3} \mathbb{R}^{1/3}\right] \qquad [3.14]$$

where ρ_{fl} is the fluid density (kg m^{-3}) and $\mathbb{R}$ is the Reynolds number for a porous medium:

$$\mathbb{R} = 2a_g\rho_{fl}Q_{col}/\mu_{fl}A_{col}n \qquad [3.15]$$

where a_g is the grain radius (m), Q_{col} is flow rate (m^3 s^{-1}), A_{col} is the

cross–sectional area of the column (m^2), and n is the porosity of the packed column (void volume/total volume).

The equilibrium constant K_s, a ratio of the rate constants, can be replaced with the expressions for the rate constants (Eqn. 3.2), yielding

$$K_s = \frac{k_{det}}{k_{att}} = \left[\frac{\gamma_{min1}}{\gamma_{min2}}\right]^{0.5} \exp\left[-(\phi_{min2}-\phi_{min1})/kT\right] \qquad [3.16]$$

Using the results of Eqns. 3.12 and 3.16, the experimental rate constant may be directly related to the intersurface potential energy profile and to hydrodynamic conditions:

$$\log k_{exp} = -\frac{\phi_{min2}-\phi_{min1}}{2.303kT} + \log \frac{D_c}{\delta_{bl}^2} + 0.5 \log \left[\frac{\gamma_{min1}}{\gamma_{min2}}\right] \qquad [3.17]$$

Under most conditions, the energy difference $-(\phi_{min2}-\phi_{min1})$ may be approximated by ϕ_{min1} alone because $\phi_{min2} \approx \phi_\infty = 0$, where ϕ_∞ is the potential energy at infinite separation distance. Thus, the rate constant dependence on the intersurface potential energy may be reduced to the thermodynamic stability of attached colloids attached in the primary minimum relative to colloids unaffected by the intersurface forces.

Potential Energy of Surface Interaction

In the absence of chemical bonds between the colloid and grain surfaces, physical interaction between approaching colloid surfaces in an ionic medium has been expressed in terms of an augmented DLVO (Derjaguin and Landau, 1941; Verwey and Overbeek, 1948) theory as the sum of the van der Waals, Born, and double layer potential energy varying with separation distance x:

$$\phi(x) = \phi^{vdw}(x) + \phi^{born}(x) + \phi^{dl}(x) \qquad [3.18]$$

Approaching colloids experience attractive forces resulting from dispersive,

dipole–dipole, and induced dipole effects known as van der Waals forces. Hamaker (1937) derived an expression for the van der Waals potential energy of attraction between two spheres with an x^{-6} dependence on separation distance:

$$\phi^{vdw} = -\frac{A}{12}\left\{\frac{y}{r^2+ry+r} + \frac{y}{r^2+ry+r+y} + 2\ln\left[\frac{r^2+ry+r}{r^2+ry+r+y}\right]\right\}$$

$$y = a_g/a_c \qquad r = x/2a_c \qquad [3.19]$$

where A is the Hamaker constant (J), a function of the atomic density and polarizability of the material constituting the colloid, and a_c and a_g are the colloid and grain radii, respectively. Retardation effects and the angular dependence of the potential interaction were ignored by assuming pairwise additivity of the interatomic potentials.

Short range repulsive forces arising from hydration or steric forces dominate $\phi(x)$ at very short separation distances (Israelachvili, 1982) and have an important effect on colloid detachment (Verwey and Overbeek, 1948; Ruckenstein and Prieve, 1976; Barouch *et al.*, 1987). However, the spatial variation of Born repulsion is not well understood. The Born repulsive potential has been formulated for sphere–sphere interaction by pairwise integration of the repulsive term of the interatomic Lennard–Jones potential for a x^{-12} dependence on separation distance (Feke *et al.*, 1984):

$$\phi^{born} = \frac{A}{75600r}\left[\frac{\sigma_{born}}{a_c}\right]^6\left[\frac{-4r^2-14(y-1)r-6(y^2-7y+1)}{(2r-1+y)^7}\right.$$

$$+\frac{-4r^2+14(y-1)r-6(y^2-7y+1)}{(2r+1-y)^7} + \frac{4r^2+14(y-1)r+6(y^2+7y+1)}{(2r+1+y)^7}$$

$$\left.+\frac{4r^2-14(y-1)r+6(y^2+7y+1)}{(2r-1-y)^7}\right] \qquad [3.20]$$

where σ_{born} is the collision parameter (m). The Hamaker constant may be estimated from theory or determined by experiment. For oxides in aqueous

suspension, A ranges from about $5 \cdot 10^{-21}$ to $5 \cdot 10^{-20}$ J (Hamaker, 1937; Israelachvili, 1985). For interatomic interactions, σ_{born} is on the order of 5 Å (Feke *et al.*, 1984).

Surfaces in contact with water develop a charge resulting from the exchange of protons, hydroxides, or other ions at surface functional groups. The surface charge gives rise to a double layer interaction potential between approaching surfaces. Hogg *et al.* (1966) calculated the double layer potential using a linearized solution to the Poisson–Boltzmann (PB) equation adapted to sphere–sphere interaction by one–dimensional integration of plate–plate interaction for the constant potential case:

$$\phi^{dl}(x) = \frac{\pi \epsilon \epsilon_0 a_c a_g}{(a_c + a_g)} \{2\psi_{oc}\psi_{og} \ln\left[\frac{1+\exp(-\kappa x)}{1-\exp(-\kappa x)}\right] + (\psi_{oc}^2 + \psi_{og}^2) \ln[1-\exp(-2\kappa x)]\} \quad [3.21]$$

where ϵ is the dielectric constant of water (dimensionless), ϵ_0 is the permittivity of free space (C V^{-1} m^{-1}) and ψ_{oi} is the surface potential of the colloid or grain. The reciprocal double layer thickness κ (m^{-1}) is expressed as:

$$\kappa^2 = \frac{2000\ N_a I\ e^2 z^2}{\epsilon \epsilon_0 kT} \quad [3.22]$$

where N_a is Avogadro's number, I is ionic strength (mole L^{-1}), e is the elementary charge (C), and z is the valence of a symmetrical electrolyte.

The constant potential case describes a double layer in which equilibrium with ions in the bulk solution is maintained with respect to the time scale of colloid attachment and detachment (Gregory, 1975; Lyklema, 1980). The constant potential case is appropriate for the equilibrium model because a rapid re–distribution of colloids between the primary and secondary minima requires rapid equilibration with changes in the bulk solution chemistry.

Owing to the linearization of the PB equation, Hogg *et al.* (1966) stated that their ϕ^{dl} expression was strictly accurate only for $\psi_o < 25$ mV and $\kappa^{-1} < a_c$.

However, the accuracy of the Hogg *et al.* (1966) expression for plate–plate geometry as compared to the exact (numerical) solution of the full PB equation (Devereux and de Bruyn, 1963) is relatively good at substantially higher surface potentials. For plates with surface potentials of 0.154 and 0.077 V, the approximate ϕ^{dl} does not vary from the exact ϕ^{dl} by more than about 60% (Hogg *et al.*, 1966). However, at larger surface potentials (*e.g.*, 0.257 and 0.154 V), the exact ϕ^{dl} greatly exceeds the approximate ϕ^{dl} at separation distances of $x < 30$ nm (Fig. 3.2). It should be noted that the exact solution of Devereux and de Bruyn (1963) exhibits abnormal behavior at the smallest separation distances. Usually, when $\psi_{o1} > \psi_{o2}$, the charge of the surface with the smaller (constant) potential reverses at very small separation distances ($\kappa x \leq 0.2$), resulting in attractive double layer energy. However, the exact double layer potential fluctuates and then increases to a very high repulsive value at small separations.

Despite the divergences from the exact solution, we used the Hogg *et al.* (1966) expression for this study because we were primarily interested in the relative change of ϕ_{dl} with solution chemistry than in absolute accuracy. However, the possible effect of the exact double layer potential on the interpretation of the detachment kinetics has also been considered in the Discussion.

Further error in the double layer potential may arise from the assumption that the charge on the surfaces of the colloids and grains is uniformly distributed, or "smeared out" (Verwey and Overbeek, 1948; Israelachvili, 1985). Actually, colloidal oxide surfaces are covered by patchy distributions of discrete surface charge. At the small separation distances involved in detachment (< 1 nm), the assumption of uniform surface charge may be particularly poor. Kostoglou and Karabelas (1992) solved the Poisson–Boltzmann equation in three dimensions to account for discrete charge and showed that discrete charge generated greater potential energy than uniform charge at all separation distances for the constant potential case.

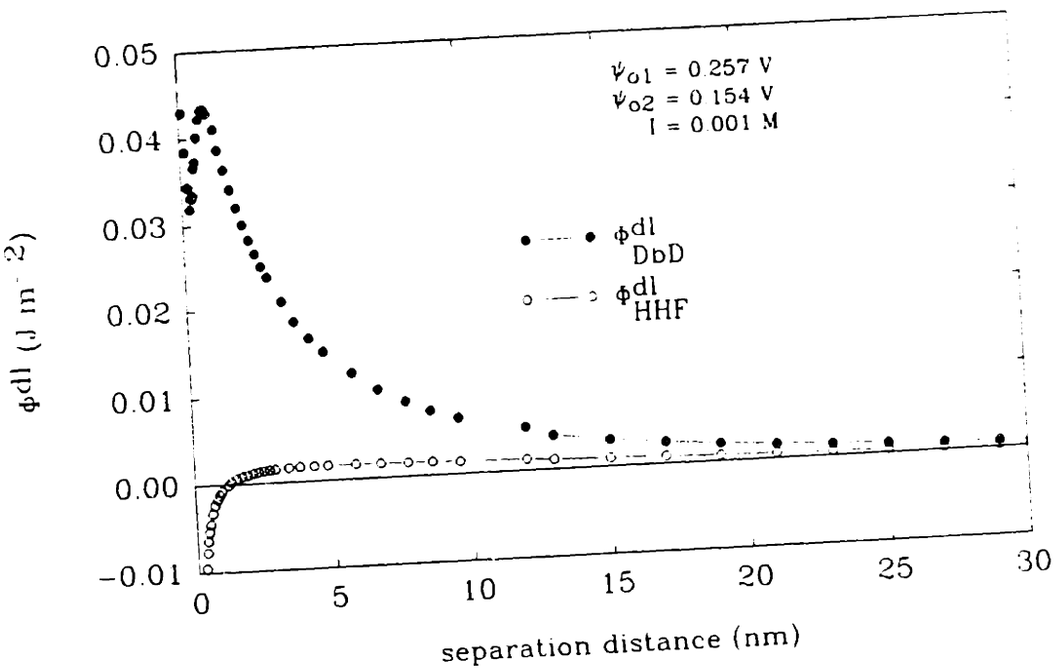

Fig. 3.2. Comparison of double layer potential energies (ϕ^{dl}) *vs.* separation distance for the interaction of two charged plates of surface potentials 0.257 and 0.154 V at $I = 0.001$ M. Double layer potential energies calculated by (1) exact (numerical) solution of the PB equation (Devereux and de Bruyn, 1963) designated ϕ^{dl}_{DbD} and (2) approximate solution of PB equation (Hogg *et al.*, 1966) designated ϕ^{dl}_{HHF}.

Surface Potentials

In most studies, zeta potentials (ζ) determined by electrokinetic measurements have been used as surface potentials (ψ_o); however, zeta potentials are insensitive to surface potentials at high surface charge and high I (Hunter, 1981). Furthermore, many researchers have not accounted for variations of I in the measurement of ζ. Estimates of surface potentials that are more sensitive to changes in surface charge and I may be obtained with surface complexation/double layer (SCDL) models (Levine and Smith, 1971, Yates *et al.*, 1974; Stumm *et al.*, 1976; Davis *et al.*, 1978).

Surface potentials may be determined for an interface described by a set of proton and hydroxide exchange reactions in the presence of a Gouy–Chapman double layer populated by indifferent counterions (Dzombak and Morel, 1990)

$$>M\text{–}OH_2^+ = >M\text{–}OH + H^+ \qquad K_{a1} = \frac{[>M\text{–}OH]\,[H^+]}{[>M\text{–}OH_2^+]} \qquad [3.23a]$$

$$>M\text{–}OH = >M\text{–}O^- + H^+ \qquad K_{a2} = \frac{[>M\text{–}O^-]\,[H^+]}{[>M\text{–}OH]} \qquad [3.23b]$$

where $>M$– is the surface metal center, $>M$–OH_2^+, $>M$–OH, and $>M$–O^- are the surface complexes, and K_{a1} and K_{a2} are the conditional equilibrium constants for the protonation reactions. The conditional equilibrium constants depend on the potential of the oxide surface:

$$K_{a1} = K_{a1}^{int} \exp\,(ze\psi_o/kT) \qquad [3.24a]$$

$$K_{a2} = K_{a2}^{int} \exp\,(ze\psi_o/kT) \qquad [3.24b]$$

where K_{a1}^{int} is the intrinsic acidity constant for $>M$–OH_2^+ and K_{a2}^{int} is the intrinsic acidity constant for $>M$–OH. The oxide surface charge per unit area σ_s (C m^{-2}) is given by

$$\sigma_s = \frac{N_a e}{S_s C_s}\{[>M\text{–}OH_2^+] - [>M\text{–}O^-]\} \qquad [3.25]$$

where S_s is the oxide specific surface area (m^2 g^{-1}) and C_s is the oxide suspension

concentration (g L^{-1}). The surface charge is related to surface potential in the Gouy–Chapman theory by

$$\sigma_s = [8\epsilon\epsilon_o N_a(1000)I\mathbf{k}T]^{0.5} \sinh (ze\psi_o/2\mathbf{k}T) \quad [3.26]$$

At the point of zero surface charge ($p\mathrm{H}_{zpc}$),

$$[>M\text{–}OH_2^+] = [>M\text{–}O^-] \quad [3.27]$$

so $p\mathrm{H}_{zpc}$ may be defined as

$$p\mathrm{H}_{zpc} = 0.5\ (pK_{a1}^{int} + pK_{a2}^{int}) \quad [3.28]$$

The surface potential is determined iteratively by solving for σ_s with initial estimates of $[>M\text{–}OH_2^+]$, $[>M\text{–}O^-]$, and ψ_o. ψ_o is determined with σ_s, and then the solution is repeated for new values of ψ_o until a consistent result is obtained (Dzombak and Morel, 1990).

METHODS

Review of Colloid Detachment Data

The kinetics of colloid detachment were measured in a series of model systems by Matijević and colleagues (Kolakowski and Matijević, 1979; Kuo and Matijević, 1979; 1980; Kallay and Matijević, 1981; Thompson *et al.*, 1984; Kallay *et al.*, 1986). From these studies, we extracted sets of experimental rate constants to compare with detachment energies calculated for the *p*H and *I* of the experiments. Other colloid detachment studies were not used because (1) parameters for modeling the colloid surface potentials were not readily identifiable (Clayfield and Lumb, 1966; 1970) or (2) hydrodynamic shear dominated colloid removal (Gotoh *et al.*, 1984; Hubbe, 1985; Sharma *et al.*, 1992).

Two types of colloid release data were examined: (1) ΔpH experiments, in which the *p*H of the flushing solution was increased by adding NaOH and (2) ΔI experiments, in which the flushing solution *I* was increased by adding $NaNO_3$, an indifferent electrolyte, at constant *p*H . Other experiments in which specifically–binding ions (*e.g.*, F^-, Ca^{2+}, Co^{2+}, ethylenediaminetetraacetic acid) were added to the flushing solution were not considered because the calculation of surface potential with the surface complexation model would require estimated unknown complexation constants for these ions.

Estimation of Detachment Rate Constants – When colloid release rate data were available, an initial experimental rate constant k^i_{exp} was calculated with this expression (Table 3.1):

$$k^i_{exp} = -\frac{1}{t} \ln \{[C_s]_t/[C_s]_0\} \qquad [3.29]$$

The initial experimental rate constant was determined for the sample time corresponding to removal of approximately half of the colloids ultimately removed, which usually was the first sample collected. When only the fraction of colloids

removed in a given time was reported (Kuo and Matijević, 1980; Thompson *et al.*, 1984; Kallay *et al.*, 1986), an overall experimental release rate k^{o}_{exp} was estimated (Table 3.1). In some cases, the overall colloid release rate had been interpreted as a combination of release from two site types, rapid and slow (Kallay and Matijević, 1981; Thompson *et al.*, 1984). Only the rapid release rates were considered in our study.

Surface Potentials – In most studies, zeta potentials (ζ) determined by electrokinetic measurements have been used as surface potentials (ψ_0) in calculating ϕ^{dl}; however, ζ–potentials are insensitive to ψ_0 at high surface charge and high I (Hunter, 1981; Dzombak and Morel, 1990). Furthermore, measurements of ζ–potential were not made at all conditions of ionic strength for which they were applied in some studies. We used both ζ–potentials and surface potentials obtained with a surface complexation/double layer model (ψ_{scdl}) to calculate ϕ^{dl}.

Electrophoretic mobilities measured by Matijević and colleagues were converted to ζ–potentials using the Henry (1931) formula. They measured ζ–potentials over the range of *p*H values used in the experiments; however, their measurements did not cover the range of ionic strengths to which the ζ–potentials were applied.

The surface complex reactions were iteratively solved with a version of MINEQL (Westall *et al.*, 1976) adapted to account for Gouy–Chapman double layer interactions (Dzombak and Morel, 1990). Parameters used to calculate ψ_{scdl} included the total site density $[>M\text{–OH}]_{tot}$, the intrinsic acidity constants pK^{int}_{a1} and pK^{int}_{a2}, and the the specific surface area S_s and suspension concentration χ_s of the oxide (Table 3.2). For oxides similar to those used in these studies (glass, SiO_2·*am*; hematite, α–Fe_2O_3; akaganéite, β–FeOOH), adsorption of H^+ and OH^- indicate a site density range of about 3 to 8 sites nm^{-2} (James and Parks, 1982). We used 4 sites nm^{-2} for all of the oxide surfaces in these experiments.

Table 3.1. Summary of solution composition, surface potential, and kinetic data for colloid detachment in model systems of Matijević and colleagues and hematite—quartz system of this study.

colloid grain experiment (ref.)	pH	$NaNO_3$	I	colloid ζ	colloid ψ_{scdl}	grain ζ	grain ψ_{scdl}	initial(i) or overall(o) rate constant
		M	M	mV	mV	mV	mV	s^{-1}
$Cr(OH)_3$	9.6		$4.0 \cdot 10^{-5}$	–32	–81.8	–18	–191	$7.46 \cdot 10^{-6}$(i)
glass	10.3		$2.0 \cdot 10^{-4}$	–37	–119	–48	–204	$9.87 \cdot 10^{-5}$
ΔpH	11.0		$1.0 \cdot 10^{-3}$	–45	–147	–89	–216	$1.48 \cdot 10^{-4}$
(1)	11.5		$3.2 \cdot 10^{-3}$	–47	–159	–137	–221	$4.56 \cdot 10^{-4}$
	12.6		$4.0 \cdot 10^{-2}$	—	–173	—	–203	$2.41 \cdot 10^{-4}$
$Cr(OH)_3$	11.5		$3.2 \cdot 10^{-3}$	–47	–159	–137	–221	$4.56 \cdot 10^{-4}$(i)
glass	11.5	$2.0 \cdot 10^{-2}$	$2.3 \cdot 10^{-2}$	—	–142	—	–197	$2.59 \cdot 10^{-4}$
ΔI	11.5	$4.0 \cdot 10^{-2}$	$4.3 \cdot 10^{-2}$	—	–137	—	–187	$1.77 \cdot 10^{-4}$
(1)	11.5	$1.0 \cdot 10^{-1}$	$1.0 \cdot 10^{-1}$	—	–128	—	–172	$5.92 \cdot 10^{-5}$
	11.5	$2.0 \cdot 10^{-1}$	$2.0 \cdot 10^{-1}$	—	–121	—	–159	$2.19 \cdot 10^{-5}$
$Cr(OH)_3$	9.5		$3.2 \cdot 10^{-5}$	—	–76.1	—	–157	$2.62 \cdot 10^{-6}$(i)
steel	11.0		$1.0 \cdot 10^{-3}$	–52	–147	–42	–186	$8.00 \cdot 10^{-5}$
ΔpH	11.3		$2.0 \cdot 10^{-3}$	–53	–155	–42	–191	$1.06 \cdot 10^{-4}$
(2)	11.7		$5.0 \cdot 10^{-3}$	–54	–163	–42	–196	$1.45 \cdot 10^{-4}$
	12.3		$2.0 \cdot 10^{-2}$	–52	–172	–41	–199	$1.91 \cdot 10^{-4}$
	12.6		$4.0 \cdot 10^{-2}$	—	–173	—	–194	$1.89 \cdot 10^{-4}$
	12.8		$6.3 \cdot 10^{-2}$	–41	–172	–41	–188	$1.02 \cdot 10^{-5}$
α—Fe_2O_3	10.5		$3.2 \cdot 10^{-4}$	–48	–158	–41	–176	$6.00 \cdot 10^{-6}$(o)
steel	11.3		$2.0 \cdot 10^{-3}$	–50	–178	–41	–190	$2.09 \cdot 10^{-5}$
ΔpH	11.7		$5.0 \cdot 10^{-3}$	–49	–185	–40	–196	$2.27 \cdot 10^{-5}$
(3)	12.1		$1.3 \cdot 10^{-2}$	–49	–189	–40	–199	$2.16 \cdot 10^{-5}$
	12.8		$6.3 \cdot 10^{-2}$	–48	–184	–40	–188	$4.96 \cdot 10^{-5}$
α—Fe_2O_3	9.0		$1.0 \cdot 10^{-5}$	—	–82.3	–40	–150	$7.94 \cdot 10^{-7}$(i)
steel	10.0		$1.0 \cdot 10^{-4}$	–46	–137	–41	–170	$3.64 \cdot 10^{-6}$
ΔpH	10.3		$2.0 \cdot 10^{-4}$	–47	–150	–41	–175	$6.51 \cdot 10^{-6}$
(4)	10.6		$4.0 \cdot 10^{-4}$	–48	–161	–41	–181	$1.49 \cdot 10^{-5}$
	10.8		$6.3 \cdot 10^{-4}$	–49	–167	–41	–185	$2.59 \cdot 10^{-5}$
	11.3		$2.0 \cdot 10^{-3}$	–50	–177	–41	–191	$1.24 \cdot 10^{-5}$
	11.6		$4.0 \cdot 10^{-3}$	–49	–184	–40	–198	$1.16 \cdot 10^{-5}$
	12.6		$4.0 \cdot 10^{-2}$	–49	–188	–40	–194	$7.94 \cdot 10^{-7}$

Table 3.1. Continued.

colloid grain experiment (ref.)	*p*H	$NaNO_3$	*I*	colloid		grain		initial(i) or overall(o) rate constant
				ζ	ψ_{scdl}	ζ	ψ_{scdl}	
		M	M	mV	mV	mV	mV	s^{-1}
β–FeOOH	10.2		$1.6 \cdot 10^{-4}$	—	−175	—	−140	$1.02 \cdot 10^{-5}$(o)
steel	10.3		$2.0 \cdot 10^{-4}$	—	−179	—	−142	$2.42 \cdot 10^{-5}$
ΔpH	10.8		$6.3 \cdot 10^{-4}$	—	−192	—	−151	$3.14 \cdot 10^{-5}$
(5)	11.4		$2.5 \cdot 10^{-3}$	—	−203	—	−162	$4.64 \cdot 10^{-5}$
	11.6		$4.0 \cdot 10^{-3}$	—	−205	—	−166	$3.88 \cdot 10^{-5}$
	12.0		$1.0 \cdot 10^{-2}$	—	−208	—	−172	$6.41 \cdot 10^{-5}$
	12.5		$3.2 \cdot 10^{-2}$	—	−202	—	−176	$5.03 \cdot 10^{-5}$
	12.8		$6.3 \cdot 10^{-2}$	—	−191	—	−175	$1.36 \cdot 10^{-5}$
β–FeOOH	11.4		$2.5 \cdot 10^{-3}$	—	−203	—	−162	$4.64 \cdot 10^{-5}$(o)
steel	11.4	$2.0 \cdot 10^{-2}$	$2.3 \cdot 10^{-2}$	—	−180	—	−143	$3.14 \cdot 10^{-5}$
ΔI	11.4	$5.0 \cdot 10^{-2}$	$5.3 \cdot 10^{-2}$	—	−170	—	−135	$2.24 \cdot 10^{-5}$
(5)	11.4	$1.0 \cdot 10^{-1}$	$1.0 \cdot 10^{-1}$	—	−160	—	−128	$8.44 \cdot 10^{-6}$
α–Fe_2O_3	9.6		$4.0 \cdot 10^{-5}$	—	−139	—	−191	$2.51 \cdot 10^{-5}$(o)
glass	10.2		$1.4 \cdot 10^{-4}$	—	−164	—	−201	$2.18 \cdot 10^{-4}$
ΔpH	10.5		$2.8 \cdot 10^{-4}$	—	−174	—	−206	$2.07 \cdot 10^{-4}$
(6)	10.6		$3.6 \cdot 10^{-4}$	—	−177	—	−208	$2.87 \cdot 10^{-4}$
	11.2		$1.6 \cdot 10^{-3}$	—	−192	—	−218	$3.40 \cdot 10^{-4}$
α–Fe_2O_3	9.6	$1.0 \cdot 10^{-4}$	$1.4 \cdot 10^{-5}$	—	−136	—	−180	$3.05 \cdot 10^{-5}$(o)
glass	9.6	$2.0 \cdot 10^{-3}$	$2.0 \cdot 10^{-3}$	—	−125	—	−156	$2.77 \cdot 10^{-5}$
ΔI	9.6	$5.0 \cdot 10^{-3}$	$5.1 \cdot 10^{-3}$	—	−119	—	−149	$1.14 \cdot 10^{-4}$
(6)	9.6	$1.0 \cdot 10^{-2}$	$1.0 \cdot 10^{-2}$	—	−114	—	−143	$1.75 \cdot 10^{-4}$
	9.6	$3.2 \cdot 10^{-2}$	$3.2 \cdot 10^{-2}$	—	−106	—	−133	$2.87 \cdot 10^{-4}$
	9.6	$5.0 \cdot 10^{-2}$	$5.0 \cdot 10^{-2}$	—	−102	—	−128	$2.78 \cdot 10^{-4}$
α–Fe_2O_3	7.0	$1.0 \cdot 10^{-3}$	$1.0 \cdot 10^{-3}$	—	+54.7	—	−99.0	0
quartz	11.0		$1.0 \cdot 10^{-3}$	—	−154	—	−248	$5.23 \cdot 10^{-5}$(i)
ΔI	11.0	$2.0 \cdot 10^{-3}$	$3.0 \cdot 10^{-3}$	—	−146	—	−235	$4.02 \cdot 10^{-5}$
(*)	11.0	$9.0 \cdot 10^{-3}$	$1.0 \cdot 10^{-2}$	—	−136	—	−217	$2.47 \cdot 10^{-5}$
	11.0	$2.9 \cdot 10^{-2}$	$3.0 \cdot 10^{-2}$	—	−127	—	−199	$6.99 \cdot 10^{-6}$
	11.0	$9.9 \cdot 10^{-2}$	$1.0 \cdot 10^{-1}$	—	−116	—	−174	$4.57 \cdot 10^{-6}$

(—) data not provided.

(1) Kolakowski and Matijević (1979).
(2) Kuo and Matijević (1979).
(3) Kuo and Matijević (1980).
(4) Kallay and Matijević (1981).
(5) Thompson *et al.* (1984).
(6) Kallay *et al.* (1986).
(*) this study.

Table 3.2. Parameters used in the calculation of surface potential with a surface complexation/double layer model. The techniques by which the parameters were measured or estimated are listed below the table.

colloid or grain	mean diameter	pH_{zpc}	ΔpK^{int}	S_S	χ_S	ref.
	μm			$m^2\ g^{-1}$	$g\ L^{-1}$	
$Cr(OH)_3$	0.28	8.2	3.0	75	0.88	(1)
	0.28	8.2	3.0	75	0.19	(2)
α—Fe_2O_3	0.17	7.6	3.0	75	0.028	(3)
	0.19	7.6	3.0	75	0.69	(4)
	0.13	7.6	3.0	75	0.69	(6)
	0.15	8.0	3.0	75	2.6	(*)
β—FeOOH	0.25x0.02‡	7.0	3.0	75	0.50†	(5)
glass	53	2.5	9.0	0.2	1800	(1)
$SiO_2 \cdot am$	110	2.5	9.0	0.2	5300	(6)
steel	53	5.0	7.6	0.2	2700	(2)
	53	5.0	7.6	0.2	6100	(3)
	53	5.0	7.6	0.2	5200	(4)
	93	5.8	7.6	0.2	3000†	(5)
quartz	250	2.5	9.0	0.1	1500	(*)

mean diameter: SEM, PCS, sieving; (‡) length and width of non—spherical colloids.
pH_{zpc}: microelectrophoresis; quartz (Parks, 1965).
ΔpK^{int}: estimated for $SiO_2 \cdot am$ (Schindler and Gamsjager, 1972); iron oxides (Sigg and Stumm, 1981; James and Parks, 1982).
S_S: estimated from BET specific surfaces area (James and Parks, 1982) and suppliers' data.
χ_C: estimated from colloid and grain size, number concentration, specific density, and column volume and porosity data; (†) estimated; data not provided.

(1) Kolakowski and Matijević (1979).
(2) Kuo and Matijević (1979).
(3) Kuo and Matijević (1980).
(4) Kallay and Matijević (1981).
(5) Thompson *et al.* (1984).
(6) Kallay *et al.* (1986).
(*) this study.

The intrinsic acidity constants were estimated by centering ΔpK^{int}, the difference between values of pK_{a1}^{int} and pK_{a2}^{int}, on the point of zero charge (pH_{zpc}) determined by microelectrophoresis. Approximate ΔpK^{int} values for Fe_2O_3, FeOOH, and SiO_2 were obtained from intrinsic acidity constants determined by acid–base titrations for similar oxides (Schindler and Gamsjager, 1972; Sigg and Stumm, 1981; James and Davis, 1982). The steel grains were modeled as mainly >Fe–OH sites with Cr (19%) and Ni (12%) impurities (Kuo and Matijević, 1979). Instead of simply using the iron oxide ΔpK^{int} for steel, the steel ΔpK^{int} was expanded because the pH_{zpc} values of Cr and Ni hydrous oxides (-7 and -11 respectively; Parks, 1965) bracket the pH_{zpc} of Fe oxides (-8; Parks, 1965). The steel ΔpK^{int} was fit by matching calculated values of ψ_{scdl} with ζ measured at low surface potential and low I (near the steel pH_{zpc} of 5.0 or 5.8). For the $Cr(OH)_3$, we used the same ΔpK^{int} and S_s as for the iron oxides.

Calculation of Detachment Energies – The total potential energy was calculated with separation distance resolutions of $\Delta x = 1 \cdot 10^{-11}$ m in the vicinity of ϕ_{min1} and ϕ_{max} and $\Delta x = 1 \cdot 10^{-10}$ m near ϕ_{min2}. We chose a value of A ($1 \cdot 10^{-20}$ J) within the range of Hamaker constants commonly observed for oxides and used it for each oxide. The Born collision parameter was chosen as $\sigma = 5 \cdot 10^{-10}$ m. Both ζ–potentials and ψ_{scdl} were used to calculate ϕ^{dl}, resulting in two $\phi(x)$ profiles for most experiments.

From each of these profiles, two detachment energies were calculated to compare the energy barrier model with the equilibrium model. For the energy barrier model, ϕ^{det} was calculated as $-(\phi_{max}-\phi_{min1})$ as in Eqn. 3.5. For the equilibrium model, ϕ^{det} was calculated as $-(\phi_{min2}-\phi_{min1})$ as in Eqn. 3.17.

Experimental Materials and Methods

Detachment of hematite colloids from quartz grains was studied in a short, wide flow–through column. The spherical hematite colloids were prepared by aging a 0.018 M $FeCl_3$ and 0.001 M HCl solution at 100° C for 24 hr (Matijević and Scheiner, 1978) in polyethylene bottles and were stored at room temperature until used in the experiments. The hydrodynamic size of the colloids was determined to be 0.15 ± 0.04 μm by photon correlation spectroscopy (PCS; Coulter N4) and cumulants analysis of the autocorrelation function. The isoelectric point of the hematite colloids in $1 \cdot 10^{-3}$, $1 \cdot 10^{-2}$, and $1 \cdot 10^{-1}$ M $NaNO_3$ solutions was *p*H 8.0 ± 0.1, as determined by microelectrophoresis (Rank Bros. MkII, cylindrical cell, 3 mW He–Ne laser). Suspension concentrations were determined by light scattering at 90° (turbidimetry; Hach Ratio X/R). A linear relationship was observed between scattering intensity (NTU) and hematite colloid concentration (H; mg L^{-1}) trapped on 0.02 μm Anotec filters ($H = [\text{NTU} - 0.004]/0.207$; $R^2 = 0.9973$).

The subrounded quartz sand grains (Aldrich Chemical Co., Inc., 50 to 70 mesh) ranged from 210 to 300 μm diameter. They were heated at 450° C for 6 hr and soaked in 1.0 N HNO_3 overnight to remove organic matter and other surface impurities, rinsed with deionized water, and dried before experiments.

The hematite colloids were attached to quartz grains by vigorously shaking 1 mL of the hematite suspension with 5.00 g quartz in 20 mL of a $1 \cdot 10^{-4}$ M HNO_3 solution for 30 min. The hematite–quartz suspension was washed three times with the $1 \cdot 10^{-4}$ M HNO_3 solution and stored 16 to 20 hr in $1 \cdot 10^{-4}$ M HNO_3 solution before experiments.

The hematite–coated quartz grains were transferred with deionized water (*p*H ≈ 6.5) to a 47 mm Millipore Swinnex filter holder containing a 0.22 μm Millipore membrane filter, a nylon screen (120 mesh) on the inlet end, and a nylon screen on the outlet end. A 40 mm diameter Viton O–ring surrounded the grains.

Flushing solutions were purged with Ar prior to being adjusted to *p*H 11.0 and pumped upward through the column with an HPLC pump. The solution reservoir was flushed with Ar during the experiment. Experiments testing the deposition of hematite colloids to uncoated quartz grains in the column showed that flow was evenly distributed across the diameter of the column.

In preliminary detachment tests, flushing at 1.0 ml min^{-1} with a *p*H 7.0, $I = 1 \cdot 10^{-3}$ M solution did not remove colloids from the column. Flushing with *p*H 10.0, $I = 1 \cdot 10^{-4}$ M solutions removed a maximum of only 1% of the total colloids. Thus, the remainder of the experiments were conducted at *p*H 11.0 to raise the colloid concentration in the effluent.

The flushing solution I was varied in the first detachment experiment (ΔI). Solutions of *p*H 11.0 and I from $1 \cdot 10^{-3}$ to $1 \cdot 10^{-1}$ M were run through columns at a flow rate of 1.0 ± 0.05 ml min^{-1}. The *p*H and I were adjusted with NaOH and $NaNO_3$. Flow rate was varied in the second detachment experiment (ΔQ_{col}). Solutions of *p*H 11 ($1 \cdot 10^{-3}$ M NaOH) were pumped through the column at flow rates ranging from 0.51 to 11.7 ml min^{-1} (pore velocities of 1.5 to 34 m d^{-1}).

Detached colloids were collected in glass vials or flasks, diluted if necessary, inverted five times to mix, sonicated for 5 s to purge bubbles, and quantified by turbidity. The experiments were stopped when the scattering intensity of the effluent fell below that of 0.22 μm–filtered deionized water (0.030 ± 0.010 NTU). Colloid size in the effluent was monitored by PCS during some experiments in 600 s analyses.

The concentrations of hematite colloids remaining in the columns were measured by turbidity after twice sonicating the residual grains in a polycarbonate tube filled with a known volume of $1 \cdot 10^{-3}$ M NaOH solution for 10 min. The colloid concentration was corrected for the presence of quartz colloids suspended during sonication by subtracting the scattering intensity of sonicated quartz grain blanks.

The amount of colloids remaining in the column and colloids in the column effluent always matched the total amount of colloids added to the quartz grains within 5%.

After some experiments, residual grains coated with Au–Pd were examined with scanning electron microscopy and energy–dispersive x–ray spectroscopy (SEM/EDX; Cambridge Stereoscan 240, Link Analytical).

The results of the colloid detachment experiments are expressed as the fraction of colloid mass remaining in the column at time t to initial total colloid mass. To account for the delay in colloid release caused by the presence of colloid–free water initially in the column, the experimental times were adjusted by subtracting the time required to flush one pore volume. The column pore volume was estimated as

$$V_{\text{pore}} = (h_{\text{col}}\ \pi R_{\text{col}}^2) - (m_{\text{g}}/\rho_{\text{g}}) \qquad [3.30]$$

where the column radius R_{col} was 2.0 cm, the column height h_{col} ranged from 0.25 to 0.30 cm, the mass of solid m_{g} was 5.00 g, and the solid density ρ_{g} was assumed to be 2.65 g cm^{-3}.

Initial experimental rate constants were evaluated as they were for the data of Matijević and colleagues. Detachment energies were estimated in the same manner outlined for the data of Matijević and colleagues using ψ_{scdl} calculated with the parameters in Table 3.2 as the surface potentials.

RESULTS

Detachment Rate – Energy Relationship

To determine if either the energy barrier or equilibrium model were consistent with the observed rate constants, we checked for direct relationships between log k_{exp} and $\phi^{det}/\mathbf{k}T$ as described by Eqns. 3.5 and 3.17.

For the ΔpH experiments, the rate constants appeared to be independent of both forms of ϕ^{det} when ζ–potential was used as ψ_0 (Fig. 3.3a and 3.3b). The ζ–potentials measured by Matijević and colleagues did not vary much with pH (Table 3.1). The small variations of the ζ–potentials led to the small variations in ϕ^{det} with pH. The potentials at the shear plane where ζ–potential is measured were relatively invariant because the increase of ionic strength with pH compressed the double layer and masked the effect of the increase in surface charge with pH. In contrast, when ψ_{scdl} was used as ψ_0, the rate constants were positively correlated to both forms of ϕ^{det} (Fig. 3.3c). The correlations were not always good because of the very low rate constants measured at the lowest pH values (when repulsion was low because surface potentials were low) and at the highest pH values (when repulsion was low because ionic strength was high).

For the Fe_2O_3–glass ΔI experiment, the rate constants appeared independent of both forms of ϕ^{det} when ζ–potentials were used as ψ_0 (Fig. 3.4). For all ΔI experiments, using ψ_{scdl} as ψ_0 produced revealing, but contradictory, results. For the $Cr(OH)_3$–glass and FeOOH–steel systems, the rate constants were positively correlated to the equilibrium ϕ^{det}, but negatively correlated to the energy barrier ϕ^{det}. For the Fe_2O_3–glass system, the rate constants were positively correlated to the energy barrier ϕ^{det}, but negatively correlated to the equilibrium ϕ^{det}.

Experimental Results

In the hematite–quartz system, a maximum of about 7% of the colloids were removed by the *p*H 11.0 solutions. SEM/EDX examination of the quartz surfaces after flushing showed that the hematite colloids were primarily situated in rough, weathered areas (Fig. 3.5). Quantitation of the Fe peak areas observed on 10 quartz grains revealed that the weathered areas contained 4.1 ± 1.4 mol% (± 1σ)and that the smooth areas contained 1.4 ± 0.7 mol% (with Fe, Si, and K peaks corrected for the presence of Au and Pd). Individual colloids could not be resolved by SEM, probably because the insulating quartz was poorly coated with Au–Pd.

The size of hematite colloids in the column effluent, as measured by PCS, ranged between 100 and 200 nm. This indicates that single colloids were detached from quartz surfaces and that colloids did not coagulate after release, even at $I = 0.1$ M. If the colloids emerged from the column as aggregates rather than as singlets, the scattering intensity – colloid concentration relationship would not be valid.

The increase in I had two effects on colloid detachment (Fig. 3.6): (1) the initial detachment rate decreased (Table 3.1) and (2) the total fraction of colloids released decreased. The rate constants were positively correlated with the equilibrium ϕ^{det} and negatively correlated with the energy barrier ϕ^{det} (Fig. 3.7). In the potential energy profiles for three values of I (Fig. 3.8), the decrease in the size of the energy barrier (ϕ_{max}–ϕ_{min1}) and the decrease in the energy difference (ϕ_{min2}–ϕ_{min1}) with increasing I are evident. The potential energy profile for *p*H 7.0, also shown in Fig. 3.8, is attractive at all separation distances, corresponding to the lack of colloid release at *p*H 7.0.

The increase in flow rate increased the initial detachment rate (Fig. 3.9). The rate constants and fractions of colloids remaining are listed in Table 3.3. The range of the fraction remaining, 0.928 to 0.948, is within 1σ of the mean total

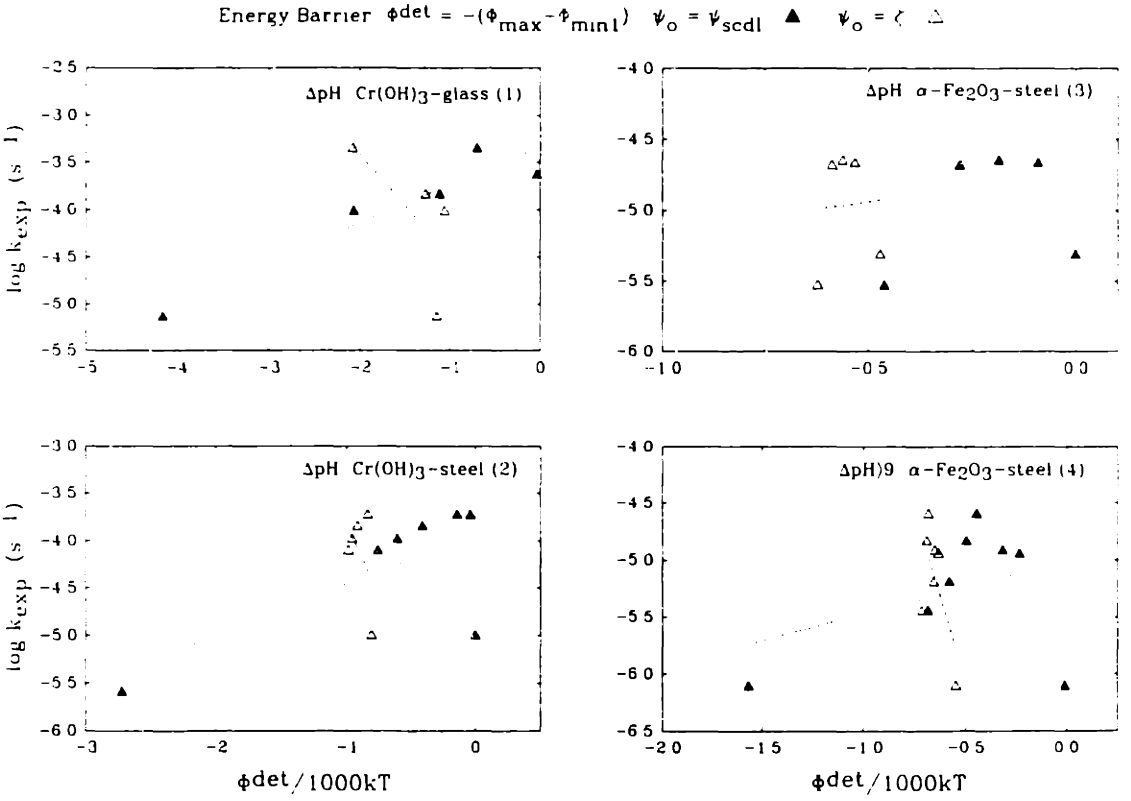

Fig. 3.3a. Plots of initial and overall experimental rate constants (log k_{exp}) *vs.* the energy barrier detachment energies ($\phi^{det}/1000\mathbf{k}T$) for the colloid release experiments of Matijević and c leagues in which *p*H was varied. Detachment energies were estimated with ζ–potentials and surface potentials calculated with a surface complex/double layer (ψ_{scdl}). Numbers in parentheses following colloid–grain system refer to references listed in Table 3.1.

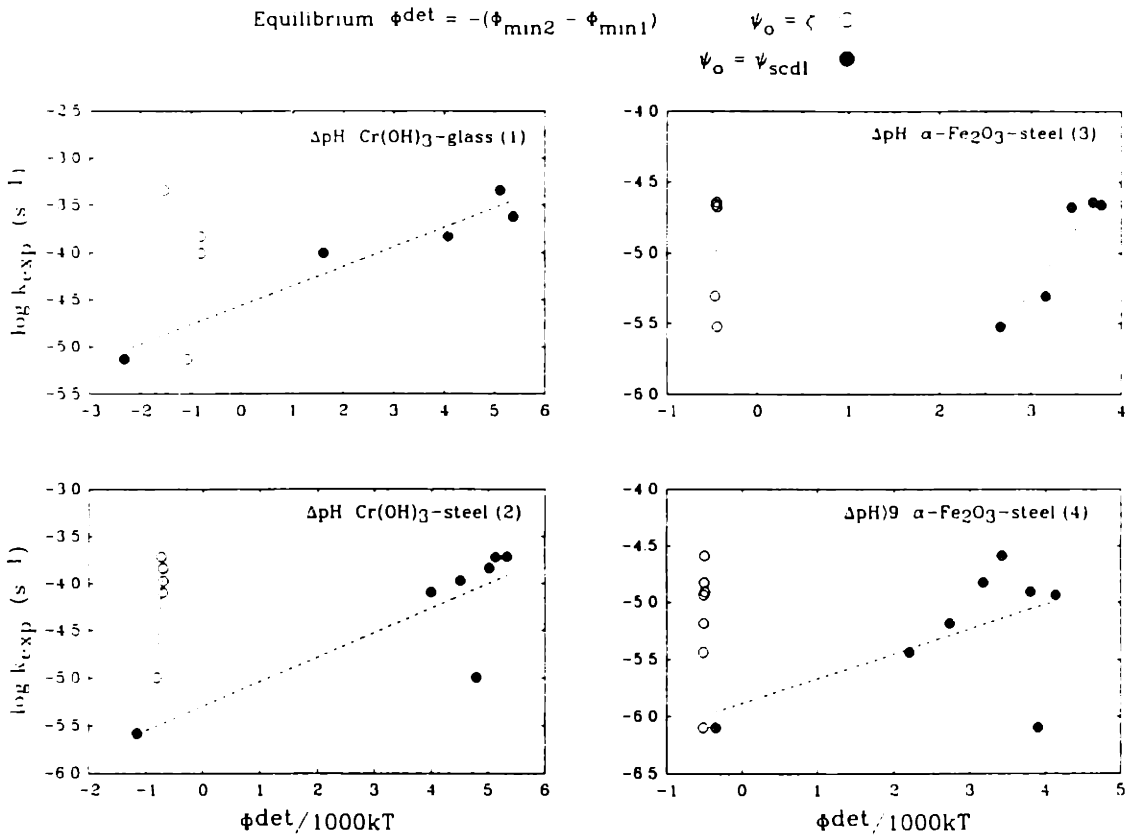

Fig. 3.3b. Plots of initial and overall experimental rate constants (log k_{exp}) *vs.* the equilibrium detachment energies (ϕ^{det}/1000kT) for the colloid release experiments of Matijević and colleagues in which *p*H was varied. Detachment energies were estimated with ζ–potentials and surface potentials calculated with a surface complex/double layer (ψ_{scdl}). Numbers in parentheses following colloid–grain system refer to references listed in Table 3.1.

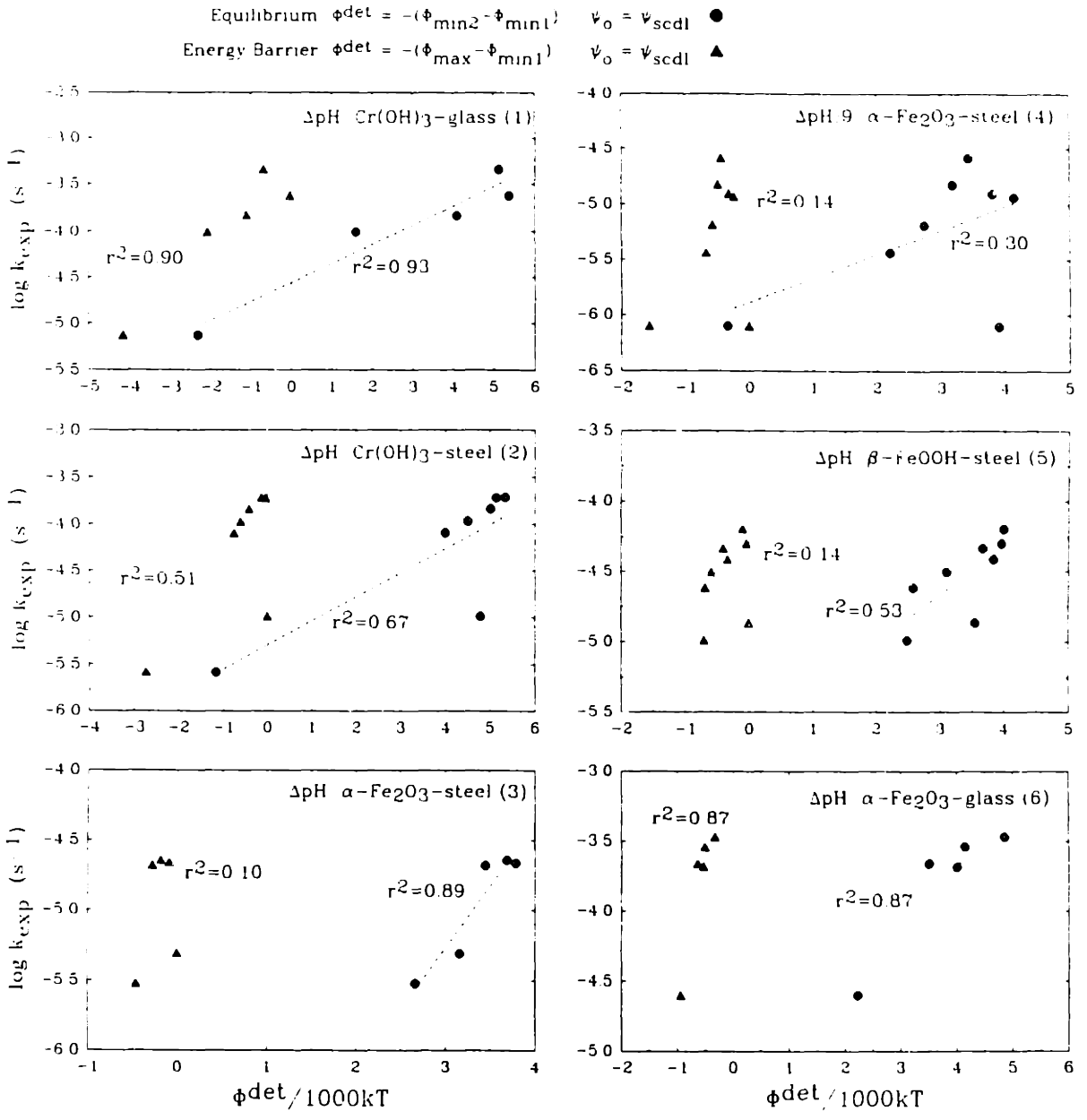

Fig. 3.3c. Plots of initial and overall experimental rate constants (log k_{exp}) *vs.* the energy barrier and equilibrium detachment energies (ϕ^{det}/1000kT) for the colloid release experiments of Matijević and colleagues in which *p*H was varied. Detachment energies were estimated with surface potentials calculated with a surface complex/double layer (ψ_{scdl}). Numbers in parentheses following colloid–grain system refer to references listed in Table 3.1.

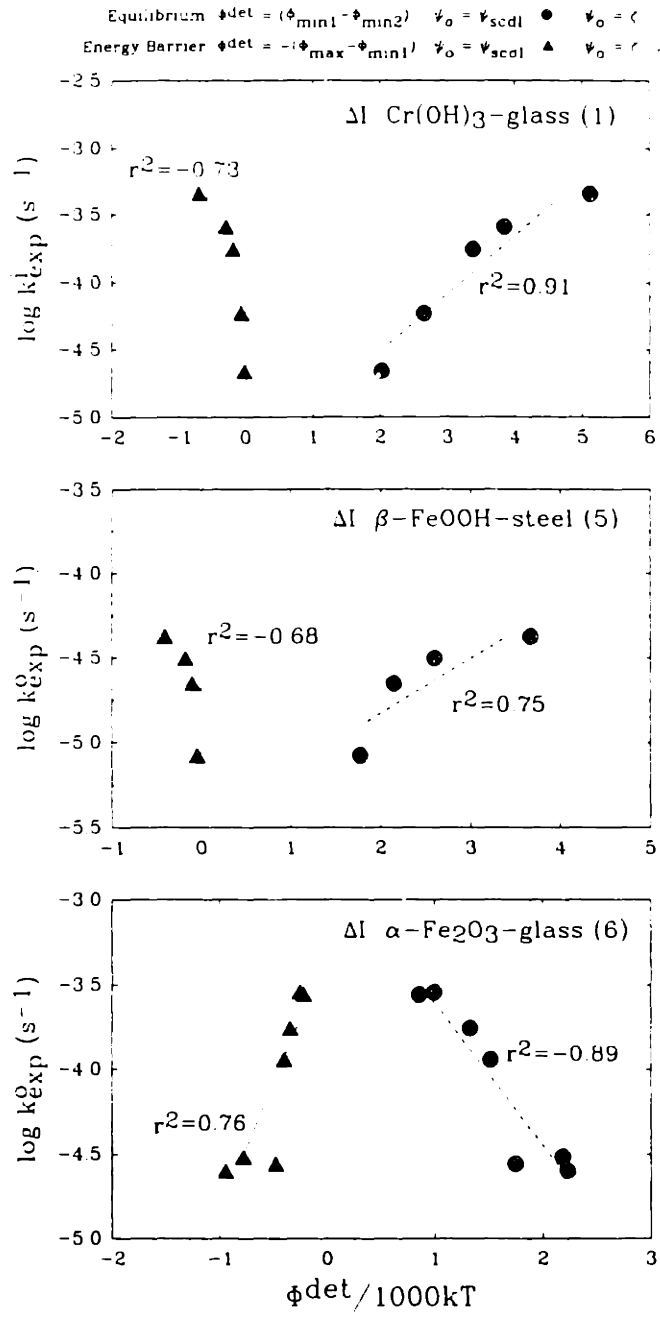

Fig. 3.4. Plots of initial and overall experimental rate constants (log k_{exp}) *vs.* the energy barrier and equilibrium detachment energies (ϕ^{det}/1000kT) for the colloid release experiments of Matijević and colleagues in which I was varied. See Fig. 3.3 for descriptions.

Fig. 3.5 is shown on the following page.

Fig. 3.5. SEM of a quartz grain following the removal of 7.2% of the originally attached colloids by 100 pore volumes of *p*H 11.0, $I = 1 \cdot 10^{-3}$ M flush solution at 0.51 ml min^{-1}. EDX spectra measured over ~4 μm^2 areas show that hematite colloids were more abundant on the weathered, irregular surface than on the smooth surface. Similar results were observed on nine other quartz grains.

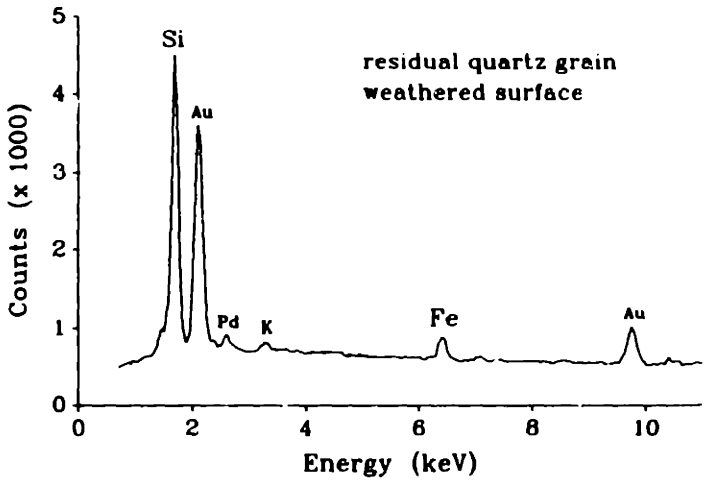
Si
Au
Pd
K
Fe
Au
residual quartz grain
weathered surface
Counts (x 1000)
Energy (keV)
0
1
2
3
4
5
0
2
4
6
8
10

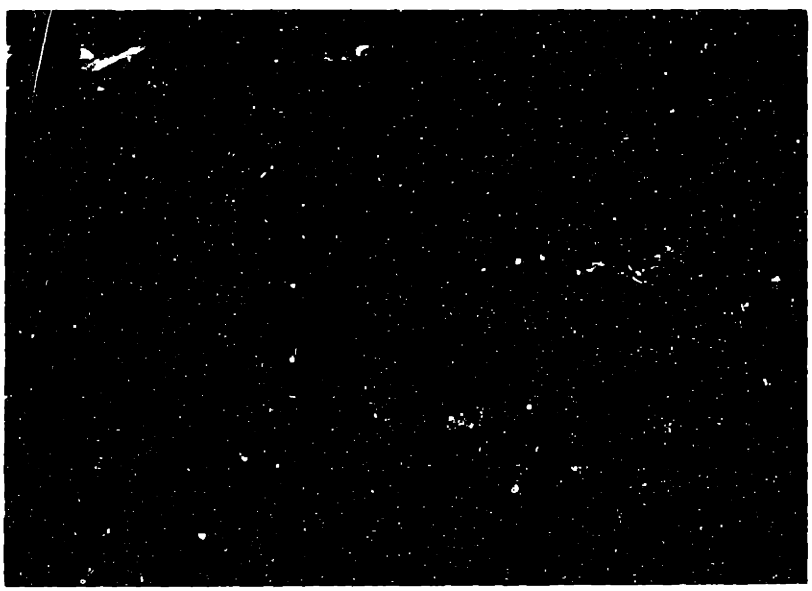

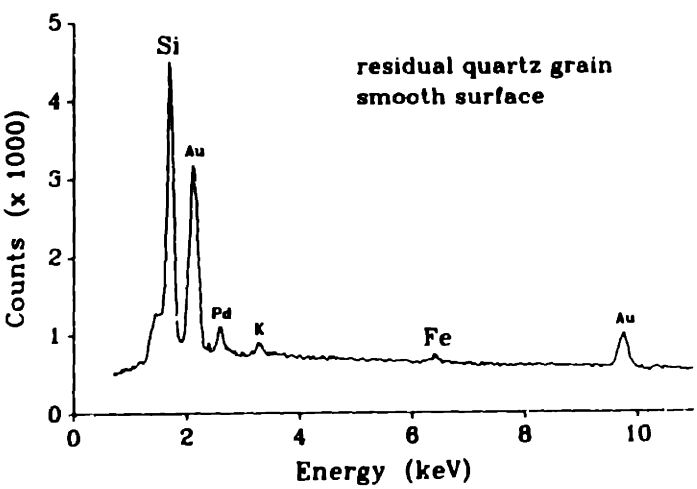
Si
Au
Pd
K
Fe
Au
residual quartz grain
smooth surface
Counts (x 1000)
Energy (keV)
0
1
2
3
4
5
0
2
4
6
8
10

fraction released, 0.940 ± 0.010. The total fraction of colloids released was not related to the variation in flow rate. The ΔQ data were fit by first–order exponential decay to show that the fraction remaining at the end of the experiment was similar to the fitted fraction remaining at equilibrium (C_{eq}). The fitted first order rate constants (k_{fit}) were about 20 to 30 times greater than k_{exp}. We surmise that k_{fit} was greater than k_{exp} because k_{fit} was sensitive to colloid diffusive transport at longer times.

A logarithmic plot of the initial rate constants *vs.* the double layer thickness calculated with Eqn. 3.14 as a function of increasing flow rate shows that $k^{i}_{exp} \propto \delta_{bl}^{-2.39}$, reasonably close to the relationship proposed in Eqn. 3.17 (Fig. 3.10).

Table 3.3. Initial rate constants and total fractions of colloids released in ΔQ experiments at *p*H 11.0 and $I = 1 \cdot 10^{-3}$ M.

flow rate Q	initial rate const k_{exp}	fitted* rate const k_{fit}	final fraction remaining	fitted* fraction remaining C_{eq}
ml min^{-1}	s^{-1}	s^{-1}		
0.51	$4.8 \cdot 10^{-5}$	$8.9 \pm 0.4 \cdot 10^{-4}$	0.928	0.930±0.001
0.98	$5.2 \cdot 10^{-5}$	$1.3 \pm 0.1 \cdot 10^{-3}$	0.948	0.949±0.001
1.9	$9.2 \cdot 10^{-5}$	$2.6 \pm 0.1 \cdot 10^{-3}$	0.941	0.941±0.001
3.2	$1.8 \cdot 10^{-4}$	$4.6 \pm 0.3 \cdot 10^{-3}$	0.939	0.940±0.001
7.3	$3.1 \cdot 10^{-4}$	$8.6 \pm 0.2 \cdot 10^{-3}$	0.947	0.948±0.001
11.7	$4.3 \cdot 10^{-4}$	$1.1 \pm 0.1 \cdot 10^{-2}$	0.936	0.944±0.001
11.7	$3.8 \cdot 10^{-4}$	$1.2 \pm 0.1 \cdot 10^{-2}$	0.941	0.939±0.001

*fitted rate constant (k_{fit}) and fraction remaining (C_{eq}) and standard errors determined by fitting data according to this equation:

$$C_t - C_{eq} = (C_0 - C_{eq}) \exp(-k_{fit} t)$$

where C_t is the fraction remaining at time t and C_0 is the fraction remaining at $t = 0$ ($C_0 = 1$).

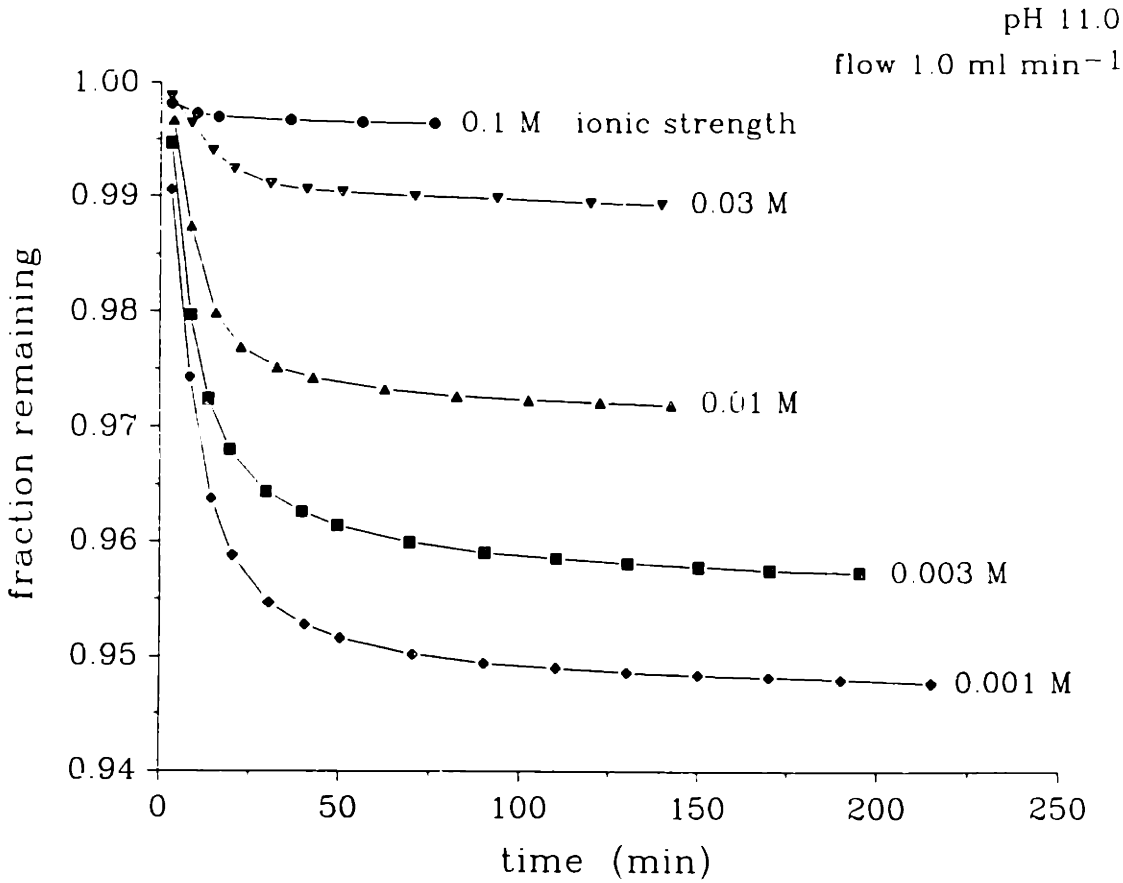

Fig. 3.6. Plot of the fraction of hematite colloids remaining attached to quartz grains *vs.* time for *p*H 11.0, $I = 1 \cdot 10^{-3}$ M flushing solution.

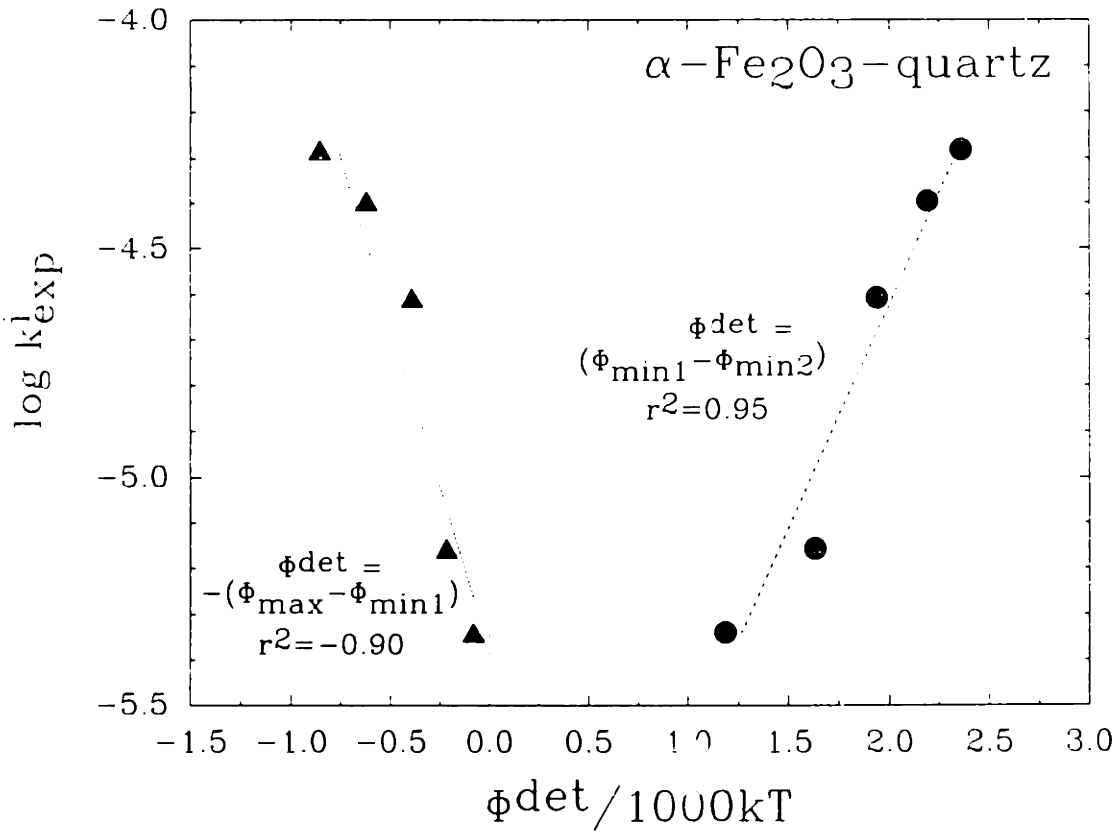

Fig. 3.7. Logarithmic plots of initial experimental rate constants (k^{i}_{exp}) *vs.* the energy barrier and equilibrium detachment energies ($\phi^{det}/1000kT$) for the Fe_2O_3–quartz system in which *I* was varied. See Fig. 3.3 for descriptions.

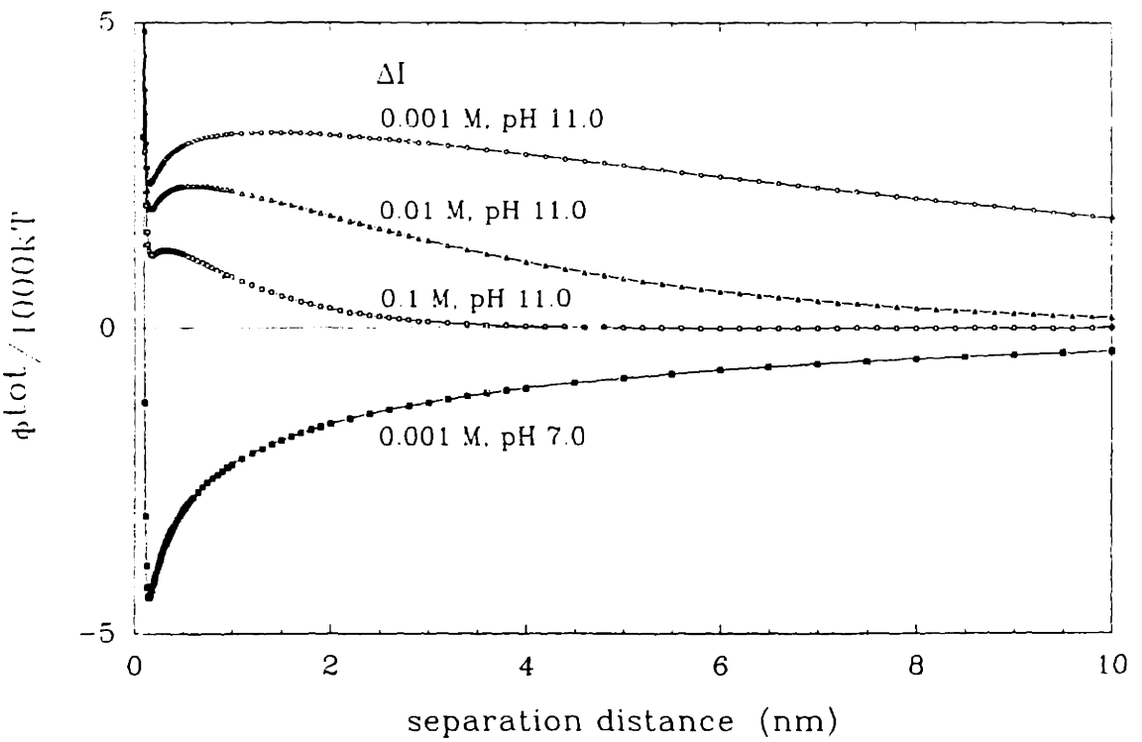

Fig. 3.8. Plot of total potential energy *vs.* separation distance for the Fe_2O_3–quartz system in which the colloid release rate decreased as I increased. As I increases, the equilibrium energy difference decreases, corresponding to slower detachment; in contrast, the size of the energy barrier decreases as I increases, corresponding to faster detachment. The total potential energy profile for *p*H 7.0 and $I = 0.001$ M is also shown – colloids were not released during *p*H 7.0 flushes.

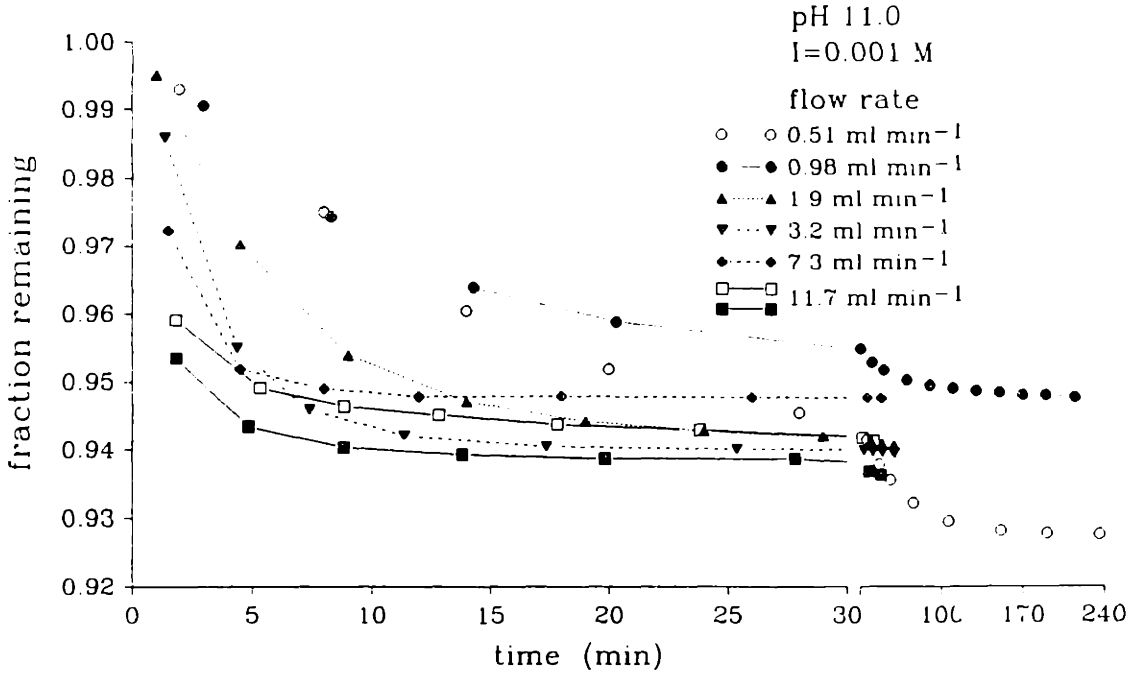

Fig. 3.9. Plot of fraction of hematite colloids remaining attached to quartz grains *vs.* time as flow rate was varied from 0.51 to 11.7 ml min^{-1}. Initial detachment rates increase with increasing flow rate, but the total fraction of colloids removed did not vary significantly with flow rate.

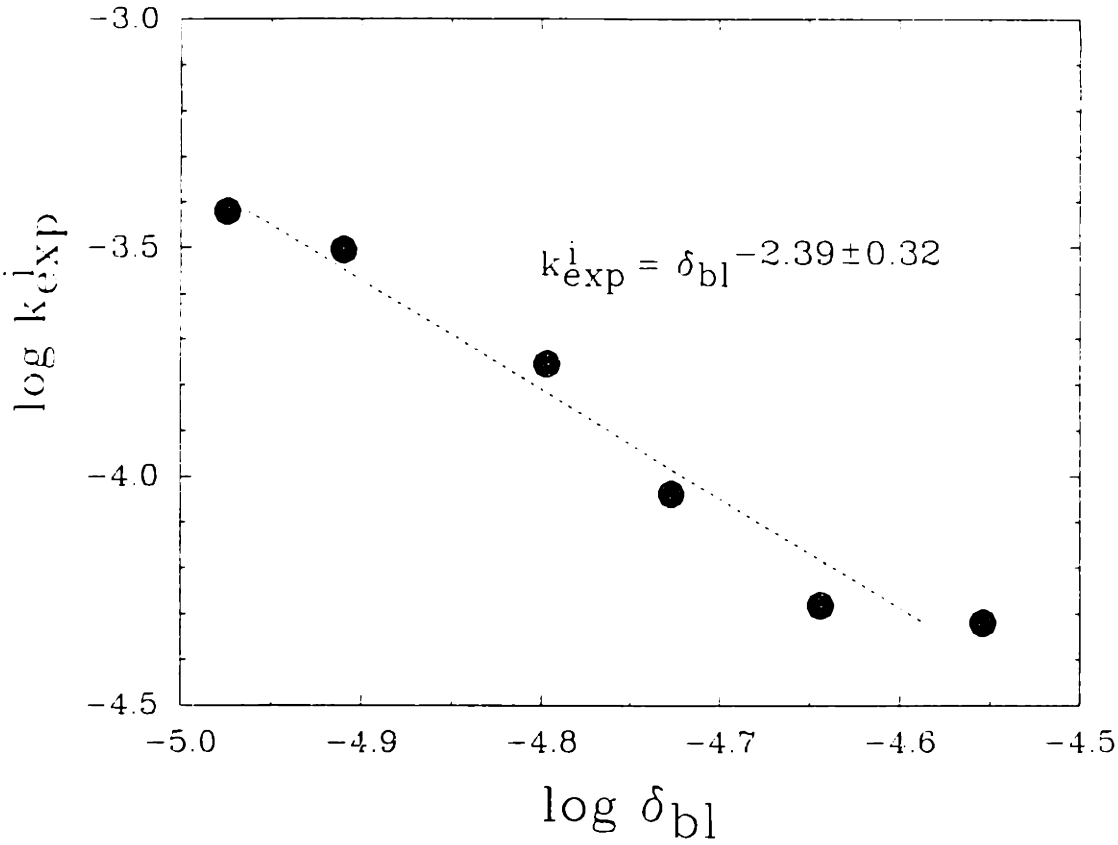

Fig. 3.10. Logarithmic plot of the initial rate constant (k^i_{exp}) *vs.* the boundary layer thickness (δ_{bl}) calculated with Eqn. 3.14. The exponent ($\pm 1\sigma$) of the relationship is close to the exponent expected for $k^i_{exp} \propto \delta_{bl}^{-2}$ (Eqn. 3.17).

DISCUSSION

Effect of Ionic Strength on Detachment Rate

In the Fe_2O_3–glass ΔI experiment, increased I resulted in more rapid colloid release (Kallay *et al.*, 1986). This result is at odds with the results obtained in the $Cr(OH)_3$–glass (Kolakowski and Matijević, 1979) and FeOOH–steel (Thompson *et al.*, 1984) experiments as well as other field and laboratory observations (Nightingale and Bianchi, 1977; Khilar and Fogler, 1984; Cerda, 1987; McDowell–Boyer, 1992). Kallay *et al.* (1987) attributed the counterintuitive result to the use of a shorter column, which supposedly reduced the probability of re–attachment of released colloids.

The probability of re–attachment might be reduced in a shorter column because the re–attachment probability is proportional to the total grain surface area passed in the column for a given flow velocity. We estimated the amount of total grain surface area (S_{col}) encountered by a colloid advected along the flow path from the grains' diameter, density, and total mass and the columns' dimensions and porosity ($n = 0.40$) (Table 3.4). The $Cr(OH)_3$ and FeOOH colloids pass about one–fourth as much surface area as the Fe_2O_3 colloids pass.

The re–attachment probability also depends on the single–collector efficiency η, the ratio of the rate of colloid collision with a grain to the rate of colloid flux toward the grain (Friedlander, 1958). For the submicrometer colloids and low flow rates used in these experiments, the collection efficiency caused by colloid diffusion is at least one order of magnitude greater than those caused by interception and sedimentation. The collection efficiency caused by diffusion is given by (Rajagopalan and Tien, 1976)

$$\eta_{dif} = 4\, A_s^{1/3} Pe^{-2/3} \qquad [3.31]$$

where A_s is a porosity–dependent flow parameter of Happel's (1958) model of a

Table 3.4. Number of grains and total grain surface areas (S_{col}) along flow path and probability of collisions following detachment in packed bed columns of ΔI experiments.

colloid grain (ref.)	Q_{col}	A_{col}	— along flow path — number of grains	tot. grain surf. area S_{col}	η_{dif}	$S_{col} \cdot \eta_{dif}$
	ml min^{-1}	cm^2		cm^2		x10^4 cm^2
$Cr(OH)_3$ glass (1)	0.75—1.0	0.64	370	0.033	0.022—0.018	7.3—5.9
β—FeOOH steel (5)	2.0	0.64	160	0.043	0.023	9.9
α—Fe_2O_3— glass (6)	1.3	0.38	450	0.17	0.011	19
α—Fe_2O_3— quartz (*)	1.0	12.6	10—12	0.020—0.024	0.072	14—17

(1) Kolakowski and Matijević (1979).
(5) Thompson *et al.* (1984).
(6) Kallay *et al.* (1986).
(*) this study.

collector grain in a porous medium ($A_s = 37.98$ for $n = 0.40$) and Pe is the Peclet number, given by $(2a_g Q_{col}/nA_{col}D_c)$. The diffusion coefficient D_c was calculated with Eqn. 3.13 and the colloid and grain radii were given in Table 3.2. In terms of the number of collisions, the product of S_{col} and η_{dif} represents the relative probability of re–attachment in the different systems (Table 3.4). Thus, the Fe_2O_3–glass system actually has a probability of re–attachment about twice as high as the $Cr(OH)_3$–glass and FeOOH–steel systems.

For two additional reasons, the probability of re–attachment of released colloids must be low in these experiments. First, the energy barrier to attachment (ϕ_{max}–ϕ_{min2}) is much larger than the energy barrier to detachment (ϕ_{max}–ϕ_{min1})

under the *p*H and I conditions of these experiments. Second, the diffusion concentration gradient away from the surface is maintained by advection of released colloids away from the grains. Kuo and Matijević (1980) concluded that colloid re–attachment was negligible after showing that Fe_2O_3 colloids passed through a column of clean steel grains at *p*H $\geq$ 9 without attachment.

Our hematite–quartz ΔI experiment was performed to test the effect of increasing I on detachment rate in a system similar to that tested by Kallay *et al.* (1986). In our column, the probability of re–attachment was just slightly less than that in the Fe_2O_3–glass system. In considering the dependence of the detachment rate constants on the detachment energies for the ΔI experiments, we have emphasized the results obtained in our hematite–quartz system and the $Cr(OH)_3$–glass and FeOOH–steel systems. We are not able to explain the behavior of the Fe_2O_3–glass system tested by Kallay *et al.* (1986).

Distinguishing Between the Energy Barrier and Equilibrium Models

Rate constants from the ΔI experiments ($Cr(OH)_3$–glass, FeOOH–steel, hematite–quartz) were positively correlated to the equilibrium ϕ^{det}. As I increased and the rate of detachment slowed, the equilibrium energy difference $-(\phi_{min2}-\phi_{min1})$ grew smaller. On the other hand, as I increased, the energy barrier ϕ^{det} became smaller, predicting faster detachment; hence, the rate constants were negatively correlated to the energy barrier ϕ^{det}.

In terms of the equilibrium model, we surmise that colloids were initially distributed between C_{min1} and C_{irr} in the near–neutral solution in the column. For grains with a smooth surface, most of the colloids would be at C_{min1}. The initial colloid concentration at C_{min2} must be very low because colloid removal by the *p*H 7.0 flush was negligible. Introduction of the *p*H 11.0 flush solution rapidly moved colloids from C_{min1} to C_{min2}, the position from which they could diffuse to

C_{fl} or C_{irr}. The kinetics of this initial redistribution were not adequately resolved in the experiments of Matijević and colleagues or in our experiment. Removing the initial volume of colloid–free water from the column obscured the initial buildup of colloids in the bulk fluid. Thus, the initial buildup of colloids at C_{min2} was treated as a "reaction" at equilibrium because it occurred much more rapidly than the overall removal of colloids from the column.

From the form of the Arrhenius relationship between rate and detachment energy, we expect a slope of 1/2.303. The slopes of the log k_{exp} *vs.* ϕ^{det}/kT plots varied from about 0.0002 to 0.0005; thus, detachment rates would be vastly underestimated by calculating the Boltzmann distribution of colloids in the primary and secondary minima. The same problem has been encountered in colloid deposition studies – predicted rates are many orders of magnitude slower than experimental rates (Hull and Kitchener, 1969; Bowen and Epstein, 1979; Gregory and Wishart, 1980).

Alternative Potential Energy Profiles

Uncertainty in the choices of potential energy expressions and parameters may affect the interpretation of the detachment kinetics. The most significant uncertainty in the potential energy seems to lie in the choice of the double layer expression. As shown in Fig. 3.2 for surface potentials corresponding to the hematite–quartz system at *p*H 11.0 and $I = 0.001$ M, the exact ϕ^{dl} (Devereux and de Bruyn, 1963) greatly exceeded the Hogg *et al.* (1966) ϕ^{dl} for plate–plate geometry at separation distances less than 30 nm. If an exact solution of ϕ^{dl} for dissimilar spheres existed and it exceeded the sphere–sphere Hogg *et al.* (1966) ϕ^{dl} by a similar amount, then the substitution of the exact ϕ^{dl} in the sum of potential energies would probably remove the primary minimum and maximum from the potential energy profile at *p*H 11.0, when colloids were released from the grains.

The resulting potential energy profile would show steadily decreasing repulsive energy with increasing separation distance until the distance of the secondary minimum is reached. At *p*H 7.0, when colloids remained attached to the grains, the use of the exact ϕ^{dl} would probably deepen the primary minimum because the hematite and quartz surfaces possess potentials of opposite sign (Table 3.1). In this case, detachment at *p*H 11.0 could be attributed to the disappearance of energy barrier. The rate of colloid release could now be related to the degree of destabilization of the colloids that resided in the primary minimum at *p*H 7.0. The relevant energy difference would be $-[\phi_{min2}-\phi(x_{min1}^{pH\ 7})]$, where $\phi(x_{min1}^{pH\ 7})$ is the total potential energy at the separation distance of the primary minimum that existed at *p*H 7.0. Under these conditions, the energy barrier model still applies when ϕ_{min1} and ϕ_{max} are present; the resulting colloid release is slow.

Variation of the Hamaker constants ($A = 4\cdot10^{-21}$, $1\cdot10^{-20}$, and $4\cdot10^{-20}$ J) and Born collision parameters ($\sigma = 3\cdot10^{-10}$, $5\cdot10^{-10}$, and $7\cdot10^{-10}$ m) through representative ranges resulted in changes in the values of ϕ_{min1}, ϕ_{max}, and ϕ_{min2} for the hematite–quartz system at *p*H 11.0 and $I = 0.001$ M (Fig. 3.11). However, the features of the potential energy profile were still present and the distinctions between the energy barrier and equilibrium kinetic models can still be made.

Fraction of Colloids Released

After 10 to 100 pore volumes of flushing in the ΔI experiments, colloid concentrations in the effluent dropped to near–zero levels. The total fraction of colloids released at the final sample time decreased with increasing I (Fig. 3.6). We surmise that the drop in the total fraction released with increasing I represents the increasing rate of colloid transport from C_{min2} to more firmly bound sites in surface irregularities. However, we cannot test this aspect of the model because the initial distribution of colloids between C_{min1} and C_{irr} cannot be determined.

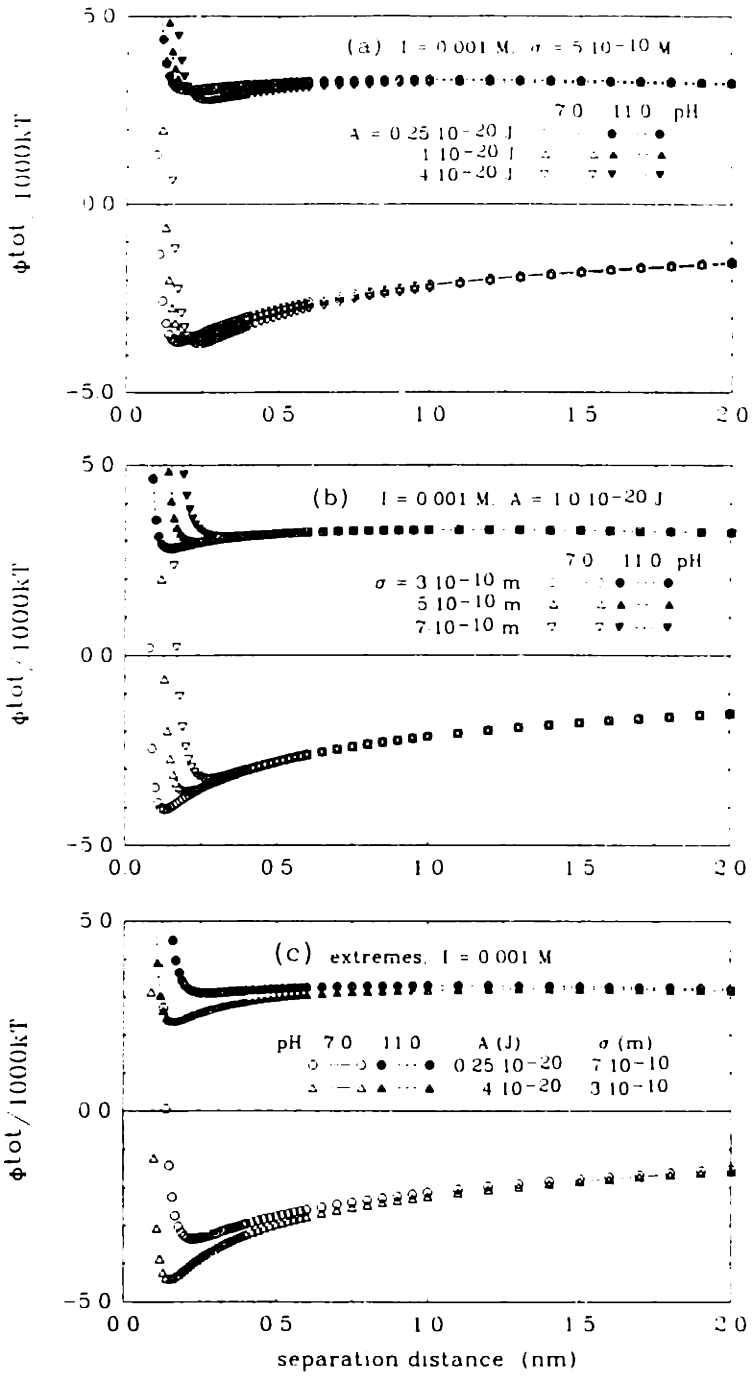

Fig. 3.11. Total potential energy *vs.* separation distance for the hematite–quartz system at *p*H 11.0 and $I = 0.001$ M for a range of Hamaker constants (A) and Born collision parameters (σ):
(a) variation of Hamaker constants.
(b) variation of Born collision parameters.
(c) extremes in Hamaker constants and Born collision parameters.
Total potential energy at *p*H 7.0, during which colloids remained attached, also shown for comparison of primary minimum positions.

In our model, all of the colloids at C_{min1} and C_{min2} will ultimately be removed to either the bulk fluid or to irregular surface sites. The ratio of the total mass of hematite removed to the total amount remaining in the column, which decreased with increasing I, represents the ratio of k_{dif} to k_{irr}. As I increases, C_{min2} moves closer to the surface. The distance δ_{bl} separating C_{min2} and C_{fl} increases, while the distance δ_{dl} separating C_{min2} and C_{irr} decreases. Because $\delta_{dl} \ll \delta_{bl}$, the variation in δ_{bl} with I is small and k_{dif} will not vary significantly with changing I. However, variations in δ_{dl} may strongly affect k_{irr}. Thus, we attribute the decrease in total fraction of colloids released to an increase in k_{irr} as I increases. We maintain that colloids must jump to C_{min2} before they can diffuse along the grain surface to a C_{irr} site because colloids at C_{min1} are much more strongly bound to the surface.

We suspect that sites of stronger attachment are associated with the deposition of colloids in geometric irregularities on the grain surfaces. Fe was concentrated on the weathered portions of the quartz surfaces (Fig. 3.5). Colloids collected in such sites are undoubtedly not subject to the same interaction potentials calculated for colloid interaction with flat surfaces. The removal of these colloids by sonication suggests that chemical bonds were not involved.

Kuo and Matijević (1980) observed similar deposition in surface irregularities in the Fe_2O_3–steel system. Colloids were transferred from smooth to crenulated surfaces on the steel grains during flushing. The colloids appeared to have aggregated into larger flocs, which would have lower diffusion coefficients than single colloids. A maximum of only 12% of the colloids were removed from these steel grains. The role of chemical bond formation between colloids and grains was discounted by Kolakowski and Matijević (1979). They suggested that F^- would detach $Cr(OH)_3$ colloids from glass more effectively than NO_3^- if >Cr–O–Si< bonds had been formed, but detachment rates were similar for F^- and NO_3^-.

Effect of Fluid Velocity on Detachment Rate

The increase in release rate with increasing flow in the hematite–quartz system further indicates that the transfer of colloids from C_{min1} is not the rate–limiting step. If it were, release rate would not vary with flow unless fluid motion disrupted the region over which the interaction potential extended. For the flow rates and porous media used in the hematite–quartz experiment, the boundary layer thickness was always much larger than the region over which the interaction potential extended.

In the equilibrium model, we propose that the transport of colloids from C_{min2} to C_{fl} controls the overall rate of the detachment reaction. We have neglected the energy barrier represented by $-(\phi_\infty - \phi_{min2})$ because the rate *vs.* ϕ^{det} relationships suggested that the primary minimum energy barrier did not control colloid release. When flow rate was varied in the hematite–quartz system, the experimental rate constants depended on the boundary layer thickness in a manner close to the proposed relationship expressed in Eqn. 3.17 (Fig. 3.10). The total fraction of colloids removed did not vary significantly. This indicated that, after rapid re–distribution of colloids between the C_{min1} and C_{min2} upon introduction of the flush solution, the same number of colloids were available to diffuse away to the bulk fluid. Thus, K_s and k_{irr} were not affected by the change in hydrodynamic conditions.

Hydrodynamic Shear

The rate of colloid transport from the surface to the bulk fluid may also be affected by hydrodynamic shear. Researchers studying the release of submicrometer colloids from grains under laminar flow in porous media have concluded that hydrodynamic shear forces are negligible compared to electrostatic adhesive forces (Clayfield and Lumb, 1966; Kolakowski and Matijević, 1979; Khilar and Fogler,

1984; Cerda, 1987). For larger colloids and more rapid flows, colloid release has been attributed to colloid rolling initiated by fluid drag force tangential to surface (Hubbe, 1985; Sharma *et al.*, 1992). The tangential force results in colloid motion away from the surface when rolling colloids hit surface irregularities. The effect of hydrodynamic lift forces on detachment are considered negligible compared to the effect of the tangential force (Gotoh *et al.*, 1984; McDowell–Boyer, 1992).

The force of fluid drag (F_d) on the attached colloid has been expressed as (Goldman *et al.*, 1968; O'Neill, 1968):

$$F_d = 1.7\ (6\pi\mu_{fl} a_c U_z) \qquad [3.32]$$

where U_z is the fluid velocity normal to the grain at the distance of the colloid radius a_c from the wall. The parabolic profile of U_z as it decreases from the open channel velocity to zero at the flat surface was expressed by Sharma *et al.* (1992) as:

$$U_z = 6\left[\frac{Q_{col}}{A_{col}}\frac{a_c}{l}\right]\left[1 - \left[\frac{a_c}{l}\right]\right] \qquad [3.33]$$

where l is the spacing between two plates (m). The interplate spacing can be approximated by the radius of the quartz grain a_g in our case.

The importance of hydrodynamic shear may be assessed by comparing the magnitude of F_d to the "critical lift force," the maximum slope of the potential energy curve, $d\phi^{tot}/dx = -F^{tot}$, where F^{tot} is the adhesive force opposing the motion of a colloid away from the surface. Although the drag and critical lift forces cannot be directly balanced because they operate in perpendicular directions, their effect on colloid release can be compared to assess the potential importance of fluid drag on colloid detachment (Gotoh *et al.*, 1984; Sharma *et al.*, 1992). F^{tot} was calculated as the sum of F^{vdw}, F^{born}, and F^{dl}, which were obtained by differentiation of ϕ^{dl} and simplified forms of ϕ^{vdw} (for $x \ll a_p$; Hamaker, 1937) and ϕ^{born} (for $x \ll a_p$; Feke *et al.*, 1984) with respect to separation distance:

$$F^{vdw} = -\frac{A}{12x^2}\frac{y a_c}{y+1} \qquad [3.34]$$

$$F^{\text{born}} = \frac{A}{180}\left[\frac{\sigma_{\text{born}}}{a_c}\right]^8 \frac{2y}{2y+1}\frac{{a_c}^7}{x^8} \qquad [3.35]$$

$$F^{\text{dl}} = \frac{2\pi\epsilon\epsilon_o a_c a_g}{(a_c+a_g)}\frac{\kappa \exp(-\kappa x)}{1-\exp(-2\kappa x)} \cdot[(\psi_{oc}^2+\psi_{og}^2)\,\kappa \exp(-\kappa x) - 2\psi_{oc}\psi_{og}] \qquad [3.36]$$

The critical lift forces were obtained for colloids in the primary and secondary minima. The increase in F_d with flow rates is compared to the critical lift force of a colloid in the secondary minimum in Fig. 3.12. At the highest flow rate, F_d approximately matched F^{tot}, so fluid drag may have contributed to detachment of colloids from the secondary minimum. However, poor agreement between the expected and observed slope of the log k_{exp} *vs.* ϕ^{det} relationship indicates that the repulsive force is greatly overestimated; thus, the adhesive force in the secondary minimum is probably much larger. Furthermore, the actual dependence of the rate of colloid detachment on fluid drag force is unknown (Hubbe, 1985; Sharma *et al.*, 1992). In any case, the detachment of colloids in the primary minimum will not be affected by drag force because the critical lift force is much larger than the fluid drag force.

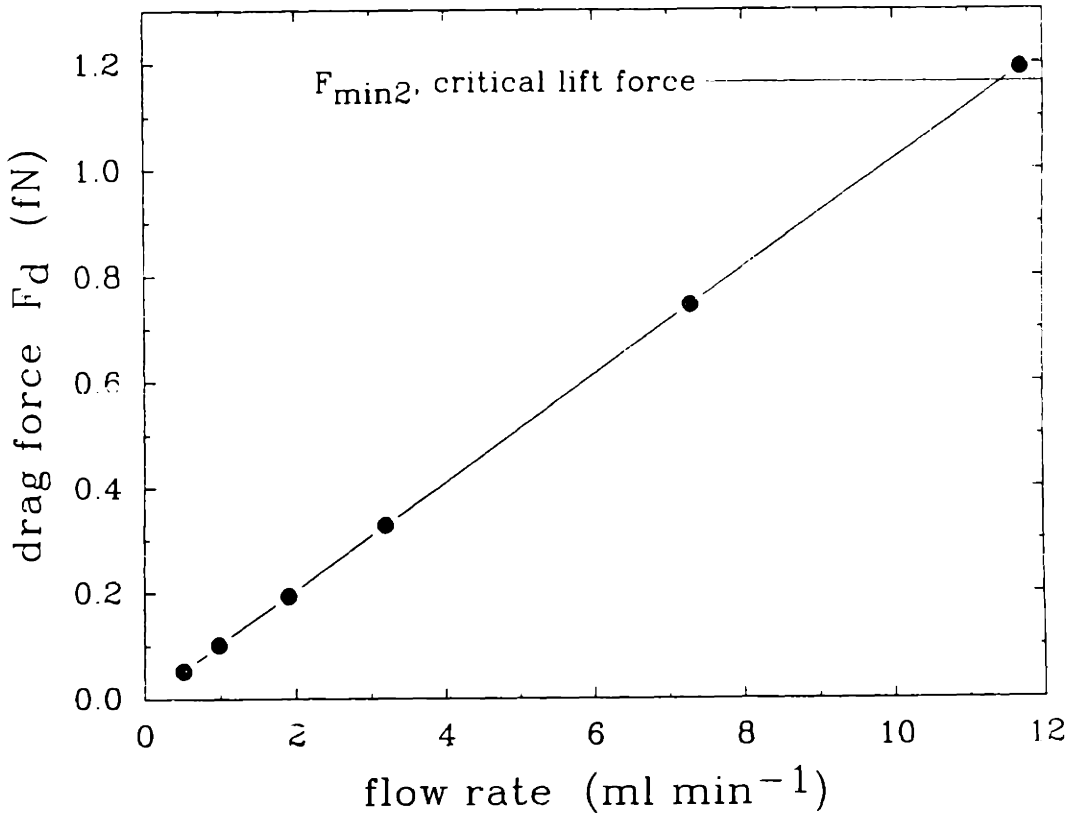

Figure 3.12. Plot of the fluid drag force (F_d) *vs.* flow rate (Q_{col}) for the hematite–quartz system. The dotted horizontal line marks the critical lift force for colloids in the secondary minimum (F_{min2} = 1.16 fN) at *p*H 11 and $I = 1 \cdot 10^{-3}$ M. Critical lift force for colloids in primary minimum (F_{min1} = 430 pN) is much greater than F_d generated by these flow rates.

CONCLUSIONS

In this research, we compared two models describing the kinetics of colloid release from grain surfaces using results from colloid detachment experiments in model systems of oxide colloids and grains:

(1) in the energy barrier model, the rate of colloid detachment is controlled by the size of the potential energy barrier. Colloids diffusing away from the surface must attain energy sufficient to exceed the barrier.

(2) in the equilibrium model, the rate of colloid detachment is controlled by the equilibrium distribution of colloids between the primary and secondary minima in potential energy, the rate of colloid diffusion from the secondary minimum to the bulk fluid, and the removal of colloids to more firmly bound sites or irregular surfaces.

We determined that the equilibrium model better explained the results of two colloid detachment experiments: (1) experiments in which an increase in I resulted in a decrease in the rate of colloid release and total fraction of colloids released, and (2) experiments in which an increase in the flushing rate caused an increase in the rate of colloid release without altering the total fraction of colloids released. We also determined that detachment energies calculated with zeta potentials did not correlate with detachment rates. Detachment energies calculated with surface potentials from surface complexation/double layer models were more sensitive to changes in I and surface charge.

In our experiment on the detachment of hematite colloids from quartz grains and in all but one of the experiments reviewed in the literature, an increase in I caused a decrease in the colloid release rate. In the energy barrier model, the size of the energy barrier decreased with increasing I, suggesting more rapid colloid release. In the equilibrium model, the energy difference between the primary and secondary

minima decreased with increasing I, corresponding to slower colloid release. Thus, the equilibrium model more accurately described the detachment kinetics behavior better than the energy barrier model.

In the equilibrium model, we explained the decrease in the total fraction of colloids released with increasing I by postulating the existence of more firmly attached sites associated with surface irregularities. At high I, colloids in the secondary minimum are much close to the colloid surface than at low I, and thus more likely to encounter sites of very low potential energy that may be associated with surface irregularities. Electron–microscopic examination of the colloids remaining after flushing supported the notion of attachment in surface irregularities.

The increase of flow rate in a hematite colloid–quartz grain system resulted in more rapid colloid release. This further indicated that the energy barrier model was inadequate because a rate–limiting step of colloid transport over the potential energy barrier should not vary with flow rate. In contrast, in the equilibrium model, the release rate would increase with increasing flow rate as the thickness of the diffusion boundary layer decreases. The initial rate constant was related to the decrease in boundary layer thickness in accordance with the proposed relationship.

We conclude that the introduction of a solution that promotes repulsion between colloids attached to grain surfaces will cause a rapid re-distribution of colloids between the primary and secondary minima in potential energy. Colloids in the secondary minimum may be removed to more firmly bound sites or released to the bulk fluid. The rate of colloid transport from the secondary minimum to the bulk fluid was related to the characteristic length scale of diffusion to the bulk fluid. The competing removal of colloids to more firmly attached sites was related to the proximity of the secondary minimum to the surface.

REFERENCES

Barouch E., Matijević E., and Wright T.H. (1987) Effects of Born repulsion on particle detachment. *Chem. Eng. Comm.* **55**, 29–40.

Batchelor G.K. (1979) Mass transfer from a particle suspended in fluid with a steady linear ambient velocity distribution. *J. Fluid Mech.* **95**, 369–400.

Bowen B.D. and Epstein N. (1979) Fine particle deposition in smooth parallel–plate channels. *J. Colloid Interface Sci.* **72**, 81–97.

Buddemeier R.W., and Hunt J.W. (1988) Transport of colloidal contaminants in groundwater: radionuclide migration at the Nevada Test Site. *Appl. Geochem.* **3**, 535–548.

Cerda C. (1987) Mobilization of kaolinite fines in porous media. *Colloids Surfaces* **27**, 219–241.

Clayfield E.J. and Lumb E.C. (1966) Detachment of adhered colloidal particles by non–aqueous surfactant solutions. *Disc. Faraday Soc.* **42**, 285–293.

Clayfield E.J. and Smith A.L. (1970) Adhesion and detachment of solid colloidal particles in aqueous ionogenic surfactant media. *Environ. Sci. Technol.* **4**, 413–416.

Dahneke B. (1975a) Kinetic theory of the escape of particles from surfaces. *J. Colloid Interface Sci.* **50**, 89–107.

Dahneke B. (1975a) Resuspension of particles. *J. Colloid Interface Sci.* **50**, 194–196.

Degueldre C., Baeyens B., Goerlich W., Riga J., Verbist J., and Stadelmann P. (1989) Colloids in water from a subsurface fracture in granitic rock, Grimsel Test Site, Switzerland. *Geochim. Cosmochim. Acta* **53**, 603–610.

Devereux O.F. and de Bruyn P.L. (1963) *Interaction of Plane–Parallel Double Layers.* MIT Press, Cambridge, MA.

Dzombak D.A. and Morel F.M.M. (1990) *Surface Complexation Modeling: Hydrous Ferric Oxide.* Wiley–Interscience.

Feke D.L., Prabhu N.D., Mann J.A. Jr., and Mann J.A. III (1984) A formulation of the short–range repulsion between spherical colloidal particles. *J. Phys. Chem.* **88**, 5735–5739.

Friedlander S.K. (1958) Theory of aerosol filtration. *Ind. Eng. Chem.* **50**, 1161–1164.

Goldman A.J., Cox R.G., and Brenner H. (1967) Slow viscous motion of a sphere parallel to a plane wall – II. Couette flow. *Chem. Eng. Sci.* **22**, 653–660.

Gotoh K., Inoue T., and Tagawa M. (1984) Adhesion of nylon particles to a quartz plate in an aqueous solution and their removal by electro–osmosis. *Colloid Polymer Sci.* **262**, 982–989.

Gregory J. (1975) Interaction of unequal double layers at constant charge. *J. Colloid Interface Sci.* **51**, 44–51.

Gregory J. and Wishart A. (1980) Deposition of latex particles on alumina fibers. *Colloids Surfaces* **1**, 313–334.

Gschwend P.G., Backhus D.A., MacFarlane J.K., and Page A.L. (1990) Mobilization of colloids in groundwater due to infiltration of water at a coal ash disposal site. *J. Contam. Hydrol.* **6**, 307–320.

Gschwend P.G. and Reynolds M.D. (1987) Monodisperse ferrous phosphate colloids in an anoxic groundwater plume. *J. Contam. Hydrol.* **1**, 309–327.

Hamaker H.C. (1937) The London–van der Waals attraction between spherical particles. *Physica* **4**, 1058–1072.

Happel J. (1958) Viscous flow in multiparticle systems: slow motion of fluids relative to beds of spherical particles. *AIChE J.* **4**, 197–201.

Henry D.C. (1931) Cataphoresis of suspended particles. Part I. – Equation of cataphoresis. *Proc. Royal Soc. (London) Ser. A* **133**, 106.

Hogg R., Healy T.W., and Fuerstenau D.W. (1966) Mutual coagulation of colloidal dispersions. *Trans. Faraday Soc.* **62**, 1638–1651.

Hubbe M.A. (1985) Detachment of colloidal hydrous oxide spheres from flat solids exposed to flow 2. Mechanism of release. *Colloids Surfaces* **16**, 249–270.

Hull M. and Kitchener J.A. (1969) Interaction of spherical colloidal particles with planar surfaces. *Trans. Faraday Soc.* **65**, 3093–3104.

Hunter R.J. (1981) *Zeta Potential in Colloid Science.* Academic Press.

Israelachvili J.N.(1982) Forces between surfaces in liquids. *Adv. Colloid Interface Sci.* **16**, 31–47.

Israelachvili J.N.(1985) *Intermolecular and Surface Forces.* Academic Press, p. 146.

James R.O. and Parks G.A. (1982) Characterization of aqueous colloids by their electrical double–layer and intrinsic surface chemical properties. In *Surface and Colloid Science*, Vol. 12 (ed. E. Matijević), Plenum Press, 119–216.

Kallay N., Barouch E., and Matijević E. (1987) Diffusional detachment of colloidal particles from solid/solution interfaces. *Adv. Colloid Interface Sci.* **27**, 1–42.

Kallay N., Biškup B., Tomić M., and Matijević E. (1986) Particle adhesion and removal in model systems X. The effect of electrolytes on particle detachment. *J. Colloid Interface Sci.* 114, 357–362.

Kallay N. and Matijević E. (1981) Particle adhesion and removal in model systems Part 2.– Monodispersed ferric oxide on steel. *J. Colloid Interface Sci.* **83**, 289–300.

Khilar K.C. and Fogler H.S. (1984) The existence of a critical salt concentration for particle release. *J. Colloid Interface Sci.* **101**, 214–224.

Kolakowski J.E. and Matijević E. (1979) Particle adhesion and removal in model systems Part 1.–Monodispersed chromium hydroxide on glass. *J. Chem. Soc. Faraday Trans. I* **75**, 65–78.

Kostoglou M. and Karabelas A.J. (1992) The effect of discrete surface charge on potential energy of repulsion between colloidal surfaces. *J. Colloid Interface Sci.* **151**, 534–545.

Kuo R.J. and Matijević E. (1979) Particle adhesion and removal in model systems Part 2.–Monodispersed chromium hydroxide on steel. *J. Chem. Soc. Faraday Trans. I* **75**, 2014–2026.

Kuo R.J. and Matijević E. (1980) Particle adhesion and removal in model systems Part 3.–Monodispersed ferric oxide on steel. *J. Colloid Interface Sci.* **78**, 407–421.

Langmuir D. (1969) Geochemistry of iron in a coastal–plain groundwater of the Camden, New Jersey area. U.S. Geol. Survey Prof. Paper 650–C, C224–C235.

Levine S. and Smith A.L. (1971) Theory of the differential capacity of the oxide/aqueous electrolyte interface. *Faraday Disc. Chem. Soc.* **52**, 290–301.

Lyklema J. (1980) Colloid stability as a dynamic phenomenon. *Pure Appl. Chem.* **52**, 1221–1227.

Magaritz M., Amiel A.J., Ronen D., and Wells M.C. (1990) Distribution of metals in a polluted aquifer: A comparison of aquifer suspended material to fine sediments in the adjacent environment. *J. Contam. Hydrol.* **5**, 333–347.

Matijević E. and Scheiner P. (1978) Ferric hydrous oxide sols III. Preparation of uniform particles by hydrolysis of Fe(III)–chloride, –nitrate, and –perchlorate solutions. *J. Colloid Interface Sci.* **63**, 509–524.

McDowell–Boyer L.M. (1992) Chemical mobilization of micron–sized particles in saturated porous media under steady flow conditions. *Environ. Sci. Technol.* **26**, 586–593.

Nightingale H.I. and Bianchi W.C. (1977) Ground–water turbidity resulting from artificial recharge. *Ground Water* **15**, 146–152.

O'Neill M.E. (1968) A sphere in contact with a plane wall in a slow linear shear flow. *Chem. Eng. Sci.* **23**, 1293–1298.

Parks G.A. (1965) The isoelectric points of solid oxides, solid hydroxides, and aqueous hydroxo complex systems. *Chem. Rev.* **65**, 177–198.

Penrose W.R., Polzer W.L., Essington E.H., Nelson D.M., and Orlandini K.A. (1990) Mobility of plutonium and americium through a shallow aquifer in a semiarid region. *Environ. Sci. Technol.* **24**, 228–234.

Rajagopalan R. and Tien C. (1976) Trajectory analysis of deep–bed filtration with the sphere–in–cell porous media model. *AIChE J.* **22**, 523–533.

Ronen D., Magaritz M., Weber U., Amiel A., and Klein E. (1992) Characterization of suspended particles collected in groundwater under natural groundwater flow conditions. *Water Resour. Res.* **28**, 1279–1291.

Ruckenstein E. and Prieve D.C. (1976) Adsorption and desorption of particles and their chromatographic separation. *AIChE J.* 22, 276–283.

Ryan J.N. and Gschwend P.M. (1990) Colloid mobilization in two Atlantic Coastal Plain aquifers: field studies. *Water Resour. Res.* **26**, 307–322.

Ryan J.N. and Gschwend P.M. (1992) Effect of iron diagenesis on the transport of colloidal clay in an unconfined sand aquifer. *Geochim. Cosmochim. Acta* **56**, 1507–1521.

Schindler P.W. and Gamsjager H. (1972) Acid–base reactions of the TiO2 (anatase) –water interface and the point of zero charge of TiO_2 suspensions. *Kolloid–Z.Z. Polym.* **250**, 759–763.

Sharma M.M., Chamoun H., Sita Rama Sarma D.S.H., and Schechter R.S. (1992) Factors controlling the hydrodynamic detachment of particles from surfaces. *J. Colloid Interface Sci.* **149**, 121–134.

Short S.A., Lowson L.T., and Ellis J. (1988) $^{234}U/^{238}U$ and $^{230}Th/^{234}U$ activity ratios in the colloidal phases of aquifers in lateritic weathered zones. *Geochim. Cosmochim. Acta* **52**, 2555–2563.

Sigg L. and Stumm W. (1981) The interactions of anions and weak acids with the hydrous goethite (α–FeOOH) surface. *Colloids Surfaces* **2**, 101–117.

Stumm W., Hohl H., and Dalang F. (1976) Interaction of metal ions with hydrous oxide surfaces. *Croatica Chem. Acta* **48**, 491–504.

Thompson G., Kallay N., and Matijević E. (1984) Particle adhesion and removal in model systems – IX Detachment of rod–like β–FeOOH particles from steel. *Chem. Eng. Sci.* **39**, 1271–1276.

Verwey E.J.W. and Overbeek J.Th.G. (1948) *Theory of the Stability of Lyophobic Colloids.* Elsevier.

Westall J.C., Zachara J.L., and Morel F.M.M. (1976) MINEQL: A computer program for the calculation of chemical equilibrium composition of aqueous systems. R.M. Parsons Laboratory Tech. Note 18, Dept. Civil Eng., Massachusetts Institute of Technology.

Yates D.E., Levine S., and Healy T.W. (1974) Site–binding model of the electrical double layer at the oxide/water interface. *J. Chem. Soc. Faraday Trans.* **70**, 1807–1818.

Chapter Four

EFFECT OF SOLUTION CHEMISTRY ON CLAY COLLOID RELEASE FROM AN IRON OXIDE-COATED SAND

With proper engineering control, suspended particles can act as a benefit to mankind. Without proper engineering control, the particles can be a scourge.

— J.B.F. Champlin (1971) *Society of Petroleum Engineers Journal* 11, 367.

ABSTRACT

To determine whether the dissolution of secondary iron oxides was required to mobilize clay colloids from an iron oxide–coated aquifer sand, we flushed the sand with solutions of varying ionic strength, *p*H, and reductant and surfactant concentrations. The rates of clay release were compared to Fe(III) oxide dissolution rates and to the interaction potential energy between the colloids and the quartz grains. Detachment energies were obtained from the intersurface potential energy profiles according to two models of colloid detachment: (1) the energy barrier model and (2) the equilibrium energy difference model. Surface potentials were estimated from zeta potentials (ζ) using an empirical relationship between ζ–potential, ionic strength (I), and surface potentials calculated with a surface complexation/double layer model for two well–characterized oxide minerals.

In most experiments, clay release rates were directly related to detachment energies and unrelated to rates of Fe(III) oxide dissolution, indicating that the intersurface potential energy dominated the binding of colloids to grain coatings. In the experiment in which ionic strength was varied, release rates were positively correlated to the equilibrium detachment energy and negatively correlated to the energy barrier detachment energy, suggesting that the colloids were rapidly redistributed between the primary and secondary minima in potential energy before diffusing to the bulk fluid. Surfactant solutions and natural groundwater released clay without dissolving iron oxides.

INTRODUCTION

Concern over the source of colloids in groundwater has escalated as cases of colloid–facilitated transport of low–solubility contaminants have been reported (*e.g.*, Buddemeier and Hunt, 1988; Penrose *et al.*, 1990; Magaritz *et al.*, 1990). However, the source of the colloids responsible for enhanced transport has not been addressed in many of these reports. Some mechanisms of groundwater colloid generation include precipitation (Langmuir, 1969; Gschwend and Reynolds, 1987), erosion in fractures (Degueldre *et al.*, 1989), mobilization by changes in *p*H and ionic strength (Nightingale and Bianchi, 1977; Khilar and Fogler, 1984), and release by dissolution of cementing phases (Harris *et al*, 1987; Gschwend *et al.*, 1990; Ronen *et al.*, 1992).

In our past research, we observed that clay mineral colloids were abundant in anoxic groundwaters and absent from oxic groundwaters in two Atlantic Coastal Plain aquifers consisting of Fe(III) oxide–coated quartz sands (Ryan and Gschwend, 1990). At the New Jersey Coastal Plain site, Fe(III) oxide and clay–sized particle contents were significantly lower in anoxic sediments below a swamp than in nearby oxic sediments (Ryan and Gschwend, 1992; Chapter 2). In the oxic sediments, the quartz grains were coated by colloidal kaolinite plates and microcrystalline Fe(III) oxide, primarily goethite (α–FeOOH), which was evenly distributed through the coatings. We hypothesized that the goethite provided a positively–charged intermediary that cemented the negatively–charged kaolinite to the negatively–charged quartz and kaolinite already attached to the coatings. Beneath the swamp, it seemed likely that the abundant organic matter gradually dissolved the goethite cement and mobilized the kaolinite layer by layer.

In this research, we wanted to determine whether chemical or physical forces bound the colloids to the coatings. Was the breaking of chemical bonds between the

microcrystalline goethite, kaolinite, and quartz by dissolving goethite required to mobilize the kaolinite, or would alteration of the physical forces described by an augmented DLVO (Derjaguin-Landau-Verwey-Overbeek) theory be adequate to release the colloids? To examine this question, we subjected a sample of the oxic sediment to solutions of varying ionic strength, *p*H, reductant concentrations, and surfactant concentrations and measured the rates of clay and Fe release. The clay release rates were compared to Fe(III) oxide dissolution rates and detachment energies to evaluate the relative importance of chemical *vs.* physical binding of colloids.

Previously, attempts have been made to relate conditions controlling colloid mobilization to intersurface potential energy. Critical salt concentrations observed for clay release leading to formation plugging were related to the sum of van der Waals and double layer potential energy calculated with zeta potentials (ζ) as surface potentials (Khilar and Fogler, 1984; Kia *et al.*, 1987; Cerda, 1987). The critical salt concentrations corresponded to potential energy profiles with primary maxima (ϕ_{max}) near zero (Fig. 4.1). However, this correspondence is not meaningful for two reasons: (1) $\phi_{max} \approx 0$ corresponds to the absence of an energy barrier to attachment, not detachment, and (2) if only van der Waals and double layer energy are considered, colloids reside in an infinitely deep potential "well", the primary minimum (ϕ_{min1}), from which there is zero probability of detachment.

A kinetic treatment of colloid detachment requires a primary minimum of finite depth, which may be obtained by including short–range Born repulsive energy (Fig. 4.1; Ruckenstein and Prieve, 1976; Barouch *et al.*, 1987; Vaidya and Fogler, 1990; McDowell–Boyer, 1992). For this case, Ruckenstein and Prieve (1976) postulated that the rate–limiting step in particle detachment is the escape of particles from ϕ_{min1} to the bulk fluid and that the detachment rate is exponentially related to the size of the energy barrier $\phi_{max}-\phi_{min1}$, in analogy with Arrhenius

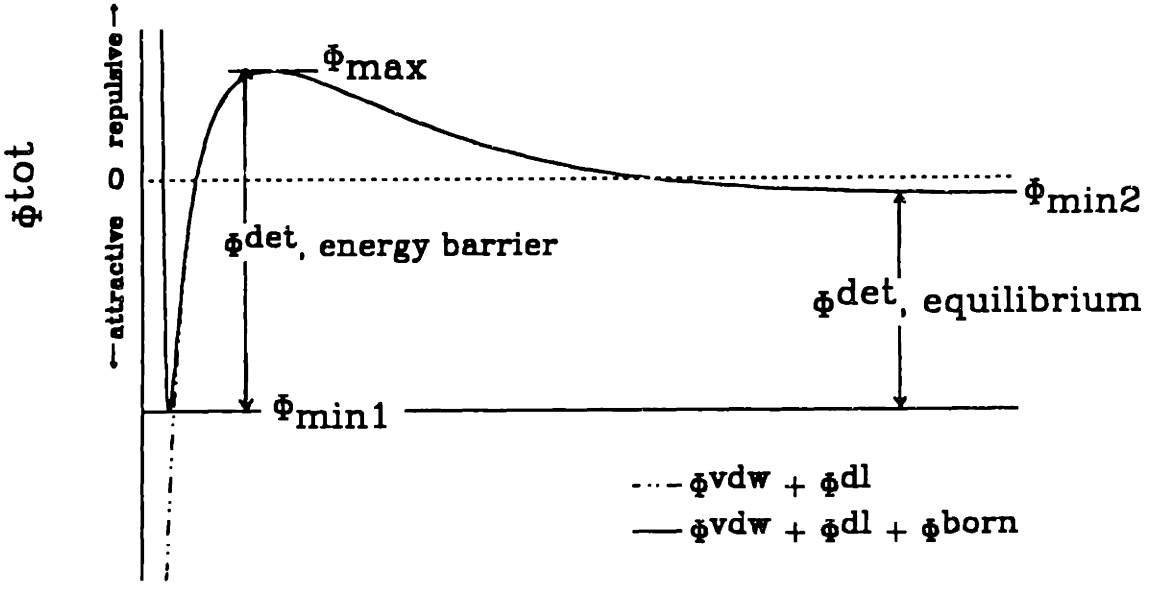

Fig. 4.1. Intersurface potential energy, ϕ^{tot}, between colloid and grain surfaces *vs.* separation distance calculated as (1) a sum of van der Waals and electrostatic energies ($\phi^{vdw} + \phi^{dl}$) and as (2) a sum of van der Waals, electrostatic, and Born energies ($\phi^{vdw} + \phi^{dl} + \phi^{born}$). The primary minimum ($\phi_{min1}$) is finite for case (2). The detachment energy (ϕ^{det}) in the energy barrier model is the difference between the primary maximum (ϕ_{max}) and minimum energies ($\phi^{det} = -[\phi_{max} - \phi_{min1}]$). In the equilibrium model, the detachment energy $\phi^{det} = -[\phi_{min2} - \phi_{min1}]$.

kinetics. In some of the studies of detachment of colloidal oxides from glass and steel beads summarized by Kallay *et al.* (1987), release rates were related to the detachment energy barrier as formulated by Dahneke (1975) to show that particle detachment was controlled by intersurface potential energy.

In examining the relationship between detachment rates and intersurface potential energy for model systems, we found that detachment energies derived from a model that included an equilibrium distribution of particles between the primary and secondary (ϕ_{min2}) minima correlated with the detachment rates, while detachment energies from the energy barrier model did not (Chapter 3). In the "equilibrium" model, the rate–limiting step was diffusive transport from ϕ_{min2} across a hydrodynamic boundary layer to the bulk fluid. Particles in ϕ_{min2} may also have been removed to more firmly attached sites in surface irregularities.

Because ζ–potential is insensitive to surface potential (ψ_0) at high I and surface charge (Verwey and Overbeek, 1948; Hunter, 1981; Dzombak and Morel, 1990), the use of ζ–potential as ψ_0 introduces large and variable errors into the calculation of the double layer potential energy. Thus, we have attempted to improve our calculation of double layer energy by converting ζ–potential to ψ_0 through an empirical relationship. The surface potentials estimated by a surface complexation/double layer (SCDL) model of surface proton exchange equilibrium were related to the measured ζ–potentials of two simple oxides (Wiese and Healy, 1975) and ionic strength to allow prediction of surface potentials with ζ–potential measurements of more complicated oxide minerals.

To our knowledge, this is the first attempt to quantify the rate of colloid release from a sediment that constitutes an important groundwater resource. In this respect, the results have an important bearing on the potential importance of the facilitation of contaminant transport by colloids.

METHODS

Field Sampling

Sediment. An unconsolidated sand sample (U.11.1) was collected in August 1989 from a saturated, oxic zone of the Late Miocene Cohansey Sand formation, the surficial aquifer underlying most of the New Jersey Coastal Plain region known as the Pine Barrens (Ryan and Gschwend, 1992; Chapter 2). The sample consists mainly of quartz sand coated by thin (<10 μm) anisopachous layers of kaolinite and goethite (Table 4.1). Scanning electron microscopy (SEM; Cambridge Stereoscan 240) and energy–dispersive x–ray spectroscopy (EDX; Link Analytical) on thin sections coated by Au and Pd showed that (1) Fe was intimately mixed with kaolinite in the coatings (Fig. 4.2a) and (2) the molar ratio of Fe/Si $\approx$ 0.1 in the coatings (Ryan and Gschwend, 1992; Chapter 2). The Fe/Si ratio determined from free Fe (39.3 μmol Fe) and clay–sized content (0.038 g clay per g sediment, assuming all clay is kaolinite, $Al_2Si_2O_5[OH]_4$) is Fe/Si = 0.13. Thus, there are are about five moles of kaolinite for every mole of goethite (assuming all Fe is goethite, α–FeOOH).

For the column experiments, the sand sample was dried at 60° C and gently sifted through 1.0 and 0.25 mm wire sieves to improve subsample homogeneity. The 0.25 to 1.0 mm fraction comprised 80 wt% of the total sample. Most of the remaining magnetic heavy minerals, mainly Fe–Ti oxides, were removed by gently vibrating the sand through an acrylic trough with a thin (0.32 cm) bottom over a 0.3 T magnet.

Groundwater. The groundwater sample was collected in November 1991 from a well screened 2 m below a swampy intermittent stream (McDonalds Branch) and 50 m upstream from where the sediment sample was obtained (Swamp Shallow, well QWH–1A; Ryan and Gschwend, 1990). Water was pumped from the well with a

Table 4.1. Composition of the natural sediment sample collected from McDonalds Branch watershed, Lebanon State Forest, New Jersey. For analytical details, see Ryan and Gschwend (1992) and Chapter 2.

	Sample U.11.1	
depth	7.3 to 8.8 m	
clay–sized fraction (< 2 μm)	3.8±0.4 wt%	sedimentation
minerals	kaolinite goethite quartz	x–ray diffraction
heavy mineral fraction (>2.89 g cm^{-3})	1.1±0.1 wt%	$CHBr_3$ sedimentation
minerals	pseudorutile ilmenite rutile	x–ray diffraction
free Fe	39±2 μmol g^{-1}	Ti(III) extraction
free Al	7.2±0.6 μmol g^{-1}	(Ryan and Gschwend, 1991)
total Fe	77±2 μmol g^{-1}	$HF/HCl/HNO_3$ digestion
total Ti	72±2 μmol g^{-1}	
organic matter	0.45±0.07 wt%	loss on ignition (450° C, 6 hr)
specific surface area	0.51±0 10 m^2 g^{-1}	before flushing
	0.15±0.03 m^2 g^{-1}	after flushing (950 pore volumes of $1 \cdot 10^{-2}$ M H_2Asc_{tot})

peristaltic pump through polytetrafluoroethylene (PTFE) and silicone tubing at a flow rate of 1 L min^{-1}. Three well volumes were purged prior to collection of samples in overflowed, ground glass–stoppered bottles. The samples were placed in a cooler for transport to the laboratory and stored at 5° C prior to experiments. The groundwater is acidic, anoxic, and contains abundant organic matter and Fe(II) (Table 4.2).

Figure 4.2 is shown on the following page.

Fig. 4.2. Secondary electron SEM images of sediments and colloids released from the sediments (clockwise):
(a) Thin–section of sample U.11.1 showing anisopachous kaolinite–Fe(III) oxide coatings on quartz grains.
(b) Sediment after high–I and low–I flush (110 pore volumes) at pH 4.8. Loose coatings of Fe(III) oxides and kaolinite remained on the quartz surfaces.
(c) Sediment after long–term 10^{-2} M ascorbic acid reduction (950 pore volumes). Coatings on smooth faces of the quartz grains were removed, while surface irregularities remained filled with Fe(III) oxides and kaolinite.
(d) Colloids mobilized from the sediment after 10^{-2} M ascorbic acid reduction (54 pore volumes). Particles were mainly kaolinitic plates in the < 2 μm size range.

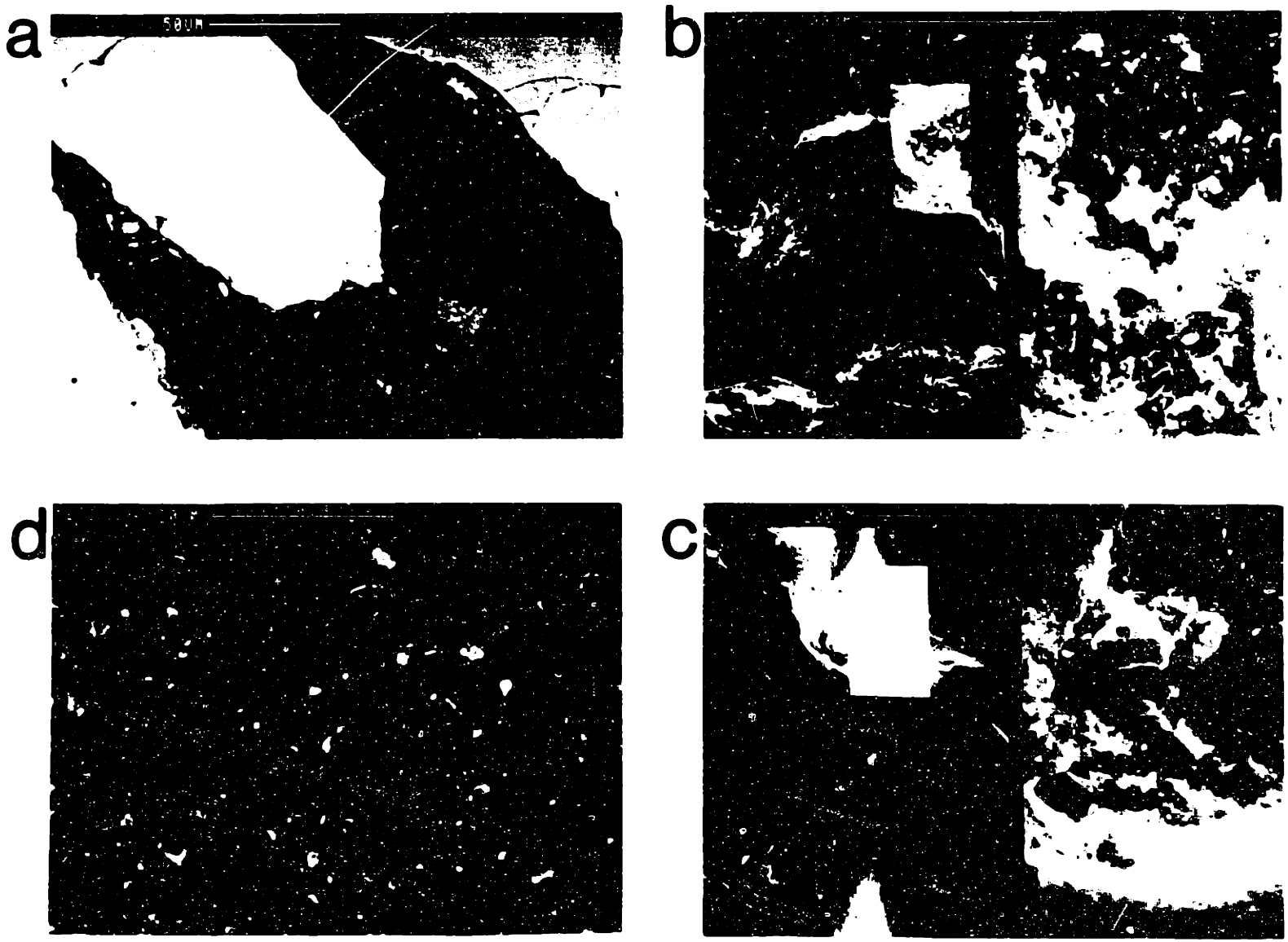
a
50UM
b
d
c

Table 4.2. Composition of the natural groundwater sample collected from McDonalds Branch watershed, Lebanon State Forest, New Jersey. For analytical details, see Ryan and Gschwend (1990).

	Well QWH—1a	
pH	4.16	combination electrode
I	1.0±0.1 mM	Ryan and Gschwend (1990)
E_h	250±25 mV	Pt electrode/4 M Ag—AgCl reference (relative to standard H electrode)
dissolved O_2	6±3 μM	colorimetric test kit (Chemetrics, Inc., Calverton, VA)
Fe(II)	42±0.6 μM	TPTZ complexation
Fe_{tot}	42±0.6 μM	NH_2OH reduction/TPTZ complexation
organic C	1.70±0.13 mM	800° C oxidation on Pt catalyst (Sugimura and Suzuki, 1988)
colloidal "clay"	0.27±0.05 mg L^{-1}	turbidity; kaolinite standard curve

Reaction Column

Experiments were conducted in the reaction column depicted in Fig. 4.3. Solutions were pumped by an HPLC pump upward through the sand, which was packed in a polypropylene filter holder (Millipore Swinnex 47 mm diameter). Solutions added to the column were sparged with argon and titrated to proper *p*H with HNO_3 or NaOH. The head space over the solution reservoir was flushed by a constant flow of argon. Ascorbic acid (H_2Asc) solutions were sparged with argon prior to H_2Asc addition and wrapped in foil to curtail photo–oxidation. The specific conductivity of the incoming solution was measured by a conductivity meter and micro–flow cell (Amber Science 1054 and 529, Eugene, OR) to determine when new solutions entered the column. The column effluent immediately entered a turbidity flow cell (fashioned from a 3 mL glass pipette) in a turbidity meter (Hach Ratio

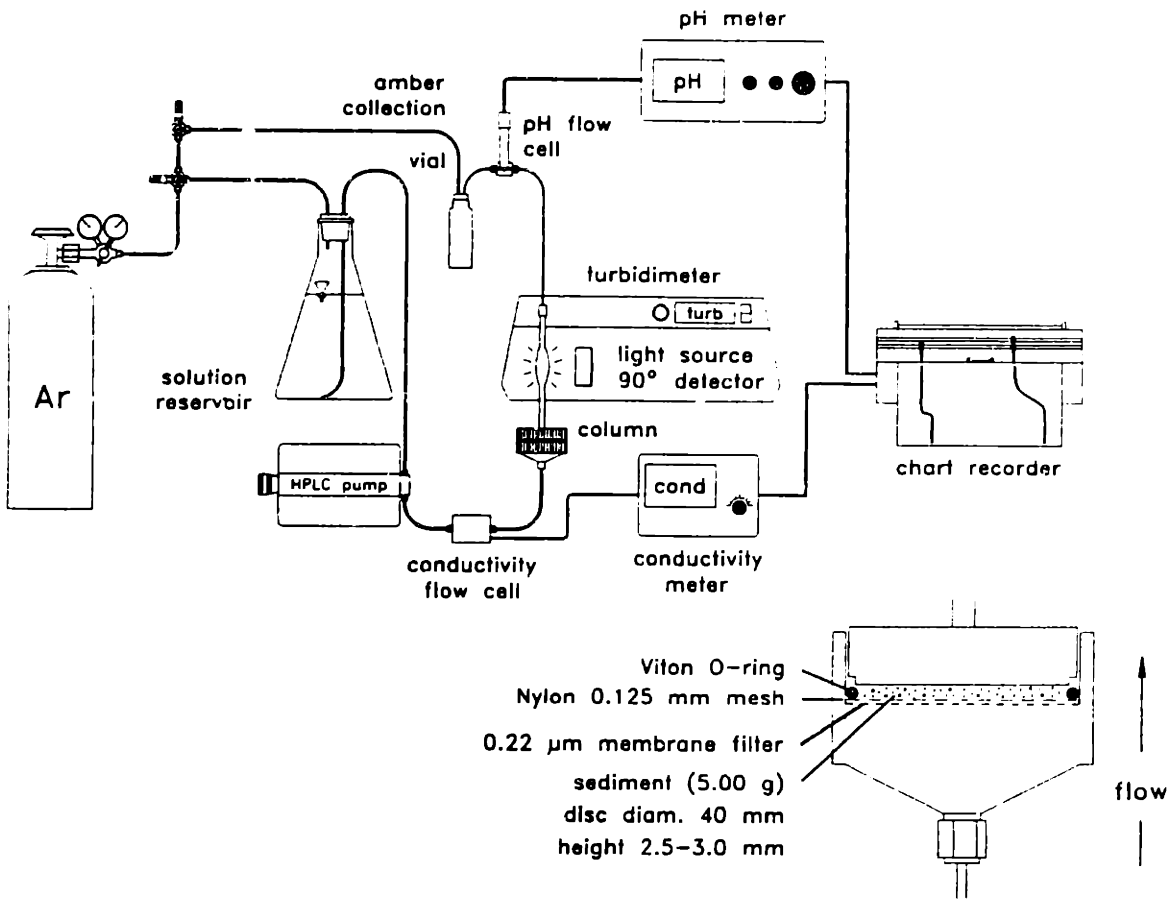

Fig. 4.3. Experimental setup with enlargement of short flow–path column.

X/R, Loveland, CO). Effluent *p*H was measured by a Ross combination electrode connected to a *p*H meter (Orion 701A) in a low–volume flow cell. The column effluent was collected in amber glass vials flushed with inert gas. PTFE tubing (1.6 mm i.d.) and fittings connected the solution reservoir, pump, flow cells, and collection vial.

A column with a short flow path was used to minimize the re–attachment of particles mobilized by the solution. The filter holder was modified by adding a 0.22 μm membrane filter to remove particles in the incoming solutions and a nylon screen (120 mesh, 0.125 mm) and Viton O–ring (40 mm diameter) to retain the sand. The entire disk of sand was exposed to the flowing solutions. The sand formed a disk of 2.5 to 3.0 mm height and 40 mm diameter, or 3.1 to 3.8 cm^3 column volume (V_{col}). The pore volume (V_{pore}) of the sand was estimated for each run by assuming a density of solids $\rho_s = 2.65$ g cm^{-3}. For example,

$$V_{pore} = V_{col} - V_{solid}$$
$$= (0.27\ cm)\pi(2.0\ cm)^2 - \left[\frac{5.00\ g}{2.65\ g\ cm^{-3}}\right] = 1.5\ cm^3 \qquad [4.1]$$

The experiments were performed at a flow rate of $Q = 0.50 \pm 0.05$ mL min^{-1}, which corresponds to column residence times of 2.3 to 4.2 min and groundwater velocities from 1.0 to 1.6 m day^{-1}. This range of groundwater velocity is within the range of velocities that have been measured in the permeable Cohansey sediments (Rhodehamel, 1979).

Reaction Column Monitoring

Reagent grade chemicals were used without further purification in the experiments. Distilled deionized water (ddW) used to prepare solutions was purified by the Millipore Milli–Q system (18 MΩ resistivity). Deionized water (dW) used to rinse laboratory ware was purified by reverse osmosis (1 MΩ). Laboratory ware was soaked in 4 N HNO_3 and rinsed in dW prior to use. The

column was sonicated in dW and soaked in 0.1 N HNO_3 overnight between each run. The turbidity flow cell was immersed in chromic–sulfuric acid solution overnight, rinsed with dW, and coated with silicone on the outer surface prior to each experiment.

Turbidity. The turbidity (intensity of light scattered by suspended particles collected at an angle of 90° to the polychromatic incident beam) of the column effluent was measured continuously. Turbidity was converted to "clay" concentration by comparing the measured turbidity to a standard curve of turbidity *vs.* kaolinite suspension concentration. Kaolinite suspensions in the range of 0.1 to 10 mg L^{-1} were prepared by dilution of a 100 mg L^{-1} suspension of < 2 μm fraction of colloidal kaolin powder (EM Science, Gibbstown, NJ) isolated by sedimentation. Turbidity (T; NTU) was linearly related to kaolinite suspension concentration ([K]; mg L^{-1}) for the flow–through glass cell arrangement by:

$$T - B = 0.623[K] + 0.004 \quad (R^2 = 0.9986) \qquad [4.2]$$

where B is the baseline turbidity (NTU) for each run, determined as the turbidity of 0.22 μm–filtered ddW. The baseline turbidity ranged between 0.050 and 0.090 NTU. The turbidity meter was zeroed and calibrated prior to each run with independent standards. Turbidity data were collected on a chart recorder, digitized, and converted into clay concentrations. The total mass of clay released in a given time was divided by the flow rate Q to determine the clay release rate (g min^{-1}). The varying baseline turbidity resulted in clay release rate detection limits of $3.7 \cdot 10^{-8}$ to $6.9 \cdot 10^{-8}$ g min^{-1}. At the low clay release rates measured in these experiments, the major source of error in the clay release rate measurement is the variable baseline.

Dissolved Fe. The amount of Fe dissolved in the column was measured as the absorption of light at 595 nm by the $Fe(II)(TPTZ)_2^{2+}$ complex (TPTZ: 2,4,6–tri(2–pyridyl)–1,3,5–triazine; Dougan and Wilson, 1973) with a Bausch &

Lomb model 100 spectrophotometer. The Fe(II) determination had a detection limit of 21 nM Fe(II) and precision of ±1.5%. Total dissolved Fe was measured by adding hydroxylamine hydrochloride ($NH_2OH \cdot HCl$) to reduce dissolved Fe(III) to Fe(II) prior to complexation. The total Fe measurement had a detection limit of 35 nM and similar precision. The Fe(III) oxide dissolution rate (mol min^{-1}) was determined in the same way as the clay release rate. The detection limit for the Fe(III) oxide dissolution rate was $1.1 \cdot 10^{-11}$ mol min^{-1} for Fe(II) and $1.8 \cdot 10^{-11}$ mol min^{-1} for total Fe.

Electrophoretic Mobility. Electrophoretic mobilities were measured at 25° C with a Rank Brothers Mk II microelectrophoresis apparatus with a cylindrical cell, Pt–blacked electrodes, and a 3 mW He–Ne laser. The mobilities (U, $m^2\ V^{-1}\ s^{-1}$) of 20 particles timed in both directions and at both stationary levels were converted to ζ–potentials (V) using the Smoluchowski formula (Hunter, 1981)

$$\zeta = \frac{U\eta}{\epsilon\ \epsilon_0} \qquad [4.3]$$

where η is the viscosity of water (kg $m^{-1}\ s^{-1}$), ϵ is the dielectric constant of water (dimensionless), and ϵ_0 is the permittivity of free space (C $V^{-1}\ m^{-1}$). Clay concentrations in the effluent were generally too low to allow measurement of the ζ–potentials of the released clay, so separate runs were made during which the columns were lightly tapped to promote clay mobilization.

Sediment and Colloid Analyses. Residual sand samples were collected after some runs and examined with SEM/EDX. Suspended particles trapped on 0.02 μm membrane filters (Anotec Separations, Ltd., Oxon, England) were also examined. The column residues and filtered particles were air–dried, mounted on Al stubs with colloidal graphite, Au–coated, and examined with SEM/EDX. The specific surface area of the sand before and after reduction was determined by single–point N_2–BET analysis (Porous Materials, Inc., Ithaca, NY).

Experimental Procedures

The experimental conditions are summarized in Table 4.3. The experiments were preceded by high–I and low–I flushes. The high–I flushes presumably removed only those particles loosened during column assembly. The various low–I flushes provided baseline clay release rates against which the experimental clay release rates could be compared. The high–I and low–I flushes were run until turbidity reached stable levels comparable to the background turbidity, which required at least 20 pore volumes in every run. Most of the solutions contained a dilute acetic acid/acetate (HAc/Ac^-) solution which buffered pH near the ambient pH of the groundwater in the oxic sediment.

In the ΔI and duplicate ΔpH experiments, successively lower I and higher pH solutions were run through single sediment columns. $NaNO_3$ was used to adjust I and HNO_3 and NaOH were used to adjust pH.

Ascorbic acid (H_2Asc), which dissolves Fe(III) oxides through complexation and reduction of surface Fe(III) (Zinder *et al.*, 1986; Suter *et al.*, 1991), was used as the reductant. ΔH_2Asc experiments were conducted at pH 4.8 and 6.0 in separate columns for each reductant concentration. The reductant solutions were followed by low–I flushes at the same pH. In the ΔpH H_2Asc experiment, the successively higher pH reductant solutions were separated by intervening low–I flushes at the next higher pH.

Dodecanoic acid ($CH_3(CH_2)_{10}COOH$, or RCOOH), a long–chain fatty acid, was used as the surfactant. In duplicate ΔRCOOH experiments, the surfactant solutions were separated by low–I flushes. In the ΔpH RCOOH experiment, the surfactant solutions were separated by low–I flushes at the next higher pH.

Table 4.3. Summary of experimental conditions including composition and number of pore volumes (no. PV) of solutions run through columns. Acetic acid/acetate (HAc/Ac^-) buffer shown in parentheses when included in all solutions of a series. Ascorbic acid (H_2Asc) and dodecanoic acid (RCOOH) added as acids. All experiments were conducted at 0.50±0.05 mL min^{-1}.

procedure	ΔI	ΔpH	ΔH_2Asc
1. high—I flush	0.5 M $NaNO_3$ $5 \cdot 10^{-4}$ M HAc/Ac^- *p*H 4.8	0.5 M $NaNO_3$ $5 \cdot 10^{-4}$ M HAc/Ac^- *p*H 2.0	0.5 M $NaNO_3$ $5 \cdot 10^{-4}$ M HAc/Ac^- *p*H 4.8, 6.0
no. PV	$\geq$ 40	$\geq$ 20	$\geq$ 20
2. low—I flush		$1 \cdot 10^{-2}$ M $NaNO_3$ $5 \cdot 10^{-4}$ M HAc/Ac^- *p*H 2.0	$5 \cdot 10^{-4}$ M HAc/Ac^- *p*H 4.8, 6.0
no. PV		$\geq$ 20	$\geq$ 20
3. experiment	$5 \cdot 10^{-1}$ M $NaNO_3$ $5 \cdot 10^{-2}$ M $NaNO_3$ $5 \cdot 10^{-3}$ M $NaNO_3$ $5 \cdot 10^{-4}$ M $NaNO_3$ $5 \cdot 10^{-5}$ M $NaNO_3$ single column	$1 \cdot 10^{-2}$ M $NaNO_3$ ($5 \cdot 10^{-4}$ M HAc/Ac^-) *p*H 2.0 to 10.0 by addition of HNO_3 and NaOH single column	$1 \cdot 10^{-4}$ M H_2Asc $1 \cdot 10^{-3}$ M H_2Asc $1 \cdot 10^{-2}$ M H_2Asc $1 \cdot 10^{-1}$ M H_2Asc ($5 \cdot 10^{-4}$ M HAc/Ac^-) *p*H 4.8, 6.0 separate columns
no. PV	20 each	20 each	$\geq$ 45
4. flush			$5 \cdot 10^{-4}$ M HAc/Ac^- *p*H 4.8, 6.0 following
no. PV			$\geq$ 45

Table 4.3. (continued). Composition and number of pore volumes (no. PV) of solutions run through sand column. Acetic acid/acetate (HAc/Ac^-) buffer shown in parentheses when included in all solutions of an experimental series. Ascorbic acid (H_2Asc) and dodecanoic acid (RCOOH) added as acids. All experiments were conducted at 0.50 ± 0.02 mL min^{-1}.

procedure	**ΔpH H_2Asc**	**ΔRCOOH**	**ΔpH RCOOH**
1. high—*I* flush	0.5 M $NaNO_3$ $5 \cdot 10^{-4}$ M HAc/Ac^- *p*H 3.0	0.5 M $NaNO_3$ $5 \cdot 10^{-4}$ M HAc/Ac^- *p*H 4.8	0.5 M $NaNO_3$ $5 \cdot 10^{-4}$ M HAc/Ac^- *p*H 3.0
no. PV	$\geq$ 20	$\geq$ 20	$\geq$ 20
2. low—*I* flush	$5 \cdot 10^{-4}$ M HAc/Ac^- *p*H 3.0	$5 \cdot 10^{-4}$ M HAc/Ac^- *p*H 4.8	$5 \cdot 10^{-4}$ M HAc/Ac^- *p*H 3.0
no. PV	$\geq$ 20	$\geq$ 20	$\geq$ 20
3. experiment	$1 \cdot 10^{-3}$ M H_2Asc ($5 \cdot 10^{-4}$ M HAc/Ac^-) *p*H 3.0 to 7.0 by addition of HNO_3 and NaOH single column	$1.2 \cdot 10^{-5}$ M to $1.6 \cdot 10^{-4}$ M RCOOH ($5 \cdot 10^{-4}$ M HAc/Ac^-) single column	$8.0 \cdot 10^{-5}$ M RCOOH ($5 \cdot 10^{-4}$ M HAc/Ac^-) *p*H 3.0 to 8.0 by addition of HNO_3 and NaOH single column
no. PV	20 each	20 each	20 each
4. flush	$5 \cdot 10^{-4}$ M HAc/Ac^- next *p*H intervening	$5 \cdot 10^{-4}$ M HAc/Ac^- *p*H 4.8 intervening	$5 \cdot 10^{-4}$ M HAc/Ac^- *p*H 4.8 intervening
no. PV	10	10	10

Calculating Detachment Energy

To estimate detachment energies, we calculated the total potential energy $\phi^{tot}(x)$ between colloid and grain surfaces as the sum of the London–van der Waals attractive, Born repulsive, and double layer potentials energies (see Chapter 3 for the complete expressions):

$$\phi^{tot}(x) = \phi^{vdw}(x) + \phi^{born}(x) + \phi^{dl}(x) \qquad [4.4]$$

The London–van der Waals potential was calculated with the Hamaker (1937) expression for the unretarded interaction of two spheres. The short–range Born repulsion potential was calculated with the Feke *et al.* (1984) expression for the interaction of two spheres. The double layer potential was calculated with a linearized solution of the Poisson–Boltzmann (PB) equation adapted for sphere–sphere interaction by a one–dimensional integration of plate–plate interaction for the constant potential case (Hogg *et al.*, 1966). Due to linearization of the PB equation, the accuracy of the Hogg *et al.* (1966) expression decreases for $\psi_0 > 25$ mV and small separation distances compared to an exact (numerical) solution of the full PB equation. Because we were more interested in the relative change of ϕ^{dl} with solution chemistry than in absolute accuracy, we used the Hogg *et al.* (1966) expression instead of a numerical solution of the full PB equation.

Although the colloids were clay plates with different charge on faces and edges, it was decided that they would be better represented as spheres because they were randomly oriented in the grain coatings. The average radii of the clay colloids and sand grains were taken as $a_c = 5 \cdot 10^{-7}$ m and $a_g = 2.5 \cdot 10^{-4}$ m. We used a Born collision parameter of $\sigma = 5$ Å and a Hamaker constant of $A = 4 \cdot 10^{-20}$ J. Hamaker constants of $1.7 \cdot 10^{-20}$ (Hough and White, 1980) and $4.4 \cdot 10^{-20}$ J (Flegmann *et al.*, 1969) have been used for pure kaolinite colloids. The reciprocal double layer thickness (κ, m^{-1}) is defined by

$$\kappa^2 = \frac{2000\ N_a I\ e^2 z^2}{\epsilon \epsilon_0 kT} \qquad [4.5]$$

where N_a is Avogadro's number, I is the ionic strength (mole L^{-1}), e is the elementary charge (C), z is the valence of a symmetrical electrolyte, k is the Boltzmann constant (J K^{-1}), and T is the absolute temperature (K).

The intersurface potential energy profile was calculated with a resolution of $\Delta x = 1 \cdot 10^{-11}$ m near ϕ_{min1} and ϕ_{max} and $\Delta x = 1 \cdot 10^{-10}$ m near ϕ_{min2}. The detachment energy ϕ^{det} was calculated in two ways: (1) as the kinetic energy barrier $\phi^{det} = -(\phi_{max} - \phi_{min1})$ and (2) as the equilibrium $\phi^{det} = -(\phi_{min2} - \phi_{min1})$, where $(\phi_{min2} - \phi_{min1})$ reflects the energy difference between the two equilibrium states (for a detailed explanation of the colloid detachment kinetics models, see Chapter 3).

The major source of error in ϕ^{det} comes from the measurement of electrophoretic mobilities and conversion to ζ–potential and then to ψ_0 (estimated error of ± 25%). At high I and low ψ_0 (< 30 mV), we estimate the precision of ϕ^{det} at < ± 5%; but at low I and high ψ_0 (>70 mV), precision is < ± 80%. The error due to the linearization of the PB equation in ϕ^{dl} is comparatively small at surface potentials less than about 150 mV (Hogg *et al.*, 1966).

Estimating Surface Potentials from Zeta Potentials

At high ionic strength and high surface charge, ζ–potentials fail to provide good estimates of ψ_0 (Hunter, 1981; Dzombak and Morel, 1990). Because ϕ^{dl} depends on ψ_0^2 and is thus very sensitive to the surface potential, we attempted to obtain more accurate values of ψ_0. Ideally, we would estimate surface potentials for kaolinite and goethite with an SCDL model; however, the clay colloids presented greater difficulty. Kaolinite contains two oxides (>Al–OH, >Si–OH) on the edges and a permanent negative charge arising from isomorphic substitution on the faces (Greenland and Mott, 1978). Carroll–Webb and Walther (1988) attempted to fit kaolinite acid–base titration data by modeling kaolinite as a two–site oxide; however, they varied the Al/Si site density ratio with *p*H and ignored the

permanent charge. As an added complexity to this approach, the modeling of our colloids would require a three–site model to include the effects of goethite attached to the kaolinite colloids.

Instead, we estimated ψ_o from ζ–potential by deriving a relationship between ζ–potentials measured for rutile (TiO_2) and alumina (γ–Al_2O_3) (Wiese and Healy, 1975) and surface potentials calculated for these simple oxides with an SCDL model (ψ_{scdl}). Details of the development of the relationship are given in Appendix 2. Values of ψ_{scdl} were calculated for the range of *p*H and I over which ζ–potentials were measured with the parameters listed in Table 4.4. The proton exchange reactions were solved iteratively with DSURF (Dzombak and Morel, 1990), a version of MINEQL (Westall *et al.*, 1976) modified to account for double layer interactions. For each of the three ionic strengths (0.01, 0.001, and 0.0001 M), ζ–potential (mV) was fit to ψ_{scdl} (mV) by least squares regression with

$$\psi_{scdl} = \zeta + \{\exp [a(I)\ \zeta] - 1\} \qquad [4.6]$$

The constant $a(I)$ was related to the variation with I through κ, yielding

$$\psi_{scdl} = \zeta + \{\exp [(4.71 \cdot 10^{-4}\ \kappa^{0.281})\ \zeta] - 1\} \qquad [4.7]$$

The ζ–potentials measured for the clay colloids were used in this equation to estimate surface potentials. These surfaces potentials were used to calculate ϕ^{dl}.

Table 4.4. Parameters used to calculate surface potentials of two oxides (Wiese and Healy, 1975) with a surface complexation/double layer model.

Parameter	alumina γ—Al_2O_3	rutile TiO_2
$[M\text{—OH}]_{tot}$ (mmol g^{-1})	0.21	0.20
pK_{a1}	7.7	3.7
pK_{a2}	10.3	8.1
S_s (m^2 g^{-1})	80	16.5
C_s (g L^{-1})	0.15	0.05

Site density ($[M\text{—OH}]_{tot}$) and intrinsic acidity constants (ΔpK_{a1}, ΔpK_{a2}): Carroll—Webb and Walther (1988), Dzombak and Morel (1990).

Specific surface area (S_s) and suspension concentration (C_s): Wiese and Healy (1975).

Morphology of Natural Sediment and Mobilized Colloids

After high– and low–I flushes, loose coatings of Fe(III) oxides and kaolinite remained on the quartz surfaces (Fig. 4.2b). Reduction with ascorbic acid removed much of the coatings on smooth faces of the quartz grains, while surface irregularities remained filled with Fe(III) oxides and kaolinite (Fig. 4.2c).

Particles released from the sediment and trapped on 0.02 μm filters had the composition of kaolinite and were generally < 2 μm in diameter (Fig. 4.2d), similar to those found in the natural groundwater (Ryan and Gschwend, 1990). However, discrete Fe(III) oxide colloids were not detected on the filters under any column conditions, although such oxides were observed suspended in the natural groundwater. Fe was detected on the kaolinite colloids in low levels (< 3 mole%) during the I, pH, and surfactant runs, and at trace levels (< 0.5 mole%) during the reductant runs.

Sediment Flushing Experiments

Sudden ΔI. The clay concentration usually rose slightly just after the low–I solution was introduced; but after a few pore volumes, no significant difference between the high–I and low–I release rate could be discerned (Fig. 4.4a). The release rates were not significantly different for the high– and low–I flushes at pH 4.8 (Fig. 4.4b).

Gradual ΔI. The clay release rate nearly doubled over the four–order of magnitude decrease in I (Fig. 4.4b), but the increase may not have been significant given the precision of the turbidity measurements. The colloid ζ–potentials became more negative with decreasing I, but surface potentials obtained with the empirical ζ–κ–ψ_{scdl} relationship were relatively constant (Fig. 4.4c).

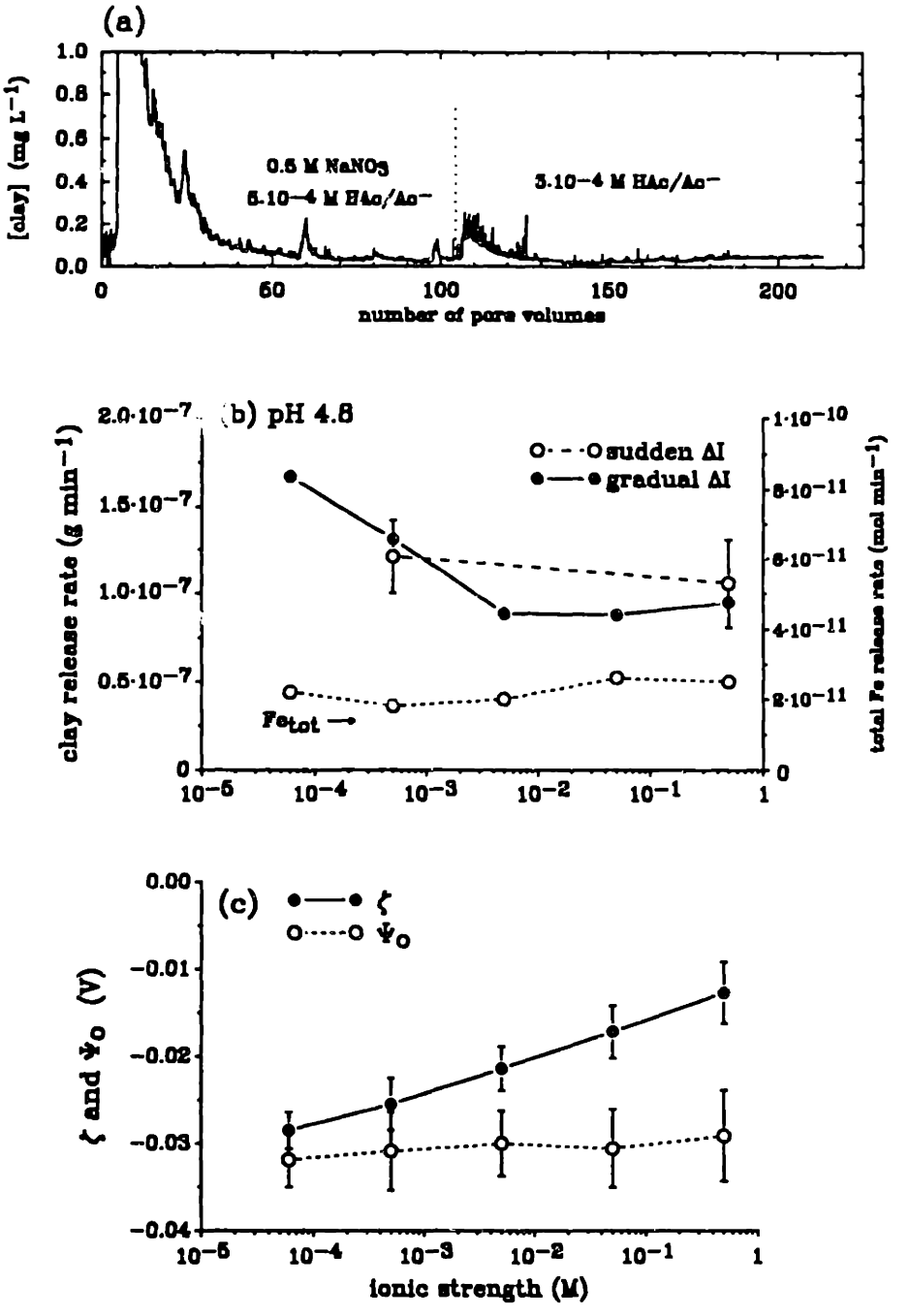

Fig. 4.4. Effect of changing I on clay release rate:
(a) Example of high–I/low–I flush at pH 4.8 used as preparation for further experiments. In initial flush, clay concentrations reached 45 mg L^{-1} (off–scale peak) as clays loosened by packing were removed.
(b) Plot of clay release and Fe(III) oxide dissolution rate *vs.* ionic strength ($[NaNO_3]$) at pH 4.8. The effects of sudden decreases in I from 0.5 M to 0.0005 M (error bars represent $\pm 1\sigma$, $n = 22$ runs) and a gradual decrease in I over four orders of magnitude are shown.
(c) Colloid zeta and surface potentials *vs.* ionic strength (error bars $\pm 1\sigma$, $n = 20$ for all zeta potential determinations).

ΔpH. The release rate roughly tripled as *p*H increased from 2.0 to 10.0 (Fig. 4.5a). Fe dissolution rates were inversely related to release rates. Colloid ζ–potentials reversed sign at approximately *p*H 3.0 (Fig. 4.5b).

ΔH_2Asc Reduction/Low–*I* Flush. The time course of an ascorbic acid reduction/low–*I* flush is shown in Fig. 4.6. The variation in release rates was not simply related to Fe(II) dissolution rates (Fig. 4.7a). Clay was released more efficiently at higher *p*H and lower $[H_2Asc]_{tot}$. Colloid ζ–potentials reached a minimum at 10^{-3} M H_2Asc_{tot} at both *p*H 4.8 and 6.0, but surface potentials became increasing more negative with increasing $[H_2Asc]_{tot}$ (Fig. 4.7b,c). When the low–*I* flush followed high $[H_2Asc]_{tot}$ reduction, much more clay was released. Most of the clay (> 80%) was released in the 5 pore volumes immediately following the introduction of the low–*I* solution. The low–*I* flush release rates were related to the Fe(III) dissolution rates measured during reduction at both *p*H 4.8 and 6.0 (Fig. 4.7a). In contrast, following the $1.0 \cdot 10^{-1}$ M H_2Asc_{tot} reduction with a high–*I* flush at *p*H 4.8 resulted in a decline of turbidity to pre–reduction levels in only 3 pore volumes.

H_2Asc Long–Term Reduction. Nine hundred fifty pore volumes of $1.0 \cdot 10^{-3}$ M H_2Asc solution were run through a sediment column (after high– and low–*I* flushes) at *p*H 4.8 (sediment residue shown in Fig. 4.2c). The release of clay and dissolution of Fe(II) were steady over the entire run. A total of 0.88 mg clay was released (at a rate of $3.09 \cdot 10^{-7}$ g min^{-1}), or only 0.5% of the total clay in the column (3.8 wt% clay content, 5.0 g in column). A total of 3.9 μmole Fe was dissolved (at a rate of $1.37 \cdot 10^{-9}$ mol min^{-1}), or 2.0% of the free Fe in the column.

ΔpH H_2Asc. Clay release rates increased with increasing *p*H while the Fe(II) dissolution rates decreased (Fig. 4.8a). The colloid ζ–potentials and surface potentials became more negative with *p*H (Fig. 4.8b).

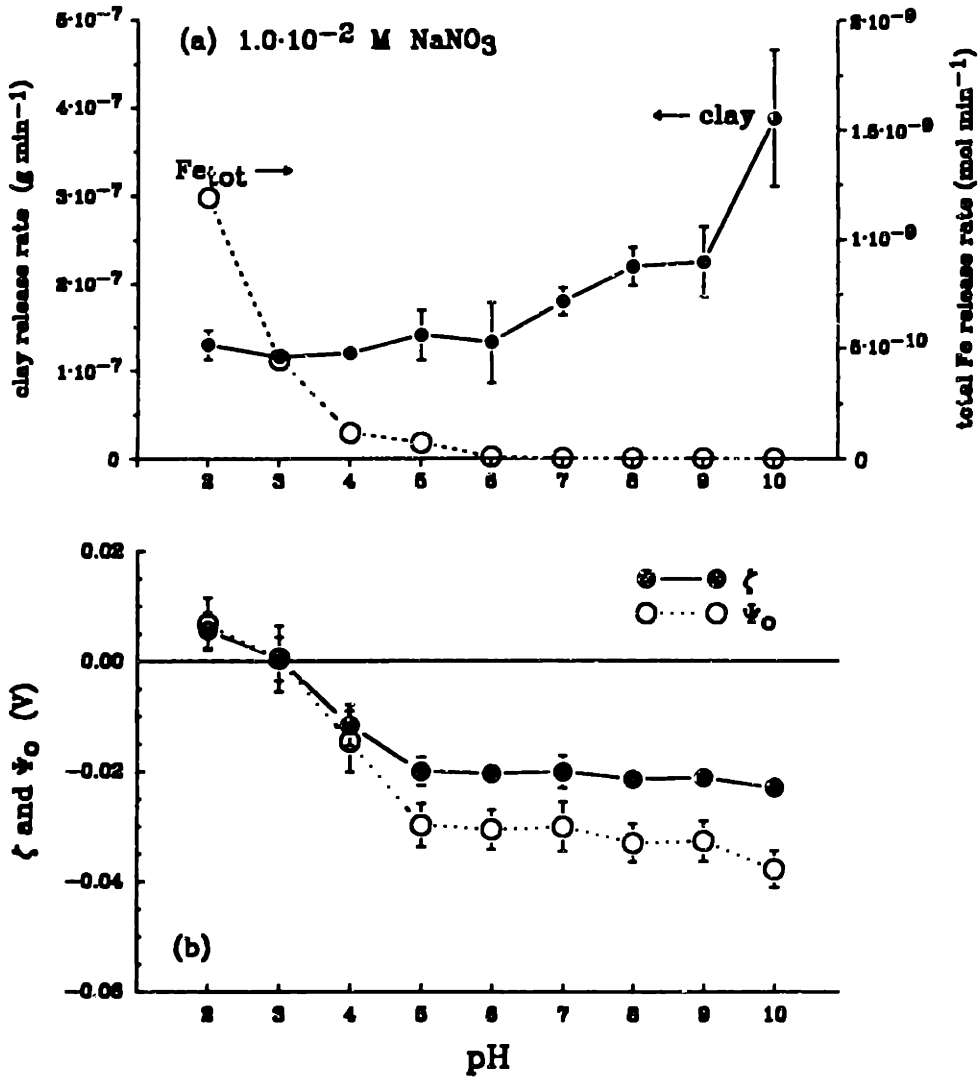

Fig. 4.5. Effect of changing *p*H on clay release rate:
(a) Plot of clay release and Fe(III) oxide dissolution rate *vs.* influent *p*H at $I = 1.0 \cdot 10^{-2}$ M $NaNO_3$. Data are mean clay release rates for two runs.
(b) Colloid zeta and surface potentials *vs.* *p*H.

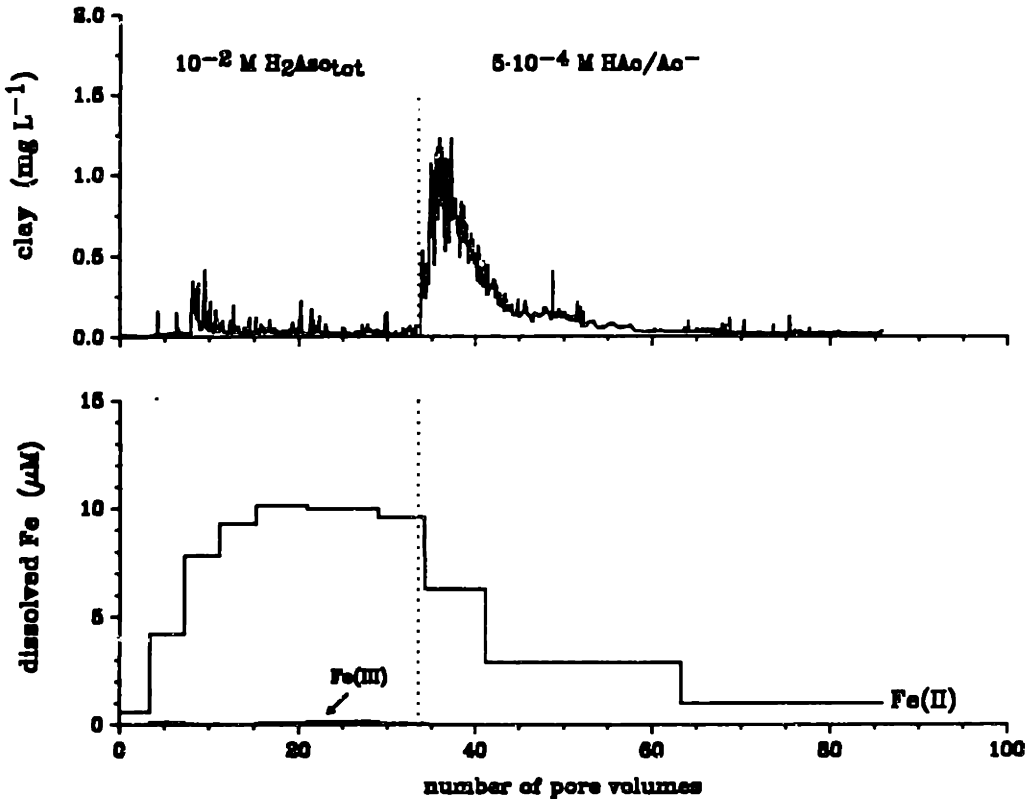

Fig. 4.6. Example of ascorbic acid/low–*I* flush for $1.0 \cdot 10^{-2}$ M H_2Asc_{tot} and $5.0 \cdot 10^{-4}$ M HAc/Ac$^-$ at *p*H 4.8. Each reduction/low–*I* flush was preceded by a high *I*/low *I* flush similar to that shown in Fig. 4.4a. Clay concentration was measured continuously; Fe was measured in integrated samples. During the low–*I* flush, most of the clay was released in the first five pore volumes.

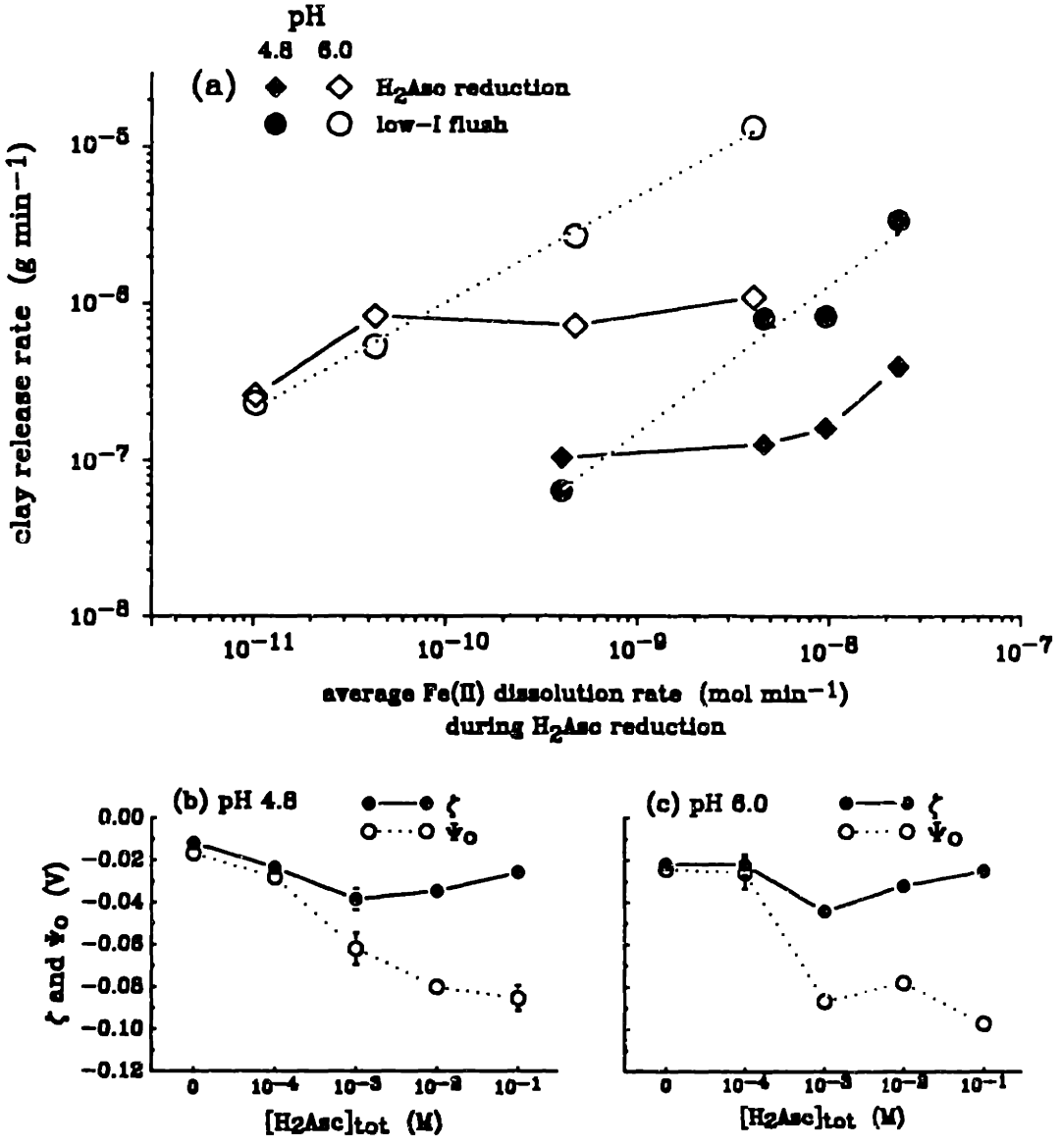

Fig. 4.7. Effect of changing ascorbic acid concentration on clay release rate at *p*H 4.8 and 6.0:
(a) Logarithmic plot of clay release rate *vs.* Fe(II) release rate during ascorbic acid reduction (circles) and ensuing low–*I* flush (diamonds) at *p*H 4.8 (filled symbols) and 6.0 (open symbols).
(b) Colloid zeta and surface potentials *vs.* ascorbic acid concentration at *p*H 4.8.
(c) Colloid zeta and surface potentials *vs.* ascorbic acid concentration at *p*H 6.0.

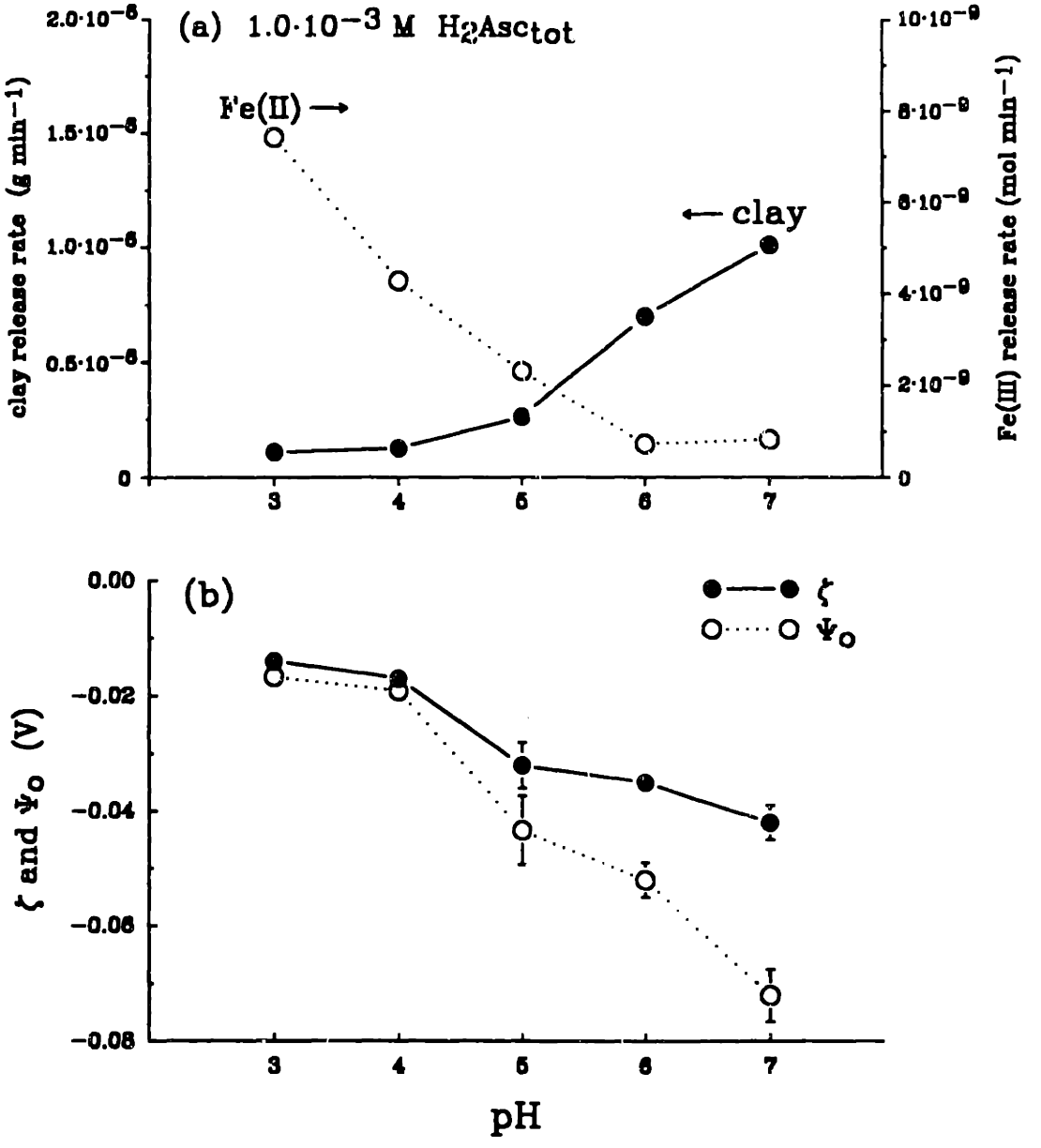

Fig. 4.8. Effect of changing *p*H on clay release rate in the presence of $1.0 \cdot 10^{-3}$ M H_2Asc_{tot}:
(a) Plot of clay release rate and Fe(II) release rate *vs.* *p*H.
(b) Colloid zeta and surface potentials *vs.* *p*H in column experiment.

ΔRCOOH. The release of clay colloids was relatively steady during flushing with the dodecanoic acid as shown in the time course of one of the ΔRCOOH experiments (Fig. 4.9a). Clay release rates increased dramatically in the presence of small amounts of dodecanoic acid (Fig. 4.9b). Colloid ζ–potentials became more negative with increasing dodecanoic acid concentration (Fig. 4.9c).

ΔpH RCOOH. Clay release rates increased with *p*H. The colloid ζ–potentials and surface potentials became more negative as *p*H increased (Fig. 4.10).

Natural Groundwater. Unamended natural groundwater was run through sediment columns following high– and low–*I* flushes at *p*H 4.2 (Table 4.5). The precision of the Fe_{tot} release rate is poor because $[Fe_{tot}]$ was determined as the difference between the effluent $[Fe_{tot}]$ and the initial $[Fe_{tot}]$ of the natural groundwater. The mean colloid ζ–potential was -0.030 V, resulting in $\psi_o = -0.049$ mV. In low–*I* flushes following the two shorter natural groundwater runs, turbidity decreased to levels measured in the preceding low–*I* flush in less than 5 pore volumes.

Clay Release Rate – Detachment Energy Relationships

The colloid ζ–potentials, surface potentials estimated with the ζ–κ–ψ_{scdl} relationship, the ϕ_{min1}, ϕ_{max}, and ϕ_{min2} values from the ϕ^{tot} profile, and the energy barrier and equilibrium model values of ϕ^{det} are listed in Table 4.6.

The persistence of the kaolinite–goethite coatings, even after reduction for 950 pore volumes, led us to assume that colloids were primarily released from grain surfaces still coated by other colloids. Therefore, the colloid and grain surface potentials were both characterized by the estimated ψ_{scdl} values of the colloids.

For the ΔH_2Asc low–*I* flushes, detachment energies were calculated with surface potentials measured during the H_2Asc reduction. If we can assume that the desorption of ascorbate from the clay colloid surfaces is no more rapid than its

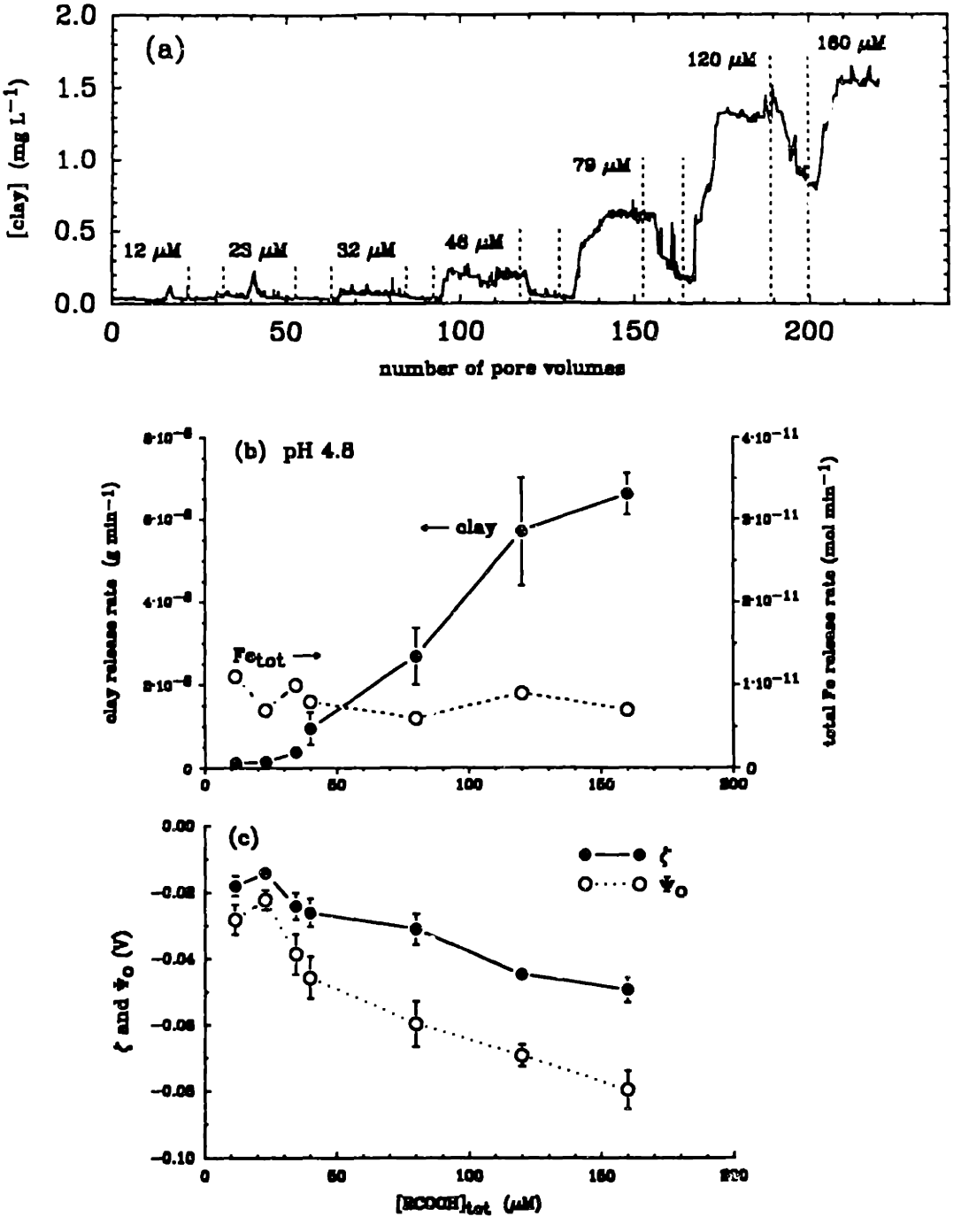

Fig. 4.9. Effect of changing dodecanoic acid concentration on clay release rate:
(a) Plot of clay concentration *vs.* number of pore volumes for ΔRCOOH experiment.
(b) Plot of clay release and Fe(III) oxide dissolution rate *vs.* dodecanoic acid concentration.
(c) Colloid zeta and surface potentials *vs.* dodecanoic acid concentration.

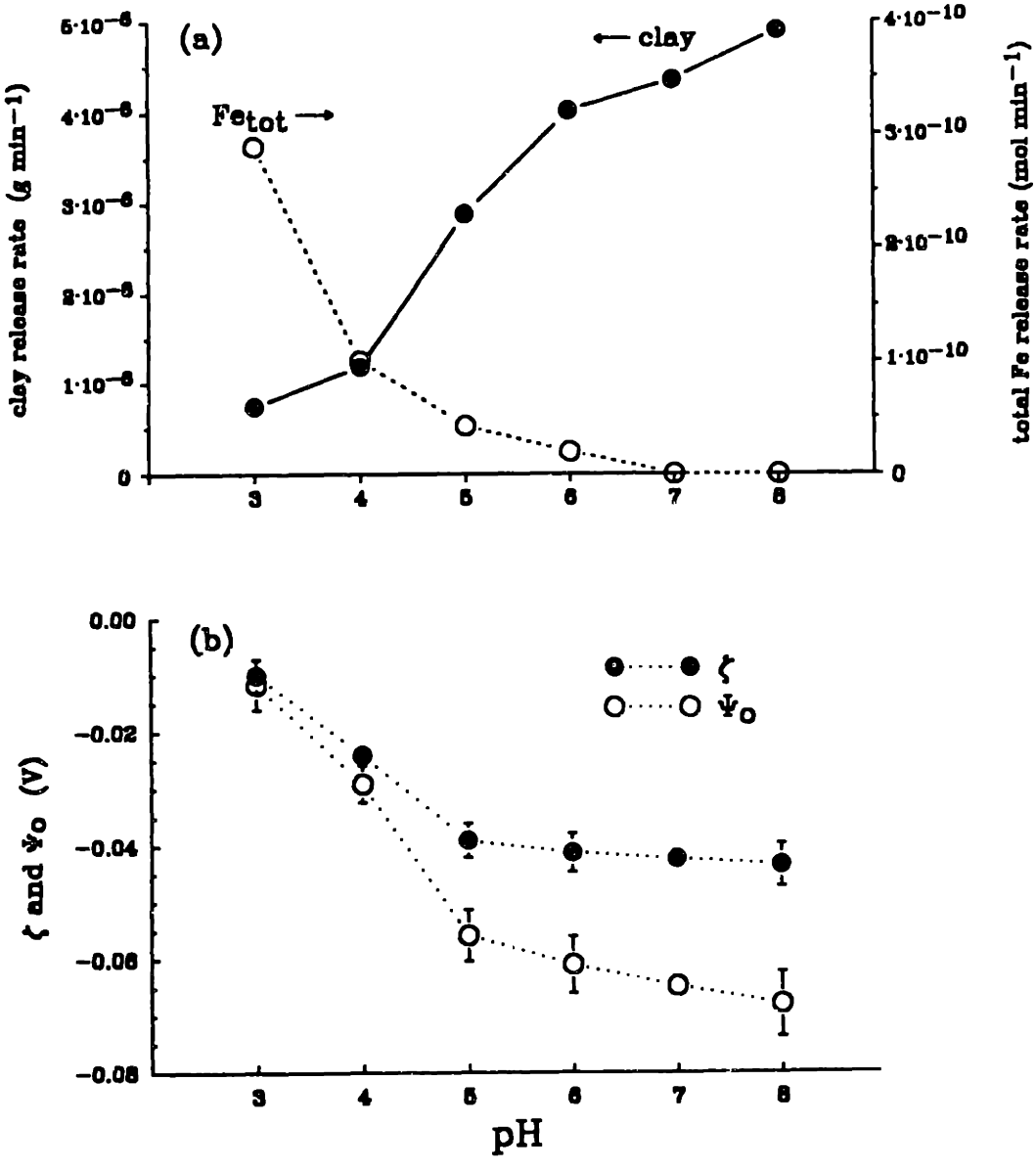

Fig. 4.10. Effect of *p*H on clay release rate in the presence of 80 μM dodecanoic acid concentration:
(a) Plot of clay release and Fe(III) oxide dissolution rate *vs.* *p*H.
(b) Colloid zeta and surface potentials *vs.* *p*H.

Table 4.5. Procedures used in three flushes of oxic sediment samples with the natural groundwater, including number of pore volumes (no. PV) of flushing solutions, and results of the three experiments.

run no.	1	2	3
1. high–I flush	——— 0.5 M $NaNO_3$ ——— $5 \cdot 10^{-4}$ M HAc/Ac^- *p*H 4.2		
no. PV		$\geq$ 20	
2. low–I flush	——— $5 \cdot 10^{-4}$ M HAc/Ac^- ——— *p*H 4.2		
no. PV		$\geq$ 20	
3. natural gw flush	——— unamended gw ——— *p*H 4.2		
no. PV	40	45	290
clay release (g min^{-1})	$2.7 \cdot 10^{-6}$	$1.8 \cdot 10^{-6}$	$2.4 \cdot 10^{-6}$
Fe_{tot} release (mol min^{-1})	$1.1 \pm 0.6 \cdot 10^{-9}$	$8.0 \pm 6.0 \cdot 10^{-10}$	$5.3 \pm 6.0 \cdot 10^{-10}$
ζ (V)	−0.031±0.004	−0.032±0.003	−0.027±0.004

adsorption to hematite and δ–Al_2O_3 surfaces (Banwart, 1989), the surface potentials measured during H_2Asc reduction may be considered valid for the first 5 pore volumes ($\leq$ 15 min) of the low–I flushes during which the bulk of clay was released.

For most of the experiments, clay release rates were positively correlated with both forms of ϕ^{det} (Fig. 4.11), with the notable exception of the ΔI experiment. For ΔI, the rates were positively correlated with the equilibrium ϕ^{det}, but negatively correlated with the energy barrier ϕ^{det}. The slope and intercepts of the

Table 4.6. Zeta potentials (ζ), estimated surface potentials (ψ_0), detachment energies calculated for equilibrium (equil) and energy barrier (en bar) models, and clay release rates for series of clay release experiments.

reductant	pH	I	ζ	ψ_0	equil $\phi^{det}/1000kT$	en bar $\phi^{det}/1000kT$	clay release rate
M		M	V	V			g min^{-1}
ΔI							
	4.8	$5.0 \cdot 10^{-1}$	−0.013	−0.029	−0.85	−0.85	$9.5 \cdot 10^{-8}$
		$5.0 \cdot 10^{-2}$	−0.017	−0.031	−0.63	−0.63	$8.8 \cdot 10^{-8}$
		$5.0 \cdot 10^{-3}$	−0.021	−0.030	−0.59	−0.85	$8.9 \cdot 10^{-8}$
		$5.0 \cdot 10^{-4}$	−0.026	−0.031	−0.53	−0.99	$1.30 \cdot 10^{-7}$
		$6.0 \cdot 10^{-5}$	−0.029	−0.032	−0.47	−1.08	$1.70 \cdot 10^{-7}$
ΔpH							
	2.0	$2.00 \cdot 10^{-2}$	0.006	0.007	−1.18	−1.18	$1.29 \cdot 10^{-7}$
	3.0	$1.10 \cdot 10^{-2}$	0.005	0.005	−1.22	−1.22	$1.15 \cdot 10^{-7}$
	4.0	$1.01 \cdot 10^{-2}$	−0.012	−0.015	−1.07	−1.07	$1.19 \cdot 10^{-7}$
	5.0	$1.00 \cdot 10^{-2}$	−0.020	−0.030	−0.61	−0.80	$1.40 \cdot 10^{-7}$
	6.0	$1.00 \cdot 10^{-2}$	−0.020	−0.031	−0.57	−0.79	$1.31 \cdot 10^{-7}$
	7.0	$1.00 \cdot 10^{-2}$	−0.020	−0.030	−0.59	−0.80	$1.78 \cdot 10^{-7}$
	8.0	$1.00 \cdot 10^{-2}$	−0.021	−0.033	−0.47	−0.76	$2.19 \cdot 10^{-7}$
	9.0	$1.00 \cdot 10^{-2}$	−0.021	−0.033	−0.48	−0.76	$2.24 \cdot 10^{-7}$
	10.0	$1.01 \cdot 10^{-2}$	−0.023	−0.038	−0.24	−0.69	$3.88 \cdot 10^{-7}$
ΔH_2Asc Reduction							
$1.0 \cdot 10^{-4}$	4.8	$5.6 \cdot 10^{-4}$	−0.024	−0.028	−0.64	−1.01	$1.03 \cdot 10^{-7}$
$1.0 \cdot 10^{-3}$		$1.1 \cdot 10^{-3}$	−0.039	−0.062	1.53	−0.70	$1.26 \cdot 10^{-7}$
$1.0 \cdot 10^{-2}$		$6.5 \cdot 10^{-3}$	−0.035	−0.080	3.25	−0.30	$1.61 \cdot 10^{-7}$
$1.0 \cdot 10^{-1}$		$6.05 \cdot 10^{-2}$	−0.026	−0.085	3.27	0.00	$3.96 \cdot 10^{-7}$
Low—I flush							
	4.8	$5.0 \cdot 10^{-4}$	−0.024	−0.028	−0.64	−1.01	$6.3 \cdot 10^{-8}$
		$5.0 \cdot 10^{-4}$	−0.039	−0.062	1.55	−0.78	$7.93 \cdot 10^{-7}$
		$5.0 \cdot 10^{-4}$	−0.035	−0.080	3.43	−0.66	$8.23 \cdot 10^{-7}$
		$5.0 \cdot 10^{-4}$	−0.026	−0.085	4.04	−0.63	$3.41 \cdot 10^{-6}$
Reduction							
$1.0 \cdot 10^{-4}$	6.0	$6.0 \cdot 10^{-4}$	−0.022	−0.026	−0.73	−1.02	$2.60 \cdot 10^{-7}$
$1.0 \cdot 10^{-3}$		$1.5 \cdot 10^{-3}$	−0.044	−0.087	4.14	−0.47	$8.28 \cdot 10^{-7}$
$1.0 \cdot 10^{-2}$		$1.05 \cdot 10^{-2}$	−0.032	−0.078	2.92	−0.24	$7.16 \cdot 10^{-7}$
$1.0 \cdot 10^{-1}$		$1.005 \cdot 10^{-1}$	−0.025	−0.097	4.36	0.00	$1.09 \cdot 10^{-6}$
Low—I flush							
	6.0	$5.0 \cdot 10^{-4}$	−0.022	−0.026	−0.73	−1.03	$2.31 \cdot 10^{-7}$
		$5.0 \cdot 10^{-4}$	−0.044	−0.087	4.20	−0.62	$5.29 \cdot 10^{-7}$
		$5.0 \cdot 10^{-4}$	−0.032	−0.078	3.16	−0.68	$2.69 \cdot 10^{-6}$
		$5.0 \cdot 10^{-4}$	−0.025	−0.097	5.61	−0.56	$1.33 \cdot 10^{-5}$

Table 4.6. (continued).

surfactant/ reductant	pH	I	ζ	ψ_0	equil ϕ^{det}/ 1000kT	en bar ϕ^{det}/ 1000kT	clay release rate
M		M	V	V			g min^{-1}
ΔpH H_2Asc							
$1.0 \cdot 10^{-3}$	3.0	$1.1 \cdot 10^{-3}$	−0.014	−0.017	−1.02	−1.08	$1.09 \cdot 10^{-7}$
	4.0	$6.0 \cdot 10^{-4}$	−0.017	−0.019	−0.95	−1.07	$1.25 \cdot 10^{-7}$
	5.0	$9.1 \cdot 10^{-4}$	−0.032	−0.043	0.14	−0.86	$2.62 \cdot 10^{-7}$
	6.0	$1.0 \cdot 10^{-3}$	−0.035	−0.052	0.73	−0.78	$7.01 \cdot 10^{-7}$
	7.0	$1.0 \cdot 10^{-3}$	−0.042	−0.072	2.52	−0.63	$1.01 \cdot 10^{-6}$
ΔRCOOH							
$1.2 \cdot 10^{-5}$	4.8	$5.1 \cdot 10^{-4}$	−0.018	−0.021	−0.91	−1.07	$1.20 \cdot 10^{-7}$
$2.3 \cdot 10^{-5}$		$5.2 \cdot 10^{-4}$	−0.014	−0.016	−1.03	−1.10	$1.50 \cdot 10^{-7}$
$3.2 \cdot 10^{-5}$		$5.2 \cdot 10^{-4}$	−0.025	−0.029	−0.59	−1.00	$3.82 \cdot 10^{-7}$
$4.6 \cdot 10^{-5}$		$5.3 \cdot 10^{-4}$	−0.026	−0.032	−0.49	−0.98	$9.53 \cdot 10^{-7}$
$7.9 \cdot 10^{-5}$		$5.5 \cdot 10^{-4}$	−0.031	−0.040	−0.08	−0.92	$2.69 \cdot 10^{-6}$
$1.2 \cdot 10^{-4}$		$5.8 \cdot 10^{-4}$	−0.041	−0.062	1.59	−0.76	$5.70 \cdot 10^{-6}$
$1.6 \cdot 10^{-4}$		$6.1 \cdot 10^{-4}$	−0.046	−0.077	3.00	−0.66	$6.61 \cdot 10^{-6}$
ΔpH RCOOH							
$8.0 \cdot 10^{-5}$	3.0	$1.5 \cdot 10^{-3}$	−0.010	−0.012	−1.12	−1.12	$7.40 \cdot 10^{-7}$
	4.0	$6.0 \cdot 10^{-4}$	−0.024	−0.029	−0.60	−1.00	$1.19 \cdot 10^{-6}$
	5.0	$5.4 \cdot 10^{-4}$	−0.039	−0.056	1.03	−0.81	$2.88 \cdot 10^{-6}$
	6.0	$5.7 \cdot 10^{-4}$	−0.041	−0.061	1.47	−0.77	$4.01 \cdot 10^{-6}$
	7.0	$5.8 \cdot 10^{-4}$	−0.042	−0.065	1.81	−0.75	$4.34 \cdot 10^{-6}$
	8.0	$5.8 \cdot 10^{-4}$	−0.043	−0.068	2.11	−0.72	$4.89 \cdot 10^{-6}$

individual rate – energy barrier ϕ^{det} relationships spanned a much larger range than did those of the rate – equilibrium ϕ^{det} relationships (Table 4.7).

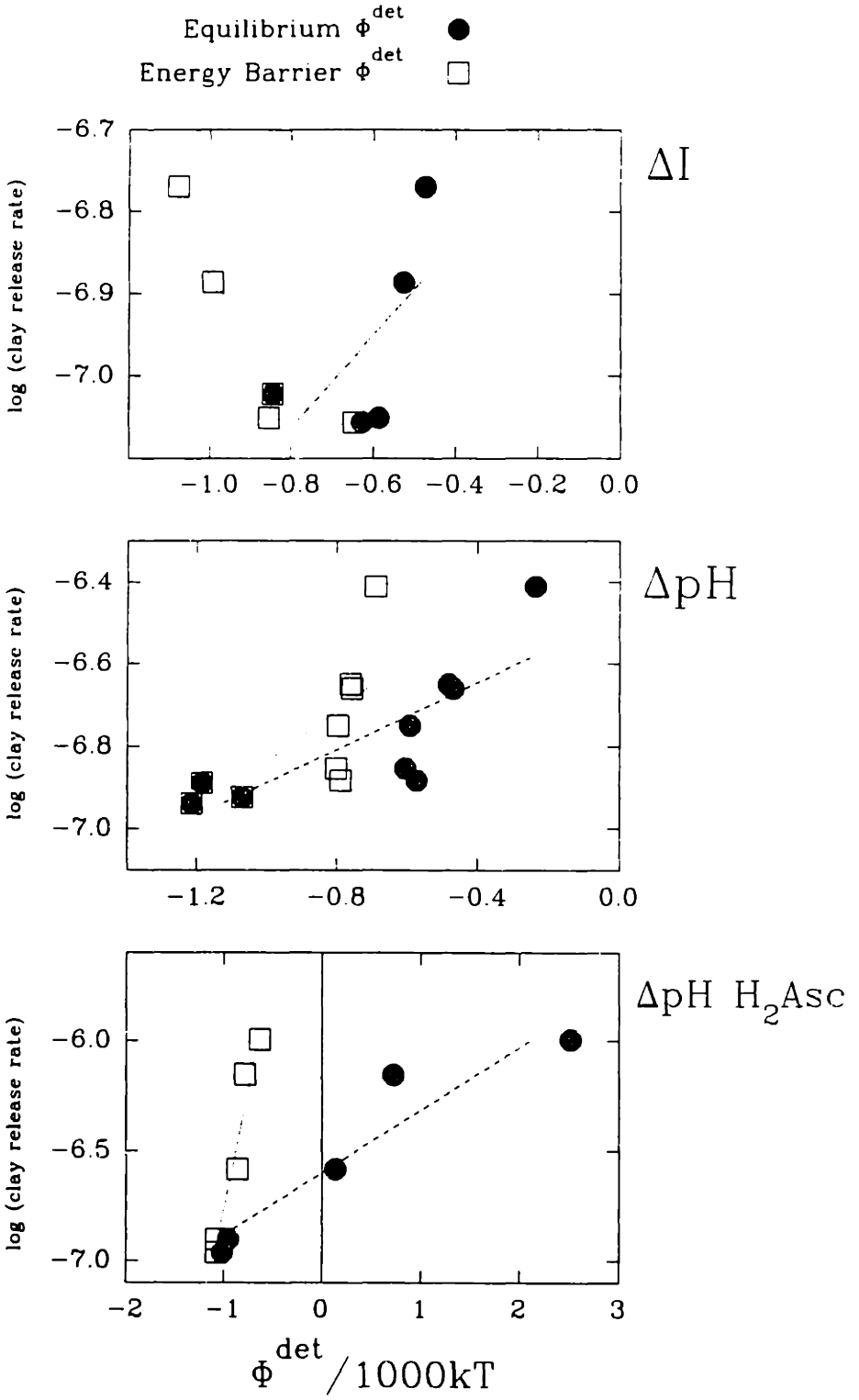

Fig. 4.11a. Plot of log (clay release rate) *vs.* $\phi_{det}/1000kT$ (detachment energy) for ΔI, ΔpH, and ΔpH H_2Asc experiments for equilibrium and energy barrier detachment energies.

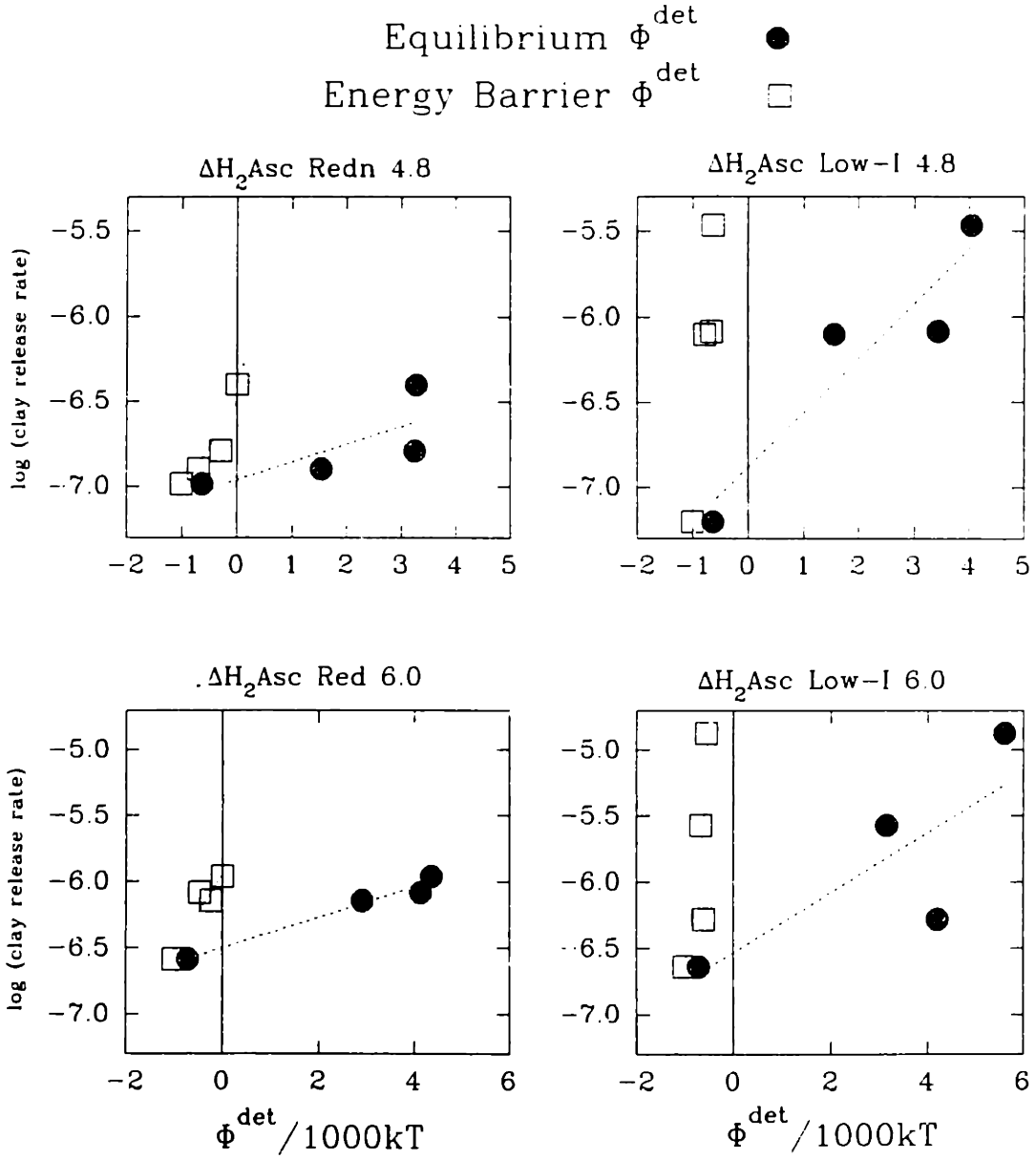

Fig. 4.11b. Plot of log (clay release rate) *vs.* $\phi_{det}/1000kT$ (detachment energy) for ΔH_2Asc reduction (redn) and low–*I* flush (low–*I*) experiments at *p*H 4.8 and 6.0 for equilibrium and energy barrier detachment energies.

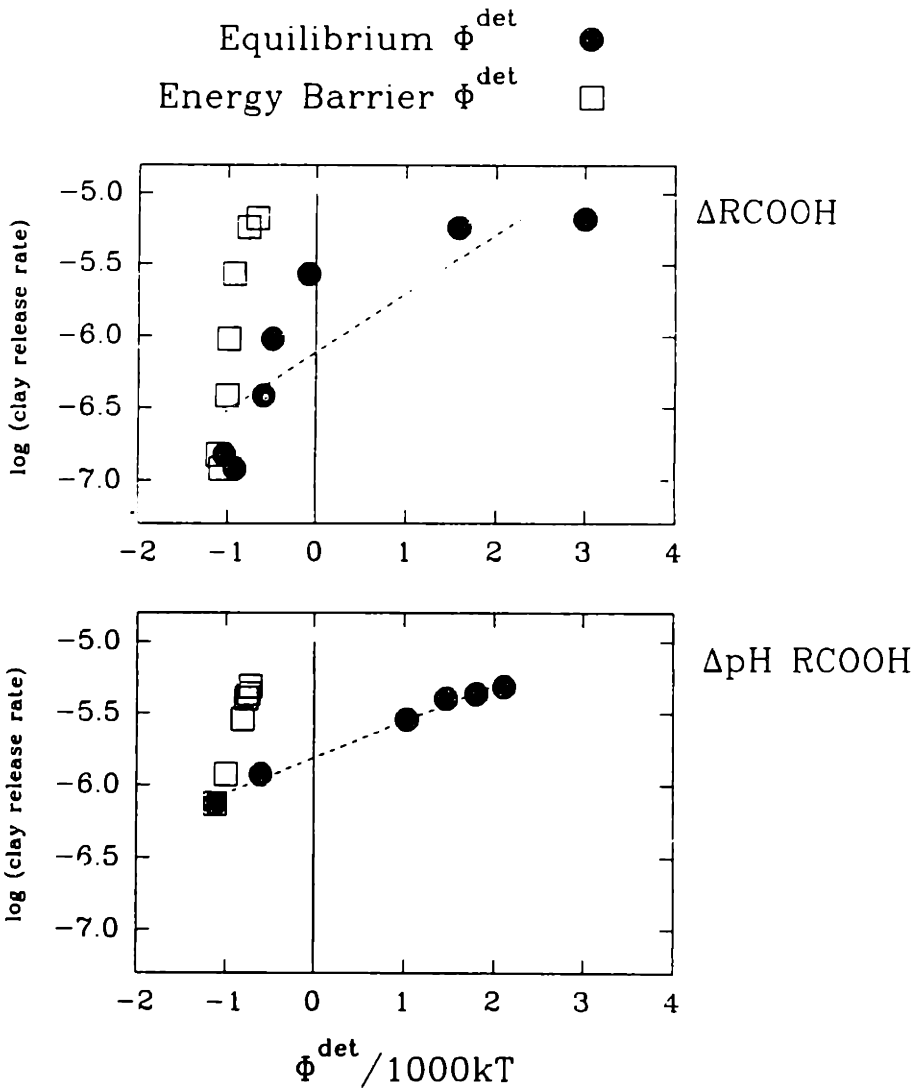

Fig. 4.11c. Plot of log (clay release rate) *vs.* $\phi_{det}/1000kT$ (detachment energy) for ΔRCOOH and Δ*p*H RCOOH experiments for equilibrium and energy barrier detachment energies.

Table 4.7. Summary of relationship between clay release rate and detachment energy. Slopes are calculated for the relationship log R *vs.* ϕ^{det}/kT without the factor of 1000 in the denominator in the detachment energy expression.

	Equilibrium			Energy Barrier		
	slope	$\phi^{det} = 0$ intercept	R^2	slope	$\phi^{det} = 0$ intercept	R^2
ΔI						
	$5.7 \pm 3.9 \cdot 10^{-4}$	−6.6±0.2	0.42	$-6.7 \pm 2.1 \cdot 10^{-4}$	−7.6±0.2	0.77
ΔpH						
	$4.1 \pm 1.1 \cdot 10^{-4}$	−6.5±0.1	0.67	$6.2 \pm 2.3 \cdot 10^{-4}$	−6.2±0.2	0.52
ΔH_2Asc pH 4.8						
Redn	$1.0 \pm 0.6 \cdot 10^{-4}$	−7.0±0.2	0.56	$5.4 \pm 1.6 \cdot 10^{-4}$	−6.5±0.1	0.85
Low I	$3.2 \pm 0.3 \cdot 10^{-4}$	−6.9±0.2	0.86	$4.0 \pm 0.9 \cdot 10^{-3}$	−3.2±0.7	0.90
ΔH_2Asc pH 6.0						
Redn	$1.1 \pm 0.1 \cdot 10^{-4}$	−6.5±0.1	0.98	$5.9 \pm 1.5 \cdot 10^{-4}$	−5.9±0.1	0.88
Low I	$2.3 \pm 1.3 \cdot 10^{-4}$	−6.5±0.5	0.62	$2.8 \pm 1.7 \cdot 10^{-3}$	−3.8±1.3	0.56
ΔpH H_2Asc						
	$2.8 \pm 0.6 \cdot 10^{-4}$	−6.6±0.1	0.90	$2.2 \pm 0.3 \cdot 10^{-3}$	−4.6±0.3	0.96
ΔRCOOH						
	$4.1 \pm 1.1 \cdot 10^{-4}$	−6.1±0.2	0.74	$4.2 \pm 0.7 \cdot 10^{-3}$	−2.2±0.7	0.86
ΔpH RCOOH						
	$2.5 \pm 0.1 \cdot 10^{-4}$	−5.8±0.1	0.99	$2.1 \pm 0.1 \cdot 10^{-3}$	−3.8±0.1	0.99

DISCUSSION

Accuracy of Surface Potentials

The surface potentials estimated for the clay colloids with the ζ–κ–ψ_{scdl} relationship seemed to more accurately describe the effects of solution chemistry on the colloid surfaces than did the zeta potentials. For example, a decrease in I would alter the surface potential slightly through an increase in the activity coefficients associated with the surface complex sites, but not to the extent by which the clay colloid ζ–potentials became more negative with decreasing I (Fig. 4c). In contrast, the estimated surface potentials were nearly constant with decreasing I as expected. Another example is the behavior of the colloid ζ–potentials as [$HAsc^-$] was increased. Initially, adsorption of the anion made the ζ–potential more negative; but, at higher [$HAsc^-$], ζ–potential became less negative (Figs. 4.7b and 4.7c). The estimated surface potentials became more negative with [$HAsc^-$] as expected.

For a number of reasons, the surface potentials estimated with the ζ–κ–ψ_{scdl} relationship may not accurately represent the true surface potentials of the colloids. First, the ζ–κ–ψ_{scdl} relationship, which was derived with data from spherical colloids, does not account for non–sphericity. The electrophoretic force on the clay colloids is opposed by fluid drag, which depends on colloid shape. The fluid drag force on an oblate ellipsoid (disk) with a major axis ratio of $b/a = 10$ is about 1.45 times greater than that on a sphere of the same radius (Hiemenz, 1986). Thus, the ζ–potential of a clay colloid suspension with the same electrophoretic mobility as a suspension of spherical colloids should actually be about 50% greater than the ζ–potential of the spherical colloids.

Second, the measured ζ–potentials may not adequately describe the effects of the heterogeneity of the clay colloid surfaces. The structure of clay minerals results in heterogeneous distribution of surface charge, with a permanent negative charge

on faces and amphoteric oxide functional groups on the edges. Also, the kaolinite colloids may still be partially coated by goethite. The potentials of the face, edge, and attached oxide surfaces are all measured as one overall, averaged ζ–potential. This overall ζ–potential would not adequately describe colloid detachment behavior if, for example, the clay edges controlled the attachment of the colloids to the coatings.

Third, the measured ζ–potentials of effluent colloids may have been substantially different than those of the colloids still attached. To get colloid concentrations high enough to measure ζ–potential, we had to slightly agitate the column in duplicate experiments. We may have been measuring ζ–potentials of colloids whose detachment was aided by some motion greater than caused by diffusion. The surface properties of such colloids probably equilibrated rapidly with the solution conditions; thus, we believe that the colloids released by agitation provided an accurate representation of the colloid zeta potentials.

Reversal of Colloid Surface Potential

The point of zero surface charge ($p\mathrm{H_{pzc}}$) of clay colloids in the column effluent was observed at $p\mathrm{H} \approx 3.0$. This $p\mathrm{H_{pzc}}$ closely matches the $p\mathrm{H_{pzc}}$ observed for the natural clay colloids in the Swamp Deep groundwater (Ryan and Gschwend, 1990). Because both the colloids released from the column and the natural colloids are composed almost entirely of kaolinite, we expected that their $p\mathrm{H_{pzc}}$ would fall within the range of $p\mathrm{H_{pzc}}$ values observed for pure kaolinites (3.3 to 5.0; by microelectrophoresis; Parks, 1967), but the $p\mathrm{H_{pzc}}$ values of the colloids were slightly lower. We postulated that adsorption of natural organic matter made the kaolinite slightly more negative and reduced the $p\mathrm{H_{pzc}}$ of the clay colloids.

Fe(III) oxides attached to the clay colloid surfaces did not contribute significantly to the colloid surface potential. If more than a trace amount of Fe(III)

oxide had been attached to the colloid surfaces, the $p\mathrm{H}_{pzc}$ of the colloids would have been shifted to a higher pH because the goethite $p\mathrm{H}_{pzc} \approx 8.0$ (Parks, 1967).

Nature of Forces Controlling Colloid Detachment

In the ΔI, ΔpH, ΔpH H_2Asc, ΔRCOOH, and ΔpH RCOOH experiments, the rate of clay release was not related to the rate of Fe(III) oxide dissolution. The Fe(III) oxide dissolution rate decreased with increasing pH in all of the experiments in which the solution pH was changed. In the ΔI and ΔRCOOH experiments, the rate of Fe(III) oxide dissolution was near the detection limit and did not vary significantly with changes in solution chemistry. With the notable exception of the ΔI experiment, the clay release rates were positively correlated with both forms of the detachment energy. The clay release rates of the ΔI experiment were positively correlated with ϕ^{det} representing the equilibrium model of colloid detachment but negatively correlated with the energy barrier ϕ^{det}. For these changes in solution chemistry, the forces controlling colloid detachment are clearly the weak electrostatic forces described by the augmented DLVO theory.

A comparison of the ΔpH and ΔpH H_2Asc experiments shows that dissolution of Fe(III) oxide must have some effect on the rate of clay release. At pH 5, clay was released about twice as rapidly in the presence of $1 \cdot 10^{-3}$ M H_2Asc; at pH 6 and 7, the clay release rate was 5 to 7 times faster in the presence of H_2Asc. Given the correlation of the clay release rates with the detachment energies in both the ΔpH and ΔpH H_2Asc experiments, we surmise that the dissolution of Fe(III) oxides enhanced the clay release rate by altering the nature of the physical interactions in the coatings. The removal of goethite from the surface of the coatings changed the colloid–colloid interactions from kaolinite–goethite–kaolinite to the more repulsive kaolinite–kaolinite. However, we could not observe this change in colloid–colloid interactions by measuring ζ–potential. Because we were measuring the overall

colloid ζ–potential, the loss of a trace amount of goethite from the colloid surfaces would not have been detected; also, the increasingly negative surface potential was attributed to loss of surface protons and adsorption of $HAsc^-$, not to loss of the Fe(III) oxide.

The experiments in which H_2Asc concentration was varied and followed by a low ionic strength flush further illustrated the effect of dissolution of the Fe(III) oxide cement. The lowest concentration of H_2Asc ($1 \cdot 10^{-4}$ M) had little effect on clay release rate relative to the release rate measured at the same *p*H without H_2Asc present. At $1 \cdot 10^{-3}$ M H_2Asc, Fe(III) oxide was dissolved more rapidly and the clay release rate tripled at *p*H 6 and increased slightly at *p*H 4.8. The increase at *p*H 4.8 is probably not significant due to the poor precision of the turbidity measurement at this low release rate. However, if we average the clay release rate measured in the ΔpH H_2Asc experiment at *p*H 5 and $1 \cdot 10^{-3}$ M H_2Asc ($2.6 \cdot 10^{-7}$ g min^{-1}) and the clay release rate measured in this experiment at *p*H 4.8 and $1 \cdot 10^{-3}$ M H_2Asc ($1.3 \cdot 10^{-7}$ g min^{-1}) to get an estimate of the error involved in (near–) replicate runs, the average clay release rate is $1.9 \cdot 10^{-7} \pm 1.0 \cdot 10^{-7}$ g min^{-1}. If we consider the average clay release rate for $1.0 \cdot 10^{-3}$ M H_2Asc at *p*H 4.8, then we see an increase in clay release rate with increasing H_2Asc (from $1 \cdot 10^{-4}$ M to $1 \cdot 10^{-3}$ M) comparable to that measured at *p*H 6.0.

At the two higher H_2Asc concentrations, the rate of Fe(III) oxide dissolution kept increasing, but the clay release rate leveled off at *p*H 6. At *p*H 4.8, the clay release rate increased by a factor of three; however, if the average clay release rate at $1 \cdot 10^{-3}$ M H_2Asc were included, the increase in release rate would be only by a factor of two. We surmise that the clay release rate reached a plateau as the Fe(III) oxide dissolution rate continued to rise because the ionic strength increased. The increase in ionic strength decreased the repulsion between the clay colloids even though the dissolution of Fe(III) oxides may have changed the colloid–colloid

interactions from kaolinite–goethite–kaolinite to kaolinite–kaolinite. When the high I H_2Asc solution was replaced by the low–I flush solution, the colloids that had been "loosened," but not released, by goethite dissolution were rapidly flushed from the column. In the low–I flushes, the rate (and total amount) of clay release were directly related to the rate (and total amount) of Fe(III) dissolution.

Decreasing the contribution of $HAsc^-$ to I by lowering pH to below ascorbic acid pK_{a1} (= 4.04) enhanced the rate of Fe(III) oxide dissolution but did not accelerate clay release as anticipated. The contribution of $[H^+]$ made up for the decrease in $[HAsc^-]$ in I. Also, low surface potentials at pH 3.0 and 4.0 did not generate sufficient repulsive energy to promote detachment, resulting in slower clay release at low pH.

Equilibrium vs. Energy Barrier Detachment Model

The rate constants measured in the ΔI experiment were positively correlated with the equilibrium ϕ^{det}, but negatively correlated with the energy barrier ϕ^{det}. This indicates that the equilibrium model, in which the initial re–distribution of particles between the primary and secondary minima is fast and the transport of particles through the diffusion boundary layer to the bulk fluid is the rate–limiting step, more accurately portrays particle escape from surfaces than the energy barrier model. Only with the ΔI experiments in model colloid–grain systems were we able to distinguish between the appropriateness of the two kinetic models (Chapter 3). The relatively consistent slopes and intercepts of the individual rate -- equilibrium ϕ^{det} relationships also suggests that the equilibrium energy difference more accurately describes the detachment kinetics (Table 4.7).

In terms of the equilibrium model, colloids are bound to the surface in either the primary or secondary minimum of potential energy or the more firmly attached sites associated with surface irregularities. A low particle release rate indicates that

(1) the primary minimum is favored over the secondary minimum and/or (2) the rate of particle transport to the surface irregularities is rapid. Introducing a solution that increases the repulsive interactions between colloids (*e.g.*, low–I flush after high–I flush) causes a rapid re–distribution of colloids from the primary to the secondary minimum. Colloids released to the secondary minimum may then diffuse across the hydrodynamic boundary layer to the bulk fluid or they may be trapped in surface irregularities. Colloid attachment in surface irregularities is more likely at high I because the secondary minimum is much closer to the surface (see detailed description in Chapter 3).

With the large number of clay colloids on the surface, we would expect to observe a quasi–steady state release rate under most conditions. For most of the experiments, we did observe constant release rates. However, in the case of the low–I flush following reduction, the release rate rose suddenly and declined gradually over about 5 pore volumes. In that case, we suspect that the low–I flush removed colloids from which the goethite cement had been removed. After the colloids loosened by Fe(III) oxide dissolution were flushed from the secondary minimum and boundary layer, the clay release rate returned to the same steady, low level measured in the ΔI experiment.

Alternative Potential Energy Profiles

The ΔI results reinforce the distinction between the energy barrier and equilibrium models. The high surface potentials (> 150 mV) involved in the model systems investigated in Chapter 3 led to concern over the discrepancy between the double layer potential energies calculated by the approximate solution of the PB equation (Hogg *et al.*, 1966) and the exact (numerical) solution (Devereux and de Bruyn, 1966). Although an exact solution does not exist for sphere–sphere geometry, the exact plate–plate solution gave much higher double layer potentials

than did the approximate plate–plate solution. The greater repulsive energy associated with the exact solution suggested that the primary minimum and maximum might disappear from the potential energy profile under conditions that led to colloid release.

In the ΔI experiment, the estimated surface potentials did not exceed 32 mV. Under these conditions, the Hogg *et al.* (1966) double layer expression is accurate within a few percent at all separation distances; thus, the interpretation of the detachment kinetics may be somewhat better constrained by these results. Variation of the Hamaker constant ($1 \cdot 10^{-20}$, $2 \cdot 10^{-20}$, $4 \cdot 10^{-20}$ J) and the Born collision parameter (3, 5, and 7 Å) did not lead to significantly different potential energy profiles for the ΔI case (Fig. 4.12).

Effect of Surfactant Adsorption on Clay Release

The adsorption of dodecanoate in the range of $[RCOOH]_{tot}$ used in these experiments is capable of reversing the surface charge of hematite at *p*H 5.2 (Liang and Morgan, 1990). Although we were not able to directly observe the effect of dodecanoate adsorption onto positively–charged oxides, we surmise that dodecanoate adsorption reversed the surface charge of goethite and the positively–charged oxide sites on the clay edges, resulting in strongly repulsive interactions and rapid colloid release. Dodecanoate adsorption, which is primarily physical (ionic exchange, hydrophobic interactions), but may include some specific complexation, particularly with Fe(III) oxides (Peck *et al.*, 1966; Han *et al.*, 1971), probably resulted in hemimicelle formation. Hemimicelle formation usually occurs at about 1/1000 to 1/100 of the critical micelle concentration (CMC) of a surfactant (Fuerstenau, 1956; Somasundaran *et al.*, 1964). The CMC of sodium dodecanoate is 24 mM (Lichtenberg *et al.*, 1983); thus, we expect hemimicelle formation at about 24 to 240 μM dodecanoate. This corresponds well with the $[RCOO^-]$ concentration

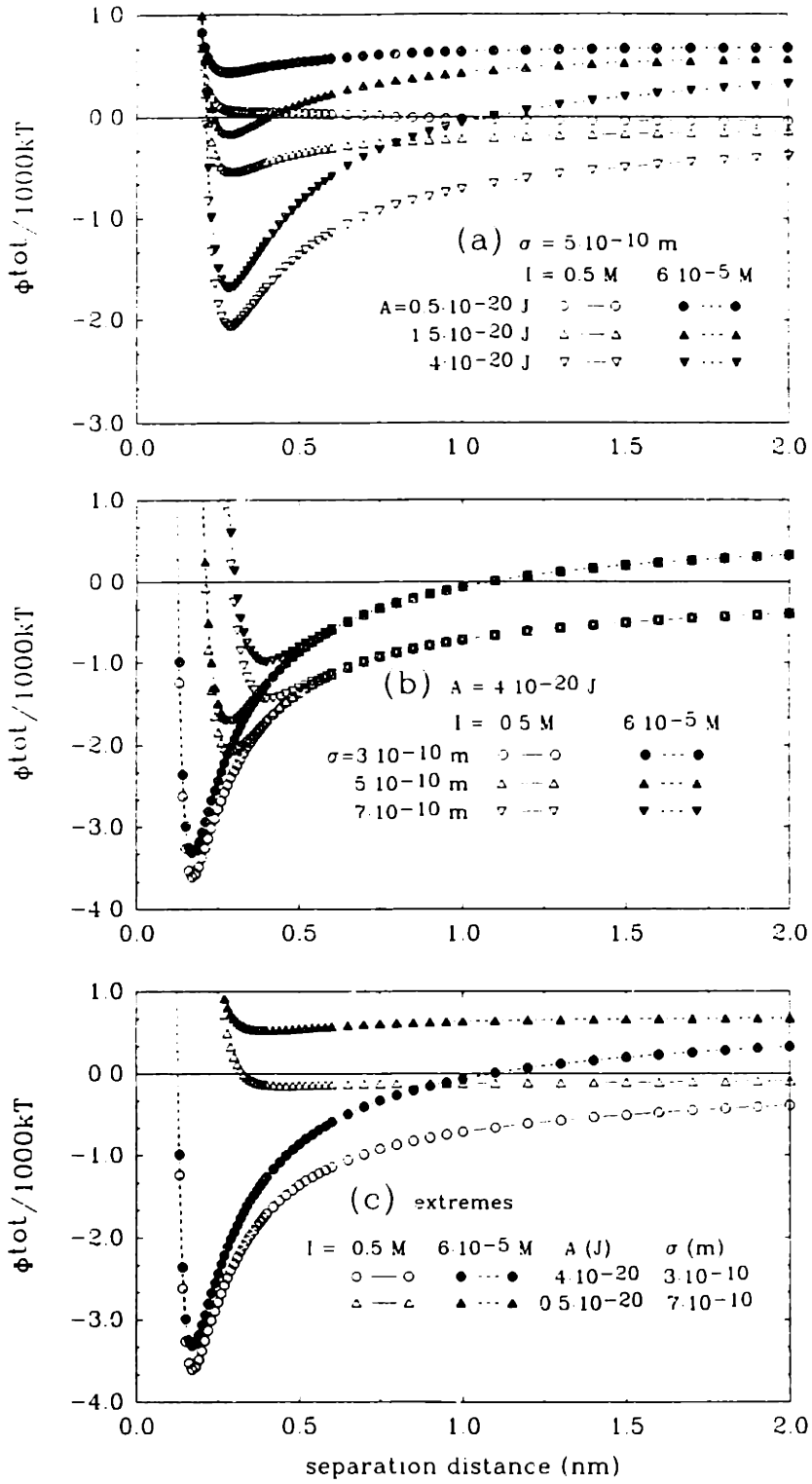

Figure 4.12. Comparison of total potential energy *vs.* separation distance for the ΔI experiment showing effect of variation of the Hamaker constant A and Born collision parameter σ. Total potential energy profiles shown for high (0.5 M) and low ($6 \cdot 10^{-5}$ M) ionic strengths.

at which the clay release rate increased rapidly, about 16 to 48 μM $RCOO^-$.

The equilibrium $\phi_{det} = 0$ intercepts of the ΔRCOOH and ΔpH RCOOH regressions (–6.1, –5.8) corresponded to clay release rates about 2.5 to 5 times faster than those corresponding to the mean of the equilibrium ϕ_{det} intercepts (–6.5 ± 0.4). This difference between the equilibrium ϕ^{det} intercepts may represent more rapid clay release caused by some repulsive "extra–DLVO" energy. Colloidal stability resulting from adsorption of organic polyelectrolytes and polymers has been attributed to short–range steric interactions (Napper, 1977; Tipping and Higgins, 1982; Warszyński, 1989; O'Melia, 1989).

Alternatively, the formation of hemimicelles may have disrupted the measurement of ζ–potential if the hydrophobic tails reached the shear plane (Cohen Stuart and Mulder, 1985). Values of ζ–potential measured at a shear plane pushed away from the surface by hemimicelles would be lower than ζ–potentials measured the shear plane of the surface without hemimicelle coverage. Thus, at the higher $[RCOOH_{tot}]$ used in these experiments, the estimated colloid surface potentials may be lower than the true surface potentials. If that were the case, then the double layer potentials were underestimated and the equilibrium and energy barrier detachment energies would be adjusted to reflect more rapid clay release.

Effect of Natural Groundwater on Clay Release

The natural groundwater–promoted Fe(III) oxide dissolution rate was only slightly greater that the proton–promoted Fe dissolution rate at pH 4.0, yet clay release increased to rates greater than any measured during the H_2Asc reduction. The relatively high clay release rate accompanied by low Fe(III) oxide dissolution rates suggested that the natural groundwater affected clay release in a manner similar to dodecanoic acid.

In Pine Barrens groundwater, organic matter consists mainly of humic and

fulvic acids (Crerar *et al.*, 1981). Terrestrial humic substances typically contain about 5 mmol g^{-1} carboxyl groups ($pK_a \approx 4.0$) (Thurman, 1986), resulting in about 4.3 mmol g^{-1} of ionized functional groups. Thus, 1.7 mM C of organic matter in the natural groundwater contained about 88 μM of ionized functional groups. At *p*H 4.2, the natural groundwater released clay at the about the same rate as 80 μM dodecanoic acid (33 μM $RCOO^-$) solution at *p*H 4.8.

Colloid Mobilization in Natural and Anthropogenically–Affected Sediments

Clay colloid release is relatively slow in the natural New Jersey Coastal Plain groundwater, despite its low ionic strength. In the acidic water, surface potentials are not high enough to generate sufficient repulsion between surfaces. Based on a clay release rate of $1.5 \cdot 10^{-7}$ g min^{-1} at 0.5 mL min^{-1} from a pore volume of 1.5 mL, $4.5 \cdot 10^{-7}$ g clay were released per pore volume of solution flushed through the column. At this rate, $1.3 \cdot 10^5$ pore volumes would be required to flush the 0.038 g clay–sized fraction contained in 1.0 g sediment. With hydraulic gradients as high as 0.17 m m^{-1} measured in the New Jersey Coastal Plain groundwater (Lord *et al.*, 1990), hydraulic conductivities ranging from 10^{-5} to 10^{-7} m s^{-1}, and porosity of 0.44 (Rhodehamel, 1979), flushing the clay from the sediment would require about 9 to 900 years.

The infiltration of organic matter–rich water from the swamp would significantly accelerate clay release. At a clay release rate of $2.3 \cdot 10^{-6}$ g min^{-1}, the clay from 1.0 g sediment could be removed in only 0.4 to 40 years without requiring the dissolution of the Fe(III) oxides. By contrast, dissolution of the 39 μmol free Fe per g sediment would require 1.1 to 110 years at the Fe(III) oxide dissolution rate of $8.1 \cdot 10^{-10}$ mol min^{-1}. Thus, clay release is about three times as fast as Fe(III) oxide dissolution. If all the clay released is kaolinite, the clay release rate could be expressed as $8.9 \cdot 10^{-9}$ mol (kaolinite) min^{-1}; thus, about 11 moles of kaolinite are

released for every mole of goethite dissolved, while the molar ratio of kaolinite/goethite ≈ 5 in the coatings.

Contaminant plumes emanating from waste sites are typically near neutral *p*H, anoxic, high in ionic strength, and capable of dissolving reducible oxides from the sediments (Kimmel and Braids, 1980; Nicholson *et al.*, 1983). While Fe(III) oxide dissolution may occur, high ionic strength may inhibit release of colloids. Contaminant plumes also contain surfactant–like compounds (Robinson and Maris, 1979; Thurman *et al.*, 1986) that may cause colloid mobilization. Surfactants containing phosphate and sulfonate functional groups, which form strong specific surface complexes with most oxides, may be even more effective than carboxylic acids at reversing the surface charge of cementing phases and mobilizing colloids.

CONCLUSIONS

In this investigation, we tested the importance of chemical *vs.* physical bonding of kaolinite colloids in an iron oxide–coated sand by subjecting the sand to changes in ionic strength, *p*H, reductant concentration, and surfactant concentration. The rates of clay release from the sand were compared to rates of Fe(III) oxide dissolution and to detachment energies representing two models of colloid detachment kinetics, the energy barrier model and the equilibrium model (Chapter 3). Zeta potentials measured by microelectrophoresis were converted to surface potentials with an empirical relationship between zeta potentials, ionic strength, and surface potentials calculated with a surface complexation/double layer model of proton exchange equilibrium for two oxides.

Clay release rates were increased by decreasing ionic strength, increasing *p*H, increasing the reductant concentration, and increasing the surfactant concentration. The reductive dissolution of Fe(III) oxides increased the rate of clay release only at low reductant (ascorbic acid) concentration (*i.e.*, at low ionic strength). Ensuing flushes at low ionic strength apparently removed clay "loosened" by the dissolution of Fe(III) oxides. Flushing the sand with natural groundwater caused rapid clay release without substantial Fe(III) oxide dissolution, as did the surfactant (dodecanoic acid) solutions. When normalized to the ionized functional group concentration, the clay release rates for the natural groundwater and the surfactant solutions were similar.

For the experiments in which the reductant was not present, the rate of clay release was unrelated to the rate of Fe(III) oxide dissolution. Release rates of most of the experiments were positively correlated with both the equilibrium and energy barrier detachment energies. One notable exception to this result involved the experiment in which the ionic strength was varied: the rate constants were

positively correlated with the equilibrium detachment energies, but negatively correlated with the energy barrier detachment energies. The slopes of the rate – equilibrium detachment energy regressions were quite similar, suggesting that detachment proceeded by a similar mechanism. Thus, the equilibrium model of colloid detachment appeared to better describe the clay release data. The zero–detachment energy intercept of the surfactant experiments was significantly higher than the overall intercept, suggesting that surfactant–promoted clay release was aided by some extra–DLVO force, perhaps short–range steric interaction.

Fe(III) oxide dissolution was not necessary to mobilize clay colloids, although decementation did accelerate clay release rates under some conditions, possibly by changing colloid–colloid interactions from kaolinite–goethite–kaolinite to the more repulsive kaolinite–kaolinite. Colloids were mobilized primarily by the breaking of physical bonds between the colloid surfaces. The results of these experiments imply that, in typical landfill leachates, surfactants may present the most effective means of generating colloids capable of facilitating contaminant transport.

REFERENCES

Banwart S. (1989) The reductive dissolution of hematite (α–Fe_2O_3) by ascorbate. Ph.D. thesis no. 8934, Swiss Federal Institute of Technology (ETH), Zurich.

Barouch E., Matijević E., and Wright T.H. (1987) Effects of Born repulsion on particle detachment. *Chem. Eng. Comm.* **55**, 29–40.

Buddemeier R.W. and Hunt J.W. (1988) Transport of colloidal contaminants in groundwater: radionuclide migration at the Nevada Test Site. *Appl. Geochem.* **3**, 535–548.

Carroll–Webb S.A. and Walther J.V. (1988) A surface complex reaction model for the *p*H–dependence of corundum and kaolinite dissolution rates. *Geochim. Cosmochim. Acta* **52**, 2609–2623.

Cerda C. (1987) Mobilization of kaolinite fines in porous media. *Colloids Surfaces* **27**, 219–241.

Crerar D.A., Means J.L., Yuretich R.F., Borcsik M.P., Amster J.L., Hastings D.W., Knox G.W., Lyon K.E., and Quiett R.F. (1981) Hydrogeochemistry of the New Jersey Coastal Plain 2. Transport and deposition of iron, aluminum, dissolved organic matter, and selected trace elements in stream, ground–, and estuary water. *Chem. Geol.* **33**, 23–44.

Cohen Stuart M.A. and Mulder J.W. (1985) Adsorbed polymers in aqueous media. The relation between zeta potential, layer thickness, and ionic strength. *Colloids Surfaces* **15**, 49–55.

Dahneke B. (1975) Kinetic theory of the escape of particles from surfaces. *J. Colloid Interface Sci.* **50**, 89–107.

Degueldre C., Baeyens B., Goerlich W., Riga J., Verbist J., and Stadelmann P. (1989) Colloids in water from a subsurface fracture in granitic rock, Grimsel Test Site, Switzerland. *Geochim. Cosmochim. Acta* **53**, 603–610.

Dougan W.K. and Wilson A.L. (1973) Absorptiometric determination of iron with T.P.T.Z. *Water Treat. Exam.* **22**, 100–113.

Dzombak D.A. and Morel F.M.M. (1990) *Surface Complex Modeling. Hydrous Ferric Oxide.* Wiley–Interscience.

Feke D.L., Prabhu N.D., Mann J.A. Jr., Mann J.A. III (1984) A formulation of the short–range repulsion between spherical colloidal particles. *J. Phys. Chem.* **88**, 5735–5739.

Flegmann A.W., Goodwin J.W., and Ottewill R.H. (1969) Rheological studies on kaolinite suspensions. *Proc. Brit. Ceram. Soc.* **13**, 31–45.

Fuerstenau D.W. (1956) Streaming potential studies on quartz in solutions of ammonium acetates in relation to the formation of hemi–micelles at the quartz–solution interface. *J. Phys. Chem.* **60**, 981–985.

Greenland D.J. and Mott C.J.B. (1978) Surfaces of soil particles. In *The Chemistry of Soil Constituents* (eds. D.J. Greenland and M.H.B. Hayes), Wiley, 321–353.

Gschwend P.G. and Reynolds M.D. (1987) Monodisperse ferrous phosphate colloids in an anoxic groundwater plume. *J. Contam. Hydrol.* **1**, 309–327.

Gschwend P.G., Backhus D.A., MacFarlane J.K., and Page A.L. (1990) Mobilization of colloids in groundwater due to infiltration of water at a coal ash disposal site. *J. Contam. Hydrol.* **6**, 307–320.

Hamaker H.C. (1937) The London–van der Waals attraction between spherical particles. *Physica* **4**, 1058–1072.

Han K.N., Healy T.W., and Fuerstenau D.W. (1973) The mechanism of adsorption of fatty acids and other surfactants at the oxide–water interface. *J. Colloid Interface Sci.* **44**, 407–414.

Harris W.G., Carlisle V.W., and Chesser S.L. (1987) Clay mineralogy as related to the morphology of Florida soils with sandy epipedons. *Soil Sci. Amer. J.* **51**, 1673–1677.

Hiemenz P.C. (1986) *Principles of Colloid and Surface Chemistry*, 2nd ed. Marcel Dekker, NY, p. 88.

Hogg R., Healy T.W., and Fuerstenau D.W. (1966) Mutual coagulation of colloidal dispersions. *Trans. Faraday Soc.* **62**, 1638–1651.

Hough D.B. and White L.R. (1980) The calculation of Hamaker constants from Lifshitz theory with applications to wetting phenomena. *Adv. Colloid Interface Sci.* **14**, 3–41.

Hunter R.J. (1981) *Zeta Potential in Colloid Science.* Academic Press.

Kallay N., Barouch E., and Matijević E. (1987) Diffusional detachment of colloidal particles from solid/solution interfaces. *Adv. Colloid Interface Sci.* **27**, 1–42.

Khilar K.C. and Fogler H.S. (1984) The existence of a critical salt concentration for particle release. *J. Colloid Interface Sci.* **101**, 214–224.

Kia S.F., Fogler H.S., and Reed M.G. (1987) Effect of *p*H on colloidally induced fines migration. *J. Colloid Interface Sci.* **118**, 158–168.

Kimmel G.E. and Braids O.C. (1980) Leachate plumes in ground water from Babylon and Islip landfills, Long Island, New York. U.S. Geological Survey Prof. Paper 1085.

Langmuir D. (1969) Geochemistry of iron in a coastal–plain groundwater of the Camden, New Jersey area. U.S. Geological Survey Prof. Paper 650–C, C224–C235.

Liang L. and Morgan J.J. (1990) Coagulation of iron oxide particles in the presence of organic materials. In *Chemical Modeling of Aqueous Systems II* (eds. D.C. Melchoir and R.L. Bassett), Amer. Chem. Soc. Symp. Ser. 416, 293–308.

Lichtenberg D., Robson R.J., and Dennis E.A. (1983) Solubilization of phospholipids by detergents. Structural and kinetic aspects. *Biochim. Biophys. Acta* 737, 285–304.

Lord D.G., Barringer J.L., Johnsson P.A., Schuster P.F., Walker R.L., Fairchild J.E., Sroka B.N., and Jacobsen E. (1990) Hydrogeochemical data from an acidic deposition study at McDonalds Branch basin in the New Jersey Pinelands, 1983–1986. U.S. Geol. Survey Open–File Report 88–500.

Magaritz M., Amiel A.J., Ronen D., and Wells M.C. (1990) Distribution of metals in a polluted aquifer: A comparison of aquifer suspended material to fine sediments in the adjacent environment. *J. Contam. Hydrol.* **5**, 333–347.

McDowell–Boyer L.M. (1992) Chemical mobilization of micron–sized particles in saturated porous media under steady flow conditions. *Environ. Sci. Technol.* **26**, 586–593.

Napper D.H. (1977) Steric stabilization. *J. Colloid Interface Sci.* **58**, 390–407.

Nicholson R.V., Cherry J.A., and Reardon E.J. (1983) Migration of contaminants in groundwater at a landfill: A case study. 6. Hydrogeochemistry. *J. Hydrol.* **63**, 131–176.

Nightingale H.I. and Bianchi W.C. (1977) Ground–water turbidity resulting from artificial recharge. *Ground Water* **15**, 146–152.

O'Melia C.R. (1989) Particle–particle interactions in aquatic systems. *Colloids Surfaces* **39**, 255–271.

Parks G.A. (1967) Aqueous surface chemistry of oxides and complex oxide minerals. In *Equilibrium Concepts in Natural Water Systems* (ed. W. Stumm), Advan. Chem. Ser. 67, Amer. Chem. Soc., Washington, DC, 121–160.

Peck A.S., Raby L.H., and Wadsworth M.E. (1966) An infrared study of the flotation of hematite with oleic acid and sodium oleate. *Trans. Amer. Inst. Min. Met. Eng.* **235**, 301–307.

Penrose W.R., Polzer W.L., Essington E.H., Nelson D.M., and Orlandini K.A. (1990) Mobility of plutonium and americium through a shallow aquifer in a semiarid region. *Environ. Sci. Technol.* **24**, 228–234.

Rhodehamel E.C. (1979) Hydrology of the New Jersey Pine Barrens. In *Pine Barrens: Ecosystem and Landscape* (ed. R.T.T. Forman), 39–60, Academic Press.

Robinson H.D. and Maris P.J. (1979) Leachate from domestic waste: generation, composition, and treatment. A review. Technical Report TR108, Water Research Centre, Bucks., UK.

Ronen D., Magaritz M., Weber U., Amiel A.J., and Klein E. (1992) Characterization of suspended particles collected in groundwater under natural gradient flow conditions. *Water Resour. Res.* **28**, 1279–1291.

Ruckenstein E. and Prieve D.C. (1976) Adsorption and desorption of particles and their chromatographic separation. *Amer. Inst. Chem. Eng. J.* **22**, 276–283.

Ryan J.N. and Gschwend P.M. (1990) Colloid mobilization in two Atlantic Coastal Plain aquifers: field studies. *Water Resour. Res.* **26**, 307–322.

Ryan J.N. and Gschwend P.M. (1991) Extraction of iron oxides from sediments using reductive dissolution by titanium (III). *Clays Clay Min.* **39**, 509–518.

Ryan J.N. and Gschwend P.M. (1992) Effect of iron diagenesis on the transport of colloidal clay in an unconfined sand aquifer. *Geochim. Cosmochim. Acta* **56**, 1507–1521.

Somasundaran P., Healy T.W., and Fuerstenau D.W. (1964) Surfactant adsorption at the solid–liquid interface – Dependence of mechanism on chain length. *J. Phys. Chem.* **68**, 3562–3566.

Sugimura Y. and Suzuki Y. (1988) A high–temperature catalytic oxidation method for the determination of non–volatile dissolved organic carbon in seawater by direct injection of a liquid sample. *Marine Chem.* **24**, 105–131.

Suter D., Banwart S., and Stumm W. (1991) Dissolution of hydrous iron(III) oxides by reductive mechanisms. *Langmuir* **7**, 809–813.

Thurman E.M. (1986) *Organic Geochemistry of Natural Waters.* Martinus Nijhoff/Dr W. Junk.

Thurman E.M., Barber L.B. Jr., and LeBlanc D. (1986) Movement and fate of detergents in groundwater: a field study. *J. Contam. Hydrol.* **1**, 143–161.

Tipping E. and Higgins D.C. (1982) The effect of adsorbed humic substances on the colloid stability of haematite particles. *Colloids Surfaces* **5**, 85–92.

Vaidya R.N. and Fogler H.S. (1990) Formation damage due to colloidally induced fines migration. *Colloids Surfaces* **50**, 215–229.

Verwey E.J.W. and Overbeek J.Th.G. (1948) *Theory of the Stability of Lyophobic Colloids.* Elsevier.

Warszyński P. (1989) The influence of polymer adsorption on deposition kinetics of colloid particles I. Theory. *Colloids Surfaces* **39**, 79–92.

Westall J.C., Zachary J.L., and Morel F.M.M. (1976) MINEQL: A computer program for the calculation of chemical equilibrium composition of aqueous systems. Tech. Note 18, Dept. Civil Engineering, MIT.

Wiese G.R. and Healy T.W. (1975) Coagulation and electrokinetic behavior of TiO_2 and Al_2O_3 colloidal dispersions. *J. Colloid Interface Sci.* **51**, 427–433.

Zinder B., Furrer G., and Stumm W. (1986) The coordination chemistry of weathering: II. Dissolution of Fe(III) oxides. *Geochim. Cosmochim. Acta* **50**, 1861–1869.

Chapter Five

CONCLUSIONS

Eventually, all things merge into one, and a river runs through it. The river was cut by the world's greatest flood and runs over rocks from the basement of time. On some of the rocks are timeless raindrops. Under the rocks are the words, and some of the words are theirs.

I am haunted by waters.

— Norman Maclean, *A River Runs Through It* (1976).

SUMMARY

The goal of these studies was to develop an understanding of the geochemical mechanisms responsible for the mobilization of clay colloids in an iron oxide–coated sediment. Starting with the hypothesis that the infiltration of anoxic, organic matter–rich groundwater caused the dissolution of the Fe(III) oxides and the release of clay colloids in the New Jersey Coastal Plain Cohansey Sand formation, we made two major efforts to elucidate the source of clay colloids.

The first effort involved examining distributions of minerals and elements in soil and sediment samples taken from the Cohansey Sand formation (Ryan and Gschwend, 1992; Chapter 2) near the wells that yielded the groundwater samples (Ryan, 1988; Ryan and Gschwend, 1990). In this investigation we presented evidence that showed that the clay and Fe(III) oxides that make up the quartz grain coatings were diagenetic alterations of the originally–deposited sediment. The clay had been transported in the groundwater and attached to the coatings. The microcrystalline Fe(III) oxides were formed by the weathering of Fe–Ti oxides under oxidizing conditions. Clay–sized fraction and Fe(III) oxide contents in the anoxic sediments below the swamp were lower than those in the oxic sediments. Based on these observations and general knowledge of the geology of the Atlantic Coastal Plain, we surmised that the influx of organic matter–rich water from the swamp, beginning about 10,000 years ago, dissolved the Fe(III) oxide coatings and released kaolinite, leading to the difference in clay content we observed between the Swamp reduced sediments and the oxidized sediments of the Upland and Swamp cores.

To determine the abundance of the secondary Fe(III) oxides in the New Jersey Coastal Plain sands, we devised a new selective extraction method that targeted the dissolution of Fe(III) oxides in soils and sediments using a mixed

chelate Ti(III) complex as the reductant (Ryan and Gschwend, 1991; Appendix). The Ti(III) method was, in most cases, as effective as the dithionite method of Mehra and Jackson (1960) in dissolving synthetic Fe(III) oxides and Fe(III) oxides in natural sediments. The Ti(III) method was much more selective in removing only the targeted Fe(III) oxides from standard clays and natural sediments than the dithionite method. We attributed the greater selectivity of the Ti(III) method to low free ligand concentrations and room temperature extractions.

The second effort involved a laboratory study of the effect of solution chemistry on the rate of clay release from the New Jersey Coastal Plain sediment (Chapter 4). By comparing the rates of clay release to the rates of Fe(III) oxide dissolution and to the intersurface potential energy associated with detachment, we showed that the weak electrostatic forces between colloid surfaces exerted the primary control over clay release. The dissolution of the Fe(III) oxides accelerated clay release by increasing the repulsive electrostatic forces between colloid surfaces. One clay release experiment, in which the flushing solution ionic strength was varied, suggested that the energy barrier model of colloid detachment kinetics (Dahneke, 1975, Ruckenstein and Prieve, 1976) did not adequately describe the release data; instead, an alternative "equilibrium" model provided a better description of the kinetics (Chapter 3). Also, surface potentials estimated with an empirical relationship between zeta potential, ionic strength, and surface potentials calculated with a surface complexation/double layer model of proton exchange equilibrium for two oxides were more appropriate for calculating the intersurface potential energy.

As a prelude to exploring the effects of solution chemistry on clay release from the New Jersey Coastal Plain sediments in laboratory columns (Chapter 4), we tested the appropriateness of two models of colloid detachment kinetics for describing the effect of solution chemistry and flow rate on colloid release rates

determined in some model systems (Kallay *et al.*, 1987) and in a hematite colloid – quartz grain system:

(1) the energy barrier model, in which the rate of colloid detachment is controlled by the size of the potential energy barrier (Dahneke, 1975; Ruckenstein and Prieve, 1976). Colloids diffusing away from the surface must attain energy sufficient to exceed the barrier.

(2) the equilibrium model, in which the rate of colloid detachment is controlled b the equilibrium distribution of colloids between the primary and secondary minima in potential energy, the rate of colloid diffusion from the secondary minimum to the bulk fluid, and the removal of colloids to "permanently" attached sites (Chapter 3).

Experiments in which the ionic strength and the flow rate of the flushing solution were altered showed that the equilibrium model better described the colloid detachment kinetics. Nevertheless, the detachment energies could only be qualitatively related to the trends in the colloid release rates. Quantitatively, the detachment energies would vastly overpredict the colloid release rates in the same way that attachment energies vastly underpredict rates of colloid deposition (O'Melia, 1989).

IMPLICATIONS

The results of these investigations advance our ability to predict the effect of solution chemistry on colloid mobilization in iron oxide–coated sediments. The ability to predict colloid mobilization will be utilized to assess (1) the extent to which contaminant transport may be facilitated by association with colloids and (2) the potential usefulness of colloids in remedial schemes. The ubiquity of iron weathered from unstable Fe(II)–bearing primary minerals to Fe(III)–bearing secondary minerals in near–surface sediments (Ronov and Yaroshevsky, 1971), and the abundance of "red beds," sediments tinted by Fe(III) oxides (Van Houten, 1973; Pye, 1983), suggests that this problem may be of widespread importance.

Predicting Colloid Mobilization in an Iron Oxide–Coated Sediment

The salient result of this work is the discovery that the weak electrostatic forces between colloid surfaces appeared to dominate the kinetics of colloid release in these iron oxide–coated sediments. Although reductive dissolution of the Fe(III) oxide cement accelerated the release of colloids, the electrostatic forces between the kaolinite colloids that remained in the coatings still controlled the rate of colloid release. However, trends in the potential energy between colloid and grain surfaces still only qualitatively describe changes in the colloid detachment rate. Further research is needed to determine if the forces between surfaces are accurately described by the potential energy expressions and if the mechanism of colloid detachment has been correctly determined.

Colloid Mobilization by Landfill Leachate

In these investigations, we have examined clay colloid mobilization in a natural, pristine setting, the iron oxide–coated sands of the New Jersey Coastal

Plain Cohansey formation. The real value in investigating this site is that we may consider the onset of reducing conditions in the sediments below the swamp as an analog for the anthropogenic input of reducing leachates from landfills.

Perhaps the most significant finding from these studies was that the dissolution of Fe(III) oxides was of secondary importance to the release of clay colloids. Instead, flushing solutions containing the surfactant, dodecanoic acid, promoted the most rapid clay release without dissolving Fe(III) oxides. At a dodecanoate concentration of about 16 μM, or about 8 mg L^{-1} total dodecanoic acid concentration at *p*H 4.8, a concentration of long chain fatty acids commonly encountered in landfill leachates (Robinson and Maris, 1979), clay was released at about $1 \cdot 10^{-6}$ g min^{-1} at a flow velocity of 1.6 m d^{-1}. At this release rate and a bulk density of 1.4 g cm^{-3}, the clay–sized particles in the six meters below the swamp would be removed in about 140 years. This release rate results in a groundwater clay colloid concentration of 9 mg L^{-1}. Surfactants in landfill leachates are present primarily as detergents like branched and linear alkyl aryl sulfonates and sodium dodecyl sulfates at a few mg L^{-1} concentrations (Thurman *et al.*, 1986; Field *et al.*, 1992). Similar concentrations of these types of surfactants have a similar effect on oxide surfaces (Dick *et al.*, 1971; Han *et al.*, 1973; Fuerstenau and Wakamatsu, 1975; Liang and Morgan, 1990).

Flushing with the natural swamp groundwater produced a similar effect: rapid clay release at low Fe(III) oxide dissolution rates. At the release rate of $2.3 \cdot 10^{-6}$ g min^{-1} measured for flushing by natural groundwater, the removal of clay from the six meters of sediments would take only about 60 years and would result in clay colloid concentrations of about 20 mg L^{-1}. Although this suspension concentration is reasonably close to what was observed in the natural groundwater from the Swamp Deep well (8 m below the swamp), about 60 mg L^{-1} (Ryan and Gschwend, 1990), the clay release time period is far shorter than the time period

over which we presume that the swamp has existed (10,000 years). We must recall that the Swamp Shallow groundwater (collected about 2 m below the swamp) contained only about 1 to 2 mg L^{-1} clay colloids (Ryan and Gschwend, 1990), suggesting that most of the clay in the upper soil and sediments must have been removed in the past. The distribution of the clay–sized fraction in the Swamp cores confirmed that most of the clay had been removed from the upper layers (Ryan and Gschwend, 1992; Chapter 2). The high clay colloid concentration at depth suggests that clays are mobilized at the rate measured in the column experiments only near the redox boundary. These clay colloids may be redeposited as groundwater carries them across the redox boundary to sediments where Fe(III) oxides are still present and uncoated by organic matter. The cycling of colloidal clay may slow the advance of the redox front, explaining the underestimate of the time required to remove clay from the six meters below the swamp.

Factors Affecting Colloidal Transport

The possibility that the mobilized clay is re–attached after it is carried across the redox front suggests that the clay colloids are transported only over short distances. Indeed, the application of the colloid filtration theory (Yao *et al.*, 1971; Rajagopalan and Tien, 1976) to colloid transport in porous media generally predicts that the concentration of mobile colloids will be 99% attenuated within 10 cm of the source if the attachment efficiency $\alpha = 1$ (O'Melia, 1990). Nevertheless, transport of inorganic and organic colloids has been observed over distances of tens to hundreds of meters (Keswick *et al.*, 1982; Robertson *et al.*, 1984; Buddemeier and Hunt, 1988; Harvey *et al.*, 1989). The ability of these colloids to avoid attachment to aquifer grains indicates that the intersurface potential energy profiles, which has been used to predict the collision efficiency α (the ratio of the number of attachments to the number of collisions), do not account for some significant

repulsive force.

Generally, this additional repulsive force has been attributed to steric repulsion caused by the adsorption of organic polyelectrolytes (O'Melia, 1989). For example, the clay colloids in the Atlantic Coastal Plain groundwater were most likely coated by natural organic matter because (1) about one–third to one–half of the total organic carbon was associated with the clay colloids and (2) the point of zero surface charge ($p\mathrm{H}_{\mathrm{pzc}}$) for the colloids were both measured at pH values below the expected ranges (Ryan, 1988; Ryan and Gschwend, 1990). The $p\mathrm{H}_{\mathrm{pzc}}$ of the clay colloids flushed from the columns in the laboratory experiments were also below the expected range (Chapter 4).

Similar surface charge effects and resulting increase in colloidal stability have been observed for particles in estuaries and coastal waters (Hunter and Liss, 1979; Newton and Liss, 1987). O'Melia (1989) suggested that a layer of adsorbed macromolecules would enhance the colloidal stability of particles through steric interactions in a solution in which the double layer is somewhat compressed (*i.e.*, a more saline environment). However, the importance of an adsorbed macromolecular layer on the clay colloids in the Swamp groundwater, where ionic strength is $\leq$ 1 mM and double layers are at least 30 nm thick, was unanticipated.

We had hoped that we could predict the rate of colloid mobilization resulting from decementation, and hence the concentration of colloids in the groundwater, simply by knowing the rate of dissolution of the cementing phase. However, we found that intersurface forces exert the primary control over colloid mobilization in the iron oxide–coated sediment of the New Jersey Coastal Plain (Chapter 4). We must rely on our knowledge of the weak, electrostatic forces between colloids and the surfaces to which they are attached to predict the rate of colloid mobilization. As we have shown, colloid detachment kinetics can be qualitatively assessed using intersurface potential energy (Chapters 3 and 4); however, a quantitative prediction

of the colloid detachment rates is still not feasible. Just as predictions of collision efficiency based on potential energy vastly underpredict the rate of attachment, rates of colloid detachment would be vastly overpredicted by potential energy. The role of additional repulsive forces (*e.g.*, steric repulsion and polymer adsorption; O'Melia, 1989), may explain the inability of intersurface potential energy to quantitatively predict colloidal interactions. However, the effect of relatively simple changes in solution ionic strength or *p*H, which alter only the double layer energy profile, on colloid attachment and detachment, still cannot be predicted accurately.

Fe(III) Oxide Dissolution by Landfill Leachate

Despite the secondary role of Fe(III) oxide dissolution in clay colloid release, the dissolution of Fe(III) oxides significantly affects other aspects of contaminant transport. The dissolution of Fe(III) and Mn(IV) oxides is accompanied by the release of hazardous metals adsorbed and co–precipitated with the oxides (Schwille, 1976; Baedecker and Back, 1979); furthermore, it represents the loss of a major portion of the capacity of the sediments to sorb hazardous metals. Organic matter sorbed to the positively–charged oxide surfaces may also be mobilized by the dissolution of these oxides, removing hydrophobic havens for sorption of non–polar organic compounds. Thus, the loss of aquifer sorption capacity caused by dissolution of Fe(III) and Mn(IV) oxides compounds may represent the most important contribution to the enhancement of contaminant transport.

From our knowledge of the geologic history of the New Jersey Coastal Plains and some assumptions about the velocity of groundwater infiltration at the site that we investigated, we estimated that the minimum amount of time required for the reductive dissolution (by organic carbon) of the goethite cement in the six meters of sediments below the swamp would be 50 to 5,000 years (Ryan and Gschwend, 1992; Chapter 2). For this estimate, we did not account for kinetic limitations on the

dissolution reaction that would lengthen the time for Fe(III) oxide removal nor did we account for re–oxidation of the dissolved Fe(II) in the sediment that remained oxic below the redox front advancing downward from the swamp. In landfill leachate plumes advancing horizontally through aquifers, Fe(III) oxides have been dissolved over distances of hundreds to thousands of meters in tens of years (Kimmel and Braids, 1980; Nicholson *et al.*, 1983).

During the investigation of the effect of solution chemistry on clay release, we measured the rate of Fe(III) oxide dissolution in the presence of the natural groundwater with 1.7 mM organic carbon. At this Fe(III) oxide dissolution rate, $8.1 \cdot 10^{-10}$ mol min^{-1} at a flow velocity of about 1.6 m d^{-1}, the dissolution of goethite cement in the six meters of sediment below the swamp would require about 160 years. This estimate, far less than the amount of time the swamp has probably existed (about 10,000 years), suggests that (1) our simple notion of groundwater flow direction and velocity is not accurate or (2) Fe may be cycled between the reducing and oxidizing zones.

The 160 year estimate is in closer agreement with the rate of dissolution encountered in leachate plumes; although, in leachate plumes, other reductants, such as phenols (LaKind and Stone, 1989) or reduced metals (Crowther *et al.*, 1983; Johnson and Xyla, 1991; Fendorf and Zasoski, 1991), may accelerate the rate of Fe(III) oxide dissolution. In Chapter 4, we showed that ascorbic acid, present at concentrations similar to those of organic reductants that could be found in contaminant plumes, accelerated Fe(III) oxide dissolution to rates resulting in removal of Fe(III) oxides from the six meters below the swamp in as little as 6 years.

Remediation Schemes and Colloid Mobilization in Iron Oxide–Coated Sediments

Four applications of our knowledge of colloid mobilization to the remediation of contaminated aquifers can be imagined: (1) prevention of colloid mobilization to reduce colloid–facilitated transport of contaminants; (2) addition of colloids to allow contaminants to re–partition to mobile phases; (3) mobilization of colloids to remove adsorbent phases; and (4) alteration of solution chemistry to avoid aquifer clogging through colloid mobilization. These applications are particularly important in the potential use of "biocolloids" (primarily bacteria) for *in situ* transformation of organic contaminants (Fontes *et al.*, 1991).

For these cases, we have developed at least a qualitative sense of how solution chemistry will affect the mobilization of inorganic colloids. The major prerequisite for this is knowledge of the surface properties of the colloid and how they vary with changes in solution chemistry. For biocolloids, these properties are not well known in all cases (Harvey and Garabedian, 1991; Gannon *et al.*, 1991; Martin *et al.*, 1992). In many cases, bacteria respond to conditions affecting their survival as well as conditions influencing their colloidal transport (*e.g.*, bacteria attach to surfactant–coated surfaces only when the surfactant can be used as a substrate; Marchesi *et al.*, 1991).

FUTURE RESEARCH

Accuracy of DLVO Theory

The major question that still exists in the determination of colloid detachment kinetics concerns the accuracy of the DLVO theory in describing the forces between colloid surfaces at separation distances of a few nanometers and less. Although experimental evidence has confirmed the accuracy of current formulations of DLVO forces at larger separation distances, the short–range forces that seem to dominate the kinetics of colloid detachment are not well characterized by experiment or theory (Israelachvili, 1982).

Measurements of the speed with which polystyrene spheres were transported along a wall by a linear shear flow were used to calculate separation distances that corresponded well with separation distances predicted by DLVO forces (Prieve and Alexander, 1986). The forces measured between approaching sheets of mica attached to very sensitive springs correspond well to DLVO theory until separation distances of about 5 nm are reached (Israelachvili and Adams, 1978; Pashley, 1981; Pashley and Israelachvili, 1984; Pashley, 1984). At smaller separation distances, these researchers concluded that the extra–DLVO short–range force was related to the expulsion of hydrated cations. Short–range forces have also been attributed to steric interactions, the repulsive forces that arise from compression and interpenetration of molecules (Napper, 1977).

Theoretically, the short–range forces have been described by Born repulsion, an adaptation of interatomic forces calculated for pairwise integration of interactions between surfaces (Feke *et al.*, 1984); however, the value of the collision parameter σ, a constant in this formulation, is taken as the value determined for interatomic potentials or used as a fitting parameter. Thus, more information is needed concerning the short–range forces.

Currently, some work into the atomic scale surface characteristics of materials used in some of the experimental investigations is being done by atomic force and scanning tunneling microscopy (P. Johnsson, Stanford University, personal communication). These sensitive techniques, capable of atomic–scale resolution, may show surface imperfections on "flat" mica surfaces that contradict the geometric assumptions upon which the short–range force theories are based. More importantly, these techniques may have the sensitivity to measure forces on the scales of interest for colloid detachment kinetics.

Model of Colloid Detachment Kinetics

The equilibrium model of colloid detachment kinetics proposed in Chapter 3 suggests many questions and opens many avenues of research. The questions mainly concern the application of the DLVO potential energy to colloid detachment kinetics. The first question: Why does the energy difference in the equilibrium positions in the DLVO potential energy profile correlate with release rate constants, but the size of the energy barrier does not? It seems contradictory for one feature of the energy profile to be related to the release kinetics while the other is not. The answer may lie in the different nature of the detachment energies. The equilibrium detachment energy merely quantifies the number of colloids eligible to diffuse to the bulk fluid from the secondary minimum. As long as the colloids achieve the distribution between the primary and secondary minima rapidly with respect to the characteristic time of diffusion to the bulk fluid, then the kinetics of the initial redistribution are of secondary importance. Use of the energy barrier detachment energy implies a concern for the balance of forces on the colloids in the primary minimum.

The second question: Why is the slope of the relationship between the experimental rate constant for colloid release (k_{exp}) and the detachment energy ϕ^{det}

(ln $k_{exp} \propto \phi^{det}/\mathbf{k}T$) much smaller than expected? If we assume that the DLVO potential energy is a good description of the forces between surfaces, then the slope of this relationship should be $\mathbf{k}T$; however, the slope was generally three to four orders of magnitude smaller than $\mathbf{k}T$ in the experiments reviewed and conducted (Chapters 3 and 4). Thus, this relationship would predict colloid release rates that are much more rapid than the measured release rates. This problem is similar to that encountered in colloid deposition studies: experimental attachment rates are much more rapid that those predicted using DLVO potential energy (Hull and Kitchener, 1969; Bowen and Epstein, 1979; Gregory and Wishart, 1980). In both cases, the poor agreement between experimental and predicted rates suggest that the predicted repulsive forces between colloid surfaces are much larger than the actual repulsive forces.

The third question involves the proposed involvement of hydrodynamics in describing the kinetics of colloid release: Under what conditions are the diffusion boundary layer conditions assumed in the formulation of the equilibrium model applicable? Other investigators of colloid release in porous media have concluded, based on both experimental and theoretical data, that colloid release rate is not flow–dependent (Khilar and Fogler, 1984; Cerda, 1987; Kallay *et al.*, 1987). These investigators may have been subjecting their porous media to flow rates so high that colloids were removed from the secondary minimum by shear. If that were the case, colloid release might involve a energy barrier jump from the primary minimum (Dahneke, 1975; Ruckenstein and Prieve, 1976). However, at such high flow rates, inertial motion of colloids in the realm of the double layer would invalidate one of the assumptions upon which the energy barrier analysis is based.

A fourth question relates to extremes in the DLVO energy profile: When the force between surfaces is repulsive at all separation distances, can separate components of the kinetic models be isolated and studied? For example, the

hydrodynamic forces controlling colloid attachment have been verified by studying systems in which every collision results in attachment. For colloid detachment, the dependence of detachment rate on the hydrodynamic parameters could be identified by working under completely repulsive interactions. The dependence of rate on the near–surface electrostatic forces could be elucidated by working under completely attractive conditions. For this case, much more sensitive means of measuring the abundance of colloids in the suspension must be devised. Radiolabelling of colloids may be promising in this respect (Champlin and Eichholz, 1968; Puls and Powell, 1992).

Dissolution of Fe(III) Oxides

Specific surface complexation has been shown to control the rate of metal oxide dissolution (Valverde and Wagner, 1976; Stumm *et al.*, 1985). In the proton–promoted dissolution of metal oxides, the dependence of the dissolution rate on the concentration of precursor surface complexes has been used to formulate a mechanism of dissolution where the valence of the metal ion dictates the number of protons that must be adsorbed to allow metal ion release (Zinder *et al.*, 1986; Furrer and Stumm, 1986; Wieland *et al.*, 1988). The rates of dissolution of natural Fe(III) oxides by protons and reductants will be evaluated with the Fe release data collected in the clay release experiments in which *p*H and ascorbic acid concentration were varied (Chapter 4). From preliminary results, we suspect that the coordinative environment of the surface metal ion must affect the number of protons required for dissolution. Further research on this subject would initially be aimed at measuring the extent of ascorbate adsorption on the goethite surface to develop an ability to predict the concentration of ascorbate surface complexes. More involved research would explore the atomic environment of reactive sites on the goethite, perhaps with atomic force microscopy.

In this investigation, we concentrated on the reduction of Fe(III) oxides by ascorbic acid under what we believed to be abiotic conditions. However, biologically–mediated reduction may dominate Fe(III) oxide dissolution in the natural sediments where bacterial populations exist (Lovley and Phillips, 1986; Macedo and Bryant, 1989; Lovley *et al.*, 1991). Indeed, bacterial mediation of ferrous iron oxidation occurs in the acidic swamp waters of the Pine Barrens, resulting in the formation of bog iron (Crerar *et al.*, 1979). The microbial reduction of Fe(III) oxides under anaerobic conditions has resulted in mobilization of trace metals coprecipitated with the oxides (Francis and Dodge, 1990). The relative contributions of biotic and abiotic Fe(III) oxide reduction should be compared in natural sediments, both pristine and contaminated.

The potential role of the solid–state electron transfer step in the weathering of the major Fe(II)–bearing primary mineral, ilmenite, in the New Jersey Coastal Plain sediments in heterogeneous organic compound transformation reactions may be of environmental interest. Homogeneous reductive dehalogenation of halogenated aliphatic compounds is slow in the presence of sulfide, but the reaction is catalyzed in the presence of Fe(II)–bearing mineral surfaces (*e.g.*, vermiculite, biotite; Kriegman–King and Reinhard, 1992). It is thought that sulfide regenerates Fe^{2+} sites on the mineral surface. In ilmenite, a semiconducting material (Shuey, 1975), electron transport is facilitated by a direct Fe–Ti bond (Sherman, 1987); thus, the ease of electron transfer in ilmenite relative to that in the Fe(II) silicates may make ilmenite a particularly effective surface by which reductive dehalogenation could occur.

REFERENCES

Baedecker M.J. and Back W. (1979) Modern marine sediments as a natural analog to the chemically stressed environment of a landfill. *J. Hydrol.* **43**, 393–414.

Bowen B.D. and Epstein N. (1979) Fine particle deposition in smooth parallel–plate channels. *J. Colloid Interface Sci.* **72**, 81–97.

Buddemeier R.W. and Hunt J.R. (1988) Transport of colloidal contaminants in groundwater: Radionuclide migration at the Nevada Test Site. *Appl. Geochem.* 3, 535–548.

Cerda, C.M. (1987) Mobilization of kaolinite fines in porous media. *Colloids Surfaces* 27, 219–241.

Champlin J.B.F. and Eichholz G.G. (1968) The movement of radioactive sodium and ruthenium through a simulated aquifer. *Water Resour. Res.* **4**, 147–158.

Crerar D.A., Knox G.W., and Means J.L. (1979) Biogeochemistry of bog iron in the New Jersey Pine Barrens. *Chem. Geol.* **24**, 111–136.

Crowther D.L., Dillard J.G., and Murray J.W. (1983) The mechanism of Co(II) oxidation on synthetic birnessite. *Geochim. Cosmochim. Acta* **47**, 1399–1403.

Dahneke B. (1975) Kinetic theory of the escape of particles from surfaces. *J. Colloid Interface Sci.* **50**, 89–107.

Dick S.G., Fuerstenau D.W., and Healy T.W. (1971) Adsorption of alkylbenzene sulfonate (A.B.S.) surfactants at the alumina–water interface. *J. Colloid Interface Sci.* **37**, 595–602.

Feke D.L., Prabhu N.D., Mann J.A. Jr., and Mann J.A. III (1984) A formulation of the short–range repulsion between spherical colloidal particles. *J. Phys. Chem.* **88**, 5735–5739.

Fendorf S.E. and Zasoski R.J. (1991) Chromium (III) oxidation by δ–MnO_2. 1. Characterization. *Environ. Sci. Technol.* **26**, 79–85.

Field J.A., Leenheer J.A., Thorn K.A., Barber L.B., II, Rostad C., Macalady D.L., and Daniel S.R. (1992) Identification of persistent anionic surfactant–derived chemicals in sewage effluent and groundwater. *J. Contam. Hydrol.* **9**, 55–78.

Fontes D.E., Mills A.L., Hornberger G.M., and Herman J.S. (1991) Physical and chemical factors influencing transport of microorganisms through porous media. *Appl. Environ. Microbiol.* **57**, 2473–2481.

Francis A.J. and Dodge C.J. (1990) Anaerobic microbial remobilization of toxic metals coprecipitated with iron oxide. *Environ. Sci. Technol.* **24**, 373–378.

Fuerstenau D.W. and Wakamatsu T. (1975) Effect of *p*H on the adsorption of sodium dodecane–sulphonate at the alumina/water interface. *Faraday Disc. Chem. Soc.* **59**, 157–168.

Furrer G. and Stumm W. (1986) The coordination chemistry of weathering: I. Dissolution kinetics of δ–Al_2O_3 and BeO. *Geochim. Cosmochim. Acta* **50**, 1847– 1860.

Gannon J.T., Manilal V.B., and Alexander M. (1991) Relationship between cell surface properties and transport of bacteria through soil. *Appl. Environ. Microbiol.* **57**, 190–193.

Gregory J. and Wishart A. (1980) Deposition of latex particles on alumina fibers. *Colloids Surfaces* **1**, 313–334.

Han K.N., Healy T.W., and Fuerstenau D.W. (1973) The mechanism of adsorption of fatty acids and other surfactants at the oxide–water interface. *J. Colloid Interface Sci.* **44**, 407–414.

Harvey R.W. and Garabedian S.P. (1991) Use of colloid filtration theory in modeling movement of bacteria through a contaminated sandy aquifer. *Environ. Sci. Technol.* **25**, 178–185.

Harvey, R.W., George, L.H., Smith, R.L., and LeBlanc, D.R. (1989) Transport of microspheres and indigenous bacteria through a sandy aquifer: Results of natural– and forced–gradient tracer experiments. *Environ. Sci. Technol.* **23**, 51–56.

Hull M. and Kitchener J.A. (1969) Interaction of spherical colloidal particles with planar surfaces. *Trans. Faraday Soc.* **65**, 3093–3104.

Hunter K.A. and Liss P.S. (1979) The surface charge of suspended particles in estuarine and coastal waters. *Nature* **282**, 823–825.

Israelachvili J.N. (1982) Forces between surfaces in liquids. *Adv. Colloid Interface Sci.* **16**, 31–47.

Israelachvili J.N. and Adams G.E. (1978) Measurement of forces between two mica surfaces in aqueous electrolyte solutions in the range 0–100 nm. *J. Chem. Soc. Faraday Trans. I* **74**, 975–1001.

Johnson C.A. and Xyla A.G. (1991) The oxidation of chromium(III) to chromium(VI) on the surface of manganite (γ–MnOOH). *Geochim. Cosmochim. Acta* **55**, 2861–2866.

Kallay N., Barouch E., and Matijević E. (1987) Diffusional detachment of colloidal particles from solid/solution interfaces. *Adv. Colloid Interface Sci.* **27**, 1–42.

Keswick, B.H., Wang, D.–S., and Gerba, C.P. (1982) The use of microorganisms as ground–water tracers: A review. *Ground Water* **20**, 142–149.

Khilar, K.C. and Fogler, H.S. (1984) The existence of a critical salt concentration for particle release. *J. Colloid Interface Sci.* **101**, 214–224.

Kimmel G.E. and Braids O.C. (1980) Leachate plumes in ground water from Babylon and Islip landfills, Long Island, New York. U.S. Geol. Survey Prof. Paper 1085, p. 20.

Kriegman–King M.R. and Reinhard M. (1992) Abiotic transformation of carbon tetrachloride in the presence of sulfide and mineral surfaces (abstract). 203rd Amer. Chem. Soc. National Meeting., **32**(1), 495–498.

LaKind J.S. and Stone A.T. (1989) Reductive dissolution of goethite by phenolic reductants. *Geochim. Cosmochim. Acta* **53**, 961–971.

Liang L. and Morgan J.J. (1990) Coagulation of iron oxide particles in the presence of organic materials. In *Chemical Modeling of Aqueous Systems II* (eds. D.C. Melchoir and R.L. Bassett), Amer. Chem. Soc. Symp. Ser. No. 416, 293–208.

Lovley D.R. and Phillips E.J.P. (1986) Organic matter mineralization with reduction of ferric iron in anaerobic sediments. *Appl. Environ. Microbiol.* **51**, 683–689.

Lovley D.R., Phillips E.J.P., and Lonergan D.J. (1991) Enzymatic versus nonenzymatic mechanisms for Fe(III) reduction in aquatic sediments. *Environ. Sci. Technol.* **25**, 1062–1067.

Macedo J. and Bryant R.B. (1989) Preferential microbial reduction of hematite over goethite in a Brazilian oxisol. *Soil Sci. Soc. Amer. J.* **53** 1114–1118.

Marchesi J.R., Russell N.J., White G.F., and House W.A. (1991) Effects of surfactant adsorption and biodegradability on the distribution of bacteria between sediments and water in a freshwater microcosm. *Appl. Environ. Microbiol.* **57**, 2507–2513.

Martin R.E., Bouwer E.J., and Hanna L.M. (1992) Application of clean–bed filtration theory to bacterial deposition in porous media. *Environ. Sci. Technol.* **26**, 1053–1058.

Mehra O.P. and Jackson M.L. (1960) Fe oxide removal from soils and clays by a dithionite–citrate system buffered with sodium bicarbonate. In *Proc. Seventh Nat. Conf. Clays Clay Min.* (ed. A. Swineford), Pergamon Press, 317–327.

Napper D.H. (1977) Steric stabilization. *J. Colloid Interface Sci.* **58**, 390–407.

Newton P.S. and Liss P.S. (1987) Positively charged suspended particles: Studies in an iron–rich river and its estuary. *Limnol. Oceanogr.* **32**, 1267–1276.

Nicholson R.V., Cherry J.A., and Reardon E.J. (1983) Migration of contaminants in groundwater at a landfill: A case study 6. Hydrogeochemistry. *J. Hydrol.* **63**, 131–176.

O'Melia C.R. (1989) Particle–particle interactions in aquatic systems. *Colloids Surfaces* **39**, 255–271.

O'Melia, C.R. (1990) Kinetics of colloid chemical processes in aquatic systems. In *Aquatic Chemical Kinetics* (ed. W. Stumm), Wiley & Sons, 447–474.

Pashley R.M. (1981) Hydration forces between mica surfaces in aqueous electrolyte solutions. *J. Colloid Interface Sci.* **80**, 153–162.

Pashley R.M. (1984) Forces between mica surfaces in La^{3+} and Cr^{3+} electrolyte solutions. *J. Colloid Interface Sci.* **102**, 23–35.

Pashley R.M. and Israelachvili J.N. (1984) DLVO and hydration forces between mica surfaces in Mg^{2+}, Ca^{2+}, Sr^{2+}, and Ba^{2+} chloride solutions. *J. Colloid Interface Sci.* **97**, 446–455.

Prieve D.C. and Alexander B.M. (1986) Hydrodynamic measurement of double–layer repulsion between colloidal particle and flat plate. *Science* **231**, 1269–1270.

Puls, R.W. and Powell, R.M. (1992) Transport of inorganic colloids through natural aquifer material: implications for contaminant transport. *Environ. Sci. Technol.* **26**, 614–621.

Pye K. (1983) Red beds. In *Chemical Sediments and Geomorphology* (eds. A.S. Goudie and K. Pye), Academic Press, 227–263.

Rajagopalan, R. and Tien, C. (1976) Trajectory analysis of deep–bed filtration with the sphere–in–cell porous media model. *AIChE J.* **22**, 523–533.

Robertson W.D., Barker J.F., LeBeau Y., and Marcoux S. (1984) Contamination of an unconfined sand aquifer by waste pulp liquor: A case study. *Ground Water* **22**, 191–197.

Robinson H.D. and Maris P.J. (1979) Leachate from domestic waste: generation, composition, and treatment. A review. Tech. Rep. TR108, Water Research Centre, Bucks., UK.

Ronov A.B. and Yaroshevsky A.A. (1971) Chemical composition of the earth's crust. In *The Earth's Crust and Mantle* (ed. P.J. Hart), Amer. Geophys. Union, 37–57.

Ruckenstein E. and Prieve D.C. (1976) Adsorption and desorption of particles and their chromatographic separation. *AIChE J.* **22**, 276–283.

Ryan J.N. (1988) Colloid mobilization in two Atlantic Coastal Plain aquifers: Colloid formation and stability. M.S. thesis, Dept. of Civil Eng., Massachusetts Institute of Technology, 250 pp.

Ryan J.N. and Gschwend P.M. (1990) Colloid mobilization in two Atlantic Coastal Plain aquifers: field studies. *Water Resour. Res.* **26**, 307–322.

Ryan J.N. and Gschwend P.M. (1991) Extraction of iron oxides from soils and sediments using reductive dissolution by titanium(III). *Clays Clay Min.* **39**, 509–518.

Ryan J.N. and Gschwend P.M. (1992) Effect of iron diagenesis on the transport of colloidal clay in an unconfined sand aquifer. *Geochim. Cosmochim. Acta* **56**, 1507–1521.

Schwille F. (1976) Anthropogenically reduced groundwater. *Hydrol. Sci.* **21**, 629–645.

Sherman D.M. (1987) Molecular orbital (SCF–Xα–SW) theory of metal–metal charge transfer processes in minerals II. Application to $Fe^{2+} \rightarrow Ti^{4+}$ charge transfer transitions in oxides and silicates. *Phys. Chem. Minerals* **14**, 364–367.

Shuey, R.T. (1975) Semiconducting ore minerals. In *Developments in Economic Geology 4*, Elsevier.

Stumm W., Furrer G., Wieland E., and Zinder B. (1985) The effects of complex–forming ligands on the dissolution of oxides and aluminosilicates. In *The Chemistry of Weathering* (ed. J.I. Drever), NATO ASI Series 149, D. Reidel Publ. Co., 55–74.

Thurman E.M., Barber L.B. Jr., and LeBlanc D. (1986) Movement and fate of detergents in groundwater: A field study. *J. Contam. Hydrol.* **1**, 143–161.

Valverde N. and Wagner C. (1976) Considerations on the kinetics and the mechanism of dissolution of metal oxides in acidic solutions. *Ber. Bunsenges. Physik. Chem.* **80**, 330–333.

Van Houten F.B. (1973) Origin of red beds; a review – 1961–1972. *Ann. Rev. Earth Planet. Sci.* **1**, 39–61.

Wieland E., Wehrli B., and Stumm W. (1988) The coordination chemistry of weathering: III. A generalization on the dissolution rate of minerals. *Geochim. Cosmochim. Acta* **52**, 1969–1981.

Yao, K.–M., Habibian, M.T., and O'Melia, C.R. (1971) Water and wastewater filtration: concepts and applications. *Environ. Sci. Technol.* **11**, 1105–1112.

Zinder B., Furrer G., and Stumm W. (1986) The coordination chemistry of weathering: II. Dissolution of Fe(III) oxides. *Geochim. Cosmochim. Acta* **50**, 1861–1870.

Appendix One

EXTRACTION OF IRON OXIDES FROM SEDIMENTS USING REDUCTIVE DISSOLUTION BY TITANIUM(III)

J.N. Ryan and P.M. Gschwend (1991)
Clays and Clay Minerals **39**, 509—518.

When we try and pick out anything by itself, we find it hitched to everything else in the Universe.

— John Muir

ABSTRACT

A new Fe oxide dissolution method designed to measure the abundance of "free" Fe oxide phases and associated elements in soils and sediments has been tested. The method employs a ternary complex of Ti(III), citrate, and ethylenediaminetetraacetate (EDTA) as a reductant and bicarbonate as a proton accepter.

The Ti(III)–citrate–EDTA–HCO_3 method dissolved more synthetic amorphous ferric oxide and goethite than the dithionite–citrate–HCO_3 method of Mehra and Jackson (1960), but less synthetic hematite. The production of acidity by the dissolution indicated that Ti(IV) is hydrolyzed to TiO_2 during the extractions. The heated dithionite method dissolved 3 to 6 times more Al from kaolinite and nontronite standard clays than the room temperature dithionite and 4 to 6 times more Al than the Ti(III)–citrate–EDTA–HCO_3 method. Furthermore, the release of Fe from the clay mineral samples consistently and rapidly reached a plateau during multiple extractions by the Ti(III)–citrate–EDTA–HCO_3 method, indicating that a well–defined Fe oxide fraction was removed. Fe released by the dithionite method continued to increase with each extraction, suggesting that some release of structural Fe occurred.

Tests on two natural sediments and one heavy mineral fraction from the Cohansey Sand in the New Jersey Coastal Plain suggested that the Ti(III)–citrate–EDTA–HCO_3 method removed Fe oxides more effectively and selectively than the dithionite method. The selectivity of the Ti(III)–citrate–EDTA–HCO_3 method is enhanced by rapid extractions at room temperature and low free ligand concentrations.

INTRODUCTION

Our interest in the dissolution of Fe oxides from sediments stems from the need to evaluate the role of Fe oxides in the attachment of clay to framework grains in Atlantic Coastal Plain surficial aquifers (Ryan and Gschwend, 1990). We hypothesized that Fe oxides cemented the clays in oxic zones of the aquifers, so we wanted to assess whether there was a correlation between the amount of secondary or "free" Fe (*e.g.*, ferrihydrite, goethite, hematite), the concentration of colloidal clay, and the amount of clay attached to the aquifer grains. We turned to the many Fe oxide extraction techniques to quantify the amount of Fe oxide coatings in sediments.

Soil scientists, geologists, and oceanographers have developed a number of Fe oxide removal techniques to enhance clay mineral characterization, to disperse sediment grains for particle size analysis, and to extract trace metals scavenged by Fe oxide fractions. These techniques have also been used to examine the role of Fe oxides in clay illuviation (Harris *et al.*, 1987; Smith and Callahan, 1987), to assess the role of Fe oxides and associated Al and Si in soil stability (Ajmone Marsan and Torrent, 1989), and to identify the transport modes and weathering products of Fe–bearing minerals in sediments (Koehnken and Stallard, 1988; Rude and Aller, 1989). In these applications, and in ours, where the measurement of Fe and associated elements in the Fe oxide fraction is the goal, the selectivity of the Fe oxide extraction technique is critical. Since the removal techniques are not perfectly selective for Fe oxides, interpretations of the results are often confounded by uncertainty related to which mineral phases are actually dissolved.

Dissolution of Fe oxides and other reducible metal oxides (*e.g.*, MnO_2) is facilitated by reductants, complexing ligands, and protons (Zinder *et al.*, 1986). Other oxide components of minerals (Al_2O_3, SiO_2, TiO_2) are dissolved only by

ligand– and proton–promoted reactions (Furrer and Stumm, 1986). The most selective Fe oxide extraction techniques take advantage of the unique sensitivity of Fe oxides to reductive dissolution. These techniques also utilize complexing ligands to bind Fe^{2+} following the reduction to prevent re–oxidation of Fe^{2+} and a buffer to avoid drastic changes in *p*H. Low *p*H results in increased aluminosilica.. dissolution by proton–promoted reaction and high *p*H results in decreasing Fe oxide solubility.

We needed an extraction method capable of dissolving crystalline Fe oxides because x–ray diffraction revealed goethite in the our soils and sediments, but we also desired a highly selective method to minimize ambiguity concerning the source of Fe and other elements dissolved. Some methods are not designed to dissolve crystalline Fe oxides: acidified NH_4^+–oxalate (McKeague and Day, 1966; Schwertmann, 1973), alkaline ethylenediaminetetraacetate (EDTA) (Borggaard, 1979). We tested $NH_2OH{\cdot}HCl$–acetic acid (Chester and Hughes, 1967) and $NH_2OH{\cdot}HCl$–citrate (Robbins *et al.*, 1984) and found they did not dissolve crystalline Fe oxides in a reasonable number of short extractions. The only widely–used selective dissolution technique capable of rapidly dissolving crystalline Fe oxides was the sodium dithionite–citrate–HCO_3 method, as described by Mehra and Jackson (1960). They reported that this combination of reductant, ligand, and buffer, augmented by heating to 80° C, dissolved 1.25 mmole of hematite in one 2–minute extraction and 2.25 mmole of goethite in three 15–minute extractions (the source of the Fe oxides was not mentioned). Dithionite is also capable of dissolving crystalline Fe oxides at room temperature in overnight extractions (Holmgren, 1967).

The strong reducing capability of dithionite methods comes at the expense of diminished selectivity, particularly when sediments contain Fe^{3+}–bearing smectite clays. Rozenson and Heller–Kallai (1976) found that dithionite readily reduced Fe^{3+} in nontronite and montmorillonite. Heath and Dymond (1977) observed that

three successive dithionite extractions of a smectite–bearing ocean sediment removed all of the Fe in the sample. Stucki *et al.* (1984) and Ericsson *et al.* (1984) observed that dithionite–citrate–HCO_3 solutions reduced structural Fe in various smectites, resulting in increased cation exchange capacities due to the higher Fe^{2+}/Fe^{3+} ratio. Citrate–HCO_3 solutions also dissolved large quantities of Al from montmorillonite and nontronite (Stucki *et al.*, 1984). Multiple extractions are often necessary to completely remove crystalline Fe oxides from some sediments, so unintended removal of structural elements may be increased. Mendelovici *et al.* (1979) extracted Fe oxides from kaolinite, separated from lateritic soils, 8 to 15 times before reaching a plateau in Fe dissolved.

In preliminary tests on our samples, dithionite (Mehra and Jackson, 1960) required multiple extractions to remove completely the free Fe oxides. In the process, Fe, Al, and Si must have been repeatedly dissolved from layer silicates and heavy minerals. We suspected that 80° C heating and the high citrate concentration (0.27 M) contributed to non–selective, ligand–promoted dissolution. We could have used dithionite in overnight room temperature extractions recommended by Holmgren (1967), but that method employs even higher citrate concentrations (0.66 M), which we feared would offset the advantage of the temperature reduction. In general, we desired short extractions because (1) at least two extractions are necessary to prove that a well–defined Fe fraction has been removed in the first extraction, and (2) short extractions favor rapid Fe oxide reduction over relatively slow ligand–promoted dissolution.

These concerns led us to formulate a new treatment for the extraction of Fe oxides from a technique used to distinguish between extra– and intracellular Fe in marine phytoplankton developed in this laboratory (Hudson and Morel, 1989). Using the ternary complex of Ti(III)–citrate–EDTA (in a molar ratio of 1:1:1) reported by Fujiwara *et al.* (1964) as a reducing agent, amorphous ferric oxides and

particulate Fe associated with cells were dissolved in 2–minute extractions in a 0.05 M Ti(III) solution. The new treatment for soils and sediments utilized the Ti(III)–citrate–EDTA ternary complex as the reducing agent and HCO_3^- as the *p*H buffer. We expected that lowering the free ligand concentration and eliminating the heating step, while keeping the extraction time short, would reduce dissolution of untargeted oxide components relative to the dithionite methods, but we were uncertain whether the Ti(III)–citrate–EDTA complex would be able to reduce crystalline Fe oxides. This communication reports a series of tests designed to compare the effectiveness and selectivity of the dithionite–citrate–HCO_3 method (Mehra and Jackson, 1960) and the Ti(III)–citrate–EDTA–HCO_3 method proposed here.

MATERIALS AND METHODS

Minerals

The reductive dissolution treatments were tested on three synthetic Fe oxides: amorphous ferric oxide, goethite, and hematite. Amorphous ferric oxide was prepared by dropwise addition of $FeCl_3$ solution to KOH solution to achieve a molar ratio of OH/Fe = 3.0. The goethite was prepared by dropwise addition of $Fe(NO_3)_3 \cdot 9H_2O$ solution to KOH solution to reach a molar ratio of OH/Fe = 1.0 (Atkinson *et al.*, 1968). The resulting suspension was aged 50 hours at room temperature, then the *p*H was raised to 12.0 by titration with KOH. The *p*H 12.0 suspension was aged 72 hours at 60° C. The amorphous ferric oxide and goethite precipitates were washed with distilled deionized water (ddW) and centrifuged three times, then dried at room temperature and ground to pass through a 120 mesh sieve (< 125 μm). Hematite was obtained as ferric oxide (Fe_2O_3, 99%) powder prepared by calcination of ferrous sulfate from EM Science and sieved through a 120 mesh sieve. The crystallinities of the Fe oxides were checked by X–ray powder diffraction (XRD) using a Diano XRD–5 diffractometer and Fe–filtered Co Kα radiation (35 kV, 15 mA). The amorphous ferric oxide sample yielded no diffraction peaks. Weak, diffuse peaks were observed only at the d_{110} and d_{130} lines for the goethite sample, indicating that the short aging period limited development of crystalline order. For the hematite sample, strong, sharp peaks appeared at all major hematite lines, indicating a high degree of crystallinity.

The standard clay minerals used in the dissolution tests include a kaolinite (API #9b, Mesa Alta, NM) and an Al–nontronite (Cheney, WA) obtained from Ward's Natural Science Establishment (Table A1.1). The clays were ground to pass through a 120 mesh sieve. The Fe and Ti contents of the kaolinite were also determined by $HF/HNO_3/HCl$ digestion in teflon–lined bombs at 110° C (Lim and

Jackson, 1982). The clay mineral crystallinities were assessed by XRD using Ni–filtered Cu Kα radiation (35 kV, 15 mA) on oriented samples of the < 2 μm fractions separated by settling in ddW, mounted on Ag membrane filters (Poppe and Hathaway, 1979), and air–dried. XRD did not reveal any crystalline impurities for either sample, although Kerr (1950) measured a total of 4.7% impurities in the kaolinite sample, which Main (1950) identified as quartz, orthoclase, sphene, leucoxene, and Fe oxides (0.5 to 1.0%).

Table A1.1. Composition of clay mineral standards and heavy mineral sample. Kaolinite data from Kerr (1950); supplementary kaolinite data from this study; nontronite data from supplier, obtained by electron microprobe analysis; heavy minerals data from this study.

Structural Oxide	Kaolinite API	Kaolinite this study	Nontronite	Heavy Minerals Sample U.11.1
	(wt%)	(wt%)	(wt%)	(wt%)
SiO_2	45.98		52.9	8.5
Al_2O_3	37.61		14.1	2.4
Fe_2O_3	0.76	0.83±0.01	23.9	24.2
TiO_2	0.50	0.86±0.01	1.2	64.9
CaO	0.35		2.6	
Na_2O	0.32		< 0.5	
K_2O	0.44		< 0.5	
H_2O	13.92		5.3	

Natural Sediments

Samples of sediments from the Cohansey Sand in the New Jersey Coastal Plain were collected using a split–tube sampler during hollow–stem auger drilling in August, 1989 (Table A1.2; Ryan and Gschwend, 1992; Chapter 2). Samples S.8.1 and S.8.2 surrounded a redox boundary at a depth of about 6 meters below a swamp. The anoxic sample (S.8.1) is a white sand bleached by reducing porewaters

from the swamp; the oxic sample (S.8.2) is a yellow sand apparently coated by Fe oxides. Total clay content was determined by suspension of the sample in ddW, 10–minute sonication in an 80 watt sonicator bath, settling to separate the < 2 μm fraction, measurement of the turbidity of the suspension, and comparison of the turbidity with turbidities of suspensions of known quantities of < 2 μm kaolinite ("colloidal kaolin powder," EM Science). The heavy mineral content was determined by settling the heavy minerals in bromoform. Color was described for dry sediments by comparison to Munsell soil color charts.

The sediment mineralogy was determined by XRD using Ni–filtered Cu Kα radiation (35 kV, 15 mA) on randomly–oriented samples of whole sediments and heavy mineral fractions ground to < 63 μm and oriented samples of the clay (< 2 μm) fraction. Equivalent masses of the clay fractions were loaded onto the Ag filters (10 mg cm^{-2}). Only quartz peaks were found in the whole sediment samples. The heavy mineral fractions of both samples revealed pseudorutile ($Fe_2O_3 \cdot 3TiO_2$), ilmenite, rutile, zircon, and augite peaks. Hematite and goethite were not detected in the heavy mineral fraction. The clay–sized (< 2 μm) fraction of the anoxic sediment revealed kaolinite and quartz peaks. In the < 2 μm fraction of sample S.8.2, kaolinite, goethite, and quartz were detected (Figure A1.1a). Crystalline Al oxides were not detected in the samples.

Heavy minerals were also separated from sample U.11.1, obtained from an oxic zone of the aquifer at a depth of 10 meters below the surface. The heavy minerals of this sample were used because the amount of heavy minerals extracted from remaining stocks of samples S.8.1 and S.8.2 was not sufficient for the heavy mineral treatments. The overall composition of the heavy mineral suite of sample U.11.1 was determined by energy–dispersive x–ray analysis (EDX) on a Au–coated sample (Table A1.1). XRD analysis showed that the major mineral constituents of this sample were the same as those of samples S.8.1 and S.8.2.

Table A1.2. Characteristics of sediment samples used in extraction tests.

	Sediment Samples	
	Oxic (S.8.2)	Anoxic (S.8.1)
Al (μmol g^{-1})	750	710
Fe (μmol g^{-1})	59	86
Ti (μmol g^{-1})	26	180
clay (< 2 μm) (wt %)	2.4	1.2
clay (< 2 μm) minerals	kaolinite goethite quartz	kaolinite quartz
heavy minerals (wt%)	0.54	2.6
Color	10YR 8/6 yellow	5YR 8/1 white

Reagents

Sodium dithionite was obtained from Aldrich Chemical Company at 78% purity. The major contaminant (~10%), sodium sulfite, and the minor contaminants identified by the supplier diminished the reducing capacity of the reagent so the amount used in the treatments was increased by a factor of 1.28. Sodium dithionite tends to be contaminated with Zn, which interferes with trace element studies (Tessier *et al.*, 1979; Shuman, 1982). The sodium dithionite was stored in a desiccator. Titanium(III) chloride was obtained from Aldrich as 12 wt% $TiCl_3$ in a 21 wt% HCl solution. The $TiCl_3$ reagent was significantly contaminated by Fe and perhaps other trace elements, but the supplier could not provide an analysis.

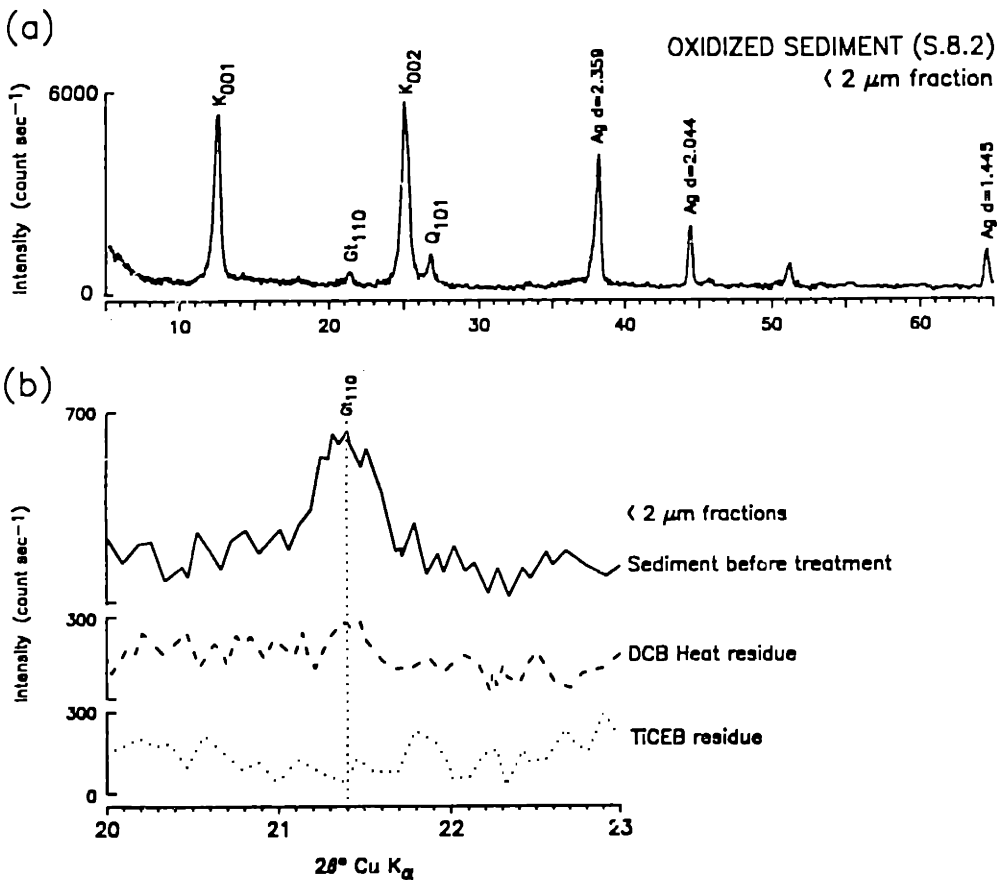

Figure A1.1. XRD results for (a) < 2 μm fraction of the oxidized sediment (S.8.2) showing the goethite (Gt), kaolinite (K), and Ag calibration peaks and (b) the major goethite peak (Gt_{110}) for < 2 μm fraction of the untreated sediment, the *DCB Heat*–treated sediment, and the *TiCEB*–treated sediment.

Reductive Dissolution Treatments

We set up a series of treatments in which only single components of the methods (reductant, ligand, buffer, heat) were changed (Table A1.3). All experiments were carried out in polyethylene and polycarbonate labware with the exception of some ground glass–stoppered reagent bottles and volumetric flasks. All labware was soaked in 4 N HNO_3 and rinsed with Fe– and Al–free 1 MΩ resistivity water produced with a reverse osmosis water purification system.

DCB Heat is a modification of the traditional Mehra and Jackson (1960) dithionite–citrate–HCO_3 method, altered to provide more complete separation of solids from the supernatant by high–speed centrifugation.

1. Mineral sample (0.1 g) or sediment sample (0.3 g) weighed in 40 mL polyethylene or polycarbonate centrifuge tube.
2. Thirty mL of 0.27 M citrate–0.11 M $NaHCO_3$ solution added to tube.
3. Suspension heated at 80° C in a water bath for 30 minutes.
4. Sodium dithionite (0.64 g at 78% purity) added to heated tube.
5. Suspension shaken for 15 minutes (sediment suspension sonicated for 5 minutes and shaken for 10 minutes).
6. Suspension centrifuged at 13,000 rpm (maximum 26,900 g) in Beckman J2–21 centrifuge with JS–13.1 tilting rotor for 60 minutes.
7. Supernatant (25 mL) carefully removed by syringe and stored for analysis.
8. Extraction repeated on reduced residue to insure complete Fe removal.

DCB and all of the following treatments omit the heating of the suspension (Step 3). *TiCB* uses the Ti(III)–citrate complex as the reductant in place of $Na_2S_2O_4$. The preparation of the reagent is best accomplished in a deaerated solution to prevent the oxidation of Ti(III) by dissolved oxygen. The following steps substituted for step 2:

2a. One liter of 0.27 M citrate solution bubbled with Ar for 60 minutes.

2b. Ti(III) chloride stock solution (64.28 g) diluted to 1 L with the deaerated citrate solution, resulting in a dark brownish–purple solution.

2c. Ti(III)–citrate solution titrated to *p*H 7.0 with NaOH while bubbling with Ar and stirring magnetically.

2d. Neutral Ti(III)–citrate solution stored in ground glass–stoppered reagent bottles (no longer than 48 hours).

2e. Thirty mL of Ti(III)–citrate solution added to tube.

2f. $NaHCO_3$ solution (3.33 mL of 1.0 M $NaHCO_3$) added to tube.

The dithionite addition (step 4) is omitted from this and all of the following treatments.

TiC omits the addition of the $NaHCO_3$ solution (step 2f).

TiCE uses a combination of citrate and EDTA to form a ternary Ti(III) complex in solution. Steps 2a and 2b are changed to the following:

2a. One liter of 0.05 M citrate–0.05 M Na_4EDTA bubbled with Ar for 60 minutes.

2b. Ti(III) chloride stock solution (64.28 g) diluted to 1 L with the deaerated citrate–EDTA solution, resulting in a transparent, deep purple solution.

The $NaHCO_3$ addition (step 2f) is omitted.

TiCEB includes the addition of the $NaHCO_3$ (step 2f) to the Ti(III)–citrate–EDTA solution. Steps 2a and 2b from the *TiCE* treatment are used.

Table A1.3. Reductive dissolution treatment reagents and conditions, with citrate abbreviated as "cit".

Method	Complexing Ligands	Buffer	Reducing Agent	Temp (°C)	Ar—purge
DCB Heat	0.27 M Na_3cit	0.11 M $NaHCO_3$	0.096 M $Na_2S_2O_4$	80	
DCB	0.27 M Na_3cit	0.11 M $NaHCO_3$	0.096 M $Na_2S_2O_4$	25	
TiCB	0.27 M Na_3cit	0.11 M $NaHCO_3$	0.05 M Ti(III)	25	√
TiC	0.27 M Na_3cit		0.05 M Ti(III)	25	√
TiCE	0.27 M Na_3cit 0.05 M Na_4EDTA		0.05 M Ti(III)	25	√
TiCEB	0.27 M Na_3cit 0.05 M Na_4EDTA	0.11 M $NaHCO_3$	0.05 M Ti(III)	25	√

Reductive Dissolution Test Procedures

We compared the Fe oxide reductive dissolution effectiveness of the six treatments by subjecting the three synthetic Fe oxides (0.1 g samples) to single extractions and measuring Fe dissolved in triplicate analyses. Before and after each extraction, *p*H was measured in the supernatant following 1 minute without drift. The reported *p*H is a mean of the triplicate analyses (standard deviations were always < 0.05 *p*H units). The Fe oxide dissolution results cannot readily be extrapolated to natural samples because these Fe oxides are synthesized under artificial conditions.

We tested the selectivity of the treatments by subjecting the clay minerals (0.1 g samples) to single extractions by the *DCB Heat, DCB, TiCE,* and *TiCEB* treatments and multiple extractions by the *DCB Heat* and *TiCEB* treatments. Fe and Al dissolved were measured in triplicate analyses.

The overall effectiveness of the *DCB Heat* and *TiCEB* treatments for extracting Fe oxides from sediments was tested by subjecting the heavy mineral (0.05 g samples) and sediment samples (0.3 g samples) to multiple extractions. Fe dissolved was measured in the heavy mineral extracts and Fe and Al dissolved were measured in the sediment sample extracts in triplicate analyses.

Dissolved Fe and Al concentrations in the supernatant were measured by inductively coupled plasma–atomic emission spectroscopy. Standards curves were prepared with blanks and standards made up in the treatment solutions. The overall results shown are means ± one standard deviation of triplicate analyses.

The removal of crystalline Fe oxides from the oxic sediment was monitored by XRD. The < 2 μm fractions were separated from the reduced residues and equivalent masses were loaded onto Ag filters in the same manner as the clay fractions of the sediments. XRD peak positions were calibrated to 2Θ position of the sharp Ag peak at d = 2.044 Å and peak intensities were normalized to the height of the same Ag peak in all samples.

RESULTS AND DISCUSSION

Iron Oxides: Single Extractions

For all treatments except DCB, the amount of Fe dissolved from the Fe oxide corresponds to the relative solubilities of the oxides: amorphous ferric oxide > goethite > hematite (Table A1.4). *DCB* dissolved significantly more hematite than goethite in the 15 minute extraction period, consistent with the results of Mehra and Jackson (1960) for their heated dithionite treatment. Torrent *et al.* (1987) and Macedo and Bryant (1989) also observed that dithionite and microbial reduction dissolved hematite more rapidly than goethite from lateritic soils. The slower dissolution of goethite was attributed to Al substitution in goethite (up to 34 mole% AlOOH), which decreased the goethite solubility (Tardy and Nahon, 1985). The composition of the goethite dissolved by Mehra and Jackson (1960) was not specified, but the goethite synthesized for this study did not contain Al, so it is not clear why *DCB* dissolved hematite more rapidly than goethite. The crystal form and shape, aggregation, or drying of the synthetic Fe oxides prepared for this study may have affected their dissolution kinetics.

The direction of *p*H change during the treatments suggests that dithionite reductions consume acidity and that Ti(III) reductions produce acidity. The major species involved in Fe oxide reduction by dithionite at an initial *p*H 7.3 include:

$$S_2O_4^{2-} + Fe_2O_3 + 2\ cit^{3-} + 2\ H^+ \rightarrow$$

$$2\ SO_3^{2-} + 2\ Fe(II)\text{–}cit^- + H_2O \qquad [A1.1]$$

according to Jepson (1988) and thermodynamic equilibrium calculations using MINEQL (Westall *et al.*, 1976). The change in *p*H is caused by consumption of one proton for each Fe^{3+} reduced, but *p*H rose only slightly during *DCB Heat* and *DCB* extractions because HCO_3^- donated protons. Initially, we expected that *p*H would increase in the Ti(III) reductions as well. Zehnder and Wuhrmann (1976) indicated

Table A1.4. Fe dissolved from three Fe oxides by six reductive dissolution methods. The amount of Fe dissolved (Fe Diss) is expressed as the fraction of Fe oxide dissolved determined by normalizing the amount of dissolved Fe to the total of amount of Fe dissolved in treatments where dissolution was complete.

	Amorphous Ferric Oxide			Goethite		Hematite	
	Initial *p*H	Fe Diss	Final *p*H	Fe Diss	Final *p*H	Fe Diss	Final *p*H
DCB Heat	7.3	0.94±0.01	7.8	0.87±0.02	7.8	0.62±0.08	7.9
DCB	7.3	0.71±0.04	7.7	0.39±0.00	7.6	0.56±0.03	7.4
TiCB	7.0	0.53±0.03	7.3	0.19±0.02	6.9	0.04±0.00	7.3
TiC	7.0	0.53±0.01	6.5	0.20±0.00	6.1	0.03±0.00	6.4
TiCE	7.0	1.00±0.03	5.1	1.00±0.01	5.4	0.38±0.01	5.4
TiCEB	7.0	0.98±0.05	6.7	0.98±0.00	6.7	0.42±0.01	6.6

that the Ti(III)–citrate complex is oxidized to Ti(IV)–citrate, resulting in the following reaction at neutral *p*H:

$$\text{Ti(III)–cit} + \tfrac{1}{2}\,\text{Fe}_2\text{O}_3 + \text{cit}^{3-} + 3\,\text{H}^+ \rightarrow \text{Ti(IV)–cit}^+ + \text{Fe(II)–cit}^- + \tfrac{3}{2}\,\text{H}_2\text{O} \qquad [\text{A1.2}]$$

However, *p*H decreased during the Ti(III)–citrate reductions (by almost one *p*H unit in the unbuffered *TiC* treatment); thus, we suspect that the oxidation of Ti(III) in Ti(III)–citrate destabilized the complex and Ti(IV) was hydrolyzed to TiO_2:

$$\text{Ti(III)–cit} + \tfrac{1}{2}\,\text{Fe}_2\text{O}_3 + \tfrac{1}{2}\,\text{H}_2\text{O} \rightarrow \text{TiO}_2 + \text{Fe(II)–cit}^- + \text{H}^+ \qquad [\text{A1.3}]$$

Stability constants for the Ti complexes are not available to evaluate the feasibility of this reaction. Ti concentrations remained high in the supernatants and the reduced residue, but crystalline TiO_2 was not detected in the reduced residues by

XRD. TiO_2 may remain in the supernatant as colloidal TiO_2 in the < 50 nm range or it may settle into the solid residue as amorphous TiO_2. Hudson and Morel (1989) observed that TiO_2 precipitation clogged filters used to separate phytoplankton cells from the reducing solution, but they did not investigate the nature of the TiO_2 solid. In either case, investigations of Ti (or trace elements present as contaminants in the $TiCl_3$ reagent) in soils and sediments will encounter high background problems.

During the unbuffered *TiCE* treatment, *p*H decreased by nearly two *p*H units. In this case, the hydrolysis of the resulting Ti(IV) liberates equimolar quantities of citrate and EDTA. EDTA outcompetes citrate for the Fe(II), forming Fe–EDTA complexes, and a proton is released:

$$\text{Ti(III)–cit–H}_2\text{EDTA}^{2-} + \tfrac{1}{2}\text{Fe}_2\text{O}_3 + \tfrac{1}{2}\text{H}_2\text{O} \longrightarrow \text{TiO}_2 + \text{Fe(II)–H}_2\text{EDTA} + \text{cit}^{3-} + \text{H}^+ \qquad [A1.4]$$

Protons are accepted by HCO_3^- in *TiCEB* to maintain near–neutral *p*H.

The substitution of Ti(III)–citrate for dithionite as the reductant (*TiCB*) resulted in far less Fe dissolution from each Fe oxide. Based only on equilibrium redox potentials calculated from free energies and stability constants, we expected that the Ti(III)–citrate reduction would be nearly as effective as the dithionite reduction (E_H = –480 mV at *p*H 7 for Ti(III)–citrate → Ti(IV)–citrate (Zehnder and Wuhrmann, 1976); E_H = –459 mV at *p*H 7.3 and $[S_2O_4^{2-}] = 0.096$ M for dithionite → sulfite). Incomplete complexation of Ti(III) probably caused the ineffectiveness of the Ti(III)–citrate solution. Titrating to neutral *p*H may destabilize the complex, as Hudson and Morel (1989) observed at *p*H 8, resulting in formation of $Ti(OH)_3$ ($K_{sp} \cong 10^{-40}$; Latimer, 1956).

Clay Minerals: Single Extractions

Single extractions of the clay minerals were designed to evaluate the selectivity of the *DCB Heat*, *DCB*, *TiCE*, and *TiCEB* treatments (Table A1.5). The *TiCB* and *TiC* treatments were not tested on the clay minerals because they were ineffective in Fe oxide dissolution.

Table A1.5. Selective reductive dissolution treatments on clay minerals.

		Kaolinite			Nontronite		
	Initial pH	Fe Diss	Al Diss	Final pH	Fe Diss	Al Diss	Final pH
		(μmole g^{-1} clay)			(μmole g^{-1} clay)		
DCB Heat	7.3	7.7±1.2	12±0.2	7.4	64±3	24±1	7.4
DCB	7.3	6.6±2.6	2.0±0.2	7.4	39±8	9.1±0.4	7.3
TiCE	7.0	2.7±0.6	2.3±0.7	6.0	55±10	10±0.5	5.8
TiCEB	7.0	4.1±0.5	2.2±0.2	6.8	47±2	5.7±0.2	6.8

In the single extractions of the kaolinite sample, the treatments removed between 2.5 and 7.4 % of the total Fe and between 0.027 and 0.15 % of the total Al, resulting in a molar ratio of Fe/Al removed that ranged from 0.6 to 3.3. Because Fe(III) substitution for Al^{3+} is usually limited to 3 mole% (Tardy and Nahon, 1985), it is apparent that much more Fe was dissolved from the samples than could have been present as structural Fe in the kaolinite. Thus, Fe dissolved from the sample must represent some portion of the 0.5% to 1.0% Fe oxide impurities reported by Main (1950). The single extraction of the kaolinite by *DCB Heat* dissolved about five times as much Al as the other three treatments, clearly showing the effect of heating to 80° C. The three room temperature treatments dissolved about the same

amount of Al. We expected that *TiCE* and *TiCEB* would dissolve less Al than the room temperature *DCB* treatment due to lower free ligand activity; however, in the 15–minute reactions, no significant difference was observed.

The single extractions of the nontronite sample dissolved Fe and Al at a molar ratio of Fe/Al that ranged from 3 to 8. Because the molar ratio of Fe/Al is 1.1 in the nontronite sample and Fe is dissolved much more extensively than Al from the sample, it is likely that reduction of structural Fe(III) in nontronite occurred. However, some of the Fe removed may have been present as Fe oxide impurities. Heating to 8[illegible]C in *DCB Heat* dissolved about 2.5 times as much Al from the nontronite sample as did the *DCB* and *TiCE* treatments. *TiCEB* dissolved the least Al, which we attribute to the combination of short, room temperature extractions, *p*H buffering, and low free ligand activity.

Clay Minerals: Multiple Extractions

The results of the kaolinite extractions show that the *TiCEB* extractions reached a plateau in Fe dissolved in the first extraction (Figure A1.2a). In contrast, the first *DCB Heat* extraction removed only half the total Fe ultimately dissolved and successive extractions continued to remove Fe. The total amount of Al dissolved increased with each extraction by both treatments, but *DCB Heat* dissolved nearly four times as much Al per extraction as *TiCEB*.

Successive *TiCEB* extractions on the nontronite sample dissolved only slightly more Fe than the amount of Fe dissolved in the first extraction, while the *DCB Heat* extractions removed Fe in relatively constant amounts (Figure A1.2b). Al dissolved increased with each successive extraction by both treatments, but *DCB Heat* dissolved nearly nine times as much Al per extraction as *TiCEB*.

TiCEB reached a plateau in Fe dissolved in the first extraction of both clay mineral samples, while successive *DCB Heat* extractions continued to dissolve Fe,

suggesting that the *TiCEB* treatment dissolved a well–defined portion of the Fe in the clays (probably a free Fe oxide phase) and that dissolution of structural Fe by *TiCEB* was minimal compared to *DCB Heat*. Al was dissolved from the clay mineral samples in nearly constant amounts in successive extractions, suggesting that structural Al was dissolved by both treatments; however, *TiCEB* extractions dissolved far less Al from each clay mineral than *DCB Heat* extractions.

Although trends in the amounts of Fe and Al dissolved in multiple extractions gave some indication whether the Fe and Al came from free oxide phases or from clay mineral structures, the origin of the Fe and Al could not be ascertained without the aid of some nondestructive analysis, such as differential XRD or Mössbauer spectroscopy. Crystalline Fe oxides were not detected in the clay mineral samples, so XRD could not be used to determine the source of the Fe dissolved.

Heavy Minerals: Multiple Extractions

The effects of multiple extractions by *DCB Heat* and *TiCEB* on the heavy mineral fraction (Figure A1.3) were compared to assess the contribution of this fraction to the Fe and Al dissolved from the natural sediment samples. The two treatments removed similar amounts of Fe in five extractions, but the *DCB Heat* extractions reached a plateau in Fe dissolved slightly more quickly than the *TiCEB* extractions. The plateau in Fe dissolved may represent a minor Fe–bearing fraction of the sample that is more susceptible to reductive dissolution.

DCB Heat extractions dissolved slightly more Al than *TiCEB* extractions. The source of the dissolved Al may be the small amounts of aluminosilicate heavy minerals detected by XRD and EDX (augite).

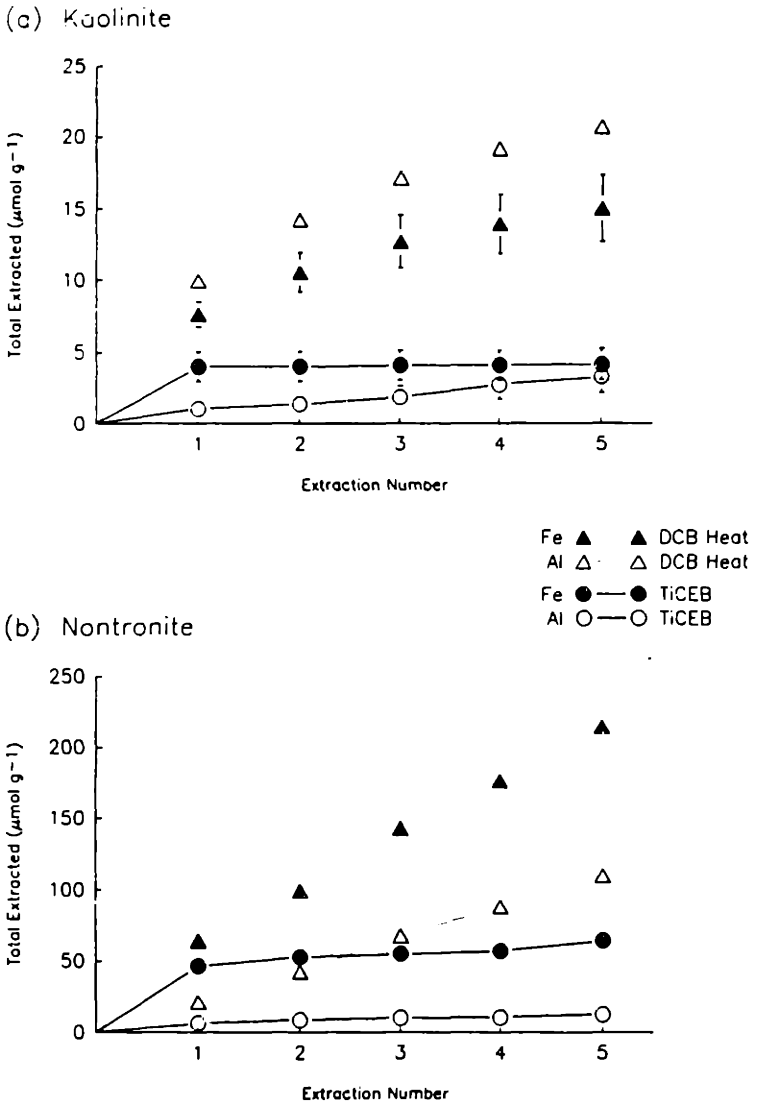

Figure A1.2. Comparison of Fe and Al dissolved from (a) kaolinite and (b) nontronite in multiple extractions by *DCB Heat* and *TiCEB*.

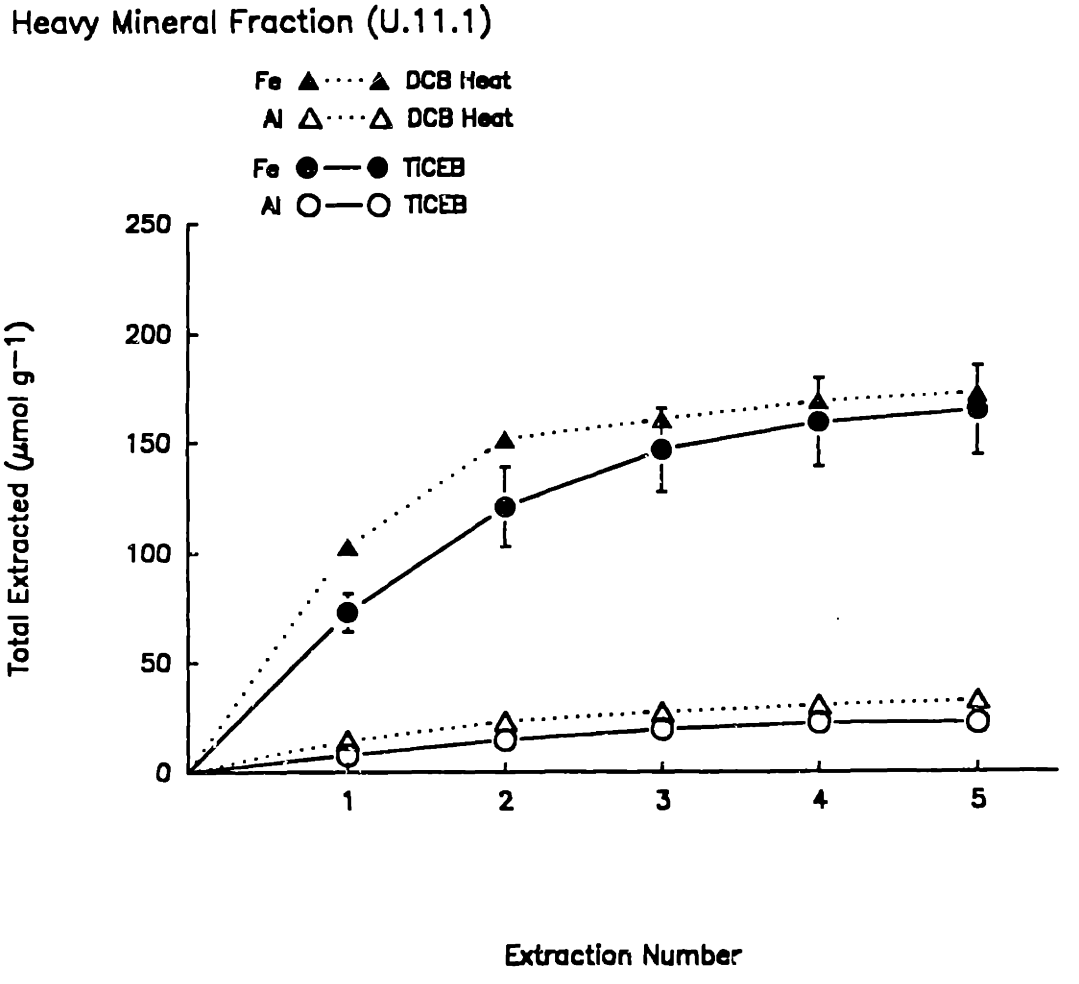

Figure A1.3. Comparison of Fe and Al dissolved from the heavy mineral fraction of sample U.11.1 in multiple extractions by *DCB Heat* and *TiCEB*.

Natural Sediment Extractions

The first *TiCEB* extraction of the oxic sediment (S.8.2) removed almost all of the Fe ultimately dissolved, while the first *DCB Heat* extraction removed only about half of the Fe ultimately dissolved (Figure A1.4a). The *DCB Heat* extractions appear to have reached a plateau in Fe dissolved, having removed only 80% of the total Fe dissolved by *TiCEB*. Both the *TiCEB* and *DCB Heat* extractions dissolved essentially all of the goethite in the oxic sediment $< 2\ \mu m$ fraction (Figure A1.1b). As with the Fe dissolved, the *TiCEB* extractions dissolved slightly more Al and reached a plateau in Al dissolved in fewer extractions than did the *DCB Heat* extractions.

The multiple extractions of the anoxic sediment (S.8.1) revealed that the first *TiCEB* extraction removed a larger portion of the Fe ultimately dissolved than did the first *DCB Heat* extraction (Figure A1.4b). The following *TiCEB* extractions dissolved less Fe per extraction than the *DCB Heat* extractions. The *DCB Heat* extractions dissolved Al from the anoxic sediment much more extensively than the *TiCEB* extractions.

To demonstrate the usefulness of the *TiCEB* method, the results of its application to the oxic and anoxic sediments are compared with those obtained by *DCB Heat*. With some knowledge of the mineralogy and some reasonable assumptions, we have estimated the amounts of Fe oxide, or "free" Fe, in each sediment. The expected free Fe content was estimated by subtracting structural Fe in clay minerals (corresponding to a clay–sized fraction composed entirely of 1 mole% Fe–substituted kaolinite) and structural Fe in the heavy mineral fraction (assuming the heavy mineral fractions have the same Fe content as that of sample U.11.1) from the total Fe measured. Other sources of structural Fe in the sediments were considered negligible. The amount of Fe removed by the two methods was amended by subtracting Fe extracted from the heavy mineral fraction of sample

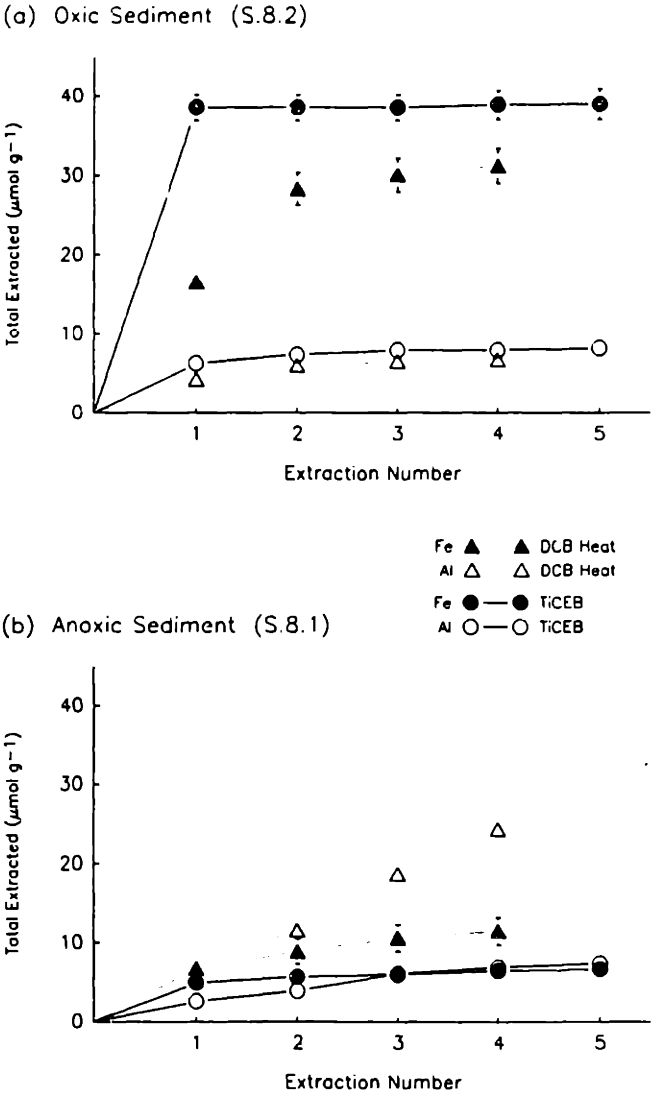

Figure A1.4. Comparison of Fe and Al dissolved from Pine Barrens (a) oxic sediment (S.8.2) and (b) anoxic sediment (S.8.1) in multiple extractions by *DCB Heat* and *TiCEB*.

U.11.1 (assuming that Fe is extracted from the heavy mineral fractions of the sediments at the same rate) from the total amount of Fe extracted from the sediments. The amount of structural Fe that may have been extracted from the clay minerals was considered negligible. The amount of Fe removed by *TiCEB* from the oxic sediment closely approximated the expected Fe oxide content, while the amount of Fe removed by *DCB Heat* fell short (Table A1.6). The small amounts of Fe removed from the anoxic sediment by both methods were both reasonable given the uncertainty in our estimated free Fe; however, the amount of Fe extracted by *DCB Heat* continued to increase slightly with each extraction.

Table A1.6. Comparison of Fe dissolved in the multiple extractions of the sediment samples with expected concentrations of Fe in various fractions of the sediments. Estimated quantities followed by (est.).

	Sediment Samples	
	Oxic (S.8.2)	Anoxic (S.8.1)
	(μmol g^{-1})	(μmol g^{-1})
Total Fe	59	86
Fe in Clay (est.)	–2.6	–0.9
Fe in Hvy Min (est.)	–16	–79
Expected free Fe	40	6.1
TiCEB		
Fe removed from sediment	39	6.7
Fe removed from hvy min	–0.9	–4.4
TiCEB Free Fe	38.1	2.3
DCB Heat		
Fe removed from sediment	31.2	11.5
Fe removed from hvy min	–0.9	–4.4
DCB Heat Free Fe	30.3	7.1

The parallel behavior of Al and Fe dissolved from the oxic sediment suggests that most of the Al (the portion removed in the first extraction) was associated with a free Fe oxide phase. After adjusting the Al removed by *TiCEB* for the amount of structural Al expected from aluminosilicates in the heavy mineral fraction, Al associated with the free Fe oxides may have been present as 15 to 20 mole% AlOOH substituting in the goethite detected by XRD, assuming that all of the Fe removed by *TiCEB* comprised the goethite and that the amount of Al released by other aluminosilicates was negligible. Goethite d_{110} peaks were shifted to smaller d–spacings in other clay fractions separated from oxic soil and sediment samples obtained in the same cores (Ryan and Gschwend, 1992; Chapter 2), indicating Al substitution in goethite (Schulze, 1984). In contrast with the similarity between the behavior of the Fe and Al dissolved from the oxic sediment, the Al dissolved from the anoxic sediment continued to increase quite steadily for both the treatments extractions, suggesting that the Al dissolved came primarily from the clay and heavy mineral phases. *DCB Heat* extractions dissolved about four times as much Al from the anoxic sediment as did *TiCEB* extractions.

CONCLUSIONS

Our attempts to characterize the abundance of the free Fe oxide phases led us to examine methods by which Fe oxides are extracted from soils and sediments. We tested the most widely–used version of the dithionite methods (Mehra and Jackson, 1960) on our samples and found that multiple extractions were required to remove a well–defined fraction of Fe from our samples. Furthermore, more Al was being dissolved in each extraction. We formulated a new Fe oxide dissolution method employing the Ti(III)–citrate–EDTA ternary complex (Fujiwara *et al.*, 1964) as the reductant and $NaHCO_3$ as a *p*H buffer.

The Ti(III)–citrate–EDTA–HCO_3 method dissolved synthetic amorphous ferric oxide and goethite slightly better than the dithionite method, but the hematite examined in this study was dissolved to a greater extent by dithionite. The change in *p*H during the experiments suggested that the Ti(III) reductions produced acidity, while the dithionite reductions consumed acidity. The heated dithionite method dissolved 3 to 6 times more Al from kaolinite and nontronite standard clays than the room temperature dithionite and 4 to 6 times more Al than the Ti(III)–citrate–EDTA–HCO_3 method. Furthermore, the release of Fe from the clay mineral samples consistently and rapidly reached a plateau during Ti(III)–citrate–EDTA–HCO_3 multiple extractions, indicating that a well–defined fraction of Fe was removed, while Fe released by dithionite continued to increase with each extraction. Multiple extractions of natural sediments and heavy minerals from the Cohansey Sand revealed that (1) the Ti(III)–citrate–EDTA–HCO_3 method extracted amounts of Fe that agreed well with the expected amount of free Fe oxides in the sediment; (2) both the Ti(III)–citrate–EDTA–HCO_3 and dithionite methods were effective at removing crystalline goethite from the oxic sample; and (3) the Ti(III)–citrate–EDTA–HCO_3 method dissolved much less Al

from the sediments than the dithionite method, Al presumed to be mainly structural in origin. Application of the *TiCEB* method to 37 other soil and sediment samples collected from cores of the Cohansey Sand consistently indicated complete free Fe removal in single extractions.

Extraction at room temperature rather than at 80° C certainly enhanced the selectivity of Ti(III)–citrate–EDTA–HCO_3 relative to dithionite, but the lower free strong ligand concentration in Ti(III)–citrate–EDTA–HCO_3 also discouraged ligand–promoted dissolution of oxide components not targeted for extraction. For our samples, the result was more complete dissolution of goethite in a small number of short extractions and less dissolution of structural components of accompanying aluminosilicate minerals. Although the usefulness of the Ti(III)–citrate–EDTA–HCO_3 method may be limited by the presence of trace elements in the "off–the–shelf" $TiCl_3$ reagent and the high concentrations of Ti left in the extraction solution and residue, we suggest that researchers concerned with the amount of Fe and associated elements in free Fe oxide phases of soils and sediments compare the effectiveness and selectivity of the Ti(III)–citrate–EDTA–HCO_3 method with traditional methods.

REFERENCES

Ajmone Marsan F. and Torrent J. (1989) Fragipan bonding by silica and Fe oxides in a soil from northwestern Italy. *Soil Sci. Soc. Amer. J.* **53** 1140–1145.

Atkinson R.J., Posner A.M., and Quirk J.P. (1968) Crystal nucleation in Fe(III) solutions and hydroxide gels. *J. Inorg. Nucl. Chem.* **30**, 2371–2381.

Borggaard O.K. (1979) Selective extraction of amorphous Fe oxides by EDTA from a Danish sandy loam. *J. Soil Sci.* **30**, 727–734.

Chester R. and Hughes M.J. (1967) A chemical technique for the separation of ferro–manganese minerals, carbonate minerals and adsorbed trace elements from pelagic sediments. *Chem. Geol.* **2**, 249–262.

Ericsson T., Linares J., and Lotse E. (1984) A Mössbauer study of the effect of dithionite–citrate–bicarbonate treatment on a vermiculite, a smectite, and a soil. *Clay Min.* **19**, 85–91.

Fujiwara S., Nagashima K., and Codell M. (1964) Mixed chelate compounds of titanium(III) as studied by electron paramagnetic resonance and spectroscopy. *Bull. Chem. Soc. Japan* **37**, 773–779.

Furrer G. and Stumm W. (1986) The coordination chemistry of weathering: I. Dissolution kinetics of α–Al_2O_3 and BeO. *Geochim. Cosmochim. Acta* **50**, 1847–1860.

Harris W.G., Carlisle V.W., and Chesser S.L. (1987) Clay mineralogy as related to morphology of Florida soils with sandy epipedons. *Soil Sci. Soc. Amer. J.* **51**, 1673–1677.

Heath G.R. and Dymond J. (1977) Genesis and transformation of metalliferous sediments from the East Pacific Rise, Bauer Deep and central region northwest Nazca plate. *Geol. Soc. Amer. Bull.* **88**, 723–733.

Holmgren G.G.S. (1967) A rapid citrate–dithionite extractable iron procedure. *Soil Sci. Soc. Amer. Proc.* **31**, 210–211.

Hudson R.J.M. and Morel F.M.M. (1989) Distinguishing between extra– and intracellular Fe in marine phytoplankton. *Limnol. Oceanogr.* **34**, 1113–1120.

Jepson W.B. (1988) Structural iron in kaolinites and in associated ancillary minerals. In *Iron in Soils and Clay Minerals* (eds. J.W. Stucki, B.A. Goodman, and U. Schwertmann). D. Reidel Publ. Co., 467–536.

Kerr P.F. (1950) Analytical data on reference clay material. Amer. Petrol. Inst. Proj. 49, Prelim. Rep. 7, Columbia Univ. Press.

Koehnken L. and Stallard R. (1988) Distribution of Fe in clays and coatings in fine–grained sediments from the Orinoco River basin. *EOS Trans. Amer. Geophys. Union* **69**, 1109.

Latimer W.M. (1956) *Oxidation Potentials*, 2nd ed. Prentice–Hall, Englewood Cliffs, NJ, p. 268.

Lim C.H. and Jackson M.L. (1982) Dissolution for total analysis. In *Methods of Soil Analysis*, Part 2 (ed. A.L. Page). Amer. Soc. Agron., Madison, WI, 5–7.

Macedo J. and Bryant R.B. (1989) Preferential microbial reduction of hematite over goethite in a Brazilian Oxisol. *Soil Sci. Soc. Amer. J.* **53**, 1114–1118.

Main M.S. (1950) Occurrence and microscopic examination of reference clay mineral specimens: Microscopic examinations. Amer. Petrol. Inst. Proj. 49, Prelim. Rep. 5, Columbia Univ. Press.

McKeague J.A. and Day J.H. (1966) Dithionite and oxalate–extractable Fe and Al as aids in differentiating various classes of soils. *Can. J. Soil Sci.* **46**, 13–22.

Mehra O.P. and Jackson M.L. (1960) Fe oxide removal from soils and clays by a dithionite–citrate system buffered with sodium bicarbonate. In *Proceedings of Seventh National Conference on Clays and Clay Minerals* (ed. A. Swineford). Pergamon Press, Washington, DC, 317–327.

Mendelovici E., Yariv Sh., and Villalba R. (1979) Fe–bearing kaolinite in Venezuelan laterites: I. Infrared spectroscopy and chemical dissolution evidence. *Clay Min.* **14**, 323–331.

Poppe L.J. and Hathaway J.C. (1979) A metal–membrane mount for x–ray powder diffraction. *Clays Clay Min.* **27**, 152–153.

Robbins J.M., Lyle M., and Heath G.R. (1984) A sequential extraction procedure for partitioning elements among co–existing phases in marine sediments. Reference 84–3, College of Oceanography, Oregon State University, Corvallis, OR, 64 pp.

Rozenson I. and Heller–Kallai L. (1976) Reduction and oxidation of Fe^{3+} in dioctahedral smectites–1: Reduction with hydrazine and dithionite. *Clays Clay Min.* **24**, 271–282.

Rude P.D. and Aller R.C. (1989) Early diagenetic alteration of lateritic particle coatings in Amazon continental shelf sediments. *J. Sed. Petrol.* **59**, 704–716.

Ryan J.N. and Gschwend P.M. (1990) Colloid mobilization in two Atlantic Coastal Plain aquifers: Field studies. *Water Resour. Res.* **26**, 307–322.

Ryan J.N. and Gschwend P.M. (1992) Effect of iron diagenesis on the transport of colloidal clay in an unconfined sand aquifer. *Geochim. Cosmochim. Acta* **56**, 1507–1521.

Schulze D.G. (1984) The influence of aluminum on iron oxides. VIII. Unit–cell dimensions of Al–substituted goethites and estimation of Al from them. *Clays Clay Min.* **32**, 36–44.

Schwertmann U. (1973) Use of oxalate for Fe extraction from soils. *Can. J. Soil Sci.* **53**, 244–246.

Shuman L.M. (1982) Separating soil Fe– and manganese–oxide fractions for microelement analysis. *Soil Sci. Soc. Amer. J.* **46**, 1099–1102.

Smith B.R. and Callahan L.L. (1987) Soils with Bx horizons in the Upper Coastal Plains of South Carolina. *Soil Sci. Soc. Amer. J.* **51**, 158–164.

Stucki J.W., Golden D.C., and Roth C.B. (1984) Effects of reduction and reoxidation of structural iron on the surface charge and dissolution of dioctahedral smectites. *Clays Clay Min.* **32**, 350–356.

Tardy Y. and Nahon D. (1985) Geochemistry of laterites, stability of Al–goethite, Al–hematite, and Fe^{3+}–kaolinite in bauxites and ferricretes: An approach to the mechanism of concretion formation. *Amer. J. Sci.* **285**, 865–903.

Tessier A., Campbell P.G.C., and Bisson M. (1979) Sequential extraction procedure for the speciation of particulate trace metals. *Anal. Chem.* **51**, 844–851

Torrent A., Schwertmann U., and Barron V. (1987) The reductive dissolution of synthetic goethite and hematite in dithionite. *Clay Min.* **22**, 329–337.

Westall J., Zachary J., and Morel F.M.M. (1976) MINEQL, a computer program for the calculation of chemical equilibrium composition of aqueous systems. Technical Note 18, Dept. Civil Eng., Mass. Inst. Tech., 91 pp.

Zehnder A.J.B. and Wuhrmann K. (1976) Titanium(III) citrate as a nontoxic oxidation–reduction buffering system for the culture of obligate anaerobes. *Science* **194**. 1165–1166.

Zinder B., Furrer G., and Stumm W. (1986) The coordination chemistry of weathering: II. Dissolution of Fe(III) oxides. *Geochim. Cosmochim. Acta* **50**, 1861–1869.

Appendix Two

ESTIMATING SURFACE POTENTIALS OF COMPLEX OXIDE MINERALS FROM ZETA POTENTIALS

It is no exaggeration to state that at this moment practically none of the values of ζ—potentials, as found in the literature, can be relied upon to give fundamental information on the double layer.

— E.J.W. Verwey and J.Th.G. Overbeek, *Theory of the Stability of Lyophobic Colloids*, p. 49 (1948).

INTRODUCTION

The surface potential of colloidal oxides is often estimated by zeta potentials. Zeta potentials are related to the electrophoretic mobility of the colloids in an electric field (Hunter, 1981). In electrophoresis measurements where solution *p*H is varied at constant ionic strength, zeta (ζ) potentials often reach a plateau at high surface charge. The surface charge at which this plateau is reached generally decreases with increasing ionic strength (*e.g.*, Wiese and Healy, 1975; James and Williams, 1982; Kallay *et al.*, 1987). In some cases where the concentration of H^+ or OH^- becomes the major contribution to ionic strength as *p*H is lowered or raised, oxide ζ–potentials decrease at high surface charge (Purcell and Sun, 1963; Williams and Williams, 1978). When solution ionic strength is varied at constant *p*H, ζ–potentials decrease as the concentration of indifferent electrolytes is increased (Fuerstenau and Modi, 1959; Kia *et al.*, 1987). From these experiments, it is apparent that ζ–potentials fail to provide good estimates of surface potentials at high ionic strength and high surface charge. Although the insensitivity of ζ–potential to surface potential has been recognized for some time (Verwey and Overbeek, 1948), ζ–potentials are still used to calculate double layer potential energy in studies of particle detachment kinetics (Kia *et al.* 1987; Cerda, 1987; Kallay *et al.*, 1987; McDowell–Boyer, 1992).

The electrokinetic experiments used to measure ζ–potential involve the tangential displacement of liquid along the charged surface in response to an applied electric field. According to the theory of these various phenomena, the value of the potential can be calculated in the plane where the liquid moves perceptibly with respect to the surface. This plane is referred to as the slipping or shear plane.

If the position of the shear plane were known, the surface potential (ψ_0) could be calculated assuming some model of potential drop from the surface (*e.g.*, Hunter

and Alexander, 1963). Unfortunately, the distance of the shear plane from the surface is not known. It is thought that the ζ–potential will resemble the the potential of the Stern plane, ψ_δ; in this case, the shear plane would be fixed at the first layer of ions adsorbed to the surface (Hunter, 1981; Van den Hul, 1983). The variation of ζ–potential with *p*H can be modeled with some accuracy by a triple–layer model assuming a fixed shear plane distance (Yates and Healy, 1980; Sprycha, 1989). However, interpretations of ζ–potential data with a two–layer Gouy–Chapman model suggest that the shear plane distance is variable (Dzombak and Morel, 1990). Basically, the behavior of the shear plane seems to depends on which electrostatic model is applied to the charged surface.

Because evidence indicates that the viscosity of vicinal water is greater than that of bulk water (Low, 1976; Hühnerfuss, 1988) and that the dielectric constant of vicinal water is much lower than that of bulk water (Neal and Cooper, 1983; Helmy and Natale, 1985), we surmise that the decrease in viscosity from the surface to the bulk water depends on the decrease in electrostatic potential from the surface. It is not unreasonable to suppose that shear plane moves as surface charge and ionic strength vary if viscosity also depends on surface charge and ionic strength because the shear plane distance must be related to the vicinal water viscosity.

We wanted to estimate accurate and consistent values of the surface potentials for the clay colloids released from the iron oxide–coated sand subjected to changes of flushing solution chemistry (Chapter 4) because the double layer potential energy as formulated by Hogg *et al.* (1966) is very sensitive to the surface potential. For simple oxides whose surface potential is determined by adsorption of potential–determining ions, we would estimate surface potentials by solving the surface complexation reactions describing the exchange of protons with surface metal hydroxyl groups in the presence of an electrostatic double layer. However, the clay colloids, composed mainly of kaolinite, could not simply be characterized as

a combination of its constituent oxides, SiO_2 and Al_2O_3. The surface chemistry of kaolinite is different for its faces and edges. The faces possess a permanent negative charge arising from isomorphic substitution of Si^{4+} sites with Al^{3+}; about one site in 25 is substituted. The edges are expected to behave as a binary mixture of two simple oxides, silica and alumina (>Si–OH, >Al–OH) . Kaolinite acid–base titration data has been modeled by Carroll–Webb and Walther (1988); however, (1) they did not account for permanent charge on the face, (2) they varied the edge Al/Si site density ratio with *p*H, and (3) their model overpredicted that amount of surface charge on kaolinite. With the added complication of a trace amount of goethite on the kaolinite, the task of estimating the surface potentials of the clay colloids would be even more daunting.

Instead, we developed an empirical relationship between the ζ–potentials of two simple oxides, rutile (TiO_2) and alumina (γ–Al_2O_3), carefully measured by Wiese and Healy (1975) at three ionic strengths, and the surface potentials estimated for these oxides by a surface complex/double layer model. We then estimated the overall surface potentials of the clay colloids released from the sand by converting their measured ζ–potentials into surface potentials with the same empirical relationship. In this Appendix, the development of the empirical relationship between the ζ–potentials and surface potentials of the model oxides is described.

MODEL OF SURFACE COMPLEXATION

Surface potentials may be determined for an interface described by a set of proton and hydroxide exchange reactions in the presence of a Gouy–Chapman double layer populated by indifferent counterions (Dzombak and Morel, 1990):

$$>M\text{–}OH_2^+ = >M\text{–}OH + H^+ \qquad K_{a1} = \frac{[>M\text{–}OH]\ [H^+]}{[>M\text{–}OH_2^+]} \qquad \text{[A2.1a]}$$

$$>M\text{–}OH = >M\text{–}O^- + H^+ \qquad K_{a2} = \frac{[>M\text{–}O^-]\ [H^+]}{[>M\text{–}OH]} \qquad \text{[A2.1b]}$$

where $>M-$ is the surface metal center, $>M\text{–}OH_2^+$, $>M\text{–}OH$, and $>M\text{–}O^-$ are the surface complexes, and K_{a1} and K_{a2} are the conditional equilibrium constants for the deprotonation reactions. The conditional equilibrium constants depend on the electrostatic potential of the oxide surface:

$$K_{a1} = K_{a1}^{int} \exp\,(ze\psi_0/\mathbf{k}T) \qquad \text{[A2.2a]}$$

$$K_{a2} = K_{a2}^{int} \exp\,(ze\psi_0/\mathbf{k}T) \qquad \text{[A2.2b]}$$

where K_{a1}^{int} is the intrinsic acidity constant for $>M\text{–}OH_2^+$, K_{a2}^{int} is the intrinsic acidity constant for $>M\text{–}OH$, z is the valence of the indifferent electrolyte, e is the elementary charge (C), $\mathbf{k}$ is the Boltzmann constant (J K^{-1}), and T is the absolute temperature (K). The oxide surface charge per unit area σ_s (C m^{-2}) is given by

$$\sigma_s = \frac{N_a e}{S_s C_s}\{[>M\text{–}OH_2^+] - [>M\text{–}O^-]\} \qquad \text{[A2.3]}$$

where S_s is the oxide specific surface area (m^2 g^{-1}), C_s is the oxide suspension concentration (g L^{-1}), and N_a is Avogadro's number. The surface charge is related to surface potential in the Gouy–Chapman theory by

$$\sigma_s = [8\epsilon\epsilon_0 N_a(1000)I\mathbf{k}T]^{0.5} \sinh\,(ze\psi_0/2\mathbf{k}T) \qquad \text{[A2.4]}$$

where ϵ is the dielectric constant of water (dimensionless), ϵ_0 is the permittivity of space (C V^{-1} m^{-1}), and I is the ionic strength (mol L^{-1}). At the point of zero surface charge (pH_{zpc}),

$$[>M\text{–}OH_2^+] = [>M\text{–}O^-] \qquad [A2.5]$$

so pH_{zpc} may be defined as

$$pH_{zpc} = 0.5\,(pK_{a1}^{int} + pK_{a2}^{int}) \qquad [A2.6]$$

The surface potential is determined iteratively by solving for σ_s with initial estimates of $[>M\text{–}OH_2^+]$, $[>M\text{–}O^-]$, and ψ_0. A better value of ψ_0 is determined with σ_s, and then the solution is repeated for new values of ψ_0 until a consistent result is obtained (Dzombak and Morel, 1990).

METHOD

Wiese and Healy (1975) carefully measured the electrophoretic mobilities of TiO_2 and γ–Al_2O_3 colloids in KNO_3 solutions of ionic strengths 0.0001 M, 0.001 M, and 0.01 M over a range of *p*H from about 4.5 to 10.0. For both oxides, the three ζ–*p*H curves coincided at the same pH_{zpc}, indicating the only H^+ and OH^- operated as potential–determining ions and that the colloidal oxides were free of impurities that could have resulting in *p*H–independent charge. They converted the electrophoretic mobilities to ζ–potentials with the tables of Wiersema *et al.* (1966).

We calculated values of surface potentials with the SCDL model (ψ_{scdl}) for the values of *p*H and *I* over which ζ–potentials were measured with total site density $[>M\text{–OH}]_{tot}$, intrinsic acidity constants pK_{a1}^{int} and pK_{a2}^{int}, surface area S_s, and suspension concentration C_s values listed in Table A2.1. The proton exchange

Table A2.1. Parameters used to calculate surface potentials of two oxides (Wiese and Healy, 1975) with a surface complexation/double layer model.

Parameter	alumina γ–Al_2O_3	rutile TiO_2
$[M\text{–OH}]_{tot}$ (sites nm^{-2})	1.6	14.6
pK_{a1}	7.7	3.7
pK_{a2}	10.3	8.1
S_s ($m^2\ g^{-1}$)	80	16.5
C_s ($g\ L^{-1}$)	0.15	0.05

Site density ($[M\text{–OH}]_{tot}$) and intrinsic acidity constants (pK_{a1}, pK_{a2}): Carroll–Webb and Walther (1988), Dzombak and Morel (1990).
Specific surface area (S_s) and suspension concentration (C_s): Wiese and Healy (1975).

reactions were solved iteratively with DSURF (Dzombak and Morel, 1990), a version of MINEQL (Westall *et al.*, 1976) modified to account for double layer interactions.

The differences between the measured ζ–potentials and the estimated values of ψ_{scdl} grow larger as ionic strength and surface charge increase (Figure A2.1). For each of three ionic strengths, ζ–potential (mV) was fit to ψ_{scdl} (mV) by a least squares regression with an expression of the form:

$$\psi_{scdl} = \zeta + (\exp [a(I)\ \zeta] - 1) \qquad [A2.7]$$

where $a(I)$ is an ionic strength–dependent fitting parameter. The form of this equation expresses the exponential increase in the difference between the absolute values of ψ_{scdl} and ζ–potential as ψ_{scdl} increases. It also expresses the relationship

$$\psi_{scdl} = \zeta = 0$$

at pH_{zpc}. The constant $a(I)$ was related to ionic strength through the reciprocal double layer thickness κ (m^{-1}) given by

$$\kappa^2 = \frac{2000\ N_a I\ e^2 z^2}{\epsilon \epsilon_0 kT} \qquad [A2.8]$$

where N_a is Avogadro's number, I is ionic strength (mole L^{-1}), e is the elementary charge (C), and z is the valence of a symmetrical electrolyte, ϵ is the dielectric constant of water (dimensionless), ϵ_0 is the permittivity of free space (C V^{-1} m^{-1}), k is the Boltzmann constant, and T is the absolute temperature. The six values of $a(I)$ were related to κ with an equation of this form:

$$a(I) = \alpha\ \kappa^{\beta} \qquad [A2.9]$$

This relationship between $a(I)$ and κ allows $a(I)$ to approach zero as ionic strength and κ decrease, corresponding to smaller differences between ζ and ψ_{scdl} at lower ionic strength. The curve calculated using the best–fit parameters $\alpha = 4.71 \pm 3.93 \cdot 10^{-4}$ and $\beta = 0.281 \pm 0.056$ is shown in Figure A2.2. This expression (Eqn. A2.9) was inserted into Eqn. A2.7 to yield the empirical relationship:

$$\psi_{scdl} = \zeta + \{\exp [(4.71 \cdot 10^{-4}\ \kappa^{0.281})\ \zeta] - 1\} \qquad [A2.10]$$

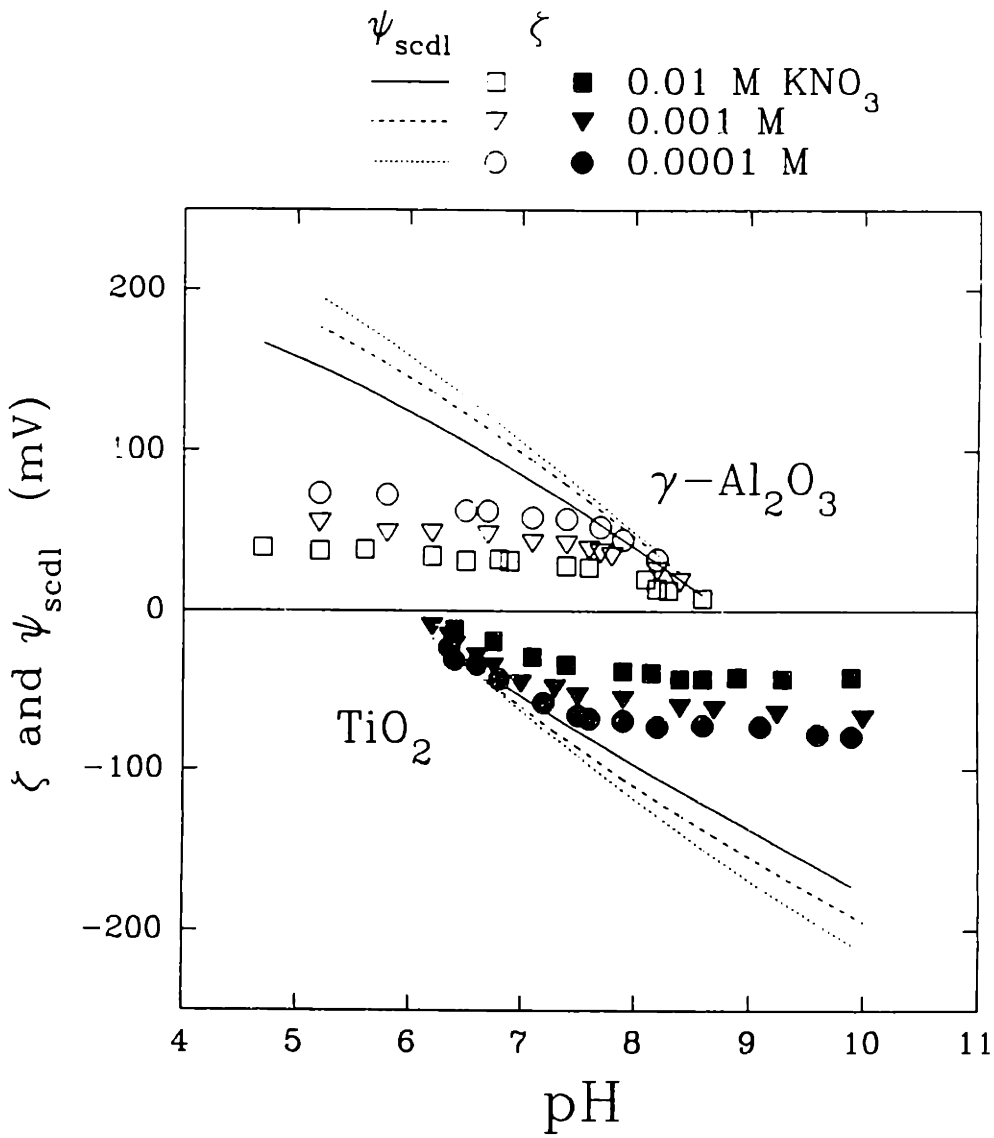

Figure A2.1 Plot of zeta potentials (ζ) and surface potentials estimated with a surface complex/double layer model (ψ_{scdl}) *vs.* *p*H for two oxides, rutile (TiO_2) and alumina (γ–Al_2O_3). The oxide ζ–potentials (filled and open symbols) were measured at three ionic strengths (KNO_3 concentrations) by Wiese and Healy (1975). The ψ_{scdl} values of the oxides (continuous curves) were calculated using the parameters shown in Table A2.1. Using Eqn. A2.7, the ζ–potentials were fit to the ψ_{scdl} values for each ionic strength, generating six values of the ionic strength–dependent fitting parameter $a(I)$.

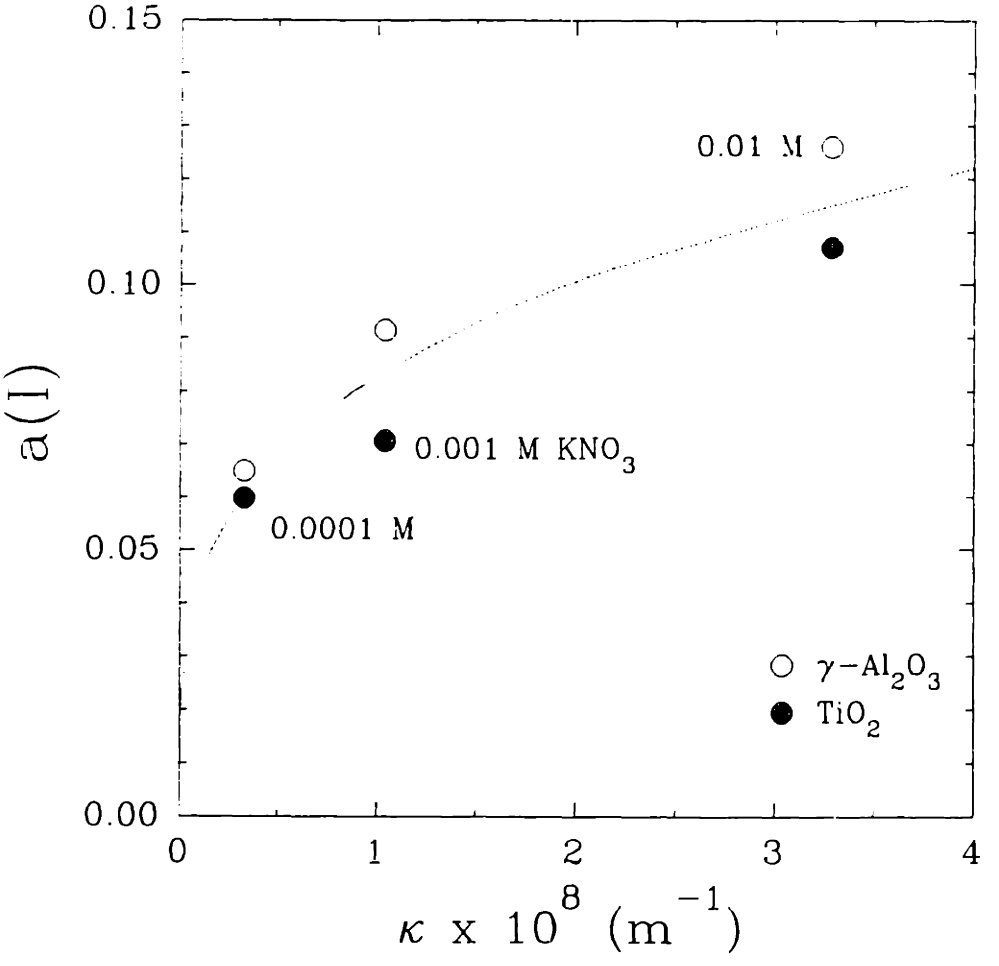

Figure A2.2. Plot of the fitting parameter $a(I)$ *vs.* the reciprocal double layer thickness κ showing the curve fit according to Eqn. A2.9. Values of $a(I)$ were obtained by fitting the oxide ζ–potentials to ψ_{scdl} values (Fig. A2.1) for each ionic strength with Eqn. A2.8. The range of κ is from zero to $4 \cdot 10^8$ m^{-1}.

RESULTS AND DISCUSSION

The fit between the TiO_2 and γ–Al_2O_3 ζ–potential data and the ψ_{scdl} values used to derive Eqn. A2.9 is shown in Figure A2.3. The ζ–κ–ψ_{scdl} relationship does a satisfactory job of predicting values ψ_o that agree well with the values of ψ_{scdl} from which the relationship was derived. The largest deviation of the predicted values of ψ_o from the calculated values of ψ_{scdl} is observed for the rutile colloids at intermediate ionic strength (0.001 M KNO_3). The value of $a(I)$ calculated with Eqn. A2.9 for this ionic strength (for which $\kappa = 1.04 \cdot 10^8$ m^{-1}) is substantially higher than the value of $a(I)$ obtained by fitting Eqn A2.7 to the $\zeta - \psi_{scdl}$ data (Figure A2.2).

This goal of deriving this ζ–κ–ψ_{scdl} relationship is to provide some means of compensation for the divergence of ζ–potential from ψ_o at high ionic strength and high surface charge. This approach is useful for correcting ζ–potentials measured for colloids composed of mixed oxides. Such mixed oxides have so far proved too complicated to model with surface complexation/double layer models. Implicit in the application of this relationship is the assumption that the adsorption of potential–determining ions by such mixed oxides should follow the same behavior as the simple oxides.

The difference in colloid shape (*e.g.*, spherical oxide colloid *vs.* clay plate) may cause some inconsistency in using the ζ–κ–ψ_{scdl} relationship to convert clay plate ζ–potentials to surface potentials. However, this is probably a second order variation in zeta potential variability compared to the insensitivity of zeta potential to surface potential at high surface charge and ionic strength.

This ζ–κ–ψ_{scdl} relationship was applied to the clay colloids that were released from the iron oxide–coated sands flushed with a variety of solutions as described in Chapter 4. An assessment of the usefulness of this relationship for the clay colloids may be found in the Discussion section of Chapter 4.

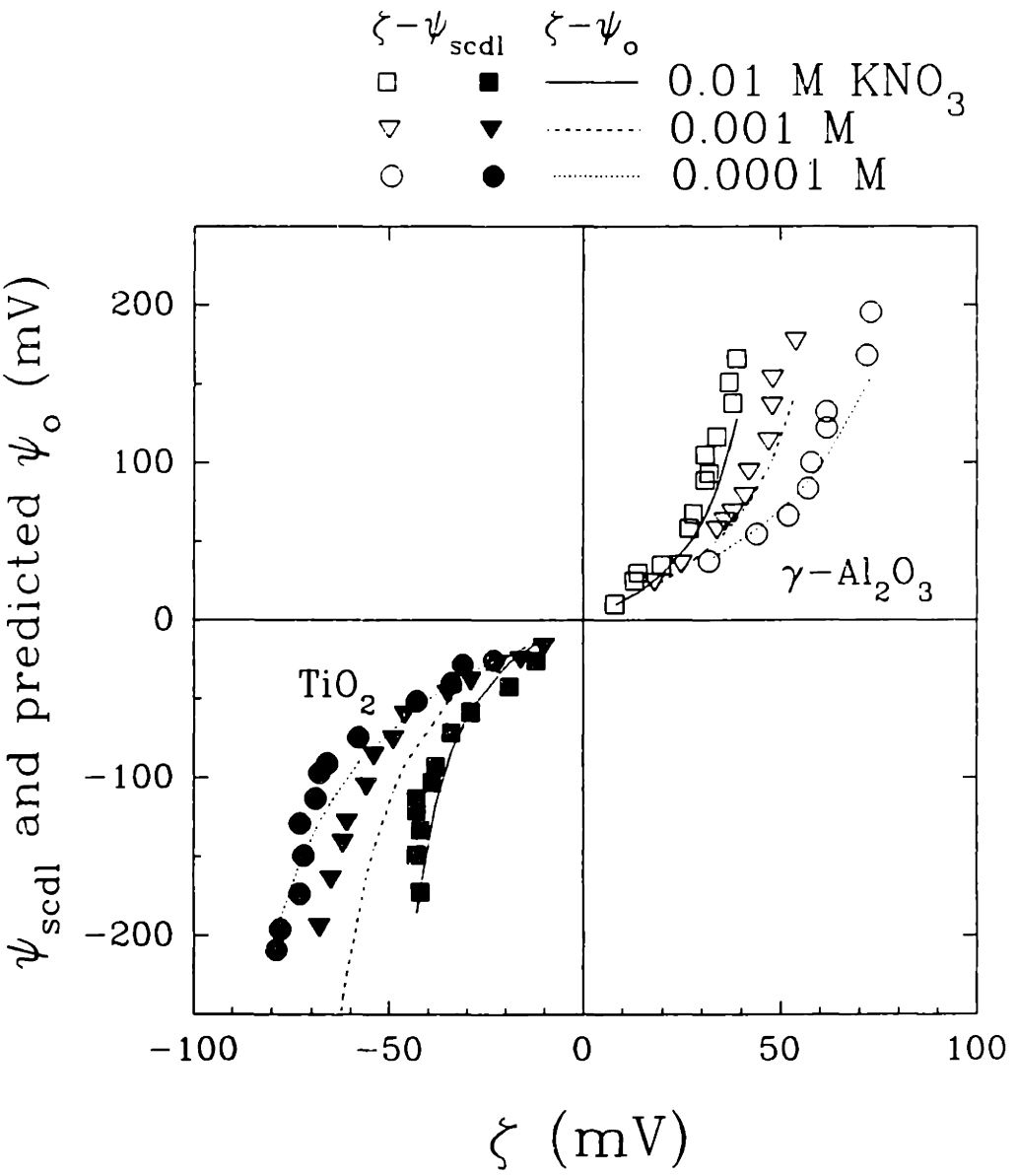

Figure A2.3. Plot of the ψ_{scdl} values and the predicted surface potentials (ψ_o) *vs.* the ζ–potentials of the two oxides. The ψ_{scdl} values are shown as filled and open symbols. The ψ_o values, predicted with Eqn. A2.10, are shown as continuous curves.

REFERENCES

Carroll–Webb S.A. and Walther J.V. (1988) A surface complex reaction model for the *p*H–dependence of corundum and kaolinite dissolution rates. *Geochim. Cosmochim. Acta* **52**, 2609–2623.

Cerda C. (1987) Mobilization of kaolinite fines in porous media. *Colloids Surfaces* **27**, 219–241.

Dzombak D.A. and Morel F.M.M. (1990) *Surface Complex Modeling. Hydrous Ferric Oxide.* Wiley–Interscience

Fuerstenau D.W. and Modi H.J. (1959) Streaming potentials of corundum in aqueous organic electrolyte solution. *J. Electrochem. Soc.* **106**, 336–341.

Helmy A.K. and Natale I.M. (1985) Effect of the dielectric constant on the double layer of clays. *Clays Clay Min.* **33**, 329–332.

Hogg R., Healy T.W., and Fuerstenau D.W. (1966) Mutual coagulation of colloidal dispersions. *Trans. Faraday Soc.* **62**, 1638–1651.

Hühnerfuss H. (1988) Hydrophilic hydration of monolayer molecules and its contribution to surface viscosity. *J. Colloid Interface Sci.* **126**, 384–385.

Hunter R.J. (1981) *Zeta Potential in Colloid Science.* Academic Press.

Hunter R.J. and Alexander A.E. (1963) Surface properties and flow behavior of kaolinite. Part I: Electrophoretic mobility and stability of kaolinite sols. *J. Colloid Sci.* **18**, 820–832.

James A.E. and Williams D.J.A. (1982) Particle interactions and rheological effects in kaolinite suspensions. *Adv. Colloid Interface Sci.* **17**, 219–232.

Kallay N., Barouch E., and Matijević E. (1987) Diffusional detachment of colloidal particles from solid/solution interfaces. *Adv. Colloid Interface Sci.* **27**, 1–42.

Kia S.F., Fogler H.S., and Reed M.G. (1984) Effect of *p*H on colloidally induced fines migration. *J. Colloid Interface Sci.* **118**, 158–168.

Low P.F. (1976) Viscosity of interlayer water in montmorillonite. *Soil Sci. Soc. Amer. J.* **40**, 500–505.

McDowell–Boyer L.M. (1992) Chemical mobilization of micron–sized particles in saturated porous media under steady flow conditions. *Environ. Sci. Technol.* **26**, 586–593.

Neal C. and Cooper D.M. (1983) Extended version of Gouy–Chapman electrostatic theory as applied to the exchange behavior of clay in natural waters. *Clays Clay Min.* **31**, 367–376.

Purcell G. and Sun S.C. (1963) Significance of double bonds in fatty acid flotation – an electrokinetic study. *Trans. Amer. Inst. Min. Met. Eng.* **226**, 6–12.

Sprycha R. (1989) Electric double layer at alumina/electrolyte interface I. Surface charge and zeta potential. *J. Colloid Interface Sci.* 127, 1–11.

Van den Hul H.J. (1983) Estimation of outer Helmholtz plane potentials from negative adsorption of co–ions. *J. Colloid Interface Sci.* **92**, 217–221.

Verwey E.J.W. and Overbeek J.Th.G. (1948) *Theory of the Stability of Lyophobic Colloids.* Elsevier.

Westall J.C., Zachara J.L., and Morel F.M.M. (1976) MINEQL: A computer program for the calculation of chemical equilibrium composition of aqueous systems. R.M. Parsons Laboratory Tech. Note 18, Dept. Civil Eng., Massachusetts Institute of Technology.

Wiersema P.H., Loeb A.L., and Overbeek J.Th.G. (1966) Calculation of the electrophoretic mobility of a spherical colloid particle. *J. Colloid Interface Sci.* **22**, 78–99.

Wiese G.R. and Healy T.W. (1975) Coagulation and electrokinetic behavior of TiO_2 and Al_2O_3 colloidal dispersions. *J. Colloid Interface Sci.* **51**, 427–433.

Williams D.J.A. and Williams K.P. (1978) Electrophoresis and zeta potential of kaolinite. *J. Colloid Interface Sci.* **65**, 79–87.

Yates D.E. and Healy T.W. (1980) Titanium dioxide–electrolyte interface. 2. Surface charge (titration) studies. *J. Chem. Soc. Faraday Trans. I* **76**, 9–18.

Appendix Three

CALCULATION OF INTERSURFACE POTENTIAL ENERGY

I believe that a colloid chemist, if asked today to explain the coagulation of a lyophobic hydrosol by electrolyte will make a rather unhappy face.

— W. Ostwald (1938) *J. Phys. Chem.* **42**, 981.

INTRODUCTION

The physical interaction between approaching surfaces has been expressed in the terms of the DLVO theory as the sum of the van der Waals and double layer potential energy varying with separation distance (Derjaguin and Landau, 1941; Verwey and Overbeek, 1948). To obtain a finite primary minimum, the short--range Born repulsive energy may be added to the total potential energy.

In this Appendix, the details of the calculation of one DLVO energy profile for the hematite colloid--quartz grain system examined in Chapter 3 are presented. Similar calculations were made for other systems considered in Chapters 2, 3, and 4. The choice of parameters for the other systems are detailed in the individual chapters.

METHOD

Intersurface Potential Energy

The total potential energy between approaching surfaces is expressed as the sum of the van der Waals, Born and double layer potential energy varying with separation distance x:

$$\phi(x) = \phi^{vdw}(x) + \phi^{born}(x) + \phi^{dl}(x) \qquad [A3.1]$$

Approaching colloids experience attractive forces resulting from dispersive, dipole–dipole, and induced dipole effects known as London–van der Waals forces. Hamaker (1937) derived an expression for the van der Waals potential energy of attraction between two spheres with an x^{-6} dependence on separation distance:

$$\phi^{vdw} = -\frac{A}{12}\left\{\frac{y}{r^2+ry+r} + \frac{y}{r^2+ry+r+y} + 2\ln\left[\frac{r^2+ry+r}{r^2+ry+r+y}\right]\right\}$$

$$y = a_g/a_c \qquad r = x/2a_c \qquad [A3.2]$$

where A is the Hamaker constant (J), a function of the atomic density and polarizability of the material constituting the colloid, and a_c and a_g are the colloid and grain radii, respectively. Retardation effects and the angular dependence of the potential interaction were ignored by assuming pairwise additivity of the interatomic potentials.

Short range repulsive forces arising from hydration or steric forces dominate $\phi(x)$ at very short separation distances (Israelachvili, 1982) and have an important effect on colloid detachment (Verwey and Overbeek, 1948; Ruckenstein and Prieve, 1976; Barouch *et al.*, 1987). However, the spatial variation of Born repulsion is not well understood. The Born repulsive potential has been formulated for sphere–sphere interaction by pairwise integration of the repulsive term of the interatomic Lennard–Jones potential for a x^{-12} dependence on separation distance

Feke *et al.*, 1984):

$$\phi^{\text{born}} = \frac{A}{75600r}\left[\frac{\sigma_{\text{born}}}{a_c}\right]^6\left[\frac{-4r^2-14(y-1)\,r-6(y^2-7y+1)}{(2r-1+y\ )^7}\right.$$
$$+\frac{-4r^2+14(y-1\,)r-6(y^2-7y+1)}{(2r+1-y)^7}+\frac{4r^2+14(y-1\,)\,r+6(y^2+7y+1)}{(2r+1+y\,)^7}$$
$$\left.+\frac{4r^2-14(y-1)r+6(y^2+7y+1)}{(2r-1-y)^7}\right] \qquad \text{[A3.3]}$$

where σ_{born} is the collision parameter (m). The Hamaker constant may be estimated from theory or determined by experiment. For oxides in aqueous suspension, A ranges from about 10^{-20} to 10^{-19} J (Hamaker, 1937; Israelachvili, 1985). For interatomic interactions, σ_{born} is on the order of 5 Å (Feke *et al.*, 1984).

Surfaces in contact with water develop a charge resulting from the exchange of protons, hydroxides, or other ions at surface functional groups. The surface charge gives rise to a double layer interaction potential between approaching surfaces. Hogg *et al.* (1966) calculated the double layer potential using a linearized solution to the Poisson–Boltzmann (PB) equation adapted to sphere–sphere interaction by one–dimensional integration of plate–plate interaction for the constant potential case:

$$\phi^{\text{dl}}(x) = \frac{\pi\epsilon\epsilon_0\,a_c a_g}{(a_c+a_g)}\{2\psi_{oc}\psi_{og}\ln\left[\frac{1\ +\ \exp(-\kappa x)}{1\ -\ \exp(-\kappa x)}\right]$$
$$+(\psi_{oc}^2+\psi_{og}^2)\ln[1-\exp(-2\kappa x)]\} \qquad \text{[A3.4]}$$

where ϵ is the dielectric constant of water (dimensionless), ϵ_0 is the permittivity of free space (C V^{-1} m^{-1}) and ψ_{oi} is the surface potential of the colloid or grain. The reciprocal double layer thickness κ (m^{-1}) is expressed as:

$$\kappa^2 = \frac{2000\ N_a I\ \ e^2z^2}{\epsilon\epsilon_0 kT} \qquad \text{[A3.5]}$$

where N_a is Avogadro's number, I is ionic strength (mole L^{-1}), e is the elementary charge (C), and z is the valence of a symmetrical electrolyte. The constant

potential case describes a double layer in which equilibrium with ions in the bulk solution is maintained with respect to the time scale of colloid attachment and detachment (Gregory, 1975; Lyklema, 1980).

Owing to the linear approximation of the PB equation, the Hogg *et al.* (1966) expression for plate–plate geometry is strictly accurate only for $\psi_0 > 25$ mV. However, the relative error between the approximate solution and the exact (numerical) solution of the full PB equation (Devereux and de Bruyn, 1963) is less than 60% even at $\psi_{01} = 0.154$ V and $\psi_{01} = 0.077$ V. At higher surface potentials, the relative error becomes more significant, but the exact solution displays some abnormal tendencies under certain conditions (see Chapter 3).

Equations A3.2, A3.3, and A3.4 were entered into a spreadsheet program (Lotus 123) on a personal computer. Appropriate values of A, σ, a_c, and a_g were chosen for each set of colloid–grain systems and kept constant as solution chemistry was varied in the experiments. Values of A and σ were chosen to allow identification of the maximum and minima in potential energies (ϕ_{max}, ϕ_{min1}, and ϕ_{min2}) for all combinations of ionic strength (I) and surface potentials (ψ_0). The changes in solution chemistry were reflected solely in the variation of ψ_{oc}, ψ_{og}, and I. The DLVO potential energy was calculated with a separation distance resolution of $\Delta x = 1 \cdot 10^{-11}$ m in the vicinity of ϕ_{min1} and ϕ_{max} and $\Delta x = 1 \cdot 10^{-10}$ m near ϕ_{min2}.

Surface Potentials

The surface potentials used to calculate the double layer potential energy ϕ^{dl} were chosen in different manners. In Chapter 2, the surface potentials (ψ_0) of the natural colloids and framework grains were chosen as zeta potentials (ζ) measured by microelectrophoresis for the clay–Fe(III) oxide–organic matter colloids (Ryan and Gschwend, 1990) and for quartz colloidal suspensions (Kia *et al.*, 1987). To

correct for the insensitivity of zeta potential to surface potential at high surface charge and high ionic strength (Verwey and Overbeek, 1948; Hunter, 1981) and to compensate for the lack of zeta potential measurements at all relevant combinations of *p*H and ionic strength, the surface potentials of the model colloids and grains were estimated with a surface complexation/double layer (SCDL) model (Dzombak and Morel, 1990) in Chapter 3. In Chapter 4, the surface potentials of the clay colloids released from the sediment were estimated by measuring their zeta potentials and converting the zeta potentials to surface potentials. The conversion of zeta potential to surface potential was done with an empirical relationship between the zeta potentials, ionic strength (in the form of the reciprocal double layer thickness κ), and surface potentials of two simple oxides characterized by Wiese and Healy (1975). The development of the ζ–κ–ψ_0 relationship is described in Appendix 2.

Calculation of Detachment Energies

From each of these profiles, detachment energies were calculated for both the energy barrier model with the equilibrium model as described in Chapter 3. For the energy barrier model, ϕ^{det} was calculated as $-(\phi_{max}-\phi_{min1})$ as in Eqn. 3.5. For the equilibrium model, ϕ^{det} was calculated as $-(\phi_{min2}-\phi_{min1})$ as in Eqn. 3.17. It should be noted that the secondary minimum exists because the exponential decay of the repulsive double layer term causes it to fall off more rapidly with separation distance than the power law of the attractive van der Waals term (Ottewill, 1977).

RESULTS

The complete results of one DLVO potential energy calculation are listed in Table A3.1. The calculation shown was done for the hematite colloid--quartz grain system at *p*H 11.0 and $I = 1 \cdot 10^{-3}$ M (this potential energy profile is shown in Fig. 3.7 in Chapter 3). The parameters used in the calculation included $A = 1 \cdot 10^{-20}$ J, $\sigma = 5 \cdot 10^{-10}$ m, $a_c = 7.5 \cdot 10^{-8}$ m, $a_g = 1.25 \cdot 10^{-4}$ m, $\psi_{oc} = -0.154$ V, $\psi_{og} = -0.248$ V, and $I = 1 \cdot 10^{-3}$ M. The physical constants used included the dielectric constant of water $\epsilon = 78.85$, the permittivity of free space $\epsilon_0 = 8.80 \cdot 10^{-12}$ C V^{-1} m^{-1}, the Boltzmann constant $\mathbf{k} = 1.38 \cdot 10^{-23}$ J K^{-1}, and the absolute temperature $T = 298$ K. The reciprocal double layer thickness κ was calculated with I, Avogadro's number $N_a = 6.023 \cdot 10^{23}$ ion mole^{-1}, the elementary charge $e = 1.602 \cdot 10^{-19}$ C, and the valence of a symmetrical electrolyte $z = 1$. The results of the calculation are shown graphically in Fig. A3.1.

Table A3.1. Results of the DLVO potential energy calculations for one DLVO potential energy profile shown in Fig. 3.7. Parameters used in calculation listed in text. The primary minimum ϕ_{min1} is shown by (−1), the primary maximum ϕ_{max} by (1), and the secondary minimum ϕ_{min2} by (−2).

separation distance z	total potential energy $\phi^{tot}/1000kT$	total potential energy ϕ^{tot}	van der Waals potential energy ϕ^{vdw}	Born potential energy ϕ^{born}	double layer potential energy ϕ^{dl}
m		J	J	J	J
1.00e−11	42180000	1.73e−10	−4.991e−17	1.735e−10	8.370e−18
2.00e−11	329500	1.36e−12	−2.493e−17	1.355e−12	9.356e−18
3.00e−11	19280	7.93e−14	−1.660e−17	7.931e−14	9.926e−18
4.00e−11	2574	1.06e−14	−1.244e−17	1.059e−14	1.033e−17
5.00e−11	540.0	2.22e−15	−9.944e−18	2.220e−15	1.063e−17
6.00e−11	151.3	6.22e−16	−8.280e−18	6.196e−16	1.088e−17
7.00e−11	52.18	2.15e−16	−7.091e−18	2.106e−16	1.109e−17
8.00e−11	21.34	8.78e−17	−6.199e−18	8.270e−17	1.127e−17
9.00e−11	10.26	4.22e−17	−5.506e−18	3.626e−17	1.143e−17
1.00e−10	5.825	2.40e−17	−4.952e−18	1.734e−17	1.156e−17
1.10e−10	3.912	1.61e−17	−4.498e−18	8.899e−18	1.169e−17
1.20e−10	3.044	1.25e−17	−4.120e−18	4.840e−18	1.180e−17
1.30e−10	2.641	1.09e−17	−3.800e−18	2.764e−18	1.190e−17
1.40e−10	2.458	1.01e−17	−3.526e−18	1.645e−18	1.199e−17
1.50e−10	2.384	9.80e−18	−3.289e−18	1.015e−18	1.208e−17
1.60e−10	2.364(−1)	9.72e−18	−3.081e−18	6.460e−19	1.216e−17
1.70e−10	2.372	9.75e−18	−2.898e−18	4.226e−19	1.223e−17
1.80e−10	2.394	9.85e−18	−2.735e−18	2.832e−19	1.230e−17
1.90e−10	2.423	9.97e−18	−2.589e−18	1.940e−19	1.236e−17
2.00e−10	2.455	1.01e−17	−2.458e−18	1.355e−19	1.242e−17
2.10e−10	2.488	1.02e−17	−2.339e−18	9.627e−20	1.248e−17
2.20e−10	2.521	1.04e−17	−2.231e−18	6.951e−20	1.253e−17
2.30e−10	2.552	1.05e−17	−2.133e−18	5.092e−20	1.258e−17
2.40e−10	2.583	1.06e−17	−2.042e−18	3.780e−20	1.263e−17
2.50e−10	2.611	1.07e−17	−1.959e−18	2.841e−20	1.267e−17
2.60e−10	2.639	1.09e−17	−1.883e−18	2.159e−20	1.271e−17
2.70e−10	2.665	1.10e−17	−1.812e−18	1.657e−20	1.275e−17
2.80e−10	2.689	1.11e−17	−1.746e−18	1.285e−20	1.279e−17
2.90e−10	2.712	1.12e−17	−1.685e−18	1.005e−20	1.283e−17
3.00e−10	2.734	1.12e−17	−1.628e−18	7.926e−21	1.286e−17
3.10e−10	2.754	1.13e−17	−1.574e−18	6.301e−21	1.290e−17
3.20e−10	2.774	1.14e−17	−1.524e−18	5.045e−21	1.293e−17
3.30e−10	2.793	1.15e−17	−1.477e−18	4.067e−21	1.296e−17
3.40e−10	2.810	1.16e−17	−1.432e−18	3.300e−21	1.299e−17
3.50e−10	2.827	1.16e−17	−1.391e−18	2.694e−21	1.301e−17
3.60e−10	2.843	1.17e−17	−1.351e−18	2.212e−21	1.304e−17
3.70e−10	2.858	1.18e−17	−1.314e−18	1.826e−21	1.307e−17
3.80e−10	2.872	1.18e−17	−1.278e−18	1.515e−21	1.309e−17
3.90e−10	2.886	1.19e−17	−1.245e−18	1.263e−21	1.311e−17

Table A3.1 (continued).

z	$\phi^{tot}/1000kT$	ϕ^{tot}	ϕ^{vdw}	ϕ^{born}	ϕ^{dl}
m		J	J	J	J
4.00e−10	2.899	1.19e−17	−1.213e−18	1.058e−21	1.314e−17
4.20e−10	2.924	1.20e−17	−1.154e−18	7.517e−22	1.318e−17
4.40e−10	2.946	1.21e−17	−1.100e−18	5.428e−22	1.322e−17
4.60e−10	2.967	1.22e−17	−1.051e−18	3.976e−22	1.325e−17
4.80e−10	2.986	1.23e−17	−1.006e−18	2.952e−22	1.329e−17
5.00e−10	3.003	1.24e−17	−9.647e−19	2.218e−22	1.332e−17
5.20e−10	3.020	1.24e−17	−9.265e−19	1.685e−22	1.334e−17
5.40e−10	3.035	1.25e−17	−8.912e−19	1.294e−22	1.337e−17
5.60e−10	3.048	1.25e−17	−8.584e−19	1.003e−22	1.339e−17
5.80e−10	3.061	1.26e−17	−8.278e−19	7.846e−23	1.342e−17
6.00e−10	3.073	1.26e−17	−7.993e−19	6.188e−23	1.344e−17
6.50e−10	3.100	1.27e−17	−7.358e−19	3.533e−23	1.348e−17
7.00e−10	3.122	1.28e−17	−6.814e−19	2.103e−23	1.352e−17
7.50e−10	3.141	1.29e−17	−6.342e−19	1.297e−23	1.355e−17
8.00e−10	3.157	1.30e−17	−5.930e−19	8.257e−24	1.357e−17
8.50e−10	3.170	1.30e−17	−5.567e−19	5.401e−24	1.359e−17
9.00e−10	3.181	1.31e−17	−5.244e−19	3.619e−24	1.361e−17
9.50e−10	3.190	1.31e−17	−4.955e−19	2.479e−24	1.361e−17
1.00e−09	3.198	1.31e−17	−4.696e−19	1.731e−24	1.362e−17
1.10e−09	3.209	1.32e−17	−4.248e−19	8.880e−25	1.362e−17
1.20e−09	3.215	1.32e−17	−3.875e−19	4.828e−25	1.361e−17
1.30e−09	3.218(1)	1.32e−17	−3.560e−19	2.756e−25	1.359e−17
1.40e−09	3.218	1.32e−17	−3.290e−19	1.640e−25	1.356e−17
1.50e−09	3.215	1.32e−17	−3.057e−19	1.012e−25	1.353e−17
1.60e−09	3.210	1.32e−17	−2.853e−19	6.439e−26	1.349e−17
1.70e−09	3.203	1.32e−17	−2.673e−19	4.211e−26	1.344e−17
1.80e−09	3.195	1.31e−17	−2.513e−19	2.822e−26	1.339e−17
1.90e−09	3.186	1.31e−17	−2.371e−19	1.932e−26	1.334e−17
2.00e−09	3.175	1.31e−17	−2.243e−19	1.349e−26	1.328e−17
2.20e−09	3.151	1.30e−17	−2.022e−19	6.920e−27	1.316e−17
2.40e−09	3.123	1.28e−17	−1.838e−19	3.762e−27	1.303e−17
2.60e−09	3.094	1.27e−17	−1.683e−19	2.147e−27	1.289e−17
2.80e−09	3.062	1.26e−17	−1.551e−19	1.278e−27	1.275e−17
3.00e−09	3.029	1.25e−17	−1.436e−19	7.879e−28	1.260e−17
3.20e−09	2.994	1.23e−17	−1.336e−19	5.013e−28	1.245e−17
3.40e−09	2.959	1.22e−17	−1.248e−19	3.278e−28	1.229e−17
3.60e−09	2.923	1.20e−17	−1.170e−19	2.196e−28	1.214e−17
3.80e−09	2.886	1.19e−17	−1.101e−19	1.503e−28	1.198e−17
4.00e−09	2.849	1.17e−17	−1.038e−19	1.049e−28	1.182e−17
4.50e−09	2.754	1.13e−17	−9.071e−20	4.596e−29	1.142e−17
5.00e−09	2.659	1.09e−17	−8.027e−20	2.196e−29	1.101e−17
5.50e−09	2.563	1.05e−17	−7.179e−20	1.125e−29	1.061e−17
6.00e−09	2.469	1.02e−17	−6.477e−20	6.114e−30	1.022e−17
6.50e−09	2.376	9.77e−18	−5.887e−20	3.487e−30	9.829e−18
7.00e−09	2.284	9.39e−18	−5.384e−20	2.073e−30	9.448e−18
7.50e−09	2.195	9.03e−18	−4.951e−20	1.278e−30	9.076e−18
8.00e−09	2.107	8.67e−18	−4.574e−20	8.124e−31	8.713e−18

Table A3.1 (continued).

z	$\phi^{tot}/1000kT$	ϕ^{tot}	ϕ^{vdw}	ϕ^{born}	ϕ^{dl}
m		J	J	J	J
8.50e−09	2.022	8.32e−18	−4.244e−20	5.308e−31	8.359e−18
9.00e−09	1.940	7.98e−18	−3.952e−20	3.554e−31	8.016e−18
9.50e−09	1.859	7.65e−18	−3.693e−20	2.431e−31	7.683e−18
1.00e−08	1.781	7.33e−18	−3.461e−20	1.696e−31	7.360e−18
1.10e−08	1.633	6.72e−18	−3.064e−20	8.683e−32	6.746e−18
1.20e−08	1.495	6.15e−18	−2.738e−20	4.712e−32	6.174e−18
1.30e−08	1.366	5.62e−18	−2.465e−20	2.684e−32	5.642e−18
1.40e−08	1.247	5.13e−18	−2.234e−20	1.594e−32	5.149e−18
1.50e−08	1.137	4.67e−18	−2.036e−20	9.813e−33	4.694e−18
1.60e−08	1.035	4.26e−18	−1.865e−20	6.231e−33	4.275e−18
1.70e−08	0.942	3.87e−18	−1.716e−20	4.067e−33	3.889e−18
1.80e−08	0.856	3.52e−18	−1.585e−20	2.720e−33	3.536e−18
1.90e−08	0.777	3.20e−18	−1.469e−20	1.858e−33	3.211e−18
2.00e−08	0.705	2.90e−18	−1.366e−20	1.295e−33	2.915e−18
2.20e−08	0.580	2.38e−18	−1.191e−20	6.613e−34	2.397e−18
2.40e−08	0.476	1.96e−18	−1.049e−20	3.580e−34	1.966e−18
2.60e−08	0.389	1.60e−18	−9.313e−21	2.034e−34	1.610e−18
2.80e−08	0.318	1.31e−18	−8.327e−21	1.205e−34	1.317e−18
3.00e−08	0.260	1.07e−18	−7.491e−21	7.401e−35	1.075e−18
3.20e−08	0.212	8.71e−19	−6.776e−21	4.688e−35	8.773e−19
3.40e−08	0.172	7.09e−19	−6.159e−21	3.052e−35	7.152e−19
3.60e−08	0.140	5.77e−19	−5.622e−21	2.036e−35	5.826e−19
3.80e−08	0.114	4.69e−19	−5.152e−21	1.388e−35	4.744e−19
4.00e−08	0.093	3.81e−19	−4.738e−21	9.643e−36	3.861e−19
4.20e−08	0.075	3.10e−19	−4.371e−21	6.820e−36	3.141e−19
4.40e−08	0.061	2.51e−19	−4.045e−21	4.900e−36	2.554e−19
4.60e−08	0.050	2.04e−19	−3.752e−21	3.572e−36	2.077e−19
4.80e−08	0.040	1.65e−19	−3.490e−21	2.639e−36	1.688e−19
5.00e−08	0.033	1.34e−19	−3.254e−21	1.973e−36	1.372e−19
5.50e−08	0.019	7.89e−20	−2.755e−21	9.998e−37	8.168e−20
6.00e−08	0.011	4.62e−20	−2.359e−21	5.369e−37	4.859e−20
6.50e−08	0.007	2.69e−20	−2.040e−21	3.027e−37	2.890e−20
7.00e−08	0.004	1.54e−20	−1.778e−21	1.779e−37	1.719e−20
7.50e−08	0.002	8.66e−21	−1.562e−21	1.083e−37	1.022e−20
8.00e−08	0.001	4.69e−21	−1.381e−21	6.804e−38	6.076e−21
8.50e−08	0.001	2.38e−21	−1.228e−21	4.392e−38	3.612e−21
9.00e−08	0.000	1.05e−21	−1.098e−21	2.905e−38	2.148e−21
9.50e−08	0.000	2.91e−22	−9.862e−22	1.963e−38	1.277e−21
1.00e−07	−0.000	−1.31e−22	−8.896e−22	1.352e−38	7.591e−22
1.10e−07	−0.000	−4.64e−22	−7.323e−22	6.753e−39	2.683e−22
1.20e−07	$-0.000^{(-2)}$	−5.16e−22	−6.109e−22	3.573e−39	9.483e−23
1.30e−07	−0.000	−4.82e−22	−5.156e−22	1.984e−39	3.352e−23
1.40e−07	−0.000	−4.28e−22	−4.395e−22	1.149e−39	1.185e−23
1.50e−07	−0.000	−3.74e−22	−3.780e−22	6.891e−40	4.187e−24
1.60e−07	−0.000	−3.26e−22	−3.277e−22	4.265e−40	1.480e−24
1.70e−07	−0.000	−2.86e−22	−2.860e−22	2.713e−40	5.230e−25
1.80e−07	−0.000	−2.51e−22	−2.513e−22	1.768e−40	1.848e−25
1.90e−07	−0.000	−2.22e−22	−2.220e−22	1.177e−40	6.533e−26

Table A3.1 (continued).

z	$\phi^{tot}/1000kT$	ϕ^{tot}	ϕ^{vdw}	ϕ^{born}	ϕ^{dl}
m		J	J	J	J
2.00e—07	—0.000	—1.97e—22	—1.972e—22	7.994e—41	2.309e—26
2.10e—07	—0.000	—1.76e—22	—1.759e—22	5.524e—41	8.161e—27
2.20e—07	—0.000	—1.58e—22	—1.577e—22	3.880e—41	2.885e—27
2.30e—07	—0.000	—1.42e—22	—1.419e—22	2.765e—41	1.019e—27
2.40e—07	—0.000	—1.28e—22	—1.282e—22	1.997e—41	3.603e—28
2.50e—07	—0.000	—1.16e—22	—1.162e—22	1.460e—41	1.274e—28
2.60e—07	—0.000	—1.06e—22	—1.057e—22	1.080e—41	4.501e—29
2.70e—07	—0.000	—9.64e—23	—9.638e—23	8.068e—42	1.591e—29
2.80e—07	—0.000	—8.82e—23	—8.816e—23	6.089e—42	5.623e—30
2.90e—07	—0.000	—8.09e—23	—8.086e—23	4.638e—42	1.987e—30
3.00e—07	—0.000	—7.43e—23	—7.434e—23	3.563e—42	7.024e—31

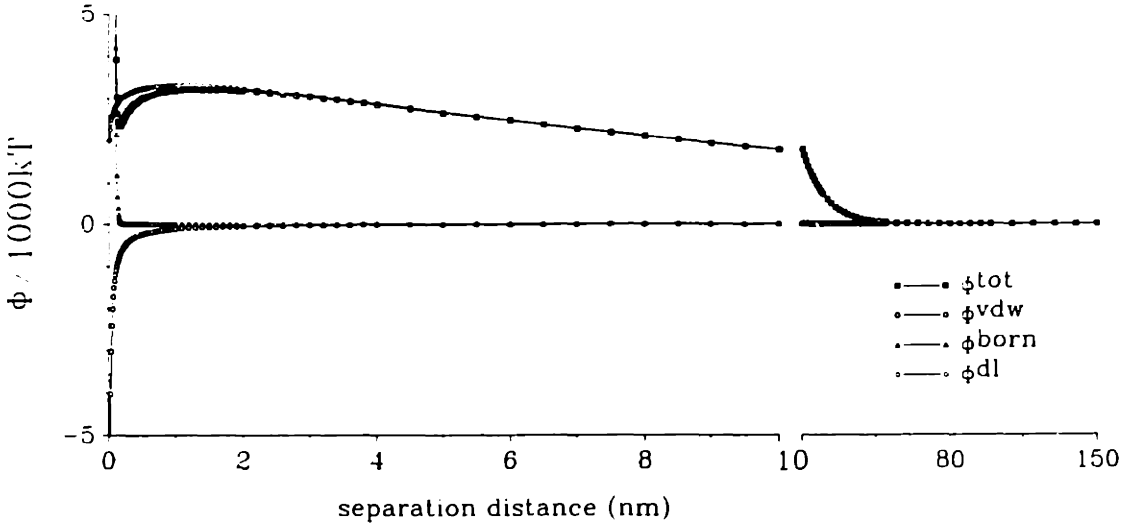

Figure A3.1. Total, van der Waals, Born, and double layer potential energy between a hematite colloid approaching a quartz grain versus separation distance for *p*H 11.0 and $I = 1 \cdot 10^{-3}$ M.

REFERENCES

Barouch E., Matijević E., and Wright T.H. (1987) Effects of Born repulsion on particle detachment. *Chem. Eng. Comm.* **55**, 29–40.

Derjaguin B.V. and Landau L. (1941) *Acta Physicochim. URSS* **14**, 633.

Devereux O.F. and de Bruyn P.L. (1963) *Interaction of Plane–Parallel Double Layers.* MIT Press, Cambridge, MA.

Dzombak D.A. and Morel F.M.M. (1990) *Surface Complexation Modeling: Hydrous Ferric Oxide.* Wiley–Interscience.

Feke D.L., Prabhu N.D., Mann J.A. Jr., and Mann J.A. III (1984) A formulation of the short–range repulsion between spherical colloidal particles. *J. Phys. Chem.* **88**, 5735–5739.

Gregory J. (1975) Interaction of unequal double layers at constant charge. *J. Colloid Interface Sci.* **51**, 44–51.

Hamaker H.C. (1937) The London–van der Waals attraction between spherical particles. *Physica* **4**, 1058–1072.

Hogg R., Healy T.W., and Fuerstenau D.W. (1966) Mutual coagulation of colloidal dispersions. *Trans. Faraday Soc.* **62**, 1638–1651.

Hunter R.J. (1981) *Zeta Potential in Colloid Science.* Academic Press.

Israelachvili J.N.(1982) Forces between surfaces in liquids. *Adv. Colloid Interface Sci.* **16**, 31–47.

Kia S.F., Fogler H.S., and Reed M.G. (1987) Effect of *p*H on colloidally induced fines migration. *J. Colloid Interface Sci.* **118**, 158–168.

Lyklema J. (1980) Colloid stability as a dynamic phenomenon. *Pure Appl. Chem.* **52**, 1221–1227.

Ottewill R.H. (1977) Stability and instability in disperse systems. *J. Colloid Interface Sci.* **58**, 357–373.

Ryan J.N. and Gschwend P.M. (1990) Colloid mobilization in two Atlantic Coastal Plain aquifers: field studies. *Water Resour. Res.* **26**, 307–322.

Ruckenstein E. and Prieve D.C. (1976) Adsorption and desorption of particles and their chromatographic separation. *AIChE J.* 22, 276–283.

Verwey E.J.W. and Overbeek J.Th.G. (1948) *Theory of the Stability of Lyophobic Colloids.* Elsevier.

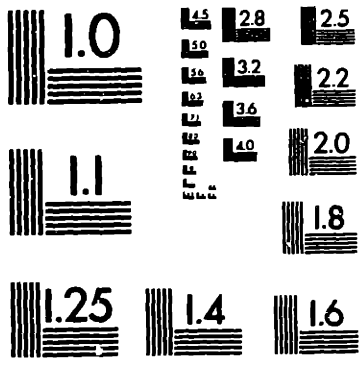

MICROCOPY RESOLUTION TEST CHART
NATIONAL BUREAU OF STANDARDS
STANDARD REFERENCE MATERIAL 1010a
(ANSI and ISO TEST CHART No. 2)